The SnRK1 kinase: novel regulatory mechanisms and its role in metabolic homeostasis

Bruno Alexandre Teixeira Peixoto

Dissertation presented to obtain the Ph.D degree in Plant Biology

Instituto de Tecnologia Química e Biológica António Xavier | Universidade Nova de Lisboa

Research work coordinated by: INSTITUTO GULBENKIAN DE CIÊNCIA; Max-Planck-Institut für Molekulare Pflanzenphysiologie

Oeiras, June, 2021

iTQB UNIVERSIDADE NOVA DE LISBOA

Financial support from Fundação para a Ciência e a Tecnologia, Portugal, through grant PD/BD/114361/2016 awarded to Bruno Peixoto

Supervisors: Elena Baena-González
Mark Stitt

Co-Supervisor: John E. Lunn

Jury Members

Supervisors:

Dr. Elena Baena González
Instituto Gulbenkian de Ciência
Oeiras, Portugal

Prof. Dr. Dr. h.c. Mark Stitt em.
Max Planck Institute of Molecular Plant Physiology
Golm, Germany

Examiners:

Dr. Camila Caldana
Max Planck Institute of Molecular Plant Physiology
Golm, Germany

Prof. Dr. James Lloyd
Stellenbosch University
Stellenbosch, South Africa

Dr. Cleverson Carlos Matiolli
Instituto de Tecnologia Química e Biológica António Xavier
Oeiras, Portugal

Dr. Rita Abranches
Instituto de Tecnologia Química e Biológica António Xavier
Oeiras, Portugal

Acknowledgments

As I write the final pages of this thesis, I cannot help looking back in contemplation of what an adventure this was. Pursuing a PhD in science was already much more challenging than I had originally imagined, and having to brave through a global pandemic at the late stages, when every second counts, only made everything that much harder. That being said, it was also an incredible experience that has forever changed who I am as a person – I met incredible people along the way that I would like to thank and acknowledge.

To all the members of the Plant Stress Signaling group ("Baenos"), both past and present, I send a very warm (covid-free) hug. You guys made everything so much easier by providing me with a vibrant and exciting working place that I have come to love and treasure. To all the members of the other plant groups with which we shared lab space at IGC, the Plant Molecular Biology and Plant Genomics groups, a very warm thank you for all the laughs, all the memories, but also all the help and interesting scientific discussions. Wine and cake are definitely needed, once covid restrictions are lifted!

I would like to highlight Diana, Joana, Mónica and Rui, for their untiring contribution both in making me a more disciplined person, but also in helping me to keep believing in myself, and that a successful end to my PhD was not only possible, but also "almost there".

To my supervisor Elena, a very heartfelt thank you for the never-ending enthusiasm and support. You believed in me even when I myself faltered, and you showed infinite patience when dealing with my convoluted way of thinking and writing. You are an incredibly important source of stability for all of us, PSS PhD students, and I see you as a role model that I intend to keep on following in the future.

I would like to thank the IGC and all of its facilities and people, for all the help and the opportunity to work in what was one of the most pleasant environments to do science that I found in Portugal.

My thanks to my thesis committee members, Isabel Abreu and Carla António, for accompanying me on this wild ride and always having the time for discussing my work and providing valuable input.

To all the members of the System Regulation group at the MPI my thanks for receiving me so warmly. You all made my move to Germany seamless, and my stay so much easier and exciting. There are far too many people I would like to mention by name, but to Brenda, David, Gian, Ginie, Sandi, Steph and Thiago I send a very warm and sunny hug from Portugal. You guys were my partners in crime during my stay at the MPI, and I will always consider you precious friends that I now have all around the globe. To Rubén and Estefanía, who have recently swapped Golm for windy Oeiras, my thanks for all the help both in life and at the bench.

To Mark and John a huge thank you for all the enthusiasm, all the help and all the patience, as they accepted my metabolically-untrained self and made me who I am today as a scientist. I really learned a lot from you two, and I acknowledge that receiving someone with so little background in this area may have been both challenging and frustrating at times. Know that I am aware of that, and all the more grateful for it.

My thanks to the MPI's greenteam, in particular to Frau Hausmann, for always keeping my tobaccos nice and happy with a smile on her face. To Regina, Melanie and all the other people whose technical expertise was essential for the success of this work – thank you.

To Mário, Mattia, Sofia and her team – know that people who feed me good food will always be my favourite people.

I thank Vera for always keeping my Portuguese plants alive, free of thrips and other nasties, and for being such a good friend and companion during this adventure.

To Umbelina and Alexandrina a very special thanks, for being my home away from home, and for going above and beyond into making my life easier during my stay with them.

To Cláudia, Vanessa and all the peeps from my previous scientific family (Lab 2.61), my warm thanks for helping me walk the road that ultimately led me to this PhD. You helped me build the foundations over which I built my PhD.

Thanks Sam, for always being there and always being proud of me. You have always believed more in me than I have.

I would also like to dedicate this work to my family - without you I would never have made it this far.

Sadly I am unable to properly recognise the contribution of all the people that were an important part of my life during this period. To all of those people, thank you for being there for me. You have all helped me reach the end of this crazy adventure.

Resumo

O metabolismo das plantas encontra-se sob um controlo rigoroso, para garantir que os recursos de carbono são investidos de uma forma optimizada, maximizando crescimento e sobrevivência. Um dos principais mecanismos de regulação metabólica é o chamado “nexo da sacarose - trehalose 6-fosfato (Tre6P)”. Neste sistema, a Tre6P acompanha os níveis de sacarose, servindo como sinal da sua disponibilidade e regulando a sua síntese e consumo, por forma a manter a sacarose dentro de níveis óptimos. Este objectivo é atingido em parte pelo direccionamento de fotoassimilados para síntese de ácidos orgânicos e aminoácidos sempre que há um aumento nos níveis de sacarose (e subsequentemente de Tre6P), permitindo a diminuição da produção de açúcar.

Outro dos componentes implicados na regulação metabólica é a SNF1-Related Protein Kinase 1 (SnRK1). A SnRK1 é uma cinase conservada evolutivamente, capaz de medir os níveis de carbono, e cuja principal função é a manutenção da homeostasia energética tanto a nível celular, como a nível do organismo. A SnRK1 é activada quando os níveis energéticos decrescem (por exemplo, durante condições de stresse), levando à implementação de um programa de conservação de energia que favorece processos catabólicos (produtores de energia) sobre processos anabólicos (consumidores de energia). Por outro lado, a SnRK1 é inibida pela Tre6P, que sinaliza a disponibilidade de sacarose. A SnRK1 opera através da fosforilação de um vasto espectro de alvos a jusante, desde enzimas do metabolismo primário a factores de transcrição. Dada a sua associação com situações de stresse, vários mutantes de ganho- e perda-de-função de SnRK1 têm sido caracterizados sob uma ampla variedade de condições de stresse.

No entanto, a relevância fisiológica da função da SnRK1 em condições de ausência de stresse, particularmente em tecidos-fonte, permanece largamente inexplorada. O facto de a manipulação da SnRK1 resultar em vários fenótipos de crescimento e desenvolvimento, aliado ao facto de que mutantes com total perda de função da SnRK1 nunca terem sido obtidos em plantas superiores, argumenta a

favor de funções essenciais da SnRK1 na manutenção da homeostasia, também em condições de ausência de stresse. Isto levou à formulação da principal hipótese de trabalho, em que **a SnRK1 desempenha um papel importante ao nível do metabolismo e expressão génica durante o ciclo diurno.**

Neste trabalho, eu demonstro que a manipulação genética da SnRK1 leva a alterações severas nos níveis de Tre6P em rosetas adultas de Arabidopsis, com a sobre-expressão da subunidade catalítica α1 a levar ao aumento da acumulação de Tre6P durante o ciclo dia-noite. Por outro lado, a depleção de subunidades catalíticas da SnRK1 leva ao fenótipo oposto, com níveis de Tre6P mal atingindo os valores mínimos observados nas plantas *wild-type* (WT). Apesar dos níveis elevados de Tre6P, as plantas sobre-expressoras de SnRK1α1 apresentaram valores WT de intermediários da via glicolítica e ciclo dos ácidos tricarboxílicos. Por outro lado, os níveis baixos de Tre6P na linha de perda-de-função de SnRK1α1 foram acompanhados por uma redução nos níveis de intermediários da via glicolítica e um aumento dos níveis de citrato e isocitrato. Isto sugere que os efeitos previamente descritos da Tre6P no metabolismo passam, pelo menos em parte, pela SnRK1. Além disso, os mutantes de SnRK1 apresentaram uma dinâmica sacarose-Tre6P alterada, devido ao efeito desproporcional que as mutações sobre a SnRK1 têm na acumulação de Tre6P. Estas observações implicam a SnRK1 na regulação da acumulação de Tre6P em resposta à sacarose.

Análises transcriptómicas de plantas WT revelaram um pico de expressão de genes induzidos pela SnRK1 ao final da noite, quando as reservas de carbono estão nos seus níveis mais baixos, e uma repressão progressiva até ao final do dia, quando as reservas de carbono atingem os seus níveis máximos. Esta observação levou à formulação da hipótese que a SnRK1 está sob o controlo da Tre6P também em tecidos diferenciados de folhas adultas, e que a sua actividade é determinada pelos ciclos diários de Tre6P. Utilizando uma linha de sobre-expressão indutível da enzima de síntese de Tre6P de *Escherichia coli* (OtsA), pudemos observar que um aumento artificial nos níveis de Tre6P durante o dia foi suficiente para reprimir a expressão de genes repórter da actividade da SnRK1.

Análises transcriptómicas revelaram também um possível papel da sinalização pela SnRK1 no metabolismo de ferro e enxofre. A perda de função da SnRK1 resultou numa repressão drástica de vários genes associados à resposta de falta de ferro. Ferro e enxofre são nutrientes altamente reactivos que necessitam ser mantidos num equilibro estequiométrico apertado para evitar danos oxidativos. Em linha com a forte repressão destes genes envolvidos na nutrição de ferro, o mutante de perda-de-função de SnRK1 apresentou um aumento na expressão de genes associados à falta de enxofre, mas apenas ao final da noite. Estes resultados revelam uma possível nova função da SnRK1 na nutrição de ferro e/ou enxofre.

Por fim, a análise do gene da *SnRK1β1* levou à identificação de *splicing* alternativo como uma fonte de diversidade de subunidades de SnRK1. Detectamos três transcriptos diferentes *in planta*, todos eles codificando proteínas diferentes. A análise de folhas de *Nicotiana benthamiana*, sobre-expressando de forma transiente as diferentes variantes de *splicing* da SnRK1β1 fundidas a um repórter GFP, por microscopia confocal de varrimento a laser, demonstrou que estas variantes se acumulavam em localizações sub-celulares distintas. Além disso, ensaios de complementação bi-fluorescente sugerem que as três variantes são capazes de interagir com a subunidade catalítica SnRK1α1 *in vivo*. A análise dos perfis metabólicos de linhas de T-DNA e de sobre-expressão de *SnRK1β1.1* revelaram apenas pequenas alterações nos níveis endógenos de nitrito, em concordância com o papel repressivo que a SnRK1 tem sobre a nitrato redutase através desta subunidade.

No seu conjunto, o trabalho descrito nesta tese identifica novos mecanismos de regulação da SnRK1 ao nível do processamento de RNA e do metabolismo. Este trabalho revelou um papel central da SnRK1 na homeostasia da sacarose, não só por bloqueio do desvio dos fluxos de carbono noutras direcções, mas também pela tradução das alterações dos conteúdos de sacarose em alterações dos níveis de Tre6P. Estes resultados realçam as funções proeminentes da SnRK1 na sincronização do metabolismo vegetal e expressão génica durante os ciclos de dia-noite.

Abstract

Plant metabolism is tightly controlled to ensure that carbon resources are optimally invested to maximize growth and fitness. One major regulatory system involved in metabolic control is the so-called sucrose-trehalose 6-phosphate (Tre6P) nexus. In this system, Tre6P mirrors sucrose levels and acts as a signal of sucrose availability, regulating its synthesis and consumption to maintain sucrose within optimal levels. This is partly achieved by the diversion of photoassimilates towards organic and amino-acid synthesis when sucrose levels (and in consequence Tre6P) rise, thereby reducing further production of sucrose.

Another component implicated in metabolic regulation is the SNF1-Related protein Kinase 1 (SnRK1). SnRK1 is an evolutionarily conserved carbon sensing kinase whose core function is to maintain cellular and whole-organism energy homeostasis. SnRK1 is activated when energy levels decrease (e.g. during stress), implementing an energy conservation programme that favours catabolic (energy-producing) over anabolic (energy-consuming) processes. Conversely, SnRK1 is inhibited by Tre6P, which signals sucrose availability. SnRK1 functions by phosphorylating a wide range of downstream targets, from enzymes of primary metabolism to transcription factors. Due to its association to stress, SnRK1 gain- and loss-of-function mutants have been mostly characterised under a wide range of stress conditions.

However, the physiological relevance of SnRK1 function under non-stress conditions, in particular in source tissues, remains largely unexplored. The fact that SnRK1 manipulation results in diverse growth and developmental phenotypes, together with the fact that full *snrk1* loss-of-function mutants could never be retrieved in higher plants, argues in favour of essential functions in homeostatic control also under stress-free conditions. This prompted the main hypothesis of this work, that **SnRK1 plays important functions in metabolism and gene expression under the regular diurnal cycles**.

In this work I show that genetic manipulation of SnRK1 leads to severely altered Tre6P levels in mature Arabidopsis rossettes, with overexpression of the α1 catalytic subunit enhancing Tre6P accumulation during the day-night cycle. On the other hand, depletion of SnRK1 catalytic subunits leads to the opposite phenotype, with Tre6P levels barely reaching the minimum values observed in wild-type (WT) plants. Despite their highly elevated Tre6P content, SnRK1α1 overexpressing plants showed WT levels of glycolytic and TCA cycle intermediates. Conversely, low Tre6P accumulation in the SnRK1α1 loss-of-function line was accompanied by reduced glycolytic intermediate accumulation and increased levels of citrate, aconitate, and isocitrate. This suggests that the previously reported effects of Tre6P on metabolism rely at least partly on SnRK1. Furthermore, the SnRK1 mutant lines presented an altered sucrose-Tre6P relationship, with a disproportionally larger effect of SnRK1 mutations on Tre6P than on sucrose. These observations implicate SnRK1 in the regulation of Tre6P accumulation in response to sucrose.

Transcriptomic analysis of WT plants revealed a peak of expression of SnRK1-induced genes at the end of the night, when carbon reserves are lowest, and a progressive downregulation towards the end of the day, when carbon reserves are highest. This prompted the hypothesis that **SnRK1 is under Tre6P regulation also in differentiated mature leaves and that its activity is determined by diurnal Tre6P cycles**. Using an inducible overexpressor of the *Escherichia coli* Tre6P-synthetizing enzyme (OtsA) we could indeed verify that an artificial increase in Tre6P levels during the day was sufficient to repress SnRK1 marker gene expression.

Transcriptomic analyses additionally revealed a putative role for SnRK1 signalling in iron and sulphur metabolism. Loss of SnRK1 function resulted in strong downregulation of genes associated with an iron starvation response. Iron and sulphur are highly reactive nutrients that must be kept under tight stoichiometric balance to avoid oxidative damage. In line with the strong repression of several iron starvation genes, the SnRK1 loss-of-function mutant showed upregulation of genes associated with sulphur starvation, but only at the end of the night. These results disclose a putative novel function of SnRK1 in iron and/or sulphur nutrition.

Finally, analysis of the *SnRK1β1* gene identified alternative splicing as a source of subunit diversity. We detected three different transcripts *in planta*, all of which encode different protein products. Confocal laser scanning microscopy analysis of *Nicotiana benthamiana* leaves, transiently overexpressing GFP-tagged SnRK1β1 splice variants, showed these different subunits accumulated in distinct subcellular compartments. Furthermore, bimolecular fluorescence complementation assays suggested all three variants possess the ability to interact with the SnRK1α1 catalytic subunit *in vivo*. Metabolite profiling of T-DNA and *SnRK1β1.1* overexpressor mutants revealed only minor changes in nitrite, which are in agreement with the previously described repressive effect of SnRK1 on nitrate reductase *via* this subunit.

Altogether, this thesis identified novel regulatory mechanisms of SnRK1 at the levels of RNA processing and metabolism. This work further uncovered a central role of SnRK1 on sucrose homeostasis, both by blocking diversion of the flux of carbon away from sucrose and by translating changes in sucrose content into mirroring Tre6P levels. These results highlight a prominent function of SnRK1 in orchestrating plant metabolism and gene expression during the normal day-night cycle.

Table of Contents

List of Abbreviations

2-OG	2-oxoglutarate
2-PGA	2-phosphoglyceric acid
3-PGA	3-phosphoglyceric acid
ABA	Abscisic acid
ADP	Adenosine Diphosphate
ADPGlc	Adenosine 5’-diphosphate-glucose
AID	Auto-inhibitory Domain
AMP	Adenosine Monophosphate
ATP	Adenosine Triphosphate
CBM	Carbohydrate-binding module
CBS	Cystathione β-synthase
CO_2	Carbon dioxide
CoA	Coenzyme A
CTD	C-Terminal Domain
DEG	Differentially Expressed Gene
DHAP	Dihydroxyacetone-phosphate
dpi	Days post-infiltration
ED	End of Day
EN	End of Night
ER	Endoplasmic Reticulum
FAD	Flavin adenine dinucleotide
FBP	Fructose 1,6-bisphosphate
FC	Fold Change

FDR	False Discovery Rate
Fru	Fructose
Fru-2,6bP	Fructose-2,6-bisphosphate
Fru6P	Fructose 6-Phosphate
GA	Golgi Apparatus
GAP	Glyceraldehyde 3-phosphate
GFP	Green Fluorescent Protein
Glc	Glucose
Glc1P	Glucose 1-Phosphate
Glc6P	Glucose 6-Phosphate
Gly3P	Glycerol 3-Phosphate
GO	Gene Ontology
HA	Hemagglutinin
IP	Immunoprecipitate
KIS	Kinase Interacting Sequence
MD	Middle of day
MW	Molecular Weight
NADP	Nicotinamide adenine dinucleotide phosphate
NR	Nitrate Reductase
OAA	Oxaloacetate
PEP	Phospho*enol* pyruvate
PEPC	Phospho*enol* Pyruvate Carboxylase
Pi	Orthophosphate
PPi	Inorganic pyrophosphate
RFP	Red Fluorescent Protein
RuBP	Ribulose-1,5-bisphoshate

SHG	Soluble Heteroglycan
SnAK	SnRK1 Activating Kinase
SnRK	Sucrose non-fermenting Related Kinase
SPS	Sucrose Phosphate Synthase
Suc6P	Sucrose 6-Phosphate
SUMO	Small Ubiquitin-like modifier
TCA	Tricarboxylic Acid
TP	Triose Phosphate
TPP	Trehalose 6-Phosphate Phosphatase
TPS	Trehalose 6-Phosphate Synthase
Tre6P	Trehalose 6-Phosphate
UBA	Ubiquitin-associated
UDPGlc	Uridine diphosphate glucose
VIGS	Virus-induced gene silencing
WT	Wildtype
Y2H	Yeast 2-hybrid
YFP	Yellow fluorescent protein
ZT	Zeitgeber time

List of Figures

List of Tables

CHAPTER 1

General Introduction

All life on Earth is dependent on the availability of energy that can fuel biochemical reactions. In the case of higher plants, this requirement is met inside the chloroplast, through photosynthesis. Sunlight is captured by photosynthetic pigments such as chlorophylls and carotenoids, exciting these molecules. This generates a flow of electrons that is transferred to the nearby plastoquinone and other components of the electron transport chain and is ultimately used to reduce nicotinamide adenine dinucleotide phosphate (NADP) to NADPH (Leegood, 2004). Concomitant with the flow of electrons, a proton gradient is generated across the thylakoid membrane that drives the synthesis of adenosine triphosphate (ATP). ATP and NADPH are subsequently used by the Calvin-Benson cycle for fuelling carbon fixation to form triose phosphates (TPs). Most of these TPs are then employed for the regeneration of the pools of the carbon acceptor ribulose-1,5-bisphosphate (RuBP), with the remainder being used for the synthesis of end-product metabolites such as starch, sucrose, and amino-acids (Leegood, 2004; Tegeder and Weber, 2006; Stitt et al., 2010).

1.1 Carbon partitioning

TPs are the organic compounds resulting from inorganic carbon assimilation *via* the Calvin-Benson cycle, and they serve as the main precursors and carbon sources for all other biosynthetic pathways in plants. Inside the chloroplasts, TPs fuel starch synthesis, but they are also exported to the cytosol, where they feed glycolysis and sucrose synthesis [reviewed in Tegeder and Weber, 2006]. The fine management of these carbon resources is essential to maximize plant growth and survival during the day-night cycle and under an ever-changing environment and is generally referred to as carbon partitioning.

1.1.1 Starch

Plants use starch as a form of storing chemical energy in a condensed, osmotically inert form. Starch can generally be classified into two different categories – storage starch or transitory starch, with most of the starch produced in photosynthetically active leaves belonging to the latter category. What makes a starch “transitory” is the fact that most of it is consumed during the dark period to sustain continuous energy production and plant growth in the absence of light and photosynthesis. Storage starch, on the other hand, is generally accumulated in non-photosynthetic tissues, such as seeds, stems, roots or tubers, and is stored for longer periods of time, with remobilisation usually occurring during germination or regrowth. Storage starch is also the primary source of dietary starch for humans (Pfister and Zeeman, 2016).

Starch is a polymer composed primarily of amylopectin (70-80%) and amylose, both of which consist of α-(1,4)-linked glucose (Glc) chains, branched *via* α-(1,6)-bonds (Badenhuizen, 1963). The highly organized structure of amylopectin leads to the semi-crystallization of starch into granules, making it water insoluble and, most importantly, osmotically inert.

In higher plants, starch is synthesized inside the plastids, such as the chloroplasts in photosynthetically active leaves. Adenosine 5’-diphosphate-glucose (ADPGlc) synthesis in leaves by ADPGlc pyrophosphorylase (AGPase) is the first committed step of starch biosynthesis, and it relies on the conversion of part of the Calvin-Benson cycle TPs into Glucose 1-phosphate (Glc1P) through a series of enzymatic steps. Afterwards, starch synthases (SSs) use the Glc moiety of ADPGlc to extend the non-reducing ends of a previously existing α-glucan chain. Branching enzymes use their glucanotransferase activity to create branching points in the existing chains, whereas debranching enzymes act upon these branches, hydrolysing them [reviewed in Pfister and Zeeman, 2016; MacNeill et al., 2017].

During the night, or in periods of insufficient photosynthetic input, transitory starch can be mobilized to fuel metabolism. Starch hydrolysis occurs at the surface

of the granule that is solubilized through the reversible phosphorylation of glucans, mediated by a glucan water dikinase (GWD1) and a phosphoglucan water dikinase (PWD). Exo-acting β-amylases and ISOAMYLASE 3 (ISA3) lead to the release of maltose and, to a smaller extent, some longer malto-oligosaccharides from the exposed non-reduced chain ends. However, in order for β-amylases and ISA3 to be able to fully complete their hydrolytic functions, glucan dephosphorylation mediated by phosphatases such as STARCH EXCESS 4 (SEX4) and LIKE SEX4 2 (LSF2) has to occur (Zeeman et al., 2010). The maltose generated from the degradation of the starch granule by these enzymes can be exported out of the chloroplast by a maltose transporter, MALTOSE EXPORTER 1 (MEX1), whereas the longer malto-oligosaccharides are further processed by DISPROPORTIONATING ENZYME 1 (DPE1), before being translocated to the cytosol in the form of Glc, through the glucose transporter GlcT. The now cytosolic maltose disaccharide, can then be hydrolysed by DISPROPORTIONATING ENZYME 2 (DPE2), which releases one of the Glc molecules, while transferring the other to an acceptor glycan, thought to be a soluble heterogeneous glycan (SHG) comprised of different sugar moieties, such as galactose, arabinose and glucose (Fettke et al., 2004; Smith and Zeeman, 2020). Glucosylated SHG can then serve as substrate for the cytosolic phosphorylase PHS2 to synthetize Glc1P (Fettke et al., 2004). This Glc1P pool subsequently serves as a substrate for the cytosolic synthesis of sucrose.

1.1.2 Regulation of starch metabolism

Transitory starch plays a pivotal function in fuelling growth during periods of stress and darkness and, consequently, its metabolism is tightly regulated. Regulation of starch metabolism relies on the coordination of starch biosynthesis and mobilization, in a process that is timed *via* the circadian clock, so that carbon stores are not prematurely exhausted. These multi-level regulatory mechanisms allow the plant to adjust its carbon reserves to the current photoperiod and environmental conditions [reviewed in MacNeill et al., 2017].

Transcriptional variation of several of the genes encoding starch metabolising enzymes has been observed, with a subset of starch degrading transcripts showing a clear peak at the end of the day, prior to the initiation of starch degradation (Smith et al., 2004). This expression pattern is known to be under control of the circadian clock, but despite strong oscillations in mRNA levels, protein abundance appears relatively constant, making the transcriptional regulation of these genes less relevant for day-to-day control of starch metabolism (Tenorio et al., 2003; Smith et al., 2004; Lu et al., 2005; Gibon et al., 2004). In plants grown under shorter photoperiods (accompanied by longer nights) there is a higher rate of starch synthesis than degradation, whereas the opposite is true for plants grown under long photoperiods (accompanied by shorter nights) (Smith and Stitt, 2007; Gibon et al., 2009; Sulpice et al., 2014). In both cases the rate of degradation shows a linear trend that has previously been observed in other plant species besides Arabidopsis (Chatterton and Silvius, 1979). Previous reports about delays in the beginning of starch synthesis at dawn (Stitt et al., 1983, 1984; Gerhardt et al., 1987), and starch degradation at dusk (Fondy and Geiger, 1985; Zeeman and Rees, 1999) are strong indicators that the regulatory mechanism is not just a light/dark switch. It is well accepted that carbon flux into transitory starch is under direct control of AGPase, which shuts down at night through allosteric inhibition by falling inorganic phosphate and falling glycerate 3-phosphate and redox inactivation (Geigenberger, 2011), although it is not clear if other enzymes involved in starch synthesis and degradation are also regulated in a similar manner.

Starch metabolism is also tightly regulated in response to changes in the environment, as exemplified by experiments in which plants subjected to sudden changes in photoperiod immediately adjust subsequent rates of starch degradation. These adjustments allow the plant to match an unexpectedly longer night with slower rates of starch mobilisation, or an unexpectedly shorter night with faster rates of starch mobilisation, and suggest that the circadian clock influences the flux of carbon into and out of starch in response to changes in the photoperiod (Lu et al., 2005; Graf et al., 2010). Further support for the control of starch metabolism by the circadian clock was provided by the observation that Arabidopsis plants are

incapable of properly adjusting starch mobilization to abnormal diurnal cycles of either 17h or 28h (Graf et al., 2010). Moreover, *cca1*/*lhy* mutants, lacking core components of the clock and with a shortened clock period, display an altered pattern of starch mobilization, with starch becoming depleted close to the perceived end of the night 2-3 hours before the external dawn, whereas long-period clock mutants do not fully exhaust their starch by dawn (Graf et al., 2010; Flis et al., 2019).

Other mechanisms, such as post-translational control over starch metabolising enzymes, have also been hypothesized to regulate starch metabolism. Large-scale phosphoproteomics studies have identified several of these enzymes as putative targets of protein kinases *in vivo*. Although the physiological relevance of these phosphorylation events has yet to be explored, it is likely that they influence protein-protein interactions and metabolon formation (Tetlow et al., 2004; Kötting et al., 2010). Other mechanisms of protein modification, such as the redox regulation of AGPase may also be in place. The sugar phosphate trehalose 6-phosphate (Tre6P) also impacts on starch dynamics and, although its effects on starch synthesis *via* redox activation of AGPase appear to be limited and less consistent, a repressive effect of Tre6P on starch mobilisation is more widely accepted (see section 1.2.3 for more details) (Kolbe et al., 2005; Lunn et al., 2006; Martins et al., 2013; Dos Anjos et al., 2018).

1.1.3 Sucrose

Sucrose is a disaccharide that is synthetized exclusively by oxygenic photosynthetic organisms, such as higher plants (Lunn, 2002; Salerno and Curatti, 2003), where it serves as the main transport carbohydrate molecule. Sucrose is synthetized in the cytoplasm, where SUCROSE-PHOSPHATE SYNTHASE (SPS) produces sucrose 6-phosphate (Suc6P) from uridine 5'-diphosphoglucose (UDPGlc) and fructose 6-phosphate (Fru6P). SUCROSE-PHOSPHATE PHOSPHATASE (SPP) further dephosphorylates Suc6P to sucrose, with the generation of an extra orthophosphate (Pi).

Newly synthetized sucrose can then either be stored in the vacuole, metabolised, or transported to other tissues through the phloem, from source (carbon fixing) to sink (carbon importing) tissues. Sucrose is transported between tissues by mechanisms that vary from species to species. So far, three different mechanisms of sucrose loading into the phloem have been identified – (1) symplastic loading, where sucrose synthetized in the mesophyll moves through plasmodesmata along a concentration gradient, towards the sieve elements; (2) apoplastic loading, where sucrose synthetized in the mesophyll is exported from the cells adjacent to the companion cells, and imported (against a concentration gradient) into the companion cells, through the aid of sugar transporters; and (3) a "polymer trapping" mechanism that relies on the synthesis of larger sugar molecules, such as stachyose, raffinose or verbascose in the companion cells. These larger sugar molecules are derived from sugars that are symplastically delivered by intermediate cells, effectively "trapping" the original sugar in the new larger polymer that cannot diffuse back through the plasmodesmata [reviewed in Slewinski and Braun, 2010; Fernie et al., 2020]. In *Arabidopsis thaliana*, sucrose loading is apoplastic (Fernie et al., 2020; Braun et al., 2014).

During apoplastic sugar loading, three members of the SUGARS WILL EVENTUALLY BE EXPORTED TRANSPORTERs (SWEETs, *viz* SWEET11, SWEET12 and SWEET13) are responsible for the efflux of sucrose from mesophyll cells into the phloem apoplast. Apoplastic sucrose is then imported through sucrose or proton SUC1-type symporters to the sieve elements and companion cells, against its concentration gradient. The proton gradient required to drive sucrose transport is generated by ATPases at the plasma membrane (Fernie et al., 2020). The high concentration of sucrose at the sieve element/companion cell complex leads to the movement of water into the phloem, increasing turgor pressure that can then drive the mass flow of photoassimilates between tissues. Once the target tissue is reached, sucrose may be cleaved by CELL WALL INVERTASE (CWIN) into Glc and Fru, before cytoplasmic uptake. CWIN expression is generally higher in sink tissues, where a high level of catalytic activity may help phloem unloading by lowering local sucrose concentrations, thereby creating a concentration gradient between the sieve

element/companion cell complex and the surrounding tissues (Ruan, 2014). This mechanism generates the necessity for sucrose synthesis to reoccur in the sink tissues, prior to storage or further intercellular transport, and in fact, SPS activity in sink tissues is correlated with starch accumulation, protein storage and cellulose biosynthesis (Weber et al., 1997; Babb and Haigler, 2001). Alternatively, sucrose can also be imported directly *via* SUC transporters, or delivered directly from the phloem through plasmodesmata, bypassing the requirement for break-down and re-synthesis [reviewed in Fernie et al., 2020].

Intracellularly, sucrose can then be metabolised in the cytoplasm *via* CYTOSOLIC INVERTASE (CIN) (Barratt et al., 2009), or imported into mitochondria (Szarka et al., 2008), chloroplasts (Gerrits et al., 2001), or vacuoles (Grennan and Gragg, 2009; Sonnewald et al., 1991), under tightly regulated processes that affect local sucrose levels and cellular metabolism with important downstream effects on plant growth and development. Direct import of sucrose to the vacuole plays an important role in controlling sucrose homeostasis, by relying on this organelle as a transient storage compartment. Sucrose can be hydrolysed irreversibly to Glc and Fru by invertases, of which several isoforms exist, with different subcellular localisations and pH optima. Sucrose can also be hydrolysed reversibly to UDPGlc and Fru by sucrose synthases. SUSY has been described as a biochemical marker of “sink strength”, particularly in tissues where internal oxygen concentrations are low (Xu et al., 2012). This likely occurs because sucrose hydrolysis *via* SUSY generates hexoses in a more ATP-efficient manner (Barratt et al., 2009; Bieniawska et al., 2007). In accordance with this idea, the expression of several SUSY isoforms has been found to increase in response to hypoxia in *Arabidopsis thaliana* roots (Bieniawska et al., 2007), as well as *Solanum tuberosum* tubers (Fu and Park, 1995).

1.1.4 Glycolysis

The glycolytic pathway consists of a series of step-wise chemical reactions that allow for the controlled oxidation of highly reduced molecules, such as carbohydrates, leading to the production of carbon dioxide (CO_2), ATP, pyruvate, and reducing equivalents (NAD(P)H and $FADH_2$). As a core section of carbon metabolism, glycolysis plays an essential role in maintaining and fuelling plant growth.

In plants, glycolysis can occur both in the plastid and cytosol, with both pathways acting in parallel and under the control of a series of distinct, nuclear-encoded isozymes (Plaxton, 1996; Givan, 1999). Because both pathways act upon the same type of substrates, and generate the same products, they interact through the action of highly specific metabolite transporters present at the plastid envelope, allowing the integration of both metabolic pathways into the overall metabolic landscape of the cell (Emes and Tobin, 1993; Plaxton, 1996; Tegeder and Weber, 2006).

At the cytosolic level, plant glycolysis expands into a series of parallel reactions, that act as effective bypasses to the classical pathway, particularly at the levels of sucrose, Fru6P, glyceraldehyde 3-phosphate (GAP) and phospho*enol* pyruvate (PEP), serving as one of the basis of plant metabolic plasticity and environmental adaptability (Black et al., 1987; Plaxton, 1996; Givan, 1999; Podestá and Plaxton, 2003). Inorganic pyrophosphate (PPi) is generated as a by-product of several anabolic reactions and can be utilized by plants to fuel these ATP-independent enzymatic reactions (Ferjani et al., 2014). In essence, the utilization of PPi results in resource optimization, as it allows plants to employ a natural by-product of anabolic metabolism to fuel glycolysis at no ATP cost (Plaxton and Podestá, 2006). In addition, it provides increased stability against environmental fluctuations, since PPi pools are much more stable under biotic and abiotic stress conditions than the adenylate pool (Duff et al., 1989; Plaxton, 1996; Stitt, 1998).

Cytosolic glycolysis begins at the level of sucrose, with its hydrolysis being mediated either by invertase or SUSY. The products resulting from sucrose cleavage are then converted into hexose phosphates by fructokinase and hexokinase, with Glc6P being processed by phosphoglucomutase and UDPGlc pyrophosphorylase into UDPGlc. Fru6P can be further phosphorylated into fructose 1,6-bisphosphate (FBP), marking what can arguably be called the first committed step of plant glycolysis (Givan, 1999). FBP can then be cleaved by aldolase, generating 3-phosphoglyceric acid (3-PGA). By the action of phosphoglyceromutase, 3-PGA is converted to 2-PGA and subsequently to PEP by enolase. PEP is the basis for the synthesis of the first organic acid molecules, either *via* pyruvate kinase (PK), or *via* Phospho*enol*pyruvate Carboxylase (PEPC), being first converted into oxaloacetate (OAA), and then into malate (Figure 1.1) [all these steps are reviewed in Plaxton and Podestá, 2006].

An increasing number of reports have shown that, rather than being randomly distributed in the cytosolic space, some of the glycolytic enzymes can organize as multi-enzyme complexes *in vivo*, capable of associating with the outer mitochondrial membrane (Giegé et al., 2003). These “metabolons” enable the micro-compartmentation of reactants and reaction products, facilitating the transfer of intermediate compounds between consecutive enzymes, reducing competition between different metabolic pathways, and allowing for a high concentration of pyruvate to be delivered directly to the mitochondrion (Giegé et al., 2003; Zhang et al., 2020). The generated pyruvate can then be used by the mitochondria to fuel the tricarboxylic acid (TCA) cycle.

For any metabolic pathway, the flux of metabolites is directly connected to the activities of the individual enzymes that comprise it. For plant glycolysis, both coarse and fine regulatory mechanisms are in place in order to accurately regulate reaction velocities *in vivo*. Coarse control is based on the total amount of each individual enzyme component and relies on the transcriptional and translational control of their respective genes, as well as on the rate of protein turnover [reviewed in Plaxton, 1996]. Fine control, on the other hand, is achieved by modulating the activity of the available enzyme pools, and can rely on several different mechanisms,

such as (1) variation in substrate and cofactor concentrations, (2) variations in pH, (3) metabolite effectors, (4) association and dissociation of different subunits, (5) post-translational modifications, and (6) association between metabolically sequential enzymes (metabolon formation) [reviewed in Plaxton, 1996].

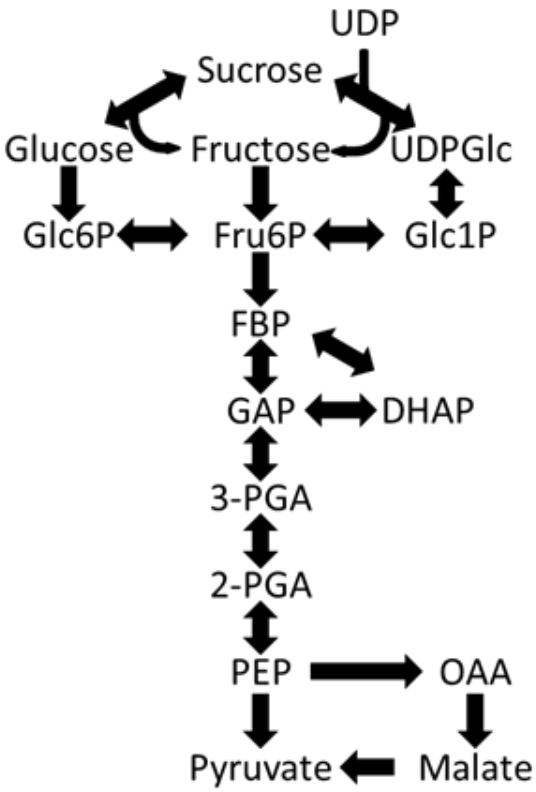

Figure 1.1 | Overview of plant cytosolic glycolysis.
Adapted from Plaxton and Podestá, 2006.

1.1.5 TCA Cycle

The TCA cycle forms the basis of mitochondrial respiratory metabolism, oxidizing carbon substrates to generate reducing equivalents (NADH and $FADH_2$), that can be further used to fuel ATP synthesis during oxidative phosphorylation. Besides fuelling ATP synthesis, the TCA cycle is also important for providing carbon skeletons for several biosynthetic processes, such as amino acid synthesis (Fatland et al., 2005), carbon/nitrogen interactions (Noguchi and Terashima, 2006), optimisation of photosynthetic activity (Nunes-Nesi et al., 2008) and redox homeostasis (Scheibe et al., 2005).

The TCA cycle begins with the entry and decarboxylation of pyruvate in the mitochondria, and is comprised of eight different enzymatic steps. Decarboxylation of pyruvate generates acetyl-CoA (Budde and Randall, 1990), which can then be condensed with OAA into citrate by citrate synthase (La Cognata et al., 1996). Citrate acts as a substrate for aconitase, generating isocitrate (Courtois-Verniquet and Douce, 1993), which can then be transformed into 2-oxoglutarate (2-OG) *via* isocitrate dehydrogenase (Gálvez et al., 1999). 2-OG can be exported to the plastid to fuel glutamate synthesis, or remain within the TCA cycle and be transformed into succinyl-CoA *via* the action of the 2-OG dehydrogenase complex (Bunik and Fernie, 2009). Succinyl-CoA ligase subsequently converts succinyl-CoA to succinate (Kaufman and Alivisatos, 1955), which can then be oxidized to fumarate by succinate dehydrogenase (Figueroa et al., 2001). Fumarase transforms fumarate to malate (Behal and Oliver, 1997), which can be further oxidized to OAA by malate dehydrogenase (Gietl, 1992), closing back the cycle (Figure 1.2).

Similarly to the glycolytic pathway, mitochondrial respiration is also subject to several layers of control. Most mitochondrial proteins are encoded in the nuclear genome, but the fact that a small number of essential proteins are encoded in the mitochondrial genome implies that gene expression has to be coordinated between both organelles, *via* anterograde and retrograde signalling pathways (Pesaresi et al., 2006; Woodson and Chory, 2008). Protein turnover is also an important level of control, with several proteases being active inside mitochondria and directly

impacting TCA cycle operation (Rigas et al., 2009; Janska et al., 2010). In addition, mitochondrial respiration is regulated by post-translational modification of enzymes, such as phosphorylation, oxidation and reduction (Bykova et al., 2003; Balmer et al., 2004; Kristensen et al., 2004; Millar et al., 2005).

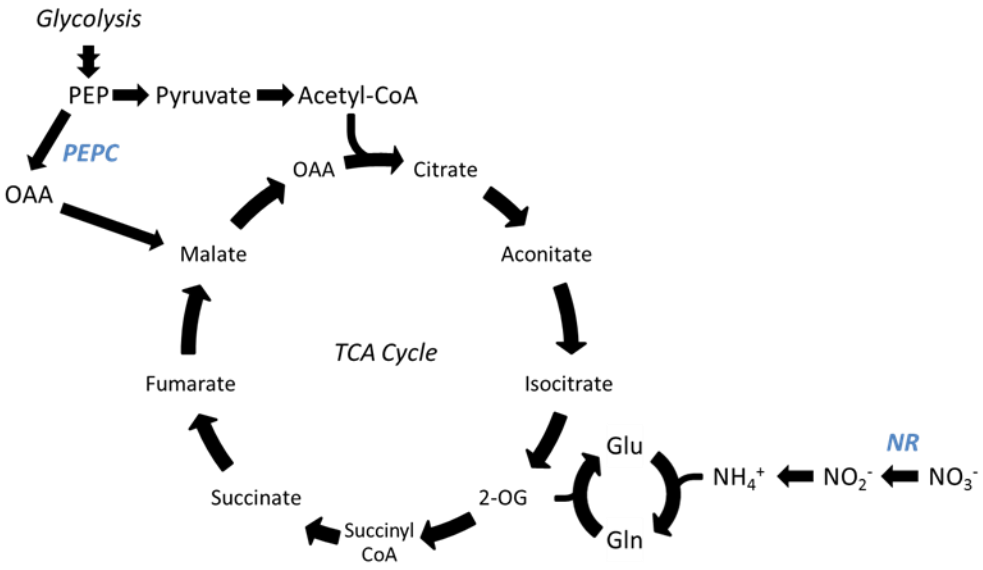

Figure 1.2 | Overview of the tricarboxylic acid (TCA) cycle and its interface with nitrogen metabolism.
Adapted from Plaxton and Podestá, 2006.

1.2 The sucrose-Tre6P nexus and its impact on sucrose homeostasis

Sucrose plays a central role in plant metabolism and growth and, accordingly, plants have evolved signalling mechanisms to allow for its precise regulation. One such mechanism relies heavily on the intermediate of trehalose metabolism, Tre6P. Trehalose is, similarly to sucrose, a non-reducing disaccharide, and it is composed by two glucosyl moieties. Trehalose can be found in all major organism groups, with the exception of vertebrates, and is known to play important roles as an osmoprotectant e.g. in *Escherichia coli* and in certain plants, such as the "resurrection plant" *Selaginella lepidophylla* (Drennan et al., 1993; Goddijn and van Dun K, 1999; Iturriaga et al., 2000; Figueroa and Lunn, 2016).

1.2.1 Tre6P-biosynthetic enzymes

In Arabidopsis, trehalose is synthetized in a two-step process, where UDPGlc and Glc6P are used by TREHALOSE 6-PHOSPHATE SYNTHASE 1 (TPS1) to produce Tre6P, which is further dephosphorylated by trehalose 6-phosphate phosphatases (TPPs), yielding trehalose (Avonce et al., 2006). The observation that constitutive overexpression of bacterial isoforms of TPS and TPP enzymes results in severe growth and developmental phenotypes in Arabidopsis contributed to the identification of the intermediate Tre6P as the molecule with the main signalling function of this pathway (Goddijn et al., 1997; Romero et al., 1997; Goddijn and van Dun K, 1999). Further investigation into trehalose metabolism in Arabidopsis led to the discovery of 11 *TPS* genes (*AtTPS1* - *AtTPS11*), and 10 *TPP* genes (*AtTPPA* - *AtTPPJ*) (Leyman et al., 2001; Avonce et al., 2006; Lunn, 2007). Of the 11 TPS proteins, only 3 (AtTPS1, AtTPS2 and AtTPS4) retain their catalytic potential (Class I TPSs), with AtTPS1 playing the most significant physiological role (Delorge et al., 2015). This conclusion was based on the fact that *tps1* null mutants are embryo lethal (Eastmond et al., 2002) and, when rescued during embryo development,

display highly compromised vegetative growth and are unable to flower (Dijken et al., 2004; Gómez et al., 2010).

Surprisingly, and even though Class II TPS proteins have been shown to lack Tre6P-synthetising activities (Ramon et al., 2009), genetic disruption of Class II TPSs results in metabolic alterations. Overexpression of the cotton *TPS11* orthologue (*GhTPS11*) in Arabidopsis led to enhanced levels of Tre6P in seeds, despite the fact that this gene presumably encodes a catalytically inactive TPS protein (Wang et al., 2016). Knocking out *TPS5* in Arabidopsis causes reduced accumulation of several soluble sugars, such as trehalose, Glc and Fru, without affecting sucrose levels (Tian et al., 2019), whereas *PvTPS9* knockout lines in *Phaseolus vulgaris* have lower trehalose content (Barraza et al., 2016). However, the mechanisms by which these non-catalytic TPS proteins affect metabolism remain unknown. Besides effects on metabolism, TPS proteins play a role in stress responses, with the overexpression of several of these genes leading to increased tolerance to abiotic stress conditions in rice (Li et al., 2011). In addition, TPS5 was described as a negative regulator of abscisic acid (ABA) signalling in Arabidopsis (Tian et al., 2019).

1.2.2 Tre6P-degrading enzymes

Even though Tre6P synthesis in Arabidopsis appears concentrated mostly on a single protein (TPS1), the same does not hold true for Tre6P catabolism. Arabidopsis possesses 10 *TPP* genes encoding catalytically active enzymes, with different specificities with regard to tissue and timing of gene expression (Vandesteene et al., 2012). These specificities raise the hypothesis that different TPP proteins may serve different functions. In *Arabidopsis*, *AtTPPA* and *AtTPPG* transcripts have been identified in the protoderm, and may play a role in cell differentiation (Houtte et al., 2013). *AtTPPB* accumulates in younger leaves, where it influences cell number (Houtte et al., 2013). *AtTPPD* is expressed in the root cap, and it has been previously linked with salt stress tolerance (Krasensky et al., 2014).

AtTPPF is induced under drought stress and may be involved in the regulation of stomatal aperture in response to ABA (Vandesteene et al., 2012; Lin et al., 2019). Finally, *AtTPPI* has been implicated in the control of stomatal aperture in response to drought stress (Lin et al., 2020), but also in the control of flowering time (Kataya et al., 2020). Besides being implicated in different processes, and being expressed in different tissues, TPP isoforms have also been found at different subcellular compartments. AtTPPA, AtTPPB, AtTPPC, AtTPPF, and AtTPPH are distributed between the cytosol and nucleus, AtTPPD and AtTPPE accumulate in the chloroplast, and AtTPPG, AtTPPI, and AtTPPJ showed an exclusively nuclear localization (with AtTPPI and AtTPPJ also labelling the nucleolus) (Krasensky et al., 2014). The whole picture might be more complex, however, with the recent report that AtTPPI can also accumulate in other organelles besides the nucleus, such as plastids and peroxisomes (Kataya et al., 2020).

1.2.3 The relationship between sucrose and Tre6P

Experiments with Arabidopsis seedlings grown in liquid culture showed that carbon starved plants had very low levels of Tre6P, which spiked quickly upon sucrose resupplementation (Lunn et al., 2006). These initial observations led to the discovery of a strong positive correlation between Tre6P and sucrose levels, that has been further confirmed in different tissues, developmental stages (Wingler et al., 2012; Carillo et al., 2013; Martins et al., 2013; Nunes, O'Hara, et al., 2013; Wahl et al., 2013; Sulpice et al., 2014; Yadav et al., 2014) and species, including *Solanum tuberosum* (Debast et al., 2011), *Triticum aestivum* (Martínez-Barajas et al., 2011), *Zea mays* (Henry et al., 2014), and *Cucumis sativa* (Zhang et al., 2015). Although the mechanisms by which a rise in sucrose results in increased Tre6P levels have not yet been elucidated, the process is known to be independent of *de novo* transcription but to require protein synthesis (Yadav et al., 2014). However, no changes in TPS1 levels were detected in response to sucrose feeding in this study, indicating that the *de novo* synthesised factor is a different protein. Further observation that constitutive overexpression of the *E. coli* TPS and TPP enzymes

(OtsA and OtsB, respectively), not only did not break the link between these two metabolites, but actually resulted in altered sucrose levels, led to the proposal of the sucrose-Tre6P nexus model (Yadav et al., 2014). In this model, Tre6P acts not only as a signal of sucrose availability, but also feeds back into its synthesis and consumption, allowing the plant to maintain sucrose at an optimal level (Yadav et al., 2014; Figueroa and Lunn, 2016). Research developed by Figueroa and colleagues using an inducible overexpressor of the OtsA transgene (iOtsA), showed how transient increases in Tre6P levels in the light period result in a shift in the flux of carbon away from glycolysis, and into the synthesis of organic acids. This phenomenon was traced back to the post-translational activation of PEPC and Nitrate Reductase (NR), allowing for an increased rate of organic and amino-acid synthesis. In addition to decreased sucrose synthesis through these mechanisms, enhanced hydrolysis is also likely to occur, altogether helping to explain the reduced carbon content in the glycolytic branch of metabolism (Figueroa et al., 2016).

Tre6P impacts also starch metabolism by promoting starch accumulation during the day, and by delaying its mobilisation during the night. It is important to note, however, that the impact of Tre6P on starch accumulation is subtle, and the underlying molecular events have not yet been resolved, with conflicting reports pointing to redox activation of AGPase as a potential mechanism (Kolbe et al., 2005; Lunn et al., 2006; Martins et al., 2013). In contrast, Tre6P has a significant impact on starch mobilisation that has been traced down to the early steps of cyclical phosphorylation and dephosphorylation of the starch granule. However, Tre6P does not affect the catalytic activities of the relevant kinase and phosphatase proteins *in vitro*. Manipulation of Tre6P levels *via* overexpression of the bacterial TPS enzyme OtsA also had no impact in the abundance of these kinases and phosphatases. For these reasons, the impact of Tre6P on starch mobilisation is thought to be indirect (Martins et al., 2013). Irrespective of the mechanism, Tre6P inhibition serves to slow down starch degradation when sucrose levels are high (Dos Anjos et al., 2018).

The molecular mechanisms behind how Tre6P affects carbon metabolism were identified in Arabidopsis rosette leaves, which act primarily as carbon sources.

Besides contributing to sucrose homeostasis, Tre6P also helps to coordinate carbon and nitrogen metabolism. By increasing the synthesis of amino-acids at the source, Tre6P allows for their transport towards metabolic sinks, fuelling the actively growing tissues with both carbon- and nitrogen-rich compounds (Figueroa et al., 2016; Figueroa and Lunn, 2016) (Figure 1.3).

1.2.4 Tre6P and development

Although the correlation between sucrose and Tre6P is very strong and resistant to outside manipulation, their relationship varies across tissues and conditions, likely as a way to accommodate a wide range of metabolic needs. High Tre6P:sucrose ratios are traditionally associated with actively growing and metabolically active tissues characteristic of sinks (Lunn et al., 2014). As an example, the work of Wahl and colleagues in Arabidopsis shoot apices showed that Tre6P:sucrose ratios in this particular sink were 1.5-fold higher than in rosettes grown under the same short-day photoperiod, but the differences increased up to 8-fold when plants were shifted to a long-day photoperiod for 7 days to induce flowering (Wahl et al., 2013; Lunn et al., 2014; Yadav et al., 2014). More recently, Fichtner and colleagues showed a correlation between the Tre6P:sucrose ratio in vascular tissues and the number of primary rosette branches, elegantly demonstrating how Tre6P can drive plant development locally, and supporting the hypothesis that the interplay between sucrose and Tre6P is crucial for the development of metabolic sinks (Fichtner, Barbier, et al., 2020).

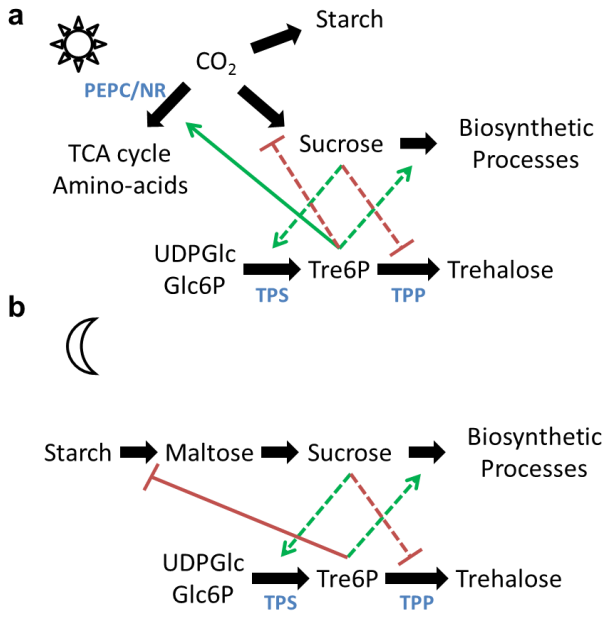

Figure 1.3 | Graphical depiction of the sucrose-Tre6P nexus in source leaves.
During the light period, Tre6P is responsible for the partitioning of photoassimilates between sucrose and the synthesis of organic acids and amino-acids. This control over partitioning relies at least partly on the post-translational modification of PEPC and NR activities **(a)**. During the dark period, Tre6P inhibits transitory starch mobilisation, rationing the supply of carbon substrates for sucrose synthesis. To a large extent, Tre6P-mediated regulation of carbon metabolism is similar between source leaves in the dark and sink tissues. The main difference is that source leaves rely mostly on the mobilisation of their transitory starch during the night period, whereas sink tissues rely also on the carbon resources available *via* the phloem **(b)**. Green arrows indicate induction, and red lines indicate inhibition. Solid lines show demonstrated interactions, and dashed lines represent hypothetical interactions. Adapted from Figueroa and Lunn, 2016.

An increasing number of studies further highlight the tight yet largely dynamic relationship between Tre6P and sucrose. For example, a time-course experiment following the developing wheat grain shows how endogenous Tre6P levels vary over 178-fold along day 1 and day 45 after anthesis. The Tre6P levels shown in this study were also much higher than those previously reported for Arabidopsis. During this entire developmental process, the strong positive correlation between Tre6P and sucrose was always maintained (Martínez-Barajas et al., 2011). Investigation into the different sugar dynamics in response to various stress treatments provided more insight into the nature of the sucrose-Tre6P nexus. In sink-limited Arabidopsis

plants, Tre6P levels were still found to correlate tightly with sucrose (Nunes, O'Hara, et al., 2013), but this relationship broke down in maize plants under conditions of starvation, caused either by extended darkness of the whole plant or by excision of the developing kernel (Henry et al., 2014; Czedik-Eysenberg et al., 2016; Bledsoe et al., 2017).

Even though the relationship between sucrose and Tre6P (rather than the absolute value of either metabolite) is widely accepted to play an important signalling role, the precise molecular mechanisms by which these two sugars interconnect and regulate metabolism remain elusive (Yadav et al., 2014; Fichtner, Barbier, et al., 2020). A recent molecular dissection of the AtTPS1 protein has increased our understanding on how this protein impacts the sucrose-Tre6P nexus. Through a mutagenesis approach, the C-terminal end of the enzyme was shown to be important for sucrose homeostasis, with its removal resulting in an uncontrolled rise in sucrose levels that appear unresponsive to the rising Tre6P levels. This disconnection between the two sugars resulted in sucrose concentrations 30 times higher than those naturally found in wild-type plants, and a Tre6P:sucrose ratio over 10-fold lower than normal. Altogether, this work underscored the prominent role of TPS1 in linking sucrose and Tre6P (Fichtner, Olas, et al., 2020).

1.2.5 Tre6P impacts on gene expression

Besides affecting metabolism and development, Tre6P impacts also gene expression. For example, *tps1* embryos have reduced expression of sucrose and starch degradation genes, and enhanced expression of genes associated with lipid mobilisation (Gómez et al., 2006). Embryo rescue of the *tps1* mutant by expression of TPS1 under the control of the *ABI3* promoter allowed these plants to grow past the embryonic stage, but these seedlings still showed altered expression of carbohydrate-associated genes (Gómez et al., 2010). More recently, a study in OtsB-expressing (low Tre6P) pea embryos also showed an overall transcriptional repression of several key enzymes for starch synthesis, such as *PGM2, AGPL* and

AGPS, as well as the auxin biosynthetic gene *TAR2*, further confirming that normal Tre6P metabolism is important for the regulation of sugar-related transcripts (Meitzel et al., 2020). However, it is difficult to interpret the exact role of Tre6P on regulating gene expression in these studies, given the vast changes in the levels of soluble sugars and starch reported in both studies and the strong growth defects of the *ABI3:TPS1* complemented *tps1* mutant.

In some of these studies, a link was found between Tre6P and the SUCROSE NON-FERMENTING RELATED KINASE 1 (SnRK1) kinase, with several of the genes under SnRK1 control being influenced by Tre6P levels in an opposite manner (Nunes, O'Hara, et al., 2013). In *in vitro* assays, Tre6P inhibits SnRK1 activity in desalted extracts of Arabidopsis seedlings, but this inhibition is not direct and requires the presence of an unknown proteinaceous factor (Zhang et al., 2009). The relationship between Tre6P and SnRK1 was explored in some of the studies that explored the dynamics of Tre6P in developing sink tissues and will be described in greater detail in section 1.3.6.

1.3 Carbon sensing and signalling via SnRK1 kinases

SnRK1 is the plant orthologue of the mammalian AMP-ACTIVATED KINASE (AMPK), and the yeast SUCROSE NON-FERMENTING 1 (SNF1). SnRK1/AMPK/SNF1 are heterotrimeric Ser/Thr protein kinase complexes that belong to the calcium-dependent protein kinase (CDPK)-SnRK superfamily. They are composed by a catalytic (kinase) α subunit and regulatory β- and γ- subunits. These kinases are known master regulators of metabolism and energy homeostasis, acting as "fuel gauges" in most eukaryotic organisms (Ghillebert et al., 2011). In Arabidopsis, three genes encode for the α subunit (*SnRK1α1*/*α2*/*α3*), three for the β subunit (*SnRK1β1*/*β2*/*β3*), and one for a *SnRK1βγ* hybrid subunit (Kleinow et al., 2000; Lumbreras et al., 2001; Ramon et al., 2013; Emanuelle et al., 2015).

1.3.1 SnRK1 subunits and their domain compositions

The catalytic α-subunits harbour an N-terminal kinase domain, and a C-terminal regulatory domain that is important for complex formation *via* interaction with the β and γ subunits (Broeckx et al., 2016). The N-terminal catalytic domain is highly conserved in all eukaryotes, including the T-loop region, whose phosphorylation at a conserved threonine (T175 for AtSnRK1α1, and T176 for AtSnRK1α2) is essential for kinase activity (Estruch et al., 1992; Hawley et al., 1996; Baena-González et al., 2007). The regulatory domain, on the other hand, is substantially less conserved. It comprises an ubiquitin-associated (UBA) domain that may be involved in the interaction with ubiquitinated proteins (Farrás et al., 2001), an auto-inhibitory domain (AID) (Jiang and Carlson, 1996; Crute et al., 1998; Leech et al., 2003; Pang et al., 2007; Chen et al., 2009), and a far C-terminal domain (αCTD) that is involved in the interaction with the regulatory β and γ subunits and upstream phosphatases (Kleinow et al., 2000; Rodrigues et al., 2013). Both *SnRK1α1* and *SnRK1α2* are expressed ubiquitously (Schmid et al., 2005), and most of the enzymatic activity detected *in vivo* can be traced back to the SnRK1α1 subunit (Jossier et al., 2009). On the other hand, *SnRK1α3* appears only weakly expressed in the pollen grain and seed tissues (Schmid et al., 2005).

The regulatory β-subunits perform a scaffolding function, and are thought to determine the subcellular localisation of the complex, substrate recognition, and kinase activity (Hedbacker et al., 2004; Polge and Thomas, 2007; Ghillebert et al., 2011; Hardie et al., 2012; Emanuelle et al., 2015). SnRK1β1 and SnRK1β2 have a conserved N-terminal domain that is myristoylated *in planta*, leading to the association of the protein with membranes (Pierre et al., 2007; Wang et al., 2020). They also harbour a carbohydrate binding module (CBM) and a β C-terminal domain (βCTD) that is important for binding the α- and the βγ subunits (Broeckx et al., 2016). Plants also have a highly divergent SnRK1β3 subunit that is N-terminally truncated and therefore does not possess the CBM domain typical of AMPK β subunits, nor can it be myristoylated. However, despite lacking the so called kinase-interacting sequence [KIS; (Schmidt, 2000; Hedbacker, 2008)] the SnRK1β3 protein

is still capable of interacting with both the yeast and plant α subunits, (Gissot et al., 2004; Emanuelle et al., 2015), and accordingly, it is able to complement the yeast *gal83 sip1 sip2* mutant, similarly to the SnRK1β1 and SnRK1β2 (Gissot et al., 2004; Polge et al., 2008).

The final subunit (SnRK1βγ) from Arabidopsis has the characteristics expected from a typical γ subunit, such as the four cystathione β-synthase (CBS) domains organized in tandem pairs (also known as the Bateman domains), and the β-interacting sequence domains, but also contains some characteristics of a β subunit, such as the CBM (Lumbreras et al., 2001; Gissot et al., 2006; Broeckx et al., 2016). This hybrid βγ subunit has been shown to complement the yeast *snf4* mutant, interact with the β subunits, and integrate the heterotrimeric complex (Ramon et al., 2013; Emanuelle et al., 2015) (Figure 1.4). The lethality of the Arabidopsis *snrk1βγ* mutant, previously attributed to a defect in pollen hydration and germination, also implies that this subunit plays unique and essential functions (Gao et al., 2016).

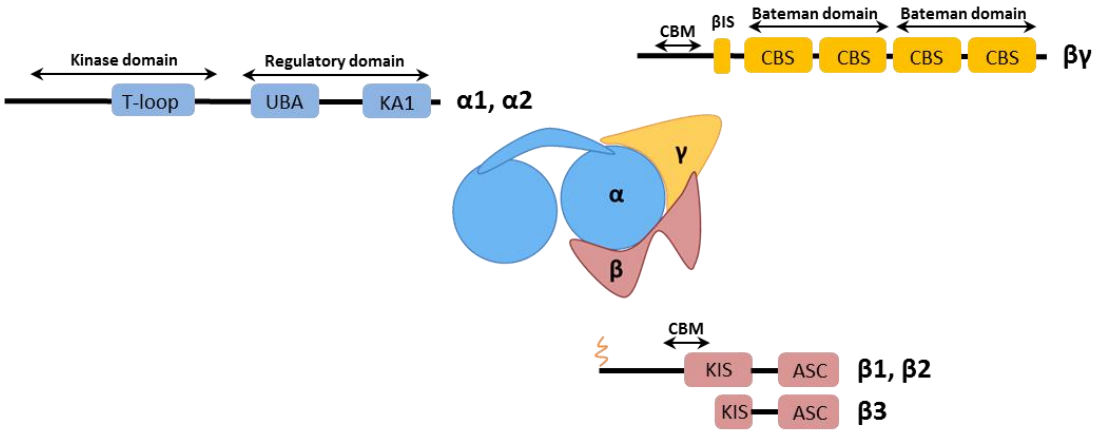

Figure 1.4 | SnRK1 is a heterotrimeric kinase complex.
The SnRK1α subunits (blue) are composed of a catalytic domain, where the T-loop is localized, and a regulatory domain, harbouring the Ubiquitin-Associated (UBA) and Kinase-Associated (KA1) domains. The KA1 domain is important for the interaction between SnRK1α with the regulatory SnRK1β and SnRK1γ subunits and with other regulatory proteins, such as PP2C. The SnRK1βγ subunit (orange) has two Bateman domains, each of them composed by two cystathionine-β-synthase (CBS) domains. The N-terminal region harbours a carbohydrate binding module (CBM), separated from the first Bateman domain by the β-Interacting Sequence (βIS). The SnRK1β subunits (red) harbour a Kinase Interacting Sequence (KIS) and the Association to the Snf1 Complex (ASC) domain. The CBM typical of the β subunits comprises part of the KIS domain and is absent from the SnRK1β3 subunit due to an N-terminal truncation. As a consequence of the truncation, also the G2 residue required for N-myristoylation is lost. Adapted from Crozet *et al.*, 2014.

1.3.2 SnRK1 is expressed over a wide range of tissues and developmental stages

The existence of different genes coding for the same subunit implies the formation of different SnRK1 αβγ complexes (Bouly et al., 1999; Gissot et al., 2004, 2006; Ramon et al., 2013, 2019; Emanuelle et al., 2015). This has the potential for creating a very complex picture, especially if homodimerization between subunits, or alternative splicing events are also considered as potential sources of SnRK1 diversity (Gissot et al., 2004; López-Paz et al., 2009; Steinberg and Kemp, 2009; Ghillebert et al., 2011).

Compatible with the fact that most of the enzymatic activity detected *in vivo* can be traced back to the α1 subunit, *SnRK1α1* can be found expressed throughout several developmental stages, from seedling to developing embryos. *SnRK1α1* expression can also be found in different tissues, with the highest levels of

expression found in leaf primordia, seedling root tips, and the vasculature. On the other hand, *SnRK1α2* expression is more restricted in both space and time, with the highest levels of expression being found at the hydathodes, and the base of newly developing leaves (Jossier et al., 2009; Williams et al., 2014; O'Brien et al., 2015). As for *SnRK1α3*, its expression was only weakly detected in pollen grains and seed tissues (Baena-González et al., 2007; Fragoso et al., 2009). The inability to obtain *snrk1α1/α2* double knock-out plants highlights the potentially redundant functions between these two subunits, as well as the more limited functionality of the SnRK1α3 subunit (Baena-González et al., 2007; Ramon et al., 2019).

Using tagged versions of the proteins, Bitrián and colleagues found SnRK1α1 and SnRK1βγ to be enriched in meristematic, elongation and differentiation zones of both primary and lateral roots, as well as in young leaf primordia (Bitrián et al., 2011). SnRK1β subunit expression was also documented *via* analysis of promoter activity, with some tissues, such as the root and mature rosette, showing expression of all three β subunits, whereas reproductive tissues, such as the developing pollen grain, the ovule and the seed being enriched for *SnRK1β3* (Polge et al., 2008). Besides tissue and developmental specificity, *SnRK1β1* expression is also strongly induced by darkness and repressed by sugar (Polge et al., 2008). This mechanism may help explain the progressively higher peaks in expression detected at dawn under progressively shorter photoperiods (Flis et al., 2016).

1.3.3 SnRK1 is regulated by post-translational modifications

There is currently a considerable gap in the literature regarding SnRK1 complex composition *in vivo*, with much of the current knowledge relying on *in vitro* studies. Much more attention has been given towards characterising SnRK1 post-translational modifications, and how they impact on and regulate kinase activity. Several of these post-translational modifications have been described for SnRK1, and they impact on the kinase activity through different mechanisms.

1.3.3.1 Phosphorylation

Similarly to AMPK and SNF1, SnRK1α activity requires phosphorylation of a highly conserved T-loop threonine residue (Sugden, Crawford, et al., 1999; Baena-González et al., 2007).

The SnRK1-activating kinases 1 and 2 (SnAK1 and SnAK2) were discovered due to their sequence similarity to the yeast SNF1 upstream kinases SAK1/PAK, ELM1 and TOS3 (Shen and Hanley-Bowdoin, 2006; Hey et al., 2007). SnAK1 and SnAK2 are also known as GRIK2 and GRIK1, respectively, as they were initially identified as Geminivirus Rep protein-Interacting Kinases (GRIKs) (Kong and Hanley-Bowdoin, 2002; Shen and Hanley-Bowdoin, 2006). In Arabidopsis, SnAKs interact with the SnRK1 catalytic subunits, phosphorylating the T-loop in a Ca^{2+}-independent manner (Shen et al., 2009) (Figure 1.5). This interaction is specific and was not observed with SnRK2 or SnRK3, belonging to the same kinase family as SnRK1. It is also possible that other phosphorylation events occur, with an impact on SnRK1 kinase activity. For example, rice OsCIPK15 interacts with SnRK1, impacting its activity in response to oxygen and sugar deficiency during flooding. However, a direct regulation of SnRK1 by CIPK15 remains to be demonstrated (Sugden, Crawford, et al., 1999; Heazlewood et al., 2008; Lee et al., 2009; Nakagami et al., 2010).

In all three systems, the AMPK/SNF1/SnRK1 upstream kinases appear to be constitutively active, with substrate availability being a major way to regulate T-loop phosphorylation and activity in AMPK (see section on adenylates below). Regulation at the substrate level is also determinant for AMPK/SNF1/SnRK1 dephosphorylation of the T-loop (Crozet et al., 2014). One particular type of protein phosphatases, the PP2C-type, has been shown to dephosphorylate these kinases in yeast, mammal and plant systems (Davies et al., 1995; Rodrigues et al., 2013; Ruiz et al., 2013), enabling their inactivation in energy-rich conditions. In plants, the same PP2C phosphatases (clade A) act as repressors of ABA signalling, *via* interaction with SnRK2 kinases and their dephosphorylation. Regulation by PP2Cs (and SnRK2s) allows therefore SnRK1 to respond not only to energy signals but also to be

activated in response to ABA (Figure 1.5) (Rodrigues et al., 2013; Belda-Palazón et al., 2020).

1.3.3.2 Ubiquitination and SUMOylation

Ubiquitination of SnRK1α1, α2 and βγ has been described in large-scale proteomic studies (Maor et al., 2007; Kim et al., 2013), and SnRK1α1 was shown to interact with both the SCF ubiquitin ligase complex and the 26S proteasome (Farrás et al., 2001). On the other hand, treatment of plants with the 26S proteasome inhibitor MG132 leads to enhanced SnRK1α accumulation (Ananieva et al., 2008; Carvalho et al., 2016; Crozet et al., 2016), suggesting that SnRK1 ubiquitination might mediate its proteasomal degradation.

SnRK1α1 was also shown to interact with the SCE1 E2 SUMO conjugating enzyme, and the ESD4 SUMO protease in a yeast 2-hybrid assay (Y2H) (Elrouby and Coupland, 2010) and to be SUMOylated *in planta* in a SIZ1 (an E3 SUMO ligase) dependent manner (Crozet et al., 2016). SUMOylation of SnRK1 was further shown to be necessary for its ubiquitination and subsequent degradation, altogether serving as a negative feedback mechanism to prevent SnRK1 overactivation (Crozet et al., 2016), as also described for yeast SNF1 (Figure 1.5) (Simpson-Lavy and Johnston, 2013). This view is further strengthened by the observation that inactive SnRK1α1 variants, such as the kinase dead SnRK1α1^{T175A}, have a longer half-life, when compared to wild-type SnRK1α1 (Baena-González et al., 2007; Crozet et al., 2014) but their degradation is triggered by fusion to a SUMO moiety, mimicking SUMOylation (Crozet et al., 2016).

1.3.3.3 Myristoylation

Myristoylation is known to play an important role in the regulation of the AMPK, SNF1 and SnRK1 complexes mostly by enabling the association of the kinase complex to membranes and thereby affecting its subcellular localisation (Hedbacker, 2008; Garcia and Shaw, 2017). In plants, disruption of the

myristoylation machinery in the *N*-MYRISTOYLTRANSFERASE 1 (NMT1) *nmt1-1* mutant led to deleterious effects that could be traced back to aberrant SnRK1 function (Pierre et al., 2007). GFP-tagged SnRK1β1 and SnRK1β2 accumulated at the plasma membrane, but a G2A mutation preventing *N*-myristoylation relocalised these subunits to the cytoplasm and nucleus. This modification thus seems to play a role in the association of these two subunits with membranes, leading to the sequestration of the SnRK1 complex outside of the nucleus and downregulating its impact on transcription (Figure 1.5) (Pierre et al., 2007; Ramon et al., 2019; Wang et al., 2020).

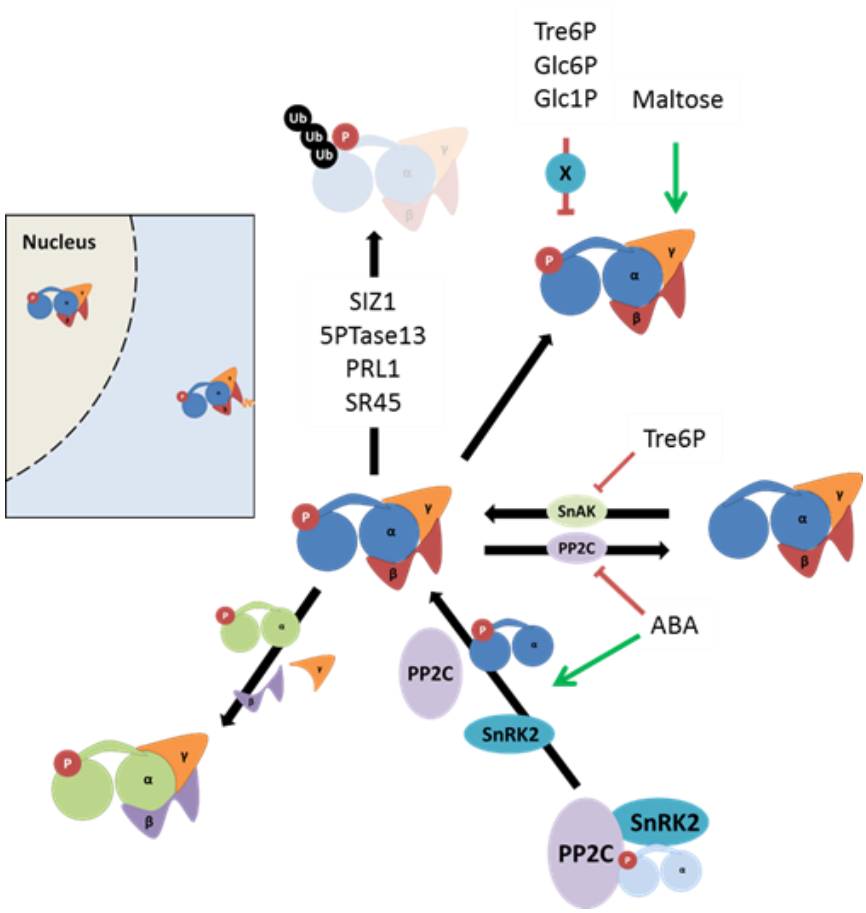

Figure 1.5 | Regulation of SnRK1 activity.
SnRK1 activity requires phosphorylation of the conserved threonine residue in the T-loop (Thr175 in SnRK1α1, Thr176 in SnRK1α2 in Arabidopsis) by the SnRK1-Activating Kinases (SnAKs). Tre6P interferes with the interaction between SnRK1α and SnAKs, preventing SnRK1α phosphorylation and thereby SnRK1 activity. Dephosphorylation may also occur *via* PP2C phosphatases, which are known repressors of ABA signalling. In the absence of ABA, SnRK2 kinases and PP2C phosphatases form repressor complexes that keep SnRK1 inactive, potentially contributing to its dephosphorylation. In the presence of ABA, the repressor complexes dissociate, releasing SnRK1α to exert its functions. SnRK1 is also ubiquitinated and degraded by the 26S proteasome to prevent over-activation of the SnRK1 pathway. Several factors have been implicated in SnRK1 ubiquitination: the SUMO E3 ligase SIZ1, the DWD protein PRL1, the splicing factor SR45, and the myo-inositol polyphosphate 5-phosphatase 5PTase13. Sugar phosphates, such as Tre6P, Glc6P or Glc1P are also known to bind to and allosterically inhibit SnRK1 activity. Tre6P has been shown to be particularly effective at inhibiting SnRK1 activity. This inhibition by sugar phosphates is dependent on the presence of an unknown protein X that can be found in extracts of young, actively growing seedlings. Maltose promotes SnRK1 activity in a SnRK1β3-dependent manner. SnRK1β1 and β2 subunits are *N*-myristoylated, leading to the association of the complex with membranes and exclusion of the catalytic subunit from the nucleus. Transcriptional regulation by SnRK1 requires its presence in the nucleus. Finally, most SnRK1 subunits are encoded by more than one gene in Arabidopsis. This raises the possibility that multiple SnRK1αβγ complexes can form *in vivo*, potentially leading to different biological activities. Adapted from Baena-González and Lunn, 2020.

1.3.4 SnRK1-interacting proteins help define its molecular functions

Besides components involved in SnRK1 regulation *via* post-translational modifications, a series of other interacting partners have been found to impact SnRK1 kinase activity. PLEIOTROPIC REGULATORY LOCUS 1 (PRL1) was initially discovered in a screen searching for sugar hypersensitive mutants (Németh et al., 1998). This WD40-repeat protein is a subunit of the nuclear spliceosome-activating Nineteen Complex (NTC) (Koncz et al., 2012) and can bind to recombinant SnRK1α1 and α2 *in vitro*, inactivating their catalytic activity (Bhalerao et al., 1999). Extracts from *prl1* loss-of-function plants also show higher SnRK1 catalytic activity, demonstrating that this effect can be reproduced *in vivo* (Bhalerao et al., 1999). Most of the phenotypes associated to this mutant, such as growth reduction, anthocyanin accumulation, and ABA, cytokinin and sugar hypersensitivities could be traced back to its elevated levels of SnRK1α1. The exact mechanism of inhibition is yet to be described, but at least part of the effect observed *in vivo* could be attributed to the absence of the PRL1-CUL4-DDB1 E3 ubiquitin ligase complex, resulting in a slower degradation rate of SnRK1α1 (Figure 1.5) (Lee et al., 2008).

SnRK1-interacting negative regulators (SKINs) were originally identified in rice, where they were found to be induced by abiotic stress, and where they bind and repress SnRK1(A), preventing its nuclear translocation. SKIN proteins possess a conserved GKSKSF motif required for their repressive effects, as well as a nuclear localisation signal (Lin et al., 2014). Putative orthologues of these SKIN proteins have been identified in Y2H experiments with Arabidopsis SnRK1α1 and SnRK1α2, although it remains to be demonstrated if these interactors can regulate AtSnRK1 activity *in planta* (Nietzsche et al., 2016).

The inositol polyphosphate 5-phosphatase 5PTase13 has also been identified as a positive regulator of SnRK1 activity in response to low nutrient levels. This enzyme is part of the myoinositol signalling pathway, and has been shown to interact with the SnRK1α1 subunit, preventing its proteasomal degradation (Figure 1.5) (Ananieva et al., 2008). This interaction is mediated by the WD40-repeat region at the N-terminal end of the 5PTase13 protein, similarly to what was described for

the PRL1 protein (Bhalerao et al., 1999; Ananieva et al., 2008). Surprisingly, 5PTase13 is also a negative regulator of SnRK1 activity in the absence of nutrients. Although the precise molecular mechanisms behind these conflicting results were not described, these suggest that 5PTase13 can modulate SnRK1 activity to adjust to the nutritional needs of the plant (Ananieva et al., 2008).

Proteins containing a domain of unknown function 581 (DUF581) are plant-specific and have been identified as major SnRK1 interactors. Arabidopsis has 19 genes encoding for different DUF581 proteins, and all have been shown to interact with both SnRK1α1 and SnRK1α2. DUF581 proteins are thought to serve as scaffolds, linking the catalytic subunits of the SnRK1 complex to a wide array of downstream targets (Nietzsche et al., 2014). The interactions between DUF581 proteins and SnRK1 targets appears to be quite specialized, allowing for a differential interactome to be formed, depending on the availability of different DUF581 members (Nietzsche et al., 2016). The SnRK1-DUF581 interactome potentially provides a molecular explanation for tissue- and stimulus-specific SnRK1 responses. It also serves as a molecular basis for linking SnRK1 to other signalling pathways such as those mediated by mitogen-activated protein kinase (MAPK), target of rapamycin (TOR), or DELLA-mediated gibberellin signalling (Broeckx et al., 2016; Nietzsche et al., 2016).

1.3.5 SnRK1 impacts on metabolism and plant development

SnRK1 is known to phosphorylate and inactivate several rate-limiting enzymes of primary metabolism, such as SPS, NR and 3-hydroxy-3-methyl-glutaryl-coenzyme A reductase (HMGR) (Figure 1.6) (Sugden, Donaghy, et al., 1999). SnRK1-mediated phosphorylation of metabolic enzymes shares a common mechanism of 14-3-3 protein recruitment and binding to the target enzyme (Moorhead et al., 1996; Ikeda et al., 2000; Bustos and Iglesias, 2003; Kulma et al., 2004).

For other enzyme targets, such as FRUCTOSE-6-PHOSPHATE 2-KINASE/FRUCTOSE-2,6-BISPHOSPHATASE (F2KP), the effects of SnRK1-mediated phosphorylation and 14-3-3 binding remain elusive (Figure 1.6). Although unclear, SnRK1-mediated phosphorylation of F2KP is hypothesised to have an impact in the levels of Fructose-2,6-bisphosphate (Fru-2,6bP) (Kulma et al., 2004). Fru-2,6bP is known to inhibit FRUCTOSE-1,6-BISPHOSPHATASE (FBPase), the enzyme responsible for catalysing the first committed step in the pathway of sucrose synthesis, effectively allowing Fru-2,6bP to coordinate sucrose synthesis and carbon assimilation rates (Stitt, 1987). If the hypothesis of SnRK1 affecting Fru-2,6bP levels holds true, that would implicate SnRK1 in the control of the photoassimilate partitioning between sucrose and starch, as well as in the regulation of glycolysis in non-photosynthetic cells.

Compatible with the former hypothesis, manipulation of SnRK1 has been shown to impact starch levels in a wide range of species and tissues. Disruption of SnRK1 signalling, either by depletion of the catalytic subunit, in barley (Zhang et al., 2001), or by depletion of the SnRK1βγ in Arabidopsis (Gao et al., 2016) led to pollen abortion and defects in starch accumulation. In the moss *Physcomitrella patens*, full SnRK1 knock-out (*snf1a/snf1*) resulted in defective starch accumulation, with plants requiring constant illumination or exogenous sugar supply to survive (Thelander et al., 2004). However, the starch phenotypes reported for SnRK1 mutants are in some cases conflicting, with overexpression of the SnRK1α1 subunit in Arabidopsis leading also to impaired starch accumulation (Jossier et al., 2009). An excess starch phenotype was in turn reported for plants whose *SnRK1α1* gene was transiently silenced (Baena-González et al., 2007), this last observation in clear contrast to what was described in *P. patens* (Thelander et al., 2004). This variable response may in part reflect the complexity of regulation of allocation between sucrose and starch, with Fru-2,6bP being just one component of a complex regulatory network (Stitt et al., 2010). It is also often challenging to distinguish if a change in starch levels reflects direct regulation of the starch synthesis or degradation pathways or is an indirect effect due to changed growth.

Enzymes of glycolysis are also under SnRK1 control. Non-phosphorylating glyceraldehyde-3-phosphate dehydrogenase (np-Ga3PDHase), which is involved in one of the ATP-independent bypass reactions of plant glycolysis, is phosphorylated and inactivated by SnRK1 (Piattoni et al., 2011). Additionally, SnRK1-antisense potato lines were unable to regulate cytosolic pyruvate kinase (PKc) activity throughout the day-night cycle, indicating an overall defect in controlling glycolysis (Figure 1.6) (Beczner et al., 2010). Furthermore, Fru-2,6bP (which may be downstream of SnRK1, see above) activates pyrophosphate:fructose 6-phosphate phosphotransferase (PFP). This enzyme is a unique feature of plant glycolysis, and catalyses a PPi-dependent bypass to ATP-phosphofructokinase. PFP is implicated in allowing increased flexibility and flux in plant glycolysis, especially in conditions where Fru-2,6bP rises, like metabolically active and growing tissues (Stitt, 1990; Stitt and Sonnewald, 1995).

Besides targeting metabolic enzymes directly, SnRK1 plays important functions in transcriptional regulation in response to energy depletion. By directly phosphorylating S1- and C-class bZIP transcription factors (Ma et al., 2011; Mair et al., 2015; Pedrotti et al., 2018), SnRK1 induces differential expression of over 1000 genes related to anabolism and catabolism (Figure 1.6). This transcriptional rewiring implements an energy-saving programme by the coordinated transcriptional upregulation of catabolic (energy-producing) and downregulation of anabolic (energy-consuming) processes (Baena-González et al., 2007; Baena-González and Sheen, 2008). This effect on transcription may also provide a more indirect way of adjusting metabolism. In fact, SnRK1 was shown to induce the expression of α-amylase genes in cereal seeds, and the expression of SUSY and AGPase in potato tubers [reviewed in MacNeill et al., 2017].

The impact of SnRK1 on enzymes controlling starch, sucrose and glycolytic metabolism, and on several bZIP transcription factors with metabolism-related gene targets, highlights the potential impact of SnRK1 on carbon expenditure by regulating both sugar and lipid metabolism (McMichael et al., 1995; Kulma et al., 2004; Ma et al., 2011; Mair et al., 2015; Robertlee et al., 2017; Frank et al., 2018).

SnRK1 has also a profound impact on plant growth and development but it is not always clear whether this is a secondary effect of altered metabolism and energy homeostasis or a more direct regulation of developmental programs (see Jamsheer K et al., 2021 for a recent review on this topic). Full *snrk1* loss-of-function mutants have never been obtained in Arabidopsis, suggesting embryo lethality or fertility problems. Silencing SnRK1 only in the seed circumvented such problems, leading to an early germination phenotype (Radchuk et al., 2006) that is in agreement with the late germination described for SnRK1 gain-of-function mutants in Arabidopsis (Radchuk et al., 2006; Tsai and Gazzarrini, 2012). SnRK1 has also been implicated in sugar and ABA signalling during early seedling development, with SnRK1α1 overexpression leading to hypersensitivity to both signals and defective true leaf formation (Jossier et al., 2009; Li et al., 2009). Finally, SnRK1 affects also flowering time, with overexpression of SnRK1α1 leading to late flowering (Tsai and Gazzarrini, 2012; Williams et al., 2014).

A common feature of these developmental phenotypes is that low SnRK1 activity is generally associated with developmental progression, whereas high SnRK1 activity is associated with developmental arrest [reviewed in Baena-González and Lunn, 2020]. However, despite acting as a developmental break, SnRK1 is also necessary for growth, as exemplified by the above-mentioned double mutant lethality and by the full growth arrest caused by systemic SnRK1 silencing via virus-induced gene silencing (VIGS) (Baena-González et al., 2007). This may be caused by defective nutrient remobilization, as shown in germinating rice seedlings (Lee et al., 2009) and/or by more direct effects on growth regulatory processes.

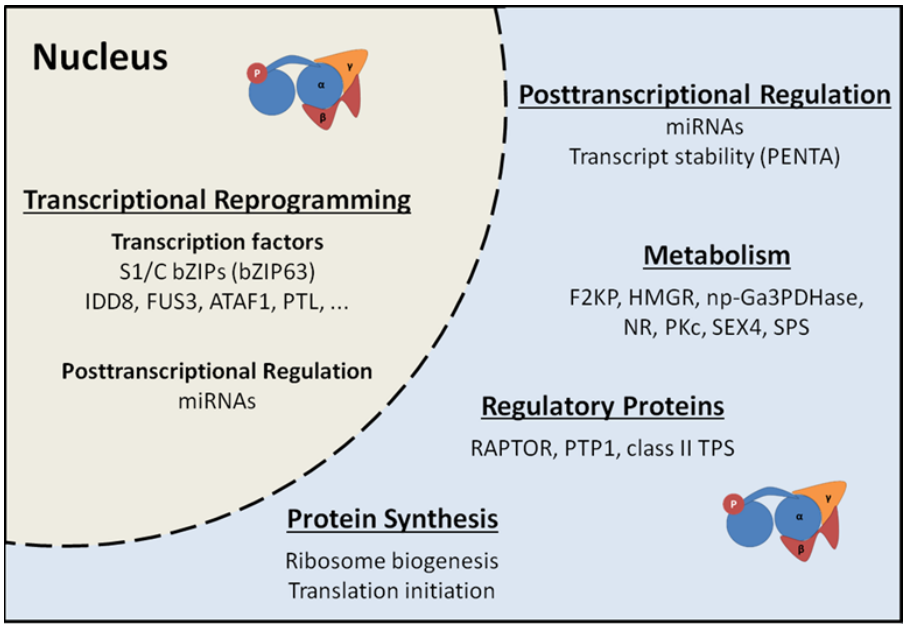

Figure 1.6 | SnRK1 affects different classes of downstream targets and biological processes. SnRK1 exerts its function by transcriptional reprogramming and direct phosphorylation of metabolic enzymes and regulatory proteins. In this way, SnRK1 can effectively implement an energy-saving programme, impacting on metabolism, growth, development and the stress response. Transcriptional reprogramming relies on the regulation of transcription factors, such as the S1/C-group bZIPs (e.g. bZIP63). Post-transcriptional regulation *via* either miRNAs or modulation of transcript stability has also been described. Metabolic reprogramming occurs *via* direct phosphorylation of key enzymes, such as NR and SPS. The effect of SnRK1 on metabolic enzymes seems to share the common mechanism of 14-3-3 protein recruitment and binding, followed by inactivation of the targeted enzyme. Other proteins targets, such as RAPTOR or TPS5 are also known targets of SnRK1. SnRK1 inhibits protein synthesis both at the level of ribosome biogenesis and translation initiation. These molecular targets have different subcellular localisations, and SnRK1 displays functions that are localisation-specific, with a particular emphasis on nuclear *versus* non-nuclear functions. See Broeckx *et al*., 2016 and Ramon *et al.*, 2019 for more details. Adapted from Broeckx *et al.*, 2016.

1.3.6 Metabolism impacts on SnRK1 function

As one of the most relevant sources of chemical energy in cells, ATP is hydrolysed to adenosine diphosphate (ADP) and Pi. The energy that is released by this hydrolysis is used by many enzymes to fuel their catalytic activities – this means that the ratio between ADP and ATP can effectively be used as a readout of the cellular energy status (Hardie et al., 2012; Broeckx et al., 2016). Further, ATP, ADP and AMP are equilibrated *via* a reversible reaction catalysed by adenylate kinase

(AK) (ATP + AMP = ADP + ADP). As ATP levels are usually higher and often much higher than ADP levels, AMP levels are usually very low and any decrease in the ATP/ADP ratio is accompanied by a much larger fold-increase of AMP than the changes of ATP or ADP. Hence, AMP is often used by cells as a readout of their energy status and regulates many key enzymes (Hardie, 2011).

In mammals, AMPK is known to be directly regulated by the adenylate charge, with adenosine monophosphate (AMP) and ADP competing with ATP for binding to the γ subunit. Increased concentrations of AMP and ADP trigger AMPK activation by inducing changes in the conformation of the kinase complex that promote its T-loop phosphorylation by upstream kinases and reduce its dephosphorylation by phosphatases. An allosteric AMP-mediated mechanism of activation that is independent of T-loop phosphorylation has also been described for mammalian AMPK (Gowans et al., 2013; Li et al., 2015). In yeast, only ADP, and not AMP, appears to affect SNF1 activity, and this is mostly by increasing the resistance of the kinase to T-loop dephosphorylation (Chandrashekarappa et al., 2011; Mayer et al., 2011). SnRK1 does not appear to be allosterically activated by AMP (Sugden, Crawford, et al., 1999; Emanuelle et al., 2015), although *in vitro* experiments have shown AMP to play a role in inhibiting T-loop dephosphorylation (Sugden, Crawford, et al., 1999; Maya-Bernal et al., 2017). Furthermore, adenosine kinase (ADK) was also identified as a direct interactor of SnRK1 *in vivo*. SnRK1 was shown to stabilize and enhance the *in vitro* activity of ADK, *via* an unknown mechanism independent of phosphorylation, leading to increases in the synthesis of 5'-AMP. These spikes in local AMP concentrations might help to stabilise SnRK1 in an active state, effectively operating as a positive-feedback loop over SnRK1 signalling. However, how such a loop could be regulated or terminated remains unresolved (Mohannath et al., 2014).

The insensitivity of SnRK1 to the perception and regulation by the adenylate charge poses a problem in regard to how metabolism feeds back into SnRK1 signalling. On the other hand, sugar phosphates, such as Glc1P and Glc6P have been shown to exert allosteric inhibition on SnRK1 (Toroser et al., 2000; Piattoni et al., 2011; Nunes, Primavesi, et al., 2013), providing an alternative mechanism for

metabolism and SnRK1 signalling to interface. Maltose, one of the main products of starch mobilisation, has also an impact on SnRK1 function, with SnRK1α1/β3/βγ, but not β1- or β2-containing recombinant heterotrimers, showing a higher than 30% increase in *in vitro* kinase activity after incubation with this sugar. A particularly relevant sugar phosphate is Tre6P, which inhibits SnRK1 activity at micromolar concentrations similar to those found *in vivo* in both Arabidopsis rosettes and sucrose-fed seedlings (Lunn et al., 2006; Zhang et al., 2009; Martins et al., 2013). The inhibitory function of these sugar phosphates is dependent on an unknown proteinaceous factor present in extracts of young seedlings but apparently not in mature leaves (Zhang et al., 2009; Martins et al., 2013), and has been described for a variety of different plant species and tissues [reviewed in Baena-González and Lunn, 2020]. The proteinaceous factor could correspond to SnAKs, given that Tre6P seems to act *via* these kinases by binding directly to SnRK1 and interfering with the SnRK-SnAK interaction (Zhai et al., 2018). However, SnAKs are not exclusive of young actively growing tissues and are also expressed in mature leaves. Thus, either further factors are also involved in the *in vitro* inhibition of SnRK1 by Tre6P in extracts from young tissues, or for some reason it is possible to detect action of Tre6P *via* SnAKs in extracts of seedlings, but not in extracts of mature leaves. In addition, in the background of the *snak1/snak2* double loss-of-function mutant, Tre6P had a stimulatory rather than inhibitory effect on SnRK1 activity, altogether suggesting that Tre6P regulates SnRK1 both *via* SnAK-dependent and SnAK-independent mechanisms (Zhai et al., 2018).

Gene expression has also been used as a read-out for the effects of Tre6P on SnRK1 activity *in vivo*, since high Tre6P levels highly correlate with reduced expression of SnRK1-induced genes and increased expression of SnRK1-repressed genes (Baena-González et al., 2007; Zhang et al., 2009). This anti-correlation between Tre6P levels and SnRK1 marker gene expression has been described for a wide range of plant species, tissues, organs and growth conditions (Debast et al., 2011; Martínez-Barajas et al., 2011; Nunes, O'Hara, et al., 2013; Henry et al., 2014, 2015; Griffiths et al., 2016; Bledsoe et al., 2017; Oszvald et al., 2018). Nevertheless, these results obtained *in vivo* do not always match results obtained *in vitro*, with

direct measurements of SnRK1 catalytic activity in plant extracts not always showing significant differences (Martínez-Barajas et al., 2011; Oszvald et al., 2018). Further, these studies are correlative, and often involve comparison of very different tissues (e.g. response of transcripts to transient overexpression of SnRK1 in protoplasts in comparison to analyses of Tre6P and transcripts in whole leaves).

1.4 Thesis aims and scope

This thesis describes novel regulatory aspects of the SnRK1 kinase and its impact on metabolic processes that contribute to sucrose homeostasis. One major aim of this work was to gain insight into how different components of the SnRK1 complex impact primary metabolism and gene expression under favourable growth conditions. A second aim was to explore the potential contribution of alternative splicing to the regulation of SnRK1.

The thesis is composed of 4 chapters (including this introductory Chapter 1) that are structured as follows:

Chapter 2. In this chapter we postulated a role for SnRK1 under the normal day-night cycle, based on the observations that complete loss-of-function of SnRK1 is lethal, and that plants manipulated for SnRK1 display a wide range of growth and developmental phenotypes. To investigate a function for SnRK1 in the absence of an overt stress treatment, we used gain- and loss-of-function mutants of the catalytic subunits to perform unbiased metabolomics time-course experiments and transcriptomic analyses. Based on the obtained data, we propose a model on how SnRK1 activity is dictated by daily fluctuations in Tre6P levels, contributing to sucrose homeostasis and gene expression during the regular day-night cycle.

Chapter 3. In this chapter we focused on the SnRK1β1 subunit for the following reasons: (1) it is predicted to suffer alternative splicing that potentially generates protein diversity; (2) it has been previously associated with primary metabolism, both *via* direct interaction with NR, and by its transcriptional response to

sugar and ammonium; (3) modelling efforts have also identified this subunit as an important link between SnRK1 and metabolism. Alternative splicing of *SnRK1β1* was confirmed *in vivo*, and the different splice variants were cloned and their subcellular localisation was analysed by confocal laser scanning microscopy. We also performed a preliminary metabolic characterization of both overexpressor and T-DNA insertional mutants for this gene. The results obtained are suggestive of a regulatory role for alternative splicing in generating subunit diversity, potentially expanding the molecular functions of SnRK1.

Chapter 4. In this chapter, I provide an overall discussion of all obtained results, and attempt to integrate the preliminary findings of Chapter 3 into the more refined model designed in Chapter 2. I discuss new hypotheses and experimental work that will drive forward research in this field and further increase our understanding of how SnRK1 regulates plant metabolism.

1.5 References

Ananieva, E.A., Gillaspy, G.E., Ely, A., Burnette, R.N., and Erickson, F. Les (2008). Interaction of the WD40 domain of a myoinositol polyphosphate 5-phosphatase with SnRK1 links inositol, sugar, and stress signaling. Plant Physiol. **148**: 1868–1882.

Dos Anjos, L., Pandey, P.K., Moraes, T.A., Feil, R., Lunn, J.E., and Stitt, M. (2018). Feedback regulation by trehalose 6-phosphate slows down starch mobilization below the rate that would exhaust starch reserves at dawn in Arabidopsis leaves. Plant Direct **2**: e00078.

Avonce, N., Mendoza-Vargas, A., Morett, E., and Iturriag, G. (2006). Insights on the evolution of trehalose biosynthesis. BMC Evol. Biol. **6**: 1–15.

Babb, V.M. and Haigler, C.H. (2001). Sucrose phosphate synthase activity rises in correlation with high-rate cellulose synthesis in three heterotrophic systems. Plant Physiol. **127**: 1234–1242.

Badenhuizen, N.P. (1963). Formation and distribution of amylose and amylopectin in the starch granule. Nature **197**: 464–467.

Baena-González, E. and Lunn, J.E. (2020). SnRK1 and trehalose 6-phosphate – two ancient pathways converge to regulate plant metabolism and growth. Curr. Opin. Plant Biol. **55**: 52–59.

Baena-González, E., Rolland, F., Thevelein, J.M., and Sheen, J. (2007). A central integrator of transcription networks in plant stress and energy signalling. Nature **448**: 938–942.

Baena-González, E. and Sheen, J. (2008). Convergent energy and stress signaling. Trends Plant Sci. **13**: 474–482.

Balmer, Y., Vensel, W.H., Tanaka, C.K., Hurkman, W.J., Gelhaye, E., Rouhier, N., Jacquot, J.P., Manieri, W., Schürmann, P., Droux, M., and Buchanan, B.B. (2004). Thioredoxin links redox to the regulation of fundamental processes of plant mitochondria. Proc. Natl. Acad. Sci. U. S. A. **101**: 2642–2647.

Barratt, D.H.P., Derbyshire, P., Findlay, K., Pike, M., Wellner, N., Lunn, J., Feil, R., Simpson, C., Maule, A.J., and Smith, A.M. (2009). Normal growth of Arabidopsis requires cytosolic invertase but not sucrose synthase. Proc. Natl. Acad. Sci. U. S. A. **106**: 13124–13129.

Barraza, A., Contreras-Cubas, C., Estrada-Navarrete, G., Reyes, J.L., Juárez-Verdayes, M.A., Avonce, N., Quinto, C., Díaz-Camino, C., and Sanchez, F. (2016). The Class II Trehalose 6-phosphate Synthase Gene PvTPS9 Modulates Trehalose Metabolism in Phaseolus vulgaris Nodules. Front. Plant Sci. **7**: 1–13.

Beczner, F., Dancs, G., Sós-Hegedus, A., Antal, F., and Bánfalvi, Z. (2010). Interaction between SNF1-related kinases and a cytosolic pyruvate kinase of potato. J. Plant Physiol. **167**: 1046–1051.

Behal, R.H. and Oliver, D.J. (1997). Biochemical and molecular characterization of fumarase from plants: Purification and characterization of the enzyme - Cloning, sequencing, and expression of the gene. Arch. Biochem. Biophys. **348**: 65–74.

Belda-Palazón, B., Adamo, M., Valerio, C., Ferreira, L.J., Confraria, A., Reis-Barata, D., Rodrigues, A., Meyer, C., Rodriguez, P.L., and Baena-González, E. (2020). A dual function of SnRK2 kinases in the regulation of SnRK1 and plant growth. Nat. Plants **6**.

Bhalerao, R.P., Salchert, K., Bakó, L., Ökrész, L., Szabados, L., Muranaka, T., Machida, Y., Schell, J., and Koncz, C. (1999). Regulatory interaction of PRL1 WD protein with Arabidopsis SNF1-like protein kinases. Proc. Natl. Acad. Sci. U. S. A. **96**: 5322–5327.

Bieniawska, Z., Paul Barratt, D.H., Garlick, A.P., Thole, V., Kruger, N.J., Martin, C., Zrenner, R., and Smith, A.M. (2007). Analysis of the sucrose synthase gene family in Arabidopsis. Plant J. **49**: 810–828.

Bitrián, M., Roodbarkelari, F., Horváth, M., and Koncz, C. (2011). BAC-recombineering for studying plant gene regulation: Developmental control and cellular localization of SnRK1 kinase subunits. Plant J. **65**: 829–842.

Black, C.C., Mustardy, L., Sung, S.S., Kormaník, P.P., Xu, D. -P, and Paz, N. (1987). Regulation and roles for alternative pathways of hexose metabolism in plants. Physiol. Plant. **69**: 387–394.

Bledsoe, S.W., Henry, C., Griffiths, C.A., Paul, M.J., Feil, R., Lunn, J.E., Stitt, M., and Lagrimini, L.M. (2017). The role of Tre6P and SnRK1 in maize early kernel development and events leading to stress-induced kernel abortion. BMC Plant Biol. **17**: 1–17.

Bouly, J.P., Gissot, L., Lessard, P., Kreis, M., and Thomas, M. (1999). Arabidopsis thaliana proteins related to the yeast SIP and SNF4 interact with AKINα1, an SNF1-like protein kinase. Plant J. **18**: 541–550.

Braun, D.M., Wang, L., and Ruan, Y.L. (2014). Understanding and manipulating sucrose phloem loading, unloading, metabolism, and signalling to enhance crop yield and food security. J. Exp. Bot. **65**: 1713–1735.

Broeckx, T., Hulsmans, S., and Rolland, F. (2016). The plant energy sensor: evolutionary conservation and divergence of SnRK1 structure, regulation, and function. J. Exp. Bot. **67**: 6215–6252.

Budde, R.J.A. and Randall, D.D. (1990). Pea leaf mitochondrial pyruvate dehydrogenase complex is inactivated in vivo in a light-dependent manner. Proc. Natl. Acad. Sci. U. S. A. **87**: 673–676.

Bunik, V.I. and Fernie, A.R. (2009). Metabolic control exerted by the 2-oxoglutarate dehydrogenase reaction: A cross-kingdom comparison of the crossroad between energy production and nitrogen assimilation. Biochem. J. **422**: 405–421.

Bustos, D.M. and Iglesias, A.A. (2003). Phosphate Dehydrogenase from Heterotrophic Cells of Wheat Interacts with 14-3-3 Proteins 1. Plant Physiol. **133**: 2081–2088.

Bykova, N. V., Egsgaard, H., and Møller, I.M. (2003). Identification of 14 new phosphoproteins involved in important plant mitochondrial processes. FEBS Lett. **540**: 141–146.

Carillo, P., Feil, R., Gibon, Y., Satoh-Nagasawa, N., Jackson, D., Bläsing, O.E., Stitt, M., and Lunn, J.E. (2013). A fluorometric assay for trehalose in the picomole range. Plant Methods **9**: 1–15.

Carvalho, R.F., Szakonyi, D., Simpson, C.G., Barbosa, I.C.R., Brown, J.W.S., Baena-González, E., and Duque, P. (2016). The arabidopsis SR45 splicing factor, a negative regulator of sugar signaling, modulates SNF1-related protein kinase 1 stability. Plant Cell **28**: 1910–1925.

Chandrashekarappa, D.G., McCartney, R.R., and Schmidt, M.C. (2011). Subunit and Domain Requirements for Adenylate-mediated Protection of Snf1 Kinase Activation Loop from Dephosphorylation*. J. Biol. Chem. **286**: 44532–44541.

Chatterton, N.J. and Silvius, J.E. (1979). Photosynthate Partitioning into Starch in Soybean Leaves. Plant Physiol. **64**: 749–753.

Chen, L., Jiao, Z.H., Zheng, L.S., Zhang, Y.Y., Xie, S.T., Wang, Z.X., and Wu, J.W. (2009). Structural insight into the autoinhibition mechanism of AMP-activated protein kinase. Nature **459**: 1146–1149.

La Cognata, U., Landschütze, V., Willmitzer, L., and Müller-Röber, B. (1996). Structure and expression of mitochondrial citrate synthases from higher plants. Plant Cell Physiol. **37**: 1022–1029.

Courtois-Verniquet, F. and Douce, R. (1993). Lack of aconitase in glyoxysomes and peroxisomes. Biochem. J. **294**: 103–107.

Crozet, P., Margalha, L., Butowt, R., Fernandes, N., Elias, C.A., Orosa, B., Tomanov, K., Teige, M., Bachmair, A., Sadanandom, A., and Baena-González, E. (2016). SUMOylation represses SnRK1 signaling in Arabidopsis. Plant J. **85**: 120–133.

Crozet, P., Margalha, L., Confraria, A., Rodrigues, A., Martinho, C., Adamo, M., Elias, C.A., and Baena-González, E. (2014). Mechanisms of regulation of SNF1/AMPK/SnRK1 protein kinases. Front. Plant Sci. **5**: 1–17.

Crute, B.E., Seefeld, K., Gamble, J., Kemp, B.E., and Witters, L.A. (1998). Functional domains of the α1 catalytic subunit of the AMP-activated protein kinase. J. Biol. Chem. **273**: 35347–35354.

Czedik-Eysenberg, A., Arrivault, S., Lohse, M.A., Feil, R., Krohn, N., Encke, B., Nunes-Nesi, A., Fernie, A.R., Lunn, J.E., Sulpice, R., and Stitt, M. (2016). The interplay between carbon availability and growth in different zones of the growing maize leaf. Plant Physiol. **172**: 943–967.

Davies, S.P., Helps, N.R., Cohen, P.T.W., and Hardie, D.G. (1995). 5′-AMP inhibits dephosphorylation, as well as promoting phosphorylation, of the AMP-activated protein kinase. Studies using bacterially expressed human protein phosphatase-2Cα and native bovine protein phosphatase-2Ac. FEBS Lett. **377**: 421–425.

Debast, S., Nunes-Nesi, A., Hajirezaei, M.R., Hofmann, J., Sonnewald, U., Fernie, A.R., and Börnke, F. (2011). Altering trehalose-6-phosphate content in transgenic potato tubers affects tuber growth and alters responsiveness to hormones during sprouting. Plant Physiol. **156**: 1754–1771.

Delorge, I., Figueroa, C.M., Feil, R., Lunn, J.E., and Van Dijck, P. (2015). Trehalose-6-phosphate synthase 1 is not the only active TPS in Arabidopsis thaliana. Biochem. J. **466**: 283–290.

Dijken, A.J.H. van, Schluepmann, H., and Smeekens, S.C.M. (2004). Arabidopsis Trehalose-6-Phosphate Synthase 1 Is Essential for Normal Vegetative Growth and Transition to Flowering. Plant Physiol. **135**: 969–977.

Drennan, P.M., Smith, M.T., Goldsworthy, D., and van Staden, J. (1993). The occurrence of trehalose in the leaves of the desiccation-tolerant angiosperm Myrothamnus flabellifolius welw. J. Plant Physiol. **142**: 493–496.

Duff, S.M.G., Moorhead, G.B.G., Lefebvre, D.D., and Plaxton, W.C. (1989). Phosphate Starvation Inducible `Bypasses' of Adenylate and Phosphate Dependent Glycolytic Enzymes in Brassica nigra Suspension Cells . Plant Physiol. **90**: 1275–1278.

Eastmond, P.J., Van Dijken, A.J.H., Spielman, M., Kerr, A., Tissier, A.F., Dickinson, H.G., Jones, J.D.G., Smeekens, S.C., and Graham, I.A. (2002). Trehalose-6-phosphate synthase 1, which catalyses the first step in trehalose synthesis, is essential for Arabidopsis embryo maturation. Plant J. **29**: 225–235.

Elrouby, N. and Coupland, G. (2010). Proteome-wide screens for small ubiquitin-like modifier (SUMO) substrates identify Arabidopsis proteins implicated in diverse biological processes. Proc. Natl. Acad. Sci. U. S. A. **107**: 17415–17420.

Emanuelle, S., Hossain, M.I., Moller, I.E., Pedersen, H.L., Van De Meene, A.M.L., Doblin, M.S., Koay, A., Oakhill, J.S., Scott, J.W., Willats, W.G.T., Kemp, B.E., Bacic, A., Gooley, P.R., and Stapleton, D.I. (2015). SnRK1 from Arabidopsis thaliana is an atypical AMPK. Plant J. **82**: 183–192.

Emes, M.J.J. and Tobin, A.K.K. (1993). Control of Metabolism and Development in Higher Plant Plastids. In International Review of Cytology (Academic Press), pp. 149–216.

Estruch, F., Treitel, M.A., Yang, X., and Carlson, M. (1992). N-terminal mutations modulate yeast SNF1 protein kinase function. Genetics **132**: 639–650.

Farrás, R., Ferrando, A., Jásik, J., Kleinow, T., Ökrész, L., Tiburcio, A., Salchert, K., Del Pozo, C., Schell, J., and Koncz, C. (2001). SKP1-SnRK protein kinase interactions mediate proteasomal binding of a plant SCF ubiquitin ligase. EMBO J. **20**: 2742–2756.

Fatland, B.L., Nikolau, B.J., and Wurtele, E.S. (2005). Reverse genetic characterization of cytosolic acetyl-CoA generation by ATP-citrate lyase in Arabidopsis. Plant Cell **17**: 182–203.

Ferjani, A., Segami, S., Asaoka, M., and Maeshima, M. (2014). Regulation of PPi Levels Through the Vacuolar Membrane H+-Pyrophosphatase. In, pp. 145–165.

Fernie, A.R., Bachem, C.W.B., Helariutta, Y., Neuhaus, H.E., Prat, S., Ruan, Y.L., Stitt, M., Sweetlove, L.J., Tegeder, M., Wahl, V., Sonnewald, S., and Sonnewald, U. (2020). Synchronization of developmental, molecular and metabolic aspects of source–sink interactions. Nat. Plants **6**: 55–66.

Fettke, J., Eckermann, N., Poeste, S., Pauly, M., and Steup, M. (2004). The glycan substrate of the cytosolic (Pho 2) phosphorylase isozyme from Pisum sativum L.: identification, linkage analysis and subcellular localization. Plant J. **39**: 933–946.

Fichtner, F., Barbier, F.F., Annunziata, M.G., Feil, R., Olas, J.J., Mueller-Roeber, B., Stitt, M., Beveridge, C.A., and Lunn, J.E. (2020). Regulation of shoot branching in Arabidopsis by trehalose 6-phosphate. New Phytol. **13**: nph.17006.

Fichtner, F., Olas, J.J., Feil, R., Watanabe, M., Krause, U., Hoefgen, R., Stitt, M., and Lunn, J.E. (2020). Functional features of TREHALOSE-6-PHOSPHATE SYNTHASE1, an essential enzyme in Arabidopsis. Plant Cell **32**: 1949–1972.

Figueroa, C.M., Feil, R., Ishihara, H., Watanabe, M., Kölling, K., Krause, U., Höhne, M., Encke, B., Plaxton, W.C., Zeeman, S.C., Li, Z., Schulze, W.X., Hoefgen, R., Stitt, M., and Lunn, J.E. (2016). Trehalose 6-phosphate coordinates organic and amino acid metabolism with carbon availability. Plant J. **85**: 410–423.

Figueroa, C.M. and Lunn, J.E. (2016). A Tale of Two Sugars : Trehalose 6-Phosphate and. Plant Physiol. **172**: 7–27.

Figueroa, P., León, G., Elorza, A., Holuigue, L., and Jordana, X. (2001). Three different genes encode the iron-sulphur subunit of succinate dehydrogenase in Arabidopsis thaliana. Plant Mol. Biol. **46**: 241–250.

Flis, A., Mengin, V., Ivakov, A.A., Mugford, S.T., Hubberten, H.-M., Encke, B., Krohn, N., Höhne, M., Feil, R., Hoefgen, R., Lunn, J.E., Millar, A.J., Smith, A.M., Sulpice, R., and Stitt, M. (2019). Multiple circadian clock outputs regulate diel turnover of carbon and nitrogen reserves. Plant. Cell Environ. **42**: 549–573.

Flis, A., Sulpice, R., Seaton, D.D., Ivakov, A.A., Liput, M., Abel, C., Millar, A.J., and Stitt, M. (2016). Photoperiod-dependent changes in the phase of core clock transcripts and global transcriptional outputs at dawn and dusk in Arabidopsis. Plant Cell Environ. **39**: 1955–1981.

Fondy, B.R. and Geiger, D.R. (1985). Diurnal Changes in Allocation of Newly Fixed Carbon in Exporting Sugar Beet Leaves. Plant Physiol. **78**: 753–757.

Fragoso, S., Espíndola, L., Páez-Valencia, J., Gamboa, A., Camacho, Y., Martínez-Barajas, E., and Coello, P. (2009). SnRK1 isoforms AKIN10 and AKIN11 are differentially regulated in Arabidopsis plants under phosphate starvation. Plant Physiol. **149**: 1906–1916.

Frank, A., Matiolli, C.C., Viana, A.J.C., Hearn, T.J., Kusakina, J., Belbin, F.E., Wells Newman, D.,

Yochikawa, A., Cano-Ramirez, D.L., Chembath, A., Cragg-Barber, K., Haydon, M.J., Hotta, C.T., Vincentz, M., Webb, A.A.R., and Dodd, A.N. (2018). Circadian Entrainment in Arabidopsis by the Sugar-Responsive Transcription Factor bZIP63. Curr. Biol. **28**: 2597-2606.e6.

Fu, H. and Park, W.D. (1995). Sink- and vascular-associated sucrose synthase functions are encoded by different gene classes in potato. Plant Cell **7**: 1369–1385.

Gálvez, S., Lancien, M., and Hodges, M. (1999). Are isocitrate dehydrogenases and 2-oxoglutarate involved in the regulation of glutamate synthesis? Trends Plant Sci. **4**: 484–490.

Gao, X.Q., Liu, C.Z., Li, D.D., Zhao, T.T., Li, F., Jia, X.N., Zhao, X.Y., and Zhang, X.S. (2016). The Arabidopsis KINβγ Subunit of the SnRK1 Complex Regulates Pollen Hydration on the Stigma by Mediating the Level of Reactive Oxygen Species in Pollen. PLoS Genet. **12**: 1–25.

Garcia, D. and Shaw, R.J. (2017). AMPK: Mechanisms of Cellular Energy Sensing and Restoration of Metabolic Balance. Mol. Cell **66**: 789–800.

Geigenberger, P. (2011). Regulation of starch biosynthesis in response to a fluctuating environment. Plant Physiol. **155**: 1566–1577.

Gerhardt, R., Stitt, M., and Heldt, H. (1987). Subcellular Metabolite Levels in Spinach Leaves: Regulation of Sucrose Synthesis during Diurnal Alterations in Photosynthetic Partitioning. Plant Physiol. **83**: 399–407.

Gerrits, N., Turk, S.C.H.J., Van Dun, K.P.M., Hulleman, S.H.D., Visser, R.G.F., Weisbeek, P.J., and Smeekens, S.C.M. (2001). Sucrose metabolism in plastids. Plant Physiol. **125**: 926–934.

Ghillebert, R., Swinnen, E., Wen, J., Vandesteene, L., Ramon, M., Norga, K., Rolland, F., and Winderickx, J. (2011). The AMPK/SNF1/SnRK1 fuel gauge and energy regulator: Structure, function and regulation. FEBS J. **278**: 3978–3990.

Gibon, Y., Blaesing, O.E., Hannemann, J., Carillo, P., Höhne, M., Hendriks, J.H.M., Palacios, N., Cross, J., Selbig, J., and Stitt, M. (2004). A robot-based platform to measure multiple enzyme activities in Arabidopsis using a set of cycling assays: Comparison of changes of enzyme activities and transcript levels during diurnal cycles and in prolonged darkness. Plant Cell **16**: 3304–3325.

Gibon, Y., Pyl, E.T., Sulpice, R., Lunn, J.E., HÖhne, M., GÜnther, M., and Stitt, M. (2009). Adjustment of growth, starch turnover, protein content and central metabolism to a decrease of the carbon supply when Arabidopsis is grown in very short photoperiods. Plant, Cell Environ. **32**: 859–874.

Giegé, P., Heazlewood, J.L., Roessner-Tunali, U., Harvey Millar, A., Fernie, A.R., Leaver, C.J., and Sweetlove, L.J. (2003). Enzymes of glycolysis are functionally associated with the mitochondrion in arabidopsis cells. Plant Cell **15**: 2140–2151.

Gietl, C. (1992). Malate dehydrogenase isoenzymes: Cellular locations and role in the flow of metabolites between the cytoplasm and cell organelles. Biochim. Biophys. Acta (BBA)/Protein Struct. Mol. **1100**: 217–234.

Gissot, L., Polge, C., Bouly, J.P., Lemaitre, T., Kreis, M., and Thomas, M. (2004). AKINβ3, a plant specific SnRK1 protein, is lacking domains present in yeast and mammals non-catalytic β-subunits. Plant Mol. Biol. **56**: 747–759.

Gissot, L., Polge, C., Jossier, M., Girin, T., Bouly, J.P., Kreis, M., and Thomas, M. (2006). AKINβγ contributes to SnRK1 heterotrimeric complexes and interacts with two proteins implicated in plant pathogen resistance through its KIS/GBD sequence. Plant Physiol. **142**: 931–944.

Givan, C. V. (1999). Evolving concepts in plant glycolysis: Two centuries of progress. Biol. Rev. **74**: 277–309.

Goddijn and van Dun K (1999). Trehalose metabolism in plants. Trends Plant Sci. **4**: 315–319.

Goddijn, O.J.M., Verwoerd, T.C., Voogd, E., Krutwagen, R.W.H.H., De Graaf, P.T.H.M., Poels, J., Van Dun, K., Ponstein, A.S., Damm, B., and Pen, J. (1997). Inhibition of trehalase activity enhances trehalose accumulation in transgenic plants. Plant Physiol. **113**: 181–190.

Gómez, L.D., Baud, S., Gilday, A., Li, Y., and Graham, I.A. (2006). Delayed embryo development in the ARABIDOPSIS TREHALOSE-6-PHOSPHATE SYNTHASE 1 mutant is associated with altered cell wall structure, decreased cell division and starch accumulation. Plant J. **46**: 69–84.

Gómez, L.D., Gilday, A., Feil, R., Lunn, J.E., and Graham, I.A. (2010). AtTPS1-mediated trehalose 6-phosphate synthesis is essential for embryogenic and vegetative growth and responsiveness to ABA in germinating seeds and stomatal guard cells. Plant J. **64**: 1–13.

Gowans, G.J., Hawley, S.A., Ross, F.A., and Hardie, D.G. (2013). AMP is a true physiological regulator of amp-activated protein kinase by both allosteric activation and enhancing net phosphorylation. Cell Metab. **18**: 556–566.

Graf, A., Schlereth, A., Stitt, M., and Smith, A.M. (2010). Circadian control of carbohydrate availability for growth in Arabidopsis plants at night. Proc. Natl. Acad. Sci. U. S. A. **107**: 9458–9463.

Grennan, A.K. and Gragg, J. (2009). How sweet it is: Identification of vacuolar sucrose transporters. Plant Physiol. **150**: 1109–1110.

Griffiths, C.A., Sagar, R., Geng, Y., Primavesi, L.F., Patel, M.K., Passarelli, M.K., Gilmore, I.S., Steven, R.T., Bunch, J., Paul, M.J., and Davis, B.G. (2016). Chemical intervention in plant sugar signalling increases yield and resilience. Nature **540**: 574–578.

Hardie, D.G. (2011). AMP-activated protein kinase: A cellular energy sensor with a key role in metabolic disorders and in cancer. Biochem. Soc. Trans. **39**: 1–13.

Hardie, D.G., Ross, F.A., and Hawley, S.A. (2012). AMPK: A nutrient and energy sensor that maintains energy homeostasis. Nat. Rev. Mol. Cell Biol. **13**: 251–262.

Hawley, S.A., Davison, M., Woods, A., Davies, S.P., Beri, R.K., Carling, D., and Hardie, D.G. (1996). Characterization of the AMP-activated protein kinase kinase from rat liver and identification of threonine 172 as the major site at which it phosphorylates AMP-activated protein kinase. J. Biol. Chem. **271**: 27879–27887.

Heazlewood, J.l., Durek, P., Hummel, J., Selbig, J., Weckwerth, W., Walther, D., and Schulze, W.X. (2008). PhosPhAt : A database of phosphorylation sites in Arabidopsis thaliana and a plant-specific phosphorylation site predictor. Nucleic Acids Res. **36**: 1015–1021.

Hedbacker, K. (2008). SNF1/AMPK pathways in yeast. Front. Biosci. **13**: 2408.

Hedbacker, K., Hong, S.-P., and Carlson, M. (2004). Pak1 Protein Kinase Regulates Activation and Nuclear Localization of Snf1-Gal83 Protein Kinase. Mol. Cell. Biol. **24**: 8255–8263.

Henry, C., Bledsoe, S.W., Griffiths, C.A., Kollman, A., Paul, M.J., Sakr, S., and Lagrimini, L.M. (2015). Differential role for trehalose metabolism in salt-stressed maize. Plant Physiol. **169**: 1072–1089.

Henry, C., Bledsoe, S.W., Siekman, A., Kollman, A., Waters, B.M., Feil, R., Stitt, M., and Lagrimini, L.M. (2014). The trehalose pathway in maize: Conservation and gene regulation in response to the diurnal cycle and extended darkness. J. Exp. Bot. **65**: 5959–5973.

Hey, S., Mayerhofer, H., Halford, N.G., and Dickinson, J.R. (2007). DNA sequences from arabidopsis, which encode protein kinases and function as upstream regulators of Snf1 in yeast. J. Biol. Chem. **282**: 10472–10479.

Houtte, H. Van, López-Galvis, L., Vandesteene, L., Beeckman, T., and Van Dijck, P. (2013). Redundant and non-redundant roles of the trehalose-6-phosphate phosphatases in leaf growth, root hair specification and energy-responses in Arabidopsis. Plant Signal. Behav. **8**: 1–5.

Ikeda, Y., Koizumi, N., Kusano, T., and Sano, H. (2000). Specific binding of a 14-3-3 protein to autophosphorylated WPK4, an SNF1-related wheat protein kinase, and to WPK4-phosphorylated nitrate reductase. J. Biol. Chem. **275**: 31695–31700.

Iturriaga, G., Gaff, D.F., and Zentella, R. (2000). New desiccation-tolerant plants, including a grass, in the central highlands of Mexico, accumulate trehalose. Aust. J. Bot. **48**: 153.

Jamsheer K, M., Kumar, M., and Srivastava, V. (2021). SNF1-related protein kinase 1: the many-faced signaling hub regulating developmental plasticity in plants. J. Exp. Bot.: 1–24.

Janska, H., Piechota, J., and Kwasniak, M. (2010). ATP-dependent proteases in biogenesis and maintenance of plant mitochondria. Biochim. Biophys. Acta - Bioenerg. **1797**: 1071–1075.

Jiang, R. and Carlson, M. (1996). Glucose regulates protein interactions within the yeast SNF1 protein kinase complex. Genes Dev. **10**: 3105–3115.

Jossier, M., Bouly, J.-P., Meimoun, P., Arjmand, A., Lessard, P., Hawley, S., Grahame Hardie, D., and Thomas, M. (2009). SnRK1 (SNF1-related kinase 1) has a central role in sugar and ABA signalling in Arabidopsis thaliana. Plant J. **59**: 316–328.

Kataya, A.R.A., Elshobaky, A., Heidari, B., Dugassa, N.-F., Thelen, J.J., and Lillo, C. (2020). Multi-targeted trehalose-6-phosphate phosphatase I harbors a novel peroxisomal targeting signal 1 and is essential for flowering and development. Planta **251**: 98.

Kaufman, S. and G. A. Alivisatos, S. (1955). Purification and properties of the phosphorylating enzymes from spinach. J Biol Chem **216**: 141–152.

Kim, D.Y., Scalf, M., Smith, L.M., and Vierstra, R.D. (2013). Advanced proteomic analyses yield a deep catalog of ubiquitylation targets in Arabidopsis. Plant Cell **25**: 1523–1540.

Kleinow, T., Bhalerao, R., Breuer, F., Umeda, M., Salchert, K., and Koncz, C. (2000). Functional identification of an Arabidopsis Snf4 ortholog by screening for heterologous multicopy suppressors of snf4 deficiency in yeast. Plant J. **23**: 115–122.

Kolbe, A., Tiessen, A., Schluepmann, H., Paul, M., Ulrich, S., and Geigenberger, P. (2005). Trehalose 6-phosphate regulates starch synthesis via posttranslational redox activation of ADP-glucose pyrophosphorylase. **102**: 2–7.

Koncz, C., deJong, F., Villacorta, N., Szakonyi, D., and Koncz, Z. (2012). The spliceosome-activating complex: Molecular mechanisms underlying the function of a pleiotropic regulator. Front. Plant Sci. **3**: 1–12.

Kong, L.J. and Hanley-Bowdoin, L. (2002). A geminivirus replication protein interacts with a protein kinase and a motor protein that display different expression patterns during plant development and infection. Plant Cell **14**: 1817–1832.

Kötting, O., Kossmann, J., Zeeman, S.C., and Lloyd, J.R. (2010). Regulation of starch metabolism: The age of enlightenment? Curr. Opin. Plant Biol. **13**: 320–328.

Krasensky, J., Broyart, C., Rabanal, F.A., and Jonak, C. (2014). The redox-sensitive chloroplast trehalose-6-phosphate phosphatase AtTPPD regulates salt stress tolerance. Antioxidants Redox Signal. **21**: 1289–1304.

Kristensen, B.K., Askerlund, P., Bykova, N. V., Egsgaard, H., and Møller, I.M. (2004). Identification

of oxidised proteins in the matrix of rice leaf mitochondria by immunoprecipitation and two-dimensional liquid chromatography-tandem mass spectrometry. Phytochemistry **65**: 1839–1851.

Kulma, A., Villadsen, D., Campbell, D.G., Meek, S.E.M., Harthill, J.E., Nielsen, T.H., and MacKintosh, C. (2004). Phosphorylation and 14-3-3 binding of Arabidopsis 6-phosphofructo-2-kinase/ fructose-2,6-bisphosphatase. Plant J. **37**: 654–667.

Lee, J.H., Terzaghi, W., Gusmaroli, G., Charron, J.B.F., Yoon, H.J., Chen, H., He, Y.J., Xiong, Y., and Deng, X.W. (2008). Characterization of Arabidopsis and rice DWD proteins and their roles as substrate receptors for CUL4-RING E3 ubiquitin ligases. Plant Cell **20**: 152–167.

Lee, K.W., Chen, P.W., Lu, C.A., Chen, S., David Ho, T.H., and Yu, S.M. (2009). Coordinated responses to oxygen and sugar deficiency allow rice seedlings to tolerate flooding. Sci. Signal. **2**: 1–10.

Leech, A., Nath, N., McCartney, R.R., and Schmidt, M.C. (2003). Isolation of mutations in the catalytic domain of the Snf1 kinase that render its activity independent of the Snf4 subunit. Eukaryot. Cell **2**: 265–273.

Leegood, R.C. (2004). Photosynthesis. **3**: 330–335.

Leyman, B., Van Dijck, P., and Thevelein, J.M. (2001). An unexpected plethora of trehalose biosynthesis genes in Arabidopsis thaliana. Trends Plant Sci. **6**: 510–513.

Li, H.-W., Zang, B.-S., Deng, X.-W., and Wang, X. (2011). Overexpression of the trehalose-6-phosphate synthase gene OsTPS1 enhances abiotic stress tolerance in rice. Planta **234**: 1007–1018.

Li, X.-F., Li, Y.-J., An, Y.-H., Xiong, L.-J., Shao, X.-H., Wang, Y., and Sun, Y. (2009). AKINβ1 is Involved in the Regulation of Nitrogen Metabolism and Sugar Signaling in Arabidopsis. J. Integr. Plant Biol. **51**: 513–520.

Li, X., Wang, L., Zhou, X.E., Ke, J., De Waal, P.W., Gu, X., Tan, M.H.E., Wang, D., Wu, D., Xu, H.E., and Melcher, K. (2015). Structural basis of AMPK regulation by adenine nucleotides and glycogen. Cell Res. **25**: 50–66.

Lin, C.R., Lee, K.W., Chen, C.Y., Hong, Y.F., Chen, J.L., Lu, C.A., Chen, K.T., David Ho, T.H., and Yu, S.M. (2014). SnRK1A-interacting negative regulators modulate the nutrient starvation signaling sensor SnRK1 in source-sink communication in cereal seedlings under abiotic stress. Plant Cell **26**: 808–827.

Lin, Q., Wang, S., Dao, Y., Wang, J., and Wang, K. (2020). Arabidopsis thaliana trehalose-6-phosphate phosphatase gene TPPI enhances drought tolerance by regulating stomatal apertures. J. Exp. Bot. **71**: 4285–4297.

Lin, Q., Yang, J., Wang, Q., Zhu, H., Chen, Z., Dao, Y., and Wang, K. (2019). Overexpression of the trehalose-6-phosphate phosphatase family gene AtTPPF improves the drought tolerance of Arabidopsis thaliana. BMC Plant Biol. **19**: 1–15.

López-Paz, C., Vilela, B., Riera, M., Pagès, M., and Lumbreras, V. (2009). Maize AKINβγ dimerizes through the KIS/CBM domain and assembles into SnRK1 complexes. FEBS Lett. **583**: 1887–1894.

Lu, Y., Gehan, J.P., and Sharkey, T.D. (2005). Daylength and circadian effects on starch degradation and maltose metabolism. Plant Physiol. **138**: 2280–2291.

Lumbreras, V., Albà, M.M., Kleinow, T., Koncz, C., and Pagès, M. (2001). Domain fusion between SNF1-related kinase subunits during plant evolution. EMBO Rep. **2**: 55–60.

Lunn, J.E. (2002). Evolution of Sucrose Synthesis. Plant Physiol. **128**: 1490–1500.

Lunn, J.E. (2007). Gene families and evolution of trehalose metabolism in plants. Funct. Plant Biol. **34**: 550–563.

Lunn, J.E., Delorge, I., Figueroa, C.M., Van Dijck, P., and Stitt, M. (2014). Trehalose metabolism in plants. Plant J. **79**: 544–567.

Lunn, J.E., Feil, R., Hendriks, J.H.M., Gibon, Y., Morcuende, R., Osuna, D., Scheible, W.R., Carillo, P., Hajirezaei, M.R., and Stitt, M. (2006). Sugar-induced increases in trehalose 6-phosphate are correlated with redox activation of ADPglucose pyrophosphorylase and higher rates of starch synthesis in Arabidopsis thaliana. Biochem. J. **397**: 139–148.

Ma, J., Hanssen, M., Lundgren, K., Hernández, L., Delatte, T., Ehlert, A., Liu, C.M., Schluepmann, H., Dröge-Laser, W., Moritz, T., Smeekens, S., and Hanson, J. (2011). The sucrose-regulated Arabidopsis transcription factor bZIP11 reprograms metabolism and regulates trehalose metabolism. New Phytol. **191**: 733–745.

MacNeill, G.J., Mehrpouyan, S., Minow, M.A.A., Patterson, J.A., Tetlow, I.J., and Emes, M.J. (2017). Starch as a source, starch as a sink: The bifunctional role of starch in carbon allocation. J. Exp. Bot. **68**: 4433–4453.

Mair, A., Pedrotti, L., Wurzinger, B., Anrather, D., Simeunovic, A., Weiste, C., Valerio, C., Dietrich, K., Kirchler, T., Nägele, T., Carbajosa, J.V., Hanson, J., Baena-González, E., Chaban, C., Weckwerth, W., Dröge-Laser, W., and Teige, M. (2015). SnRK1-triggered switch of bZIP63 dimerization mediates the low-energy response in plants. Elife **4**: 1–33.

Maor, R., Jones, A., Nühse, T.S., Studholme, D.J., Peck, S.C., and Shirasu, K. (2007). Multidimensional protein identification technology (Mud(PIT) analysis of ubiquitinated proteins in plants. Mol. Cell. Proteomics **6**: 601–610.

Martínez-Barajas, E., Delatte, T., Schluepmann, H., de Jong, G.J., Somsen, G.W., Nunes, C., Primavesi, L.F., Coello, P., Mitchell, R.A.C., and Paul, M.J. (2011). Wheat grain development is characterized by remarkable trehalose 6-phosphate accumulation pregrain filling: Tissue distribution and relationship to SNF1-related protein kinase1 activity. Plant Physiol. **156**: 373–381.

Martins, M.C.M., Hejazi, M., Fettke, J., Steup, M., Feil, R., Krause, U., Arrivault, S., Vosloh, D., Figueroa, C.M., Ivakov, A., Yadav, U.P., Piques, M., Metzner, D., Stitt, M., and Lunn, J.E. (2013). Feedback inhibition of starch degradation in Arabidopsis leaves mediated by trehalose 6-phosphate. Plant Physiol. **163**: 1142–1163.

Maya-Bernal, J.L., Ávila, A., Ruiz-Gayosso, A., Trejo-Fregoso, R., Pulido, N., Sosa-Peinado, A., Zúñiga-Sánchez, E., Martínez-Barajas, E., Rodríguez-Sotres, R., and Coello, P. (2017). Expression of recombinant SnRK1 in E. coli. Characterization of adenine nucleotide binding to the SnRK1.1/AKINβγ-β3 complex. Plant Sci. **263**: 116–125.

Mayer, F. V., Heath, R., Underwood, E., Sanders, M.J., Carmena, D., McCartney, R.R., Leiper, F.C., Xiao, B., Jing, C., Walker, P.A., Haire, L.F., Ogrodowicz, R., Martin, S.R., Schmidt, M.C., Gamblin, S.J., and Carling, D. (2011). ADP Regulates SNF1, the Saccharomyces cerevisiae Homolog of AMP-Activated Protein Kinase. Cell Metab. **14**: 707–714.

McMichael, R.W., Bachmann, M., and Huber, S.C. (1995). Spinach leaf sucrose-phosphate synthase and nitrate reductase are phosphorylated/inactivated by multiple protein kinases in vitro. Plant Physiol. **108**: 1077–1082.

Meitzel, T., Radchuk, R., McAdam, E.L., Thormählen, I., Feil, R., Munz, E., Hilo, A., Geigenberger, P., Ross, J.J., Lunn, J.E., and Borisjuk, L. (2020). Trehalose 6-phosphate promotes seed filling by activating auxin biosynthesis. New Phytol.

Millar, A.H., Heazlewood, J.L., Kristensen, B.K., Braun, H.P., and Møller, I.M. (2005). The plant mitochondrial proteome. Trends Plant Sci. **10**: 36–43.

Mohannath, G., Jackel, J.N., Lee, Y.H., Buchmann, R.C., Wang, H., Patil, V., Adams, A.K., and Bisaro, D.M. (2014). A complex containing SNF1-related kinase (SnRK1) and adenosine kinase in arabidopsis. PLoS One **9**.

Moorhead, G., Douglas, P., Morrice, N., Scarabel, M., Aitken, A., and MacKintosh, C. (1996). Phosphorylated nitrate reductase from spinach leaves is inhibited by 14- 3-3 proteins and activated by fusicoccin. Curr. Biol. **6**: 1104–1113.

Nakagami, H., Sugiyama, N., Mochida, K., Daudi, A., Yoshida, Y., Toyoda, T., Tomita, M., Ishihama, Y., and Shirasu, K. (2010). Large-scale comparative phosphoproteomics identifies conserved phosphorylation sites in plants. Plant Physiol. **153**: 1161–1174.

Németh, K., Salchert, K., Putnoky, P., Bhalerao, R., Koncz-Kálmán, Z., Stankovic-Stangeland, B., Bakó, L., Mathur, J., Ökrész, L., Stabel, S., Geigenberger, P., Stitt, M., Rédei, G.P., Schell, J., and Koncz, C. (1998). Pleiotropic control of glucose and hormone responses by PRL1, a nuclear WD protein, in Arabidopsis. Genes Dev. **12**: 3059–3073.

Nietzsche, M., Landgraf, R., Tohge, T., and Börnke, F. (2016). A protein-protein interaction network linking the energy-sensor kinase SnRK1 to multiple signaling pathways in Arabidopsis thaliana. Curr. Plant Biol. **5**: 36–44.

Nietzsche, M., Schießl, I., and Börnke, F. (2014). The complex becomes more complex: Protein-protein interactions of SnRK1 with DUF581 family proteins provide a framework for cell- and stimulus type-specific SnRK1 signaling in plants. Front. Plant Sci. **5**: 1–13.

Noguchi, K. and Terashima, I. (2006). Responses of spinach leaf mitochondria to low N availability. Plant, Cell Environ. **29**: 710–719.

Nunes-Nesi, A., Sulpice, R., Gibon, Y., and Fernie, A.R. (2008). The enigmatic contribution of mitochondrial function in photosynthesis. J. Exp. Bot. **59**: 1675–1684.

Nunes, C., O'Hara, L.E., Primavesi, L.F., Delatte, T.L., Schluepmann, H., Somsen, G.W., Silva, A.B., Fevereiro, P.S., Wingler, A., and Paul, M.J. (2013). The trehalose 6-phosphate/snRK1. signaling pathway primes growth recovery following relief of sink limitation. Plant Physiol. **162**: 1720–1732.

Nunes, C., Primavesi, L.F., Patel, M.K., Martinez-Barajas, E., Powers, S.J., Sagar, R., Fevereiro, P.S., Davis, B.G., and Paul, M.J. (2013). Inhibition of SnRK1 by metabolites: Tissue-dependent effects and cooperative inhibition by glucose 1-phosphate in combination with trehalose 6-phosphate. Plant Physiol. Biochem. **63**: 89–98.

O'Brien, M., Kaplan-Levy, R.N., Quon, T., Sappl, P.G., and Smyth, D.R. (2015). PETAL LOSS, a trihelix transcription factor that represses growth in Arabidopsis thaliana, binds the energy-sensing SnRK1 kinase AKIN10. J. Exp. Bot. **66**: 2475–2485.

Oszvald, M., Primavesi, L.F., Griffiths, C.A., Cohn, J., Basu, S.S., Nuccio, M.L., and Paul, M.J. (2018). Trehalose 6-phosphate regulates photosynthesis and assimilate partitioning in reproductive tissue. Plant Physiol. **176**: 2623–2638.

Pang, T., Xiong, B., Li, J.Y., Qiu, B.Y., Jin, G.Z., Shen, J.K., and Li, J. (2007). Conserved α-helix acts as autoinhibitory sequence in AMP-activated protein kinase α subunits. J. Biol. Chem. **282**: 495–506.

Pedrotti, L., Weiste, C., Nägele, T., Wolf, E., Lorenzin, F., Dietrich, K., Mair, A., Weckwerth, W., Teige, M., Baena-González, E., and Dröge-Laser, W. (2018). Snf1-RELATED KINASE1-controlled C/S1-bZIP signaling activates alternative mitochondrial metabolic pathways to ensure plant survival in extended darkness. Plant Cell **30**: 495–509.

Pesaresi, P., Masiero, S., Eubel, H., Braun, H.P., Bhushan, S., Glaser, E., Salamini, F., and Leister, D. (2006). Nuclear photosynthetic gene expression is synergistically modulated by rates of protein synthesis in chloroplasts and mitochondria. Plant Cell **18**: 970–991.

Pfister, B. and Zeeman, S.C. (2016). Formation of starch in plant cells. Cell. Mol. Life Sci. **73**: 2781–2807.

Piattoni, C.V., Bustos, D.M., Guerrero, S.A., and Iglesias, A.Á. (2011). Nonphosphorylating glyceraldehyde-3-phosphate dehydrogenase is phosphorylated in wheat endosperm at serine-404 by an snf1-related protein kinase allosterically inhibited by ribose-5-phosphate. Plant Physiol. **156**: 1337–1350.

Pierre, M., Traverso, J.A., Boisson, B., Domenichini, S., Bouchez, D., Giglione, C., and Meinnel, T. (2007). N-myristoylation regulates the SnRK1 pathway in arabidopsis. Plant Cell **19**: 2804–2821.

Plaxton, W.C. (1996). The organization and regulation of plant glycolysis. Annu. Rev. Plant Physiol. Plant Mol. Biol. **47**: 185–214.

Plaxton, W.C. and Podestá, F.E. (2006). The functional organization and control of plant respiration. CRC. Crit. Rev. Plant Sci. **25**: 159–198.

Podestá, F.E. and Plaxton, W.C. (2003). Fluorescence study of ligand binding to potato tuber pyrophosphate-dependent phosphofructokinase: Evidence for competitive binding between fructose-1,6-bisphosphate and fructose-2,6-bisphosphate. Arch. Biochem. Biophys. **414**: 101–107.

Polge, C., Jossier, M., Crozet, P., Gissot, L., and Thomas, M. (2008). β-subunits of the SnRK1 complexes share a common ancestral function together with expression and function specificities; physical interaction with nitrate reductase specifically occurs via AKINβ1-subunit. Plant Physiol. **148**: 1570–1582.

Polge, C. and Thomas, M. (2007). SNF1/AMPK/SnRK1 kinases, global regulators at the heart of energy control? Trends Plant Sci. **12**: 20–28.

Radchuk, R., Radchuk, V., Weschke, W., Borisjuk, L., and Weber, H. (2006). Repressing the expression of the SUCROSE NONFERMENTING-1-RELATED PROTEIN KINASE gene in pea embryo causes pleiotropic defects of maturation similar to an abscisic acid-insensitive phenotype. Plant Physiol. **140**: 263–278.

Ramon, M., Dang, T.V.T., Broeckx, T., Hulsmans, S., Crepin, N., Sheen, J., and Rolland, F. (2019). Default activation and nuclear translocation of the plant cellular energy sensor SnRK1 regulate metabolic stress responses and development. Plant Cell **31**: 1614–1632.

Ramon, M., Ruelens, P., Li, Y., Sheen, J., Geuten, K., and Rolland, F. (2013). The hybrid Four-CBS-Domain KINβγ subunit functions as the canonical γ subunit of the plant energy sensor SnRK1. Plant J. **75**: 11–25.

Ramon, M., De Smet, I., Vandesteene, L., Naudts, M., Leyman, B., Van Dijck, P., Rolland, F., Beeckman, T., and Thevelein, J.M. (2009). Extensive expression regulation and lack of heterologous enzymatic activity of the Class II trehalose metabolism proteins from Arabidopsis thaliana. Plant. Cell Environ. **32**: 1015–32.

Rigas, S., Daras, G., Laxa, M., Marathias, N., Fasseas, C., Sweetlove, L.J., and Hatzopoulos, P. (2009). Role of Lon1 protease in post-germinative growth and maintenance of mitochondrial function in Arabidopsis thaliana. New Phytol. **181**: 588–600.

Robertlee, J., Kobayashi, K., Suzuki, M., and Muranaka, T. (2017). AKIN10, a representative Arabidopsis SNF1-related protein kinase 1 (SnRK1), phosphorylates and downregulates plant HMG-CoA reductase. FEBS Lett. **591**: 1159–1166.

Rodrigues, A., Adamo, M., Crozet, P., Margalha, L., Confraria, A., Martinho, C., Elias, A., Rabissi, A., Lumbreras, V., González-Guzmán, M., Antoni, R., Rodriguez, P.L., and Baena-González, E. (2013). ABI1 and PP2CA phosphatases are negative regulators of Snf1-related protein kinase1 signaling in Arabidopsis. Plant Cell **25**: 3871–3884.

Romero, C., Bellés, J.M., Vayá, J.L., Serrano, R., and Culiáñez-Macià, F.A. (1997). Expression of the yeast trehalose-6-phosphate synthase gene in transgenic tobacco plants: pleiotropic phenotypes include drought tolerance. Planta **201**: 293–297.

Ruan, Y.L. (2014). Sucrose metabolism: Gateway to diverse carbon use and sugar signaling. Annu. Rev. Plant Biol. **65**: 33–67.

Ruiz, A., Xu, X., and Carlson, M. (2013). Ptc1 protein phosphatase 2C contributes to glucose regulation of SNF1/AMP-activated protein kinase (AMPK) in Saccharomyces cerevisiae. J. Biol. Chem. **288**: 31052–31058.

Salerno, G.L. and Curatti, L. (2003). Origin of sucrose metabolism in higher plants: When, how and why? Trends Plant Sci. **8**: 63–69.

Scheibe, R., Backhausen, J.E., Emmerlich, V., and Holtgrefe, S. (2005). Strategies to maintain redox homeostasis during photosynthesis under changing conditions. J. Exp. Bot. **56**: 1481–1489.

Schmid, M., Davison, T.S., Henz, S.R., Pape, U.J., Demar, M., Vingron, M., Schölkopf, B., Weigel, D., and Lohmann, J.U. (2005). A gene expression map of Arabidopsis thaliana development. Nat. Genet. **37**: 501–506.

Schmidt, M.C. (2000). beta-subunits of Snf1 kinase are required for kinase function and substrate definition. EMBO J. **19**: 4936–4943.

Shen, W. and Hanley-Bowdoin, L. (2006). Geminivirus infection up-regulates the expression of two arabidopsis protein kinases related to yeast SNF1- and mammalian AMPK-activating kinases. Plant Physiol. **142**: 1642–1655.

Shen, W., Reyes, M.I., and Hanley-Bowdoin, L. (2009). Arabidopsis protein kinases GRIK1 and GRIK2 specifically activate SnRK1 by phosphorylating its activation loop. Plant Physiol. **150**: 996–1005.

Simpson-Lavy, K.J. and Johnston, M. (2013). SUMOylation regulates the SNF1 protein kinase. Proc. Natl. Acad. Sci. U. S. A. **110**: 17432–17437.

Slewinski, T.L. and Braun, D.M. (2010). Current perspectives on the regulation of whole-plant carbohydrate partitioning. Plant Sci. **178**: 341–349.

Smith, A.M. and Stitt, M. (2007). Coordination of carbon supply and plant growth. Plant, Cell Environ. **30**: 1126–1149.

Smith, A.M. and Zeeman, S.C. (2020). Starch: A Flexible, Adaptable Carbon Store Coupled to Plant Growth. Annu. Rev. Plant Biol. **71**: 217–245.

Smith, S.M., Fulton, D.C., Chia, T., Thorneycroft, D., Chapple, A., Dunstan, H., Hylton, C., Zeeman, S.C., and Smith, A.M. (2004). Diurnal Changes in the Transcriptome Encoding Enzymes of Starch Metabolism Provide Evidence for Both Transcriptional and Posttranscriptional Regulation of Starch Metabolism in Arabidopsis Leaves. Plant Physiol. **136**: 2687–2699.

Sonnewald, U., Brauer, M., von Schaewen, A., Stitt, M., and Willmitzer, L. (1991). Transgenic tobacco plants expressing yeast-derived invertase in either the cytosol, vacuole or apoplast: a powerful tool for studying sucrose metabolism and sink/source interactions. Plant J. **1**: 95–106.

Steinberg, G.R. and Kemp, B.E. (2009). AMPK in health and disease. Physiol. Rev. **89**: 1025–1078.

Stitt, M. (1990). Fructose-2,6-bisphosphate as a regulatory molecule in plants. Annu. Rev. Plant Physiol. Plant Mol. Biol. **41**: 153–185.

Stitt, M. (1987). Fructose 2,6-Bisphosphate and Plant Carbohydrate Metabolism. Plant Physiol. **84**: 201–204.

Stitt, M. (1998). Pyrophosphate as an energy donor in the cytosol of plant cells: An enigmatic alternative to ATP. Bot. Acta **111**: 167–175.

Stitt, M., Gerhardt, R., Kürzel, B., and Heldt, H.W. (1983). A Role for Fructose 2,6-Bisphosphate in the Regulation of Sucrose Synthesis in Spinach Leaves. Plant Physiol. **72**: 1139–1141.

Stitt, M., Kürzel, B., and Heldt, H.W. (1984). Control of Photosynthetic Sucrose Synthesis by Fructose 2,6-Bisphosphate. Plant Physiol. **75**: 554–560.

Stitt, M., Lunn, J., and Usadel, B. (2010). Arabidopsis and primary photosynthetic metabolism - More than the icing on the cake. Plant J. **61**: 1067–1091.

Stitt, M. and Sonnewald, U. (1995). Regulation of Metabolism in Transgenic Plants. Annu. Rev. Plant Physiol. Plant Mol. Biol. **46**: 341–368.

Sugden, C., Crawford, R.M., Halford, N.G., and Hardie, D.G. (1999). Regulation of spinach SNF1-related (SnRK1) kinases by protein kinases and phosphatases is associated with phosphorylation of the T loop and is regulated by 5'-AMP. Plant J. **19**: 433–439.

Sugden, C., Donaghy, P.G., Halford, N.G., and Hardie, D.G. (1999). Two SNF1-related protein kinases from spinach leaf phosphorylate and inactivate 3-hydroxy-3-methylglutaryl-coenzyme a reductase, nitrate reductase, and sucrose phosphate synthase in vitro. Plant Physiol.

Sulpice, R., Flis, A., Ivakov, A.A., Apelt, F., Krohn, N., Encke, B., Abel, C., Feil, R., Lunn, J.E., and Stitt, M. (2014). Arabidopsis coordinates the diurnal regulation of carbon allocation and growth across a wide range of Photoperiods. Mol. Plant **7**: 137–155.

Szarka, A., Horemans, N., Passarella, S., Tarcsay, Á., Örsi, F., Salgó, A., and Bánhegyi, G. (2008). Demonstration of an intramitochondrial invertase activity and the corresponding sugar transporters of the inner mitochondrial membrane in Jerusalem artichoke (Helianthus tuberosus L.) tubers. Planta **228**: 765–775.

Tegeder, M. and Weber, A.P.M. (2006). Metabolite Transporters in the Control of Plant Primary Metabolism. In Annual Plant Reviews online (John Wiley & Sons, Ltd: Chichester, UK), pp. 85–120.

Tenorio, G., Orea, A., Romero, J.M., and Mérida, Á. (2003). Oscillation of mRNA level and activity of granule-bound starch synthase I in Arabidopsis leaves during the day/night cycle. Plant Mol. Biol. **51**: 949–958.

Tetlow, I.J., Wait, R., Lu, Z., Akkasaeng, R., Bowsher, C.G., Esposito, S., Kosar-Hashemi, B., Morell, M.K., and Emes, M.J. (2004). Protein phosphorylation in amyloplasts regulates starch branching enzyme activity and protein-protein interactions. Plant Cell **16**: 694–708.

Thelander, M., Olsson, T., and Ronne, H. (2004). Snf1-related protein kinase 1 is needed for growth in a normal day-night light cycle. EMBO J. **23**: 1900–1910.

Tian, L., Xie, Z., Lu, C., Hao, X., Wu, S., Huang, Y., Li, D., and Chen, L. (2019). The trehalose-6-phosphate synthase TPS5 negatively regulates ABA signaling in Arabidopsis thaliana. Plant Cell Rep. **38**: 869–882.

Toroser, D., Plaut, Z., and Huber, S.C. (2000). Regulation of a plant SNF1-related protein kinase by glucose-6-phosphate. Plant Physiol. **123**: 403–411.

Tsai, A.Y.L. and Gazzarrini, S. (2012). AKIN10 and FUSCA3 interact to control lateral organ development and phase transitions in Arabidopsis. Plant J. **69**: 809–821.

Vandesteene, L., López-Galvis, L., Vanneste, K., Feil, R., Maere, S., Lammens, W., Rolland, F., Lunn, J.E., Avonce, N., Beeckman, T., and van Dijck, P. (2012). Expansive evolution of the TREHALOSE-6-PHOSPHATE PHOSPHATASE gene family in Arabidopsis. Plant Physiol. **160**: 884–896.

Wahl, V., Ponnu, J., Schlereth, A., Arrivault, S., Langenecker, T., Franke, A., Feil, R., Lunn, J.E., Stitt, M., and Schmid, M. (2013). Regulation of Flowering by Trehalose-6-Phosphate Signaling in Arabidopsis thaliana. Science (80-.). **339**: 704–707.

Wang, C., Zhang, S., Qi, S., Zheng, C., and Wu, C. (2016). Delayed germination of Arabidopsis seeds under chilling stress by overexpressing an abiotic stress inducible GhTPS11. **575**: 206–212.

Wang, Y., Wang, L., Micallef, B.J., Tetlow, I.J., Mullen, R.T., Feil, R., Lunn, J.E., and Emes, M.J. (2020). AKINβ1, a subunit of SnRK1, regulates organic acid metabolism and acts as a global modulator of genes involved in carbon, lipid, and nitrogen metabolism. J. Exp. Bot. **71**: 1010–1028.

Weber, H., Borisjuk, L., and Wobus, U. (1997). Sugar import and metabolism during seed development. Trends Plant Sci. **2**: 169–174.

Williams, S.P., Rangarajan, P., Donahue, J.L., Hess, J.E., and Gillaspy, G.E. (2014). Regulation of Sucrose non-Fermenting Related Kinase 1 genes in Arabidopsis thaliana. Front. Plant Sci. **5**: 1–13.

Wingler, A., Delatte, T.L., Hara, L.E.O., Primavesi, L.F., Jhurreea, D., Paul, M.J., and Schluepmann, H. (2012). Trehalose 6-Phosphate Is Required for the Onset of Leaf Senescence Associated with High. Plant Physiol. **158**: 1241–1251.

Woodson, J.D. and Chory, J. (2008). Coordination of gene expression between organellar and nuclear genomes. Nat. Rev. Genet. **9**: 383–395.

Xu, S., Brill, E., Llewellyn, D.J., Furbank, R.T., and Ruan, Y. (2012). Overexpression of a Potato Sucrose Synthase Gene in Cotton Accelerates Leaf Expansion , Reduces Seed Abortion , and Enhances Fiber Production. Mol. Plant **5**: 430–441.

Yadav, U.P., Ivakov, A., Feil, R., Duan, G.Y., Walther, D., Giavalisco, P., Piques, M., Carillo, P., Hubberten, H.M., Stitt, M., and Lunn, J.E. (2014). The sucrose-trehalose 6-phosphate (Tre6P) nexus: Specificity and mechanisms of sucrose signalling by. J. Exp. Bot. **65**: 1051–1068.

Zeeman, S.C., Kossmann, J., and Smith, A.M. (2010). Starch: Its metabolism, evolution, and biotechnological modification in plants. Annu. Rev. Plant Biol. **61**: 209–234.

Zeeman, S.C. and Rees, T.A. (1999). Changes in carbohydrate metabolism and assimilate export in starch-excess mutants of Arabidopsis. Plant, Cell Environ. **22**: 1445–1453.

Zhai, Z., Keereetaweep, J., Liu, H., Feil, R., Lunn, J.E., and Shanklin, J. (2018). Trehalose 6-phosphate positively regulates fatty acid synthesis by stabilizing wrinkled1[open]. Plant Cell **30**: 2616–2627.

Zhang, Y., Primavesi, L.F., Jhurreea, D., Andralojc, P.J., Mitchell, R.A.C., Powers, S.J., Schluepmann, H., Delatte, T., Wingler, A., and Paul, M.J. (2009). Inhibition of SNF1-related protein kinasel activity and regulation of metabolic pathways by trehalose-6-phosphate1[w][OA]. Plant Physiol. **149**: 1860–1871.

Zhang, Y., Sampathkumar, A., Kerber, S.M.L., Swart, C., Hille, C., Seerangan, K., Graf, A., Sweetlove, L., and Fernie, A.R. (2020). A moonlighting role for enzymes of glycolysis in the co-localization of mitochondria and chloroplasts. Nat. Commun. **11**.

Zhang, Y., Shewry, P.R., Jones, H., Barcelo, P., Lazzeri, P.A., and Halford, N.G. (2001). Expression of antisense SnRK1 protein kinase sequence causes abnormal pollen development and male sterility in transgenic barley. Plant J. **28**: 431–441.

Zhang, Z.P., Deng, Y., Song, X., and Miao, M. (2015). Trehalose-6-phosphate and SNF1-related protein kinase 1 are involved in the first-fruit inhibition of cucumber. J. Plant Physiol. **177**: 110–120.

CHAPTER 2

An impact of SnRK1 on sucrose homeostasis and the transcriptome during the diel cycle in Arabidopsis

Author contributions: Bruno Peixoto, John E. Lunn, Mark Stitt, and Elena Baena-González conceived the research plan and designed the experiments. Bruno Peixoto and Leonor Margalha (TPS1 immunoblots) performed the experiments. Thiago A. Moraes assisted with sample collection and metabolite data analyses. Virginie Mengin, Melanie Höehne and Regina Feil assisted with sample collection and metabolite profiling. António G. G. Sousa and Jingtao Lilue assisted with RNA-seq data analyses. Bruno Peixoto and Elena Baena-González analysed, interpreted data, and wrote the manuscript. John E. Lunn, Mark Stitt, and Rubén Vicente interpreted data and edited the manuscript. All the authors proofread the manuscript.

2.1 Abstract

Sucrose Non-Fermenting1-Related Kinase1 (SnRK1) is an evolutionarily conserved protein kinase with key functions in energy management during stress responses in plants. To address a potential role of SnRK1 under favourable conditions, we performed a metabolomic and transcriptomic characterization of 20 d-old rosettes of Arabidopsis (*Arabidopsis thaliana*) SnRK1 gain- and loss-of-function mutants during the regular diel cycle. Our results show that SnRK1 manipulation alters the sucrose and trehalose 6-phosphate (Tre6P) relationship, influencing how the Suc content is translated into Tre6P accumulation and modulating the flux of carbon to the tricarboxylic acid cycle downstream of Tre6P-signalling. On the other hand, daily cycles of Tre6P accumulation were accompanied by changes in SnRK1 signaling, leading to a maximum in the expression of SnRK1-induced genes at the end of the night, when Tre6P levels are lowest, and to a minimum at the end of the day, when Tre6P levels peak. The expression of SnRK1-induced genes was strongly reduced by transient Tre6P accumulation in an inducible Tre6P synthase (otsA) line, further suggesting the involvement of Tre6P in the diel oscillations in SnRK1 signaling. Transcriptional profiling of wild type plants and SnRK1 mutants uncovered also defects that are suggestive of an iron sufficiency response and of a matching induction of sulphur acquisition and assimilation when SnRK1 is depleted. In conclusion, under favourable growth conditions, SnRK1 plays a role in sucrose homeostasis and transcriptome remodelling in autotrophic tissues and its activity is influenced by diel fluctuations in Tre6P levels.

2.2 Introduction

In most plants, sucrose is a major product of photosynthesis and the most common form in which carbon is exported to sink organs for growth, development and storage (Ruan, 2014). Sucrose metabolism is tightly controlled (i) to ensure that sucrose synthesis is neither too slow nor too fast to limit CO_2 fixation and (ii) to balance sucrose synthesis and export with the accumulation of carbon reserves that

enable survival and growth through the night (Smith and Stitt, 2007). The inability to efficiently manage carbon resources has clear penalties on plant growth. On the one hand, incomplete starch mobilization results in yield losses due to non-productive carbon sequestration. On the other hand, if starch is prematurely depleted during the night, the ensuing carbon starvation leads to metabolic and transcriptional responses that inhibit growth (Smith and Stitt, 2007; Stitt and Zeeman, 2012).

Although the underlying mechanisms are still poorly understood, several of the components involved in the coordinated regulation of carbon assimilation, storage and growth are known. One is trehalose 6-phosphate (Tre6P) signaling. Tre6P is a regulatory sugar that modulates primary metabolism, growth and development. Tre6P is synthesized from glucose 6-phosphate (Glc6P) and UDP-glucose by Tre6P synthase (TPS) and is further metabolized into trehalose by Tre6P phosphatase (TPP) (Lunn et al., 2014; Fichtner and Lunn, 2021). The Arabidopsis genome harbors 11 genes encoding TPS or TPS-like proteins (*TPS1-TPS11*) and 10 genes encoding TPP proteins (*TPPA–TPPJ*). Class I TPS proteins (TPS1 to TPS4) contain a catalytically active glucosyltransferase domain and a non-catalytic TPP-like domain. The class II proteins (TPS5 to TPS11) have a similar domain structure and most of the active site residues are conserved, but they do not appear to have TPS or TPP activity (Ramon et al., 2009; Lunn et al., 2014; Delorge et al., 2015; Fichtner and Lunn, 2021).

Normally, Tre6P concentrations are very low in Arabidopsis plants (0.01–2 nmol g^{-1} FW), but their levels respond to daily sucrose peaks and also rise dramatically in response to exogenous sucrose feeding (Lunn et al., 2006; Nunes et al., 2013; Yadav et al., 2014). Indeed, a strong correlation between Tre6P and sucrose levels has been reported in many tissues and species, suggesting that Tre6P is an evolutionarily conserved proxy for the plant sucrose status (Lunn et al., 2014; Fichtner and Lunn, 2021). Most importantly, Tre6P regulates sucrose levels by promoting sucrose consumption and preventing further synthesis when Tre6P levels are high, whilst promoting sucrose synthesis and decreasing sucrose consumption when Tre6P levels are low (Lunn et al., 2014; Fichtner and Lunn, 2021). Using an

inducible system for Tre6P production in combination with metabolomics, proteomics, and flux analyses, it was demonstrated that high Tre6P reduces sucrose production in source leaves by diverting photoassimilates into organic and amino acid synthesis [by activating nitrate reductase (NR) and phosphoenolpyruvate carboxylase (PEPC)] during the day (Figueroa et al., 2016) and by inhibiting starch degradation at night (Martins et al., 2013).

Another component of the energy management network is SnRK1, an evolutionarily conserved heterotrimeric protein kinase complex composed of an α-catalytic subunit and regulatory β and γ-subunits [SnRK1α1/α2, SnRK1β1/β2/β3, and SnRK1βγ in Arabidopsis; (Broeckx et al., 2016)]. SnRK1 is inhibited, directly or indirectly, by sugars such as Tre6P, Glc6P, and glucose 1-phosphate (Glc1P) (Zhang et al., 2009; Nunes et al., 2013; Zhai et al., 2018; Baena-González and Lunn, 2020) while SnRK1 signaling is activated in response to low energy levels, often associated with stress (Baena-González et al., 2007; Baena-González and Sheen, 2008; Crepin and Rolland, 2019). Upon activation, SnRK1 triggers transcriptional and metabolic responses to stimulate energy-producing catabolic processes and inhibit energy-consuming biosynthetic processes and growth (Baena-González and Sheen, 2008; Nukarinen et al., 2016), ultimately promoting stress tolerance and survival. The relevance of SnRK1 for stress responses has been validated *in planta*, where overexpression of the main catalytic subunit SnRK1α1 enhances tolerance to abiotic and biotic stresses whilst the opposite is true for *snrk1α* knockdown mutants (Hulsmans et al., 2016; Margalha et al., 2019).

In this study, we hypothesized that SnRK1 plays important roles in daily carbon management in the absence of any overt form of abiotic of biotic stress treatment. To investigate this, we compared wild-type and SnRK1 gain- and loss-of-function mutants at the metabolite and transcriptional levels at different timepoints of the day and night. Our results implicate SnRK1 in sucrose homeostasis and transcriptional regulation during normal day-night cycles in rosette leaves. They further show that this is at least partly determined by diel oscillations in Tre6P accumulation that impact on SnRK1 activity.

2.3 Results

To investigate the function of SnRK1 during the regular diel cycle, we grew plants under conditions that are only slightly limiting for growth of Arabidopsis Col-0 plants [12-h photoperiod with an irradiance of 160 µmol m^{-2} s^{-1}; (Sulpice et al., 2014)]. We used a SnRK1α1 overexpression line [*SnRK1α1-OE*; (Jossier et al., 2009)], and a partial SnRK1α loss-of-function mutant [*snrk1α1*$^{-/-}$ *snrk1α2*$^{+/-}$, *sesquiα2*; (Belda-Palazón et al., 2020)]. The *sesquiα2* line was selected as a loss-of-function mutant for two reasons. Firstly, the molecular phenotypes of the *snrk1α1* and *snrk1α2* single mutants are mild even under stress conditions (Nukarinen et al., 2016; Belda-Palazón et al., 2020) due to functional redundancy between the two *α*-subunits (Baena-González et al., 2007). Secondly, despite being a stronger loss-of-function mutant than the single *snrk1α* mutants, the *sesquiα2* line does not show obvious growth phenotypes under our standard laboratory growth conditions in soil (Supplemental Figure 2.1A). This makes this mutant ideal for investigating a potential impact of SnRK1 on metabolism and gene expression without confounding effects derived from altered growth and development. The *SnRK1α1-OE* line was selected as a gain-of-function mutant also because it did not show obvious growth alterations under our growth conditions (Supplemental Figure 2.1A) and because it was generated in the same background as the *sesquiα2* mutant [(Col-0; (Jossier et al., 2009)]. Mutants and Col-0 control plants were grown for 20 days and then harvested at 4-h intervals over a period of 40 h starting at ZT8 (Supplemental Figure 2.1B). Using both enzymatic, as well as LC-MS/MS methodologies, we analysed these samples for the contents of a total of 38 different metabolites related to pathways of carbon and nitrogen primary metabolism (Supplemental Table 2.1).

2.3.1 Impact on Suc and Tre6P levels

As shown in Figure 2.1A-B, Col-0 rosettes displayed the expected diel changes of sucrose and Tre6P, with sucrose levels peaking at the end of the day (ED) and being closely mirrored by Tre6P. The average sucrose content ranged from

0.84 to 2.08 µmol (hexose equivalents) g^{-1} FW at the end of the night (EN) and ED, respectively, whilst Tre6P ranged from 0.10 to 0.40 nmol g^{-1} FW at EN and ED, respectively. This resulted in Tre6P:sucrose ratios of 0.12 at EN and 0.19 at ED, consistent with values previously reported for Col-0 rosettes grown under equinoctial conditions (Yadav et al., 2014) (Table 2.1). Qualitatively similar diel changes of sucrose and Tre6P accumulation were observed for *SnRK1α1-OE* and *sesquiα2* (Figure 2.1A-B). However, *SnRK1α1-OE* contained higher levels of both metabolites. The differences were significant at nine time points for Tre6P (Figure 2.1B), and at four for sucrose (Figure 2.1A). Importantly, the change in Tre6P was proportionally larger than that of sucrose (2- and 1.4-fold higher at ED and EN, respectively). This led to Tre6P:sucrose ratios that were 1.9- and 1.4-fold higher than in Col-0 at ED and EN, respectively, with the main cause for this being higher Tre6P levels (Table 2.1, ED: 2.4-fold, EN: 1.6-fold higher). In contrast, *sesquiα2* contained lower levels of both metabolites. The differences were significant at all the eleven time points for Tre6P (Figure 2.1B), but only at six for sucrose (Figure 2.1A). The change in Tre6P was again proportionally larger than that of sucrose (2.9- and 2.4-fold lower at ED and EN, respectively). This led to Tre6P:sucrose ratios that were 2.8- and 2.5-fold lower than in Col-0 at ED and EN, respectively, with the main cause for this being lower Tre6P levels (Table 1; ED: 3.5-fold, EN: 2.7-fold lower). Fructose and glucose showed very small and variable differences (Supplemental Figure 2.2).

The proposal that Tre6P is a signal of the sucrose status was originally prompted by the tight correlation observed between the levels of Tre6P and sucrose (Lunn et al., 2006). We therefore wondered whether manipulation of SnRK1 had any effect on the relationship between these two sugars and generated the corresponding sucrose-Tre6P regression plots to assess this. A strong positive correlation between Tre6P and sucrose was observed in all lines, with *R* values of 0.95, 0.94 and 0.86 in Col-0, *SnRK1α1-OE*, and *sesquiα2*, respectively (Figure 2.1C and Table 2.2). However, compared to Col-0, the slope of the regression was markedly lower in the *SnRK1α1-OE* and higher in the *sesquiα2* mutant.

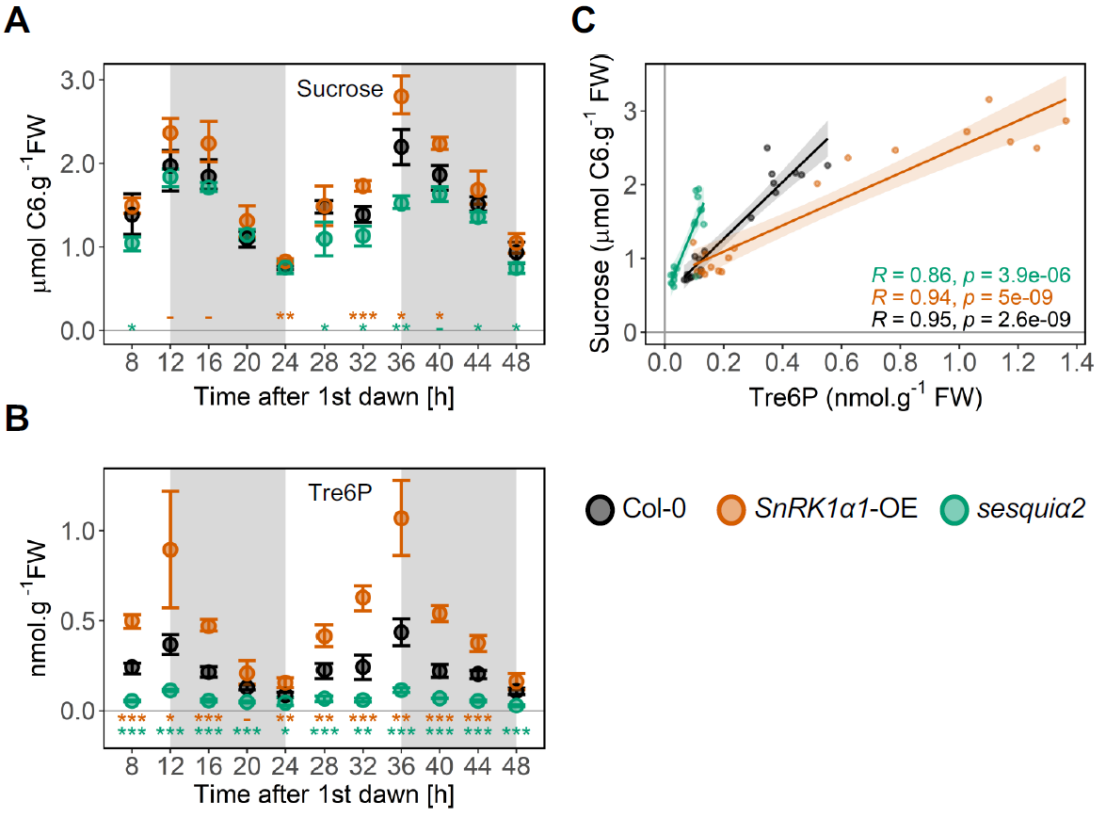

Figure 2.1 | Impact of SnRK1 on sucrose and Tre6P accumulation and relationship.
Sucrose **(A)** and Tre6P **(B)** levels were quantified from 20-day old Col-0, *SnRK1α1-OE*, and *sesquiα2* plants grown under a 12:12 photoperiod and harvested every 4 h. The night period is marked in grey. Graphs show the average of 4-5 biological replicates (each composed of a pool of 4-5 randomly sampled whole rosettes) at each time point, with error bars representing the 95% confidence interval. Asterisks denote statistically significant differences tested at each ZT for both genotypes separately (one-way ANOVA with Tukey's post-hoc test of honestly significant differences, HSD). (-), p<0.1 cases in which the Tukey's HSD resulted non-significant differences; (*), p<0.05; (**), p<0.01; (***), p<0.001. **C**, Impact of SnRK1 on the Tre6P-sucrose relationship. The Tre6P content of samples at the end of the day (ED, 12h and 36h after first dawn) and end of the night (EN, 24h and 48h after first dawn) was plotted against the corresponding values of sucrose. *R*, Pearson correlation coefficient. Sucrose levels correspond to hexose equivalents.

A previous study (Yadav et al., 2014) compared the diel levels of Tre6P and sucrose in three different photoperiods in plants constitutively expressing a bacterial TPS or TPP (*E. coli* OtsA or OtsB; *TPS-OE* and *TPP-OE*, respectively). We retrieved the data from the 12:12 photoperiod of this study and re-calculated the average values at ED and EN (Table 2.1). The Tre6P:sucrose ratios of *TPS-OE* were higher than those of Col-0, qualitatively resembling *SnRK1α1-OE* plants. However, the differences in *TPS-OE* plants were much more pronounced than in *SnRK1α1-OE* (8.4-fold and 21.2-fold higher than in Col-0 at ED and EN, respectively), and were due to lower sucrose as well as increased Tre6P. In *TPP-OE*, Tre6P:sucrose ratios were, like the *sesquiα2* mutant, lower than in Col-0 plants (2-fold and 1.5-fold lower than in Col-0 at ED and EN, respectively), and were exclusively due to high sucrose.

We next asked what could be the cause for the changed Tre6P levels in the SnRK1 mutants. The magnitude of the SnRK1-dependent change in Tre6P levels was smallest when sucrose content reached its minimum at EN (1.6-fold higher in *SnRK1α1-OE* and 2.7-fold lower in *sesquiα2* vs. Col-0), and largest when sucrose peaked at ED (2.4-fold higher in *SnRK1α1-OE* and 3.5-fold lower in *sesquiα2* vs. Col-0). This is clearly seen in the corresponding sucrose:Tre6P regression plots (Supplemental Figure 2.3A), and suggests that SnRK1 affects the sensitivity of Tre6P synthesis and/or degradation in response to sucrose, leading to sucrose hypersensitivity of Tre6P in *SnRK1α1-OE* and sucrose hyposensitivity of Tre6P in the *sesquiα2* mutant.

Table 2.1 | Impact of SnRK1 on Tre6P:sucrose ratios.
Ratios are means ± standard deviation and were calculated using only end of day (ED, 12h and 36h after first dawn), and end of night (EN, 24h and 48h after first dawn) time points. *p*-values refer to statistically significant differences (Student's *t*-test) between Col-0 and each of the indicated SnRK1 mutants. This data is graphically represented in Figure 2.1C, and uses the Tre6P and sucrose values of Figure 2.1A-B. The values previously obtained for plants with altered Tre6P accumulation (*TPS-OE* and TPP-OE, 12:12 photoperiod, EN and ED) by Yadav and colleagues (Yadav *et al.*, 2014) are also shown for comparison. FW, Fresh weight. Sucrose levels correspond to hexose equivalents.

Genotype	Time of day	Tre6P (nmol g^{-1} FW)	Suc (µmol g^{-1} FW)	Tre6P:Suc	*p*-value (*vs.* control)	Reference
Col-0	ED	0,401 ± 0,08	2,083 ± 0,28	0,195 ± 0,04	NA	Fig. 1 (*n*=8)
	EN	0,099 ± 0,02	0,843 ± 0,14	0,119 ± 0,03	NA	Fig. 1 (*n*=10)
SnRK1α1-OE	ED	0,981 ± 0,31	2,584 ± 0,34	0,376 ± 0,10	6,00E-04	Fig. 1 (*n*=8)
	EN	0,159 ± 0,05	0,939 ± 0,16	0,170 ± 0,04	1,15E-02	Fig. 1 (*n*=10)
sesquiα2	ED	0,114 ± 0,01	1,678 ± 0,20	0,069 ± 0,01	2,00E-04	Fig. 1 (*n*=8)
	EN	0,037± 0,02	0,749 ± 0,09	0,047 ± 0,03	3,00E-04	Fig. 1 (*n*=10)

Genotype	Time of day	Tre6P (nmol g^{-1} FW)	Suc (µmol g^{-1} FW)	Tre6P:Suc	*p*-value (*vs.* control)	Reference
Col-0	ED	0,417 ± 0,06	1,802 ± 0,29	0,232 ± 0,02	NA	Yadav *et al.* (*n*=5)
	EN	0,097 ± 0,01	0,729 ± 0,11	0,134 ± 0,00	NA	Yadav *et al.* (*n*=5)
TPS-OE	ED	2,388 ± 0,27	1,222 ± 0,11	1,955 ± 0,16	1,60E-02	Yadav *et al.* (*n*=4)
	EN	1,025 ± 0,34	0,362 ± 0,10	2,831 ± 0,53	7,90E-03	Yadav *et al.* (*n*=5)
TPP-OE	ED	0,399 ± 0,04	3,423 ± 0,52	0,118 ± 0,02	7,90E-03	Yadav *et al.* (*n*=5)
	EN	0,088 ± 0,02	0,995 ± 0,13	0,088 ± 0,01	7,90E-03	Yadav *et al.* (*n*=5)

To look further into the underlying mechanisms, we quantified the levels of TPS1, the predominant Tre6P-synthesizing enzyme in Arabidopsis (Delorge et al., 2015; Fichtner et al., 2020). Surprisingly, TPS1 levels were lower at ED in *SnRK1α1-OE* (Figure 2.2A), but no differences were observed at EN (Figure 2.2B). *TPS1* mRNA levels were unchanged (Supplemental Figure 2.3B). Given the high Tre6P accumulation of *SnRK1α1-OE*, decreased TPS1 levels could be due to product-mediated negative feedback, *via* translational regulation or stability of the TPS1 protein. For *sesquiα2*, no differences were observed compared to Col-0 (Figure 2.2C-D).

Collectively, these results show that Tre6P and sucrose are affected in the SnRK1 mutants. Furthermore, the responsiveness of Tre6P to changes in sucrose is also altered in these plants, suggesting that SnRK1 links sucrose to Tre6P synthesis and/or degradation through mechanisms other than TPS1 accumulation.

Table 2.2 | Impact of SnRK1 on the Tre6P-sucrose relationship.
The Tre6P content of Col-0, *SnRK1α1-OE*, and *sesquiα2* rosettes at end of the day (ED, 12h and 36h after first dawn), and end of night (EN, 24h and 48h after first dawn) was plotted against the corresponding values of sucrose. *R,* Pearson correlation coefficient. Slope, slopes of the corresponding Tre6P-sucrose regression curves (Figure 2.1C) Data previously obtained for the *TPS-OE* and *TPP-OE* lines by Yadav and colleagues (Yadav et al., 2014) are also shown for comparison.

Genotype	*R*	*p*-value	slope
Col-0	0,95	2,60E-09	3,80
SnRK1α1-OE	0,94	5,00E-09	1,80
sesquiα2	0,86	3,90E-06	9,70

Genotype	*R*	*p*-value	slope
Col-0 (Yadav *et al*.)	0,99	1,90E-07	3,40
TPS-OE (Yadav *et al*.)	0,97	1,90E-05	0,58
TPP-OE (Yadav *et al*.)	0,96	7,90E-06	7,70

2.3.2 Impact on diel starch turnover

In all genotypes, starch showed qualitatively similar diel changes, being accumulated and mobilized in a near-linear manner during the day and night, respectively, and almost fully exhausted at EN (Supplemental Figure 2.4A). However, starch levels were moderately but significantly higher in *SnRK1α1-OE* and lower in *sesquiα2*, particularly towards the ED (Supplemental Figure 2.4A). Accordingly, the rate of starch accumulation was significantly lower in *sesquiα2* compared to Col-0 (Supplemental Figure 2.4B). The rates of degradation mirrored those of starch accumulation in all the genotypes, consistent with starch mobilization being determined by the amount of starch reserves and the length of the night (Graf et al., 2010; Scialdone et al., 2013). The changes of starch and sucrose were qualitatively similar in the mutants (higher levels in *SnRK1α1-OE* and lower in *sesquiα2,* as compared to Col-0), but the changes of sucrose were larger than those of starch. Hence, the starch:sucrose ratio was lower in *SnRK1α1-OE* and higher in *sesquiα2* (Supplemental Figure 2.4C) with differences being most significant at ED, when sucrose levels are most divergent in these mutants. Altogether, this suggests decreased use of carbon in the *SnRK1α1-OE* and increased use of carbon in the *sesquiα2* mutant.

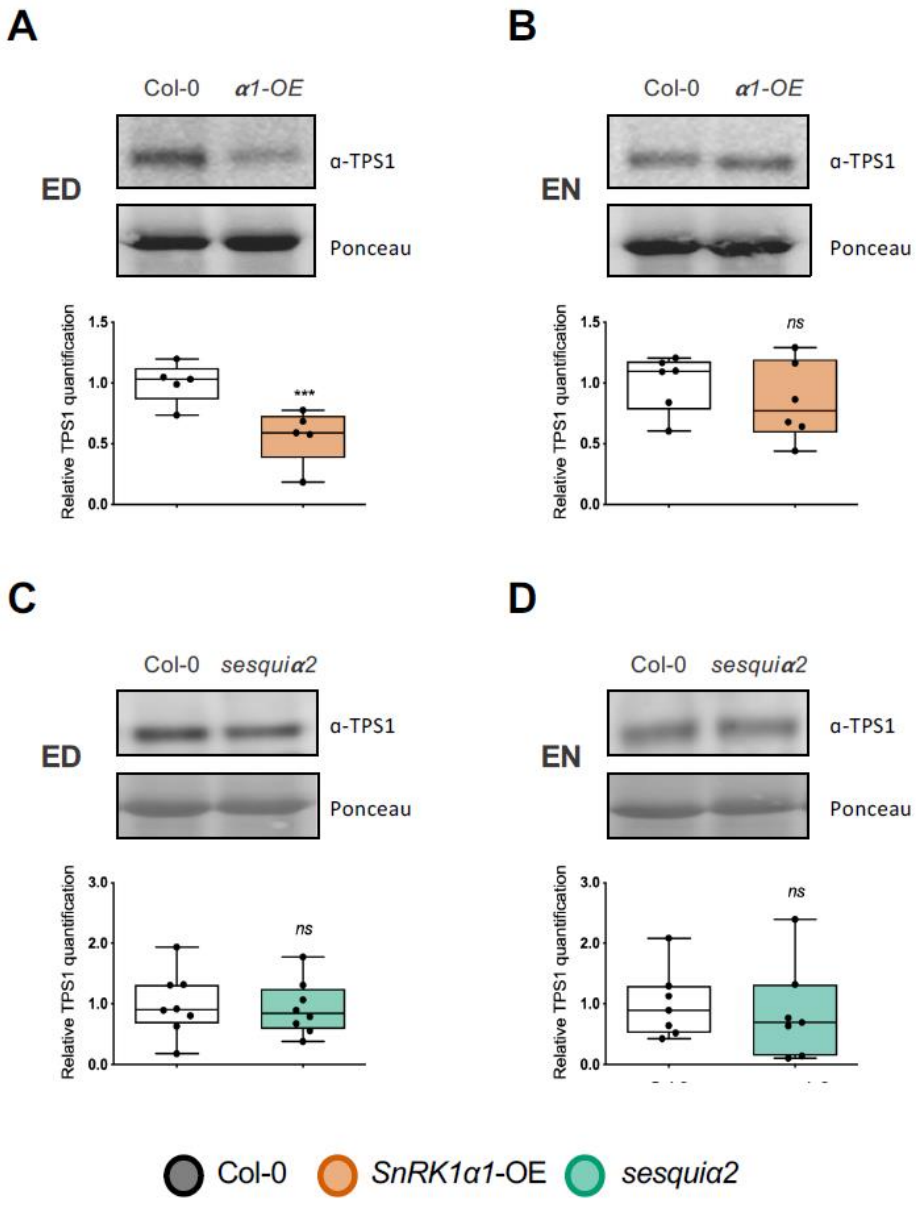

Figure 2.2 | Impact of SnRK1 on TPS1 protein accumulation.
Levels of TPS1 protein were quantified by immunoblot analyses in Col-0 control plants and *SnRK1α1-OE* **(A, B)** and *sesquiα2* **(C, D)** mutants at ED **(A, C)** and EN **(B, D)**. Upper panels, representative immunoblots for the TPS1 protein. Lower panels, boxplots representing a minimum of 4 biological replicates (each consisting of a pool of 3 randomly harvested rosettes). Lower and upper box boundaries represent the first and third quantiles, respectively, horizontal lines mark the median and whiskers mark the highest and lowest values. Dots represent individual datapoints. *p*-values denote statistically significant differences between SnRK1 mutants and Col-0 at the indicated times of the day (paired *t*-test); (*ns*), non-significant; (***), $p<0.001$.

2.3.3 Impact on sugar phosphates and organic acids

The levels of sugar phosphates and glycolytic intermediates tended to be lower in *sesquiα2* than in Col-0, in particular in the case of Fru6P and 3-PGA, for which differences were significant at four and five time points, respectively (Figure 2.3A; Supplemental Table 2.1D-E). For Glc6P and PEP, differences reached significance only at two time points. In the case of organic acids, citrate, aconitate, and isocitrate accumulated to significantly higher levels in *sesquiα2* at four, eleven, and ten time points, respectively. Remarkably, an opposite pattern was observed for succinate, which was significantly decreased in *sesquiα2* at ten time points. For 2-OG, a subtle yet significant reduction was also visible at two time points. Malate and fumarate showed inconsistent and mostly non-significant alterations. A significant and marked increase in total protein accumulation was also observed in *sesquiα2* at all eleven time points (Figure 2.3B)

In *SnRK1α1-OE*, the levels of sugar phosphates, glycolytic intermediates, TCA cycle intermediates and total protein were mostly similar to Col-0. The only exception was 2-OG, which accumulated to significantly lower levels in *SnRK1α1-OE* at four time points (Figure 2.3A-B; Supplemental Table 2.1B-C).

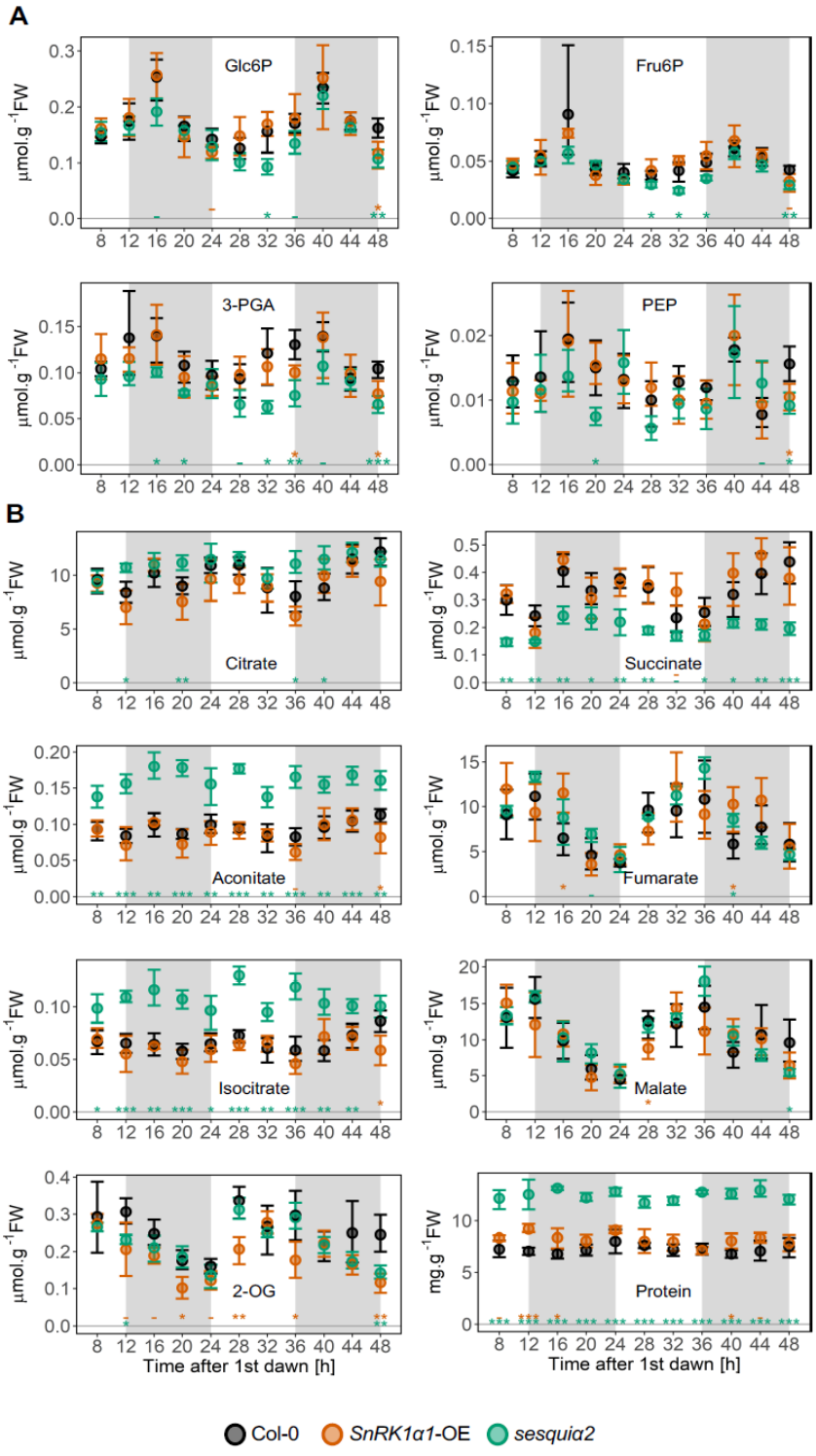

Figure 2.3 | Impact of SnRK1 on the levels of glycolytic and TCA cycle intermediates and total protein.
Levels of glycolytic intermediates **(A),** TCA cycle intermediates, and total protein **(B)** were quantified

from 20-day old Col-0, *SnRK1α1-OE*, and *sesquiα2* plants grown under a 12:12 photoperiod and harvested every 4 h. The night period is marked in grey. Graphs show average values for the same samples as Fig. 1 (n=4-5 biological replicates, each composed of a pool of 4-5 randomly sampled whole rosettes at each time point), with error bars representing the 95% confidence interval. Asterisks denote statistically significant differences tested at each ZT for both genotypes separately (one-way ANOVA with Tukey HSD post-hoc test); (-), p<0.1 cases in which the Tukey's HSD resulted non-significant differences; (*), p<0.05; (**), p<0.01; (***), p<0.001. G6P, glucose 6-phosphate; F6P, fructose 6-phosphate; 3-PGA, 3-phosphoglycerate; PEP, phosphoenolpyruvate 2-OG, 2-oxoglutarate.

2.3.4 Impact on *the transcriptome*

To investigate the relevance of SnRK1 for gene expression during the regular diel cycle, we extracted RNA from the samples collected for metabolite quantification at ED and EN (three replicates per genotype and condition; Supplemental Figure 2.1B) and performed RNA sequencing (RNA-seq) analyses. Volcano plots show differentially expressed genes for each pairwise comparison [*SnRK1α1-OE* vs. Col-0 and *sesquiα2* vs. Col-0] and time point (FDR<0.05), revealing the greatest differences, by far, for *sesquiα2* at EN (Figure 2.4). For all subsequent comparisons we considered as differentially expressed genes (DEGs) those with an absolute logFC equal or greater than 1 (ABSlogFC≥1; two-fold change).

The *SnRK1α1-OE* mutant showed mild defects in transcript abundance, with only 24 (19 up- and 5 downregulated) and 15 (10 up- and 5 downregulated) DEGs at ED and EN, respectively (Figure 2.4A-B; Supplemental Table 2.2A-D). These genes showed very poor overlap with those induced by transient SnRK1α1 overexpression in protoplasts (Baena-González et al., 2007), with only At3g62550 (an adenine nucleotide alpha hydrolase-like protein), being induced in both conditions. This suggests that constitutive *SnRK1α1* overexpression in plants may trigger negative feedback mechanisms to attenuate SnRK1 activity.

We used MapMan (Thimm et al., 2004; Schwacke et al., 2019) categorization to assign these genes to specific MapMan BIN codes. At ED, from the genes upregulated in *SnRK1α1-OE* and with an assigned function, the largest differences were observed for *QQS*, involved in the C:N balance (Li et al., 2015) and for *CSLA1*, a cellulose synthase like gene. Additional upregulated genes included the iron responsive *IRP3* (Rodríguez-Celma et al., 2013). From the downregulated genes

with assigned functions, the most prominent ones encoded a cyclophilin (*CYP21-2*)

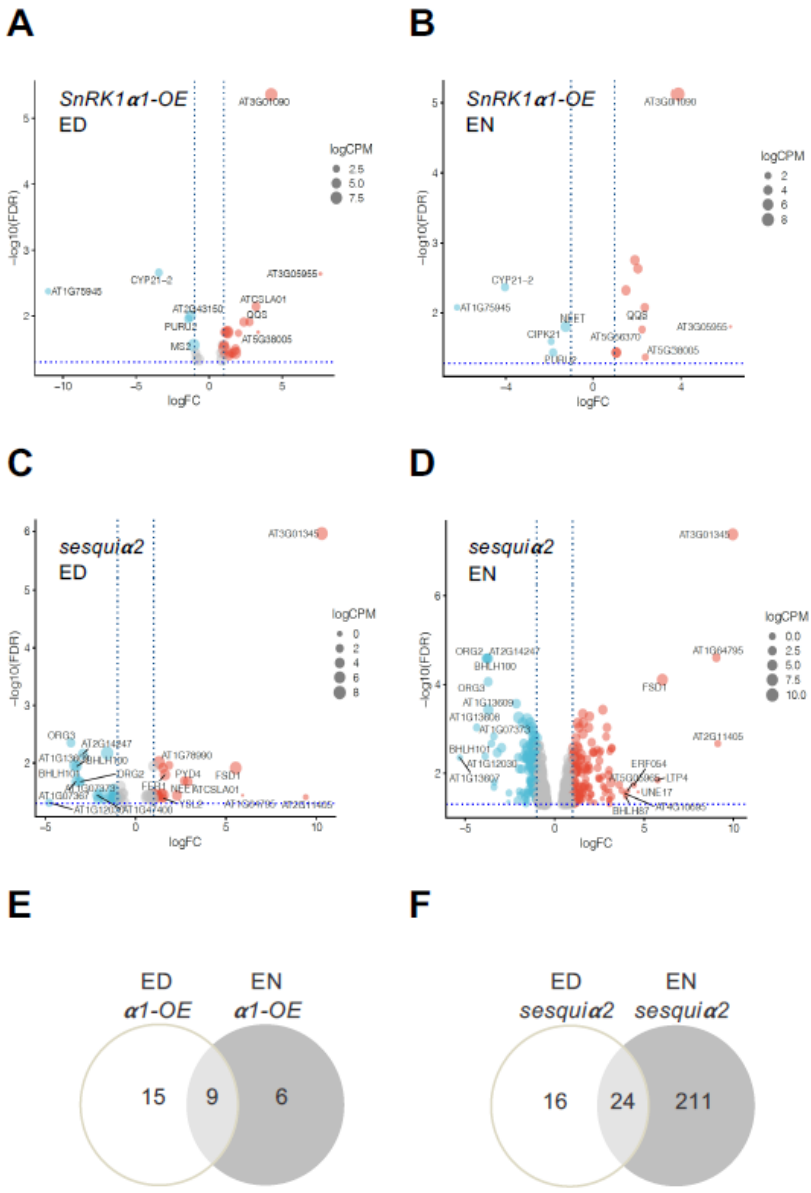

Figure 2.4 | Impact of SnRK1 on the transcriptome.
Volcano plot representation of RNA-seq analyses of the *SnRK1α1-OE* **(A, B)** and *sesquiα2* **(C, D)** mutants in comparison to Col-0 plants at the end of the day [ED, **(A, C)**] and end of the night [EN, **(B, D)**]. Up- and downregulated genes are reported as red and light blue dots, respectively. Grey dots represent genes whose differential expression is considered not significant [absolute $\log_2$ FC≤1, vertical dotted blue lines, and FDR≥0.05, horizontal dotted blue line]. Comparison of the DEG lists for the *SnRK1α1-OE* **(E)** and *sesquiα2* **(F)** mutants reveals genes that are similarly affected at the ED and EN time points.

and a 10-formyl tetrahydrofolate deformylase essential for photorespiration [*PURU2*, (Collakova *et al.*, 2008)].

Eight of the genes that were differentially expressed at ED were also differentially expressed at EN (Supplemental Table 2.3A; Figure 2.4E), suggesting SnRK1α1 overexpression causes constitutive defects in their expression. Five of these were upregulated in *SnRK1α1-OE*, including *QQS,* and the other three were strongly repressed, including *PURU2* and *CYP21-2*. Only six genes were differentially expressed in *SnRK1α1-OE* specifically at EN, including the downregulated gene *NEET*, which encodes a protein crucial for iron homeostasis (Nechushtai et al., 2012).

For the *sesquiα2* mutant, we identified a total of 40 DEGs at ED (18 up- and 22 downregulated) and 235 DEGs at EN (129 up- and 106 downregulated) (Figure 2.4C-D; Supplemental Table 2.2G-H). From the genes differentially expressed at ED, 60% showed also differential expression at EN (Supplemental Table 2.3B, Figure 2.4F), pointing to constitutive defects due to SnRK1 depletion. We analysed these DEGs with AgriGOv2 (Tian et al., 2017) and found a significant overrepresentation of 16 functional categories, with the top GO category being *iron ion homeostasis* (*p*=4.10E-10; Supplemental Table 2.4A). For the genes that were differentially expressed only in the EN or ED conditions, the top categories were *response to endogenous stimulus* (*p*=3.50E-12; Supplemental Table 2.4B), and *chemical homeostasis* (*p*=1.20E-06; Table S4C), respectively.

From the 24 genes affected in *sesquiα2* both at ED and EN, 11 are part of a conserved set of genes responding to iron deficiency in leaves and roots (Rodríguez-Celma et al., 2013) (Table 2.3). In all cases, genes downregulated in the *sesquiα2* are induced by iron deficiency whilst those upregulated in the *sesquiα2* are repressed by iron deficiency. Although not comprised in the list of iron core response genes (Table 2.3), depletion of SnRK1 led to defects both at EN and ED in other iron-responsive genes (Supplemental Table 2.2E-H), including *IMA3, IMA4, IMA6*, *bHLH101*, and *YSL2*. Other iron-responsive genes were affected specifically at EN

(e.g. *NAS1, NAS3, ZIP5,* and *IRT3*), or at ED (e.g *NEET*, *HEMA1* and *ZIF1*), altogether suggesting an iron excess response in the *sesquiα2* mutant.

Table 2.3 | Expression of genes related to iron acquisition and metabolism in the *SnRK1* mutants. Expression levels of 17 core genes responsive to iron in both leaves and roots (Rodriguez-Celma et al., 2013; Table 2.1) in the indicated genotypes at ED and EN. The response of these genes to iron deficiency is indicated for comparison (UP, upregulated; DOWN, downregulated compared to control conditions). None of these genes were retrieved as DEGs in the *SnRK1α1-OE* at EN (not shown). Numbers indicate log2 ratios of *sesquiα2* compared to the Col-0 control.

ID	Symbol	Description	Response to Fe deficiency (1)	sesquiα2 EN	sesquiα2 ED	SnRK1α1-OE ED
AT1G47400	IRP1/IMA1	Iron-responsive protein	UP	-3,20	-2,12	-
AT1G47395	IRP2/IMA2	Iron-responsive protein	UP	-2,07	-2,95	-
AT2G14247	IRP3	Iron-responsive protein	UP	-3,70	-2,91	1,03
AT1G13609	IRP4	Iron-responsive protein	UP	-3,70	-3,38	-
AT3G56360	IRP5	Iron-responsive protein	UP	-	-	-
AT5G05250	IRP6	Iron-responsive protein	UP	-1,57	-1,22	-
AT3G56970	ORG2/bHLH38	Basic helix-loop-helix protein	UP	-3,83	-3,04	-
AT3G56980	ORG3/bHLH39	Basic helix-loop-helix protein	UP	-3,71	-3,58	-
AT2G41240	bHLH100	Basic helix-loop-helix protein	UP	-3,76	-3,25	-
AT1G23020	FRO3	Ferric reduction oxidase	UP	-1,53	-1,92	-
AT4G16370	OPT3	Oligopeptidetransporter	UP	-	-	-
AT5G53450	ORG1/PAP14	OBP3-responsive gene	UP	-1,11	-1,57	-
AT1G56430	NAS4	Nicotine amine synthase	UP	-	-1,34	-
AT4G08390	SAPX	Stromal ascorbate peroxidase	DOWN	-	-	-
AT4G25100	FSD1	Fe superoxide dismutase 1	DOWN	6,02	5,53	-
AT5G01600	DFER1	Ferritin1	DOWN	-	1,63	-
AT1G48300	DGAT3	Diacylglycerol acyltransferase	DOWN	-	-	-

(1) Rodriguez-Celma et al. 2013

At ED only a few genes unrelated to iron metabolism were affected in *sesquiα2* (Supplemental Table 2.2E-F), including *CSLA1*, which was surprisingly upregulated as in the *SnRK1α1-OE.*

At EN, a clear impact was also observed in sulphur-responsive genes (Supplemental Table 2.2G-H). From the 20 genes reported to be most responsive to sulphur deprivation in leaves (Forieri *et al.*, 2017), eight were affected in the *sesquiα2* rosettes (Table 2.4). These genes are induced by sulphur deprivation and, in all but one of the cases (At1g12030), they were upregulated in the *sesquiα2* mutant. In addition, *RVE2*, repressed by sulphur deficiency in roots (Forieri *et al.*,

2017), was downregulated in the *sesquiα2,* altogether suggesting a sulphur starvation response when SnRK1 is depleted.

Table 2.4 | Expression of genes related to sulfur acquisition and metabolism in the *sesquiα2* mutant.
Expression levels of genes reported to be most responsive to sulfur deprivation (Forieri et al., 2017; Table S4) in the *sesquiα2* mutant at ED and EN. Numbers indicate log2 ratios of *sesquiα2* compared to the Col-0 control.

ID	Symbol	Description	Response to S deficiency (1)	*sesquiα2* ED	*sesquiα2* EN
AT5G48850	*ATSDI1*	SULFUR DEFICIENCY-INDUCED 1	UP (leaves)	-	1,95
AT3G49580	*LSU1*	RESPONSE TO LOW SULFUR 1	UP (leaves)	-	2,14
AT3G49570	*LSU3*	RESPONSE TO LOW SULFUR 3	UP (leaves)	-	2,17
AT5G26220	*GGCT2;1*	GAMMA-GLUTAMYL CYCLOTRANSFERASE 2;1	UP (leaves)	-	2,21
AT3G08860	*PYD4*	PYRIMIDINE 4	UP (leaves)	2,69	3,21
AT4G35640	*SERAT3;2*	SERINE ACETYLTRANSFERASE 3;2	UP (leaves)	-	1,04
AT4G31330		Putative transmembrane protein (DUF599)	UP (leaves)	-	1,21
AT1G12030		Putative phosphoenolpyruvate carboxylase (DUF506)	UP (leaves)	-4,78	-3,88
AT5G37260	*RVE2*	REVEILLE 2	DOWN (roots)	-	-1,25

(1) Forieri et al. 2017

Despite the metabolic differences caused by SnRK1 depletion in *sesquiα2* plants (Figure 2.1 and Figure 2.3), transcripts related to primary metabolism remained mostly unaffected, with the exception of *TPPD*, *TPPG*, *TPPJ* and *TPPH*, which were all upregulated at EN. Given the potential relevance of this finding for the observed Tre6P phenotype (Figure 2.1B), we sought to confirm these results for selected *TPP* genes by quantitative RT-PCR (qPCR), including also the ED and the *SnRK1α1-OE* samples (Supplemental Figure 2.5A). These analyses corroborated the RNAseq results, revealing a significant upregulation of *TPPG*, *TPPH*, and *TPPJ* in *sesquiα2* specifically at EN. In the *SnRK1α1-OE* mutant, these *TPP* genes were in most cases mildly downregulated compared to Col-0 but the differences did not reach statistical significance

We noticed a significant overlap between the genes downregulated in *sesquiα2* at EN and those previously reported to be induced by transient SnRK1α1 overexpression in protoplasts (Baena-González et al., 2007) (Figure 2.5A; p =1.93E-13, hypergeometric test). To confirm this, we analyzed several of the overlapping genes (*BGAL4*, *DIN10*, and *PYL5*) by quantitative RT-PCR (qPCR), including also the ED and the *SnRK1α1-OE* samples (Figure 2.5B). As controls, we included genes that were affected specifically in *SnRK1α1-OE* or *sesquiα2* in both time points (Supplemental Figure 2.5B). These analyses revealed lower expression of *BGAL4*, *DIN10*, and *PYL5* in the *sesquiα2* mutant at EN compared to Col-0, confirming the RNAseq results (Figure 2.5B). Interestingly, in Col-0, these genes had low expression at ED but were induced at EN, consistent with their activation by SnRK1α1 overexpression (Baena-González et al., 2007). Furthermore, at ED, these genes tended to have higher expression in *SnRK1α1-OE* than in Col-0, although differences were not significant. Other genes originally identified as markers of SnRK1 signaling (Baena-González et al., 2007) showed a similar pattern of expression, but the differences were again small, explaining why they were not retrieved as DEGs in the RNAseq analysis (Supplemental Figure 2.5C). To assess more broadly the behavior of the DEGs downregulated in *sesquiα2* at EN, we compared their expression levels in *SnRK1α1-OE vs*. Col-0 at ED and in Col-0 at EN *vs*. ED (Figure 2.5C). In general, all of these genes showed a mild upregulation in *SnRK1α1-OE* at ED. However, they fell into two distinct groups with regard to their expression in Col-0. Group A included genes like *BGAL4*, *DIN10*, and *PYL5* (blue asterisks in Figure 2.5C), with higher expression at EN than at ED in Col-0 and with decreased levels at EN in *sesquiα2* compared to Col-0. This suggests that SnRK1 is normally activated towards the EN, triggering amongst others the induction of these genes. Group B contained many of the genes previously identified as iron-responsive (Table 2.3; grey asterisks in Figure 2.5C). Their expression was higher at ED than at EN in Col-0, but they appeared to be constitutively downregulated in *sesquiα2* (EN and ED). This suggests that the effect of SnRK1 on these genes is more indirect than on Group A genes, and is also independent of time-of-day.

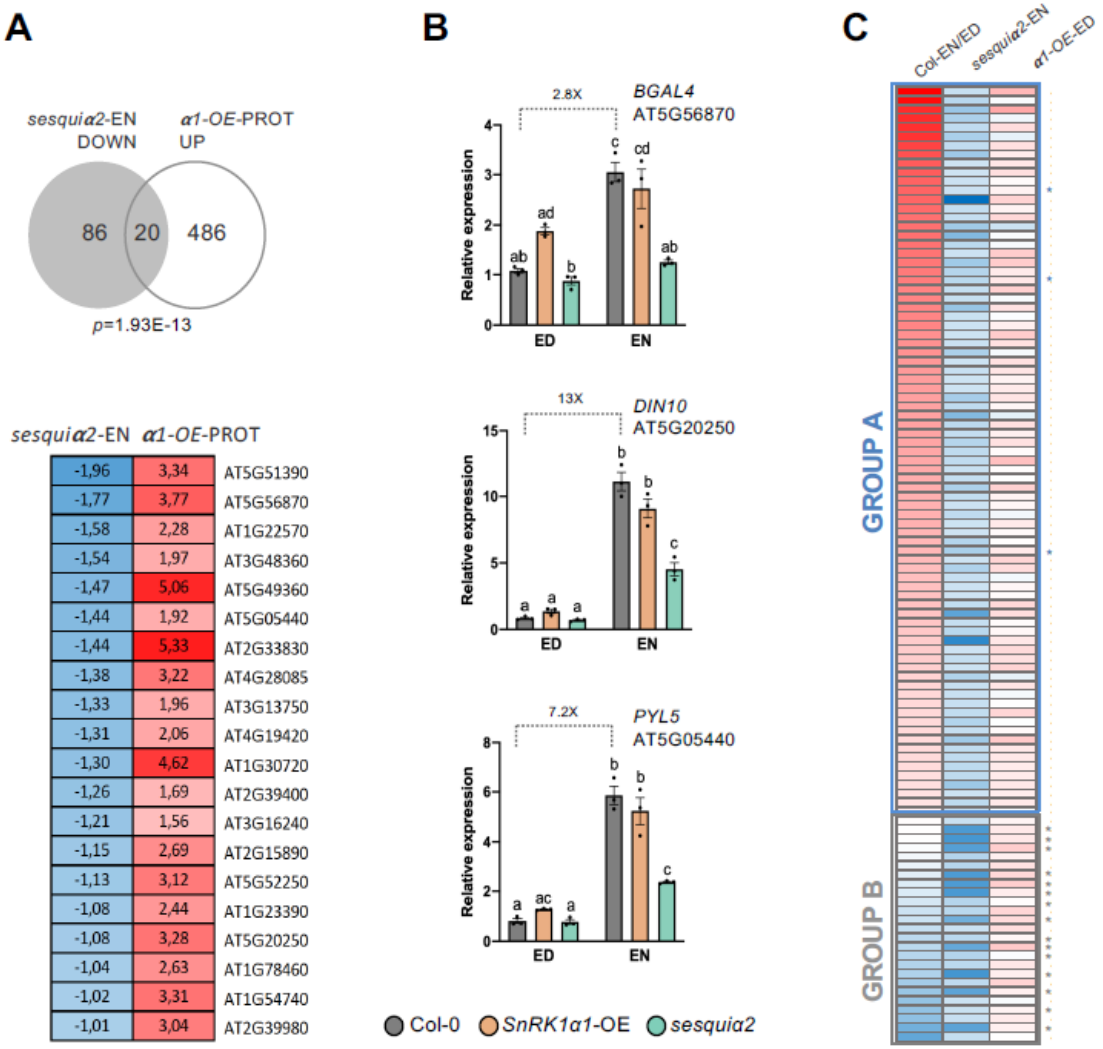

Figure 2.5 | Basal expression of SnRK1-regulated genes at the end of the day (ED) and night (EN) periods.

A, Upper panel, overlap of genes downregulated in the *sesquiα2* mutant at EN ("*sesquiα2*-EN DOWN") and those induced by transient SnRK1α1 overexpression in protoplasts ("α1-OE-PROT UP") (Baena-González et al., 2007). *p*-value denotes statistical significance (hypergeometric test). Lower panel, expression values (log_2FC) of the overlapping genes in each of the indicated datasets. Red indicates upregulation and blue, downregulation. **B**, qPCR analyses of genes (*BGAL4*, *DIN10*, and *PYL5*) from the overlapping set in **(A)** in rosettes of the indicated genotypes at ED and EN. Graphs correspond to the average of 3 independent experiments (error bars, SEM). Letters indicate significantly different groups assessed using the ANOVA and Tukey's HSD post-test. **C**, Genes downregulated in the *sesquiα2* mutant at EN ("*sesquiα2*-EN DOWN") are mildly upregulated in *SnRK1α1-OE* at ED. In Col-0, many of these genes are upregulated at EN *vs.* ED (Group A, blue rectangle; asterisks correspond to *BGAL4*, *DIN10*, and *PYL5*). A smaller group of genes show either unchanged or lower expression in Col-0 at EN *vs.* ED (Group B, grey rectangle). Asterisks correspond to the following genes, retrieved as DEGs in *sesquiα2* at ED (see Supplemental Table 2.3B): *IMA1/IRP1, IMA2/IRP2, IMA3, IMA4, IMA6, IRP3, IRP4, IRP6, PAP14/ORG1, BHLH38/ORG2, BHLH39/ORG3, BHLH100, BHLH101, FRO3,* AT1G12030.

2.3.5 Diel fluctuations in Tre6P levels modulate SnRK1 activity

The expression of Group A genes was highest when Tre6P levels are low at EN and lowest when Tre6P levels are high at ED (Figure 2.5B-C and Figure 2.1B), prompting the hypothesis that Tre6P build-up during the day inhibits SnRK1 activity at ED. If true, we reasoned that inducing Tre6P accumulation should repress these genes during the day. To test this, we used an ethanol inducible OtsA (iOtsA) line in which OtsA expression drives Tre6P production, and an AlcR control line, harboring the corresponding empty vector (Martins et al., 2013). AlcR and iOtsA plants were sprayed with ethanol at ZT0 or ZT6 and harvested 6 h later, at ZT6 (middle of the day, MD) and ZT12 (end of the day, EN). Expression of OtsA in all iOtsA samples was confirmed by qPCR (Figure 2.6A) Group A genes had higher expression in the AlcR control line at MD than at ED (Figure 2.6B) , showing that the high expression uncovered in the RNAseq analyses for Col-0 at EN extends into the first half of the day. However, the differences between EN and ED (Figure 2.5B) were clearly larger than those between MD and ED (Figure 2.6B), supporting the idea that these genes are increasingly repressed as the day progresses. In contrast, OtsA induction in the iOtsA line resulted in a marked repression of these genes (Figure 2.6B). The repression tended to be larger at MD, when the expression of these genes in the AlcR control line was higher, but was also visible at ED. For genes whose expression was already very low towards the ED, Tre6P accumulation did not have any further repressive effect (Supplemental Figure 2.5D).

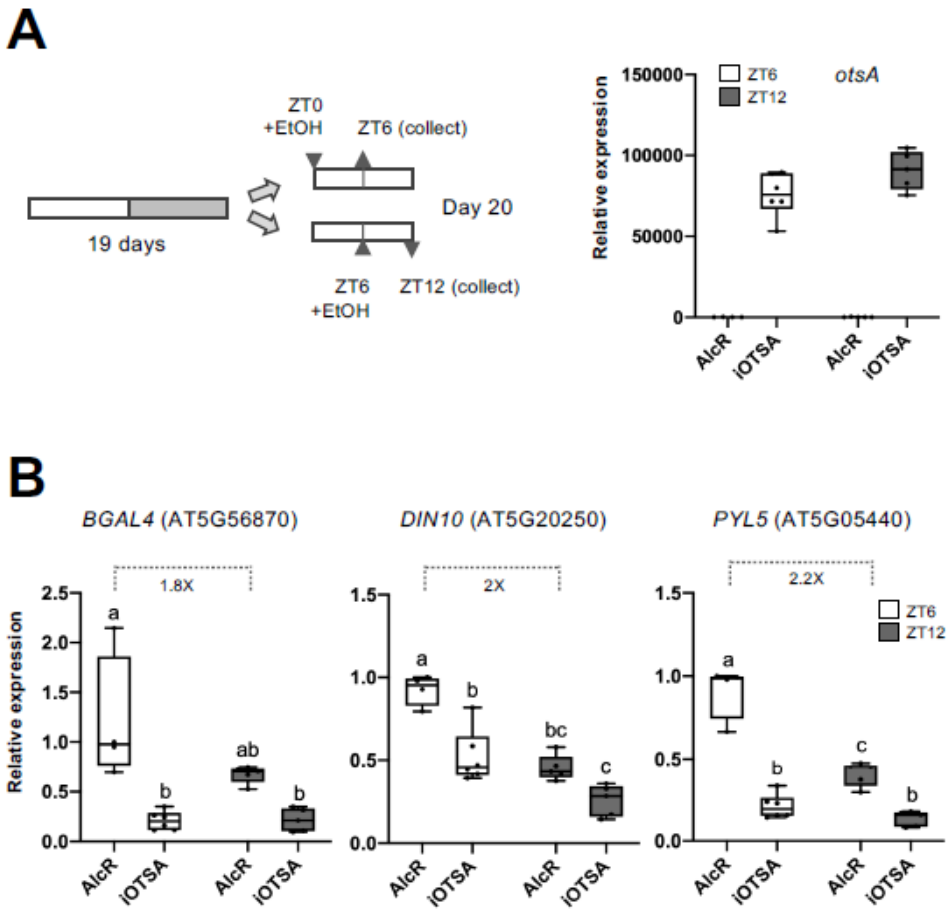

Figure 2.6 | Impact of Tre6P on the basal expression of SnRK1-regulated genes.
A, Induction of otsA expression in an ethanol-inducible line (iOtsA) and the corresponding empty vector control (AlcR). Plants were grown on soil, under a 12:12 photoperiod for 19d. Ethanol (2% v/v) was sprayed over the plants at ZT0 or at ZT6 and whole rosettes were harvested after 6h (ZT6 and ZT12 indicate the time of harvest) for qPCR analyses of otsA (A, right panel) and of the same set of SnRK1 marker genes as in Figure 2.5B **(B)**. Values denote expression relative to the ZT6 time point of the AlcR line. Boxplots represent 4-5 biological replicates (each consisting of a pool of 3 randomly harvested rosettes). Lower and upper box boundaries represent the first and third quantiles, respectively, horizontal lines mark the median and whiskers mark the highest and lowest values. Dots represent individual datapoints. Different letters indicate statistically significant differences (p<0.05, one-way ANOVA with Tukey HSD test).

2.4 Discussion

Our results show that SnRK1 plays important functions in the regulation of sucrose homeostasis and the transcriptome under standard laboratory growth conditions that are favourable for Arabidopsis. They further suggest that diel oscillations in Tre6P levels contribute to the regulation of basal SnRK1 activities during the regular day-night cycle, consistent with a recent study linking diel oscillations in sucrose and SnRK1 activity with rhythms of nitrogen accumulation in maize seeds (Li et al., 2020).

2.4.1 SnRK1 modulates the Tre6P-sucrose relationship

According to the sucrose-Tre6P nexus model, Tre6P is essential for sucrose homeostasis, acting both as a signal of sucrose availability, and as a feedback regulator of sucrose production and consumption (Yadav et al., 2014; Figueroa and Lunn, 2016). The ratio of Tre6P:sucrose is important for maintaining sucrose levels within an adequate range, with high Tre6P:sucrose ratios in actively growing tissues being thought to promote sucrose utilization and import (Lunn et al., 2014; Yadav et al., 2014; Fichtner and Lunn, 2021). In our study with Arabidopsis rosettes, SnRK1α1 overexpression and depletion resulted in increased and decreased Tre6P:sucrose ratios, respectively (Table 2.1) . Whilst being initially surprising in view of the known growth-inhibitory functions of SnRK1, these results are not unexpected because SnRK1 is also required for growth (Margalha et al., 2019; Baena-González and Lunn, 2020).

Although Tre6P and sucrose were still highly correlated in the SnRK1 mutants (Figure 2.1C), their relationship was clearly altered, as evidenced by the slopes of the Tre6P:sucrose regression lines (Table 2.2). SnRK1α1 overexpression may cause “Tre6P hyposensitivity” partly by blocking the effect of Tre6P on sucrose metabolism, as suggested by the rather weak effect of high Tre6P on organic acid levels in *SnRK1α1-OE* (Table 2.1; Figure 2.3B). Conversely, SnRK1α depletion may

cause “Tre6P hypersensitivity”, allowing changes in sucrose metabolism in response to Tre6P levels that are lower than in control plants. Accordingly, we observed an enhanced accumulation of citrate, aconitate, and isocitrate in *sesquiα2* (Figure 2.3B), suggesting that the flux of photoassimilates into the TCA cycle increases when SnRK1 is depleted. Although enhanced accumulation of these organic acids could also result from their decreased consumption, the fact that total protein content is higher in the *sesquiα2* mutant argues that this may not be the case (see below for further discussion). An enhanced flux of photoassimilates into the TCA cycle is the opposite of what would be expected for a plant with low Tre6P, given the increased organic acid content of iOtsA lines with elevated Tre6P (Figueroa et al., 2016), and may indicate that the reported effects of Tre6P on sucrose utilization rely at least partly on inhibition of SnRK1. This may involve stimulation of anaplerotic reactions through PEPC, as shown for Tre6P (Figueroa et al., 2016), but could also involve alternative or additional mechanisms. Interestingly, TCA cycle intermediates were not equally affected in the *sesquiα2* mutant. The higher levels of citrate, aconitate, and isocitrate, and the lower levels of 2-OG and, in particular succinate, suggest an increased diversion of 2-OG towards nitrogen assimilation and/or photorespiration. This is consistent with the known inhibitory effect of SnRK1 on NR activity (Sugden et al., 1999; Jossier et al., 2009; Li et al., 2009) and the higher total protein content of *sesquiα2* (Figure 2.3B). The observed downregulation of *PURU2,* essential for photorespiration (Collakova et al., 2008), in the *SnRK1α1-OE* mutant, may on the other hand support a link between SnRK1 and photorespiration.

Our results with the *sesquiα2* mutant are in agreement with the low sucrose and high organic acid content reported for an inducible *snrk1* knockdown during an extended night treatment (Nukarinen et al., 2016). However, they are opposite to those reported for silenced SnRK1 in pea embryos, potentially due to differences between source and sink tissues or to secondary effects derived from severe SnRK1 depletion and consequent embryo growth arrest (Radchuk et al., 2006; Radchuk et al., 2010). Opposite effects on sucrose and organic acids were also reported for a *snrk1β1* mutant (Wang et al., 2020). However, whether these effects are caused by

the lack of SnRK1β1 itself or from compensatory effects from other β-subunits, remains to be determined.

Although SnRK1 had a strong impact on sucrose and especially on Tre6P, it had a much smaller effect on starch, suggesting that the latter is an indirect effect. The slight but significantly higher starch in *SnRK1α1-OE* and lower starch in *sesquiα2* (Supplemental Figure 2.4A-B) is consistent with decreased and increased use of fixed carbon, respectively, and might reflect restricted starch mobilization by elevated Tre6P in *SnRK1α1-OE* and faster mobilization in *sesquiα2,* with lower Tre6P. The fact that we actually observed the opposite (slower starch mobilization in *sesquiα2*; Supplemental Figure 2.4B), may suggest that SnRK1 mediates the effects of Tre6P on starch mobilization. Alternatively, these effects on the rate of starch mobilization may be unrelated to Tre6P and simply mirror changes in the amount of starch accumulated during the day (Scialdone et al., 2013). The faster starch accumulation in *SnRK1α1-OE* and slower starch accumulation in *sesquiα2* might itself be an indirect response to the higher and lower sucrose levels. It is well-established that sucrose synthesis is subject to feedback regulation mediated by post-translational inhibition of sucrose-phosphate synthase, recycling of sucrose *via* reducing sugar to hexose phosphates, and an increase in the level of fructose 2,6-bisphosphate which inhibits cytosolic fructose-1,6.bisphophase (Stitt et al., 2010). This results in increased allocation to starch when sucrose is high.

2.4.2 SnRK1 modulates the sucrose-Tre6P relationship

The main cause for the altered Tre6P:sucrose ratios of the SnRK1 mutants was a change in Tre6P level (Figure 2.1A-B; Table 2.1). Furthermore, Tre6P accumulation was not constitutively altered in the SnRK1 mutants but instead followed the dynamics of sucrose accumulation with a modified relationship. This observation points to SnRK1 being an important part of the regulatory network that connects Tre6P levels to the sucrose status. Thus, increased SnRK1 activity (as in *SnRK1α1-OE*) leads to sucrose hypersensitivity and a proportionally higher level of

Tre6P than in Col-0 plants for the same amount of sucrose, and decreased SnRK1 activity (as in *sesquiα2*) leads to the opposite behavior. Such interpretation is in accordance with the sugar hypersensitivity of *SnRK1α1-OE* seedlings during early development, manifested as delayed germination and reduced growth under sugar concentrations that do not affect the wild-type (Baena-González et al., 2007; Rodrigues et al., 2013).

It is presently unclear how information on the sucrose status is conveyed *via* SnRK1 and other routes to regulate Tre6P levels, but could potentially involve altered Tre6P synthesis by TPS1, altered Tre6P dephosphorylation by TPP proteins or both. The modified Tre6P content of SnRK1 mutants could not be explained by changes in TPS1 protein abundance, which was unaltered or even decreased in the case of *SnRK1α1-OE* (Figure 2.2). Thus, if Tre6P accumulation is primarily determined by TPS1 activity, other mechanisms may be involved, such as synthesis of additional uncharacterized proteins or post-translational modification of TPS1 (Yadav et al., 2014; Fichtner et al., 2020). The lower TPS1 protein abundance in *SnRK1α1-OE* at ED (Figure 2.2A) suggests that the high Tre6P in this mutant may trigger negative feedback regulation on TPS1 *via* translational regulation or stability of the TPS1 protein. Such mechanisms might become apparent only when plants are exposed to high Tre6P levels over long periods, as in *SnRK1α1-OE,* because Tre6P accumulation in response to sucrose treatment did not alter TPS1 abundance within 3 h of supplying sucrose (Yadav et al., 2014). Although the low Tre6P levels of *sesquiα2* were accompanied by increased expression of four *TPP* genes at EN (Supplemental Table 2.2G and Supplemental Figure 2.5A), *SnRK1α1-OE* plants showed only mild non-significant downregulation of *TPP* expression (Supplemental Figure 2.5A). This suggests that transcriptional regulation of TPPs may not be the main mechanism by which SnRK1 affects Tre6P levels. Analyses of TPP protein abundance and activity in *SnRK1α1-OE* and *sesquiα2* mutants will therefore be needed in the future to assess if altered TPP activities contribute to the altered accumulation of Tre6P in these lines.

2.4.3 SnRK1 impacts iron and sulphur metabolism genes

Very few of the DEGs in the SnRK1 mutants were related to metabolism, suggesting that the metabolic alterations observed in these plants involve post-transcriptional rather than transcriptional regulation. By contrast, SnRK1 had a profound impact on genes related to iron and sulphur acquisition and homeostasis, with iron metabolism genes being strongly downregulated in *sesquiα2* plants both at ED and EN and sulphur metabolism genes being upregulated in *sesquiα2* plants at EN.

Iron acquisition and metabolism are repressed by sulphur deprivation and *vice versa*, possibly as a way to coordinate the synthesis of Fe-S clusters (Forieri et al., 2013; Forieri et al., 2017; Mendoza-Cózatl et al., 2019). Considering this, our interpretation is that in the *sesquiα2* mutant, iron acquisition may be aberrantly high, generating a demand for sulphur to match the iron levels and the consequent induction of sulphur starvation genes. Two observations support the hypothesis that the primary defect of *sesquiα2* might be in iron metabolism. Firstly, the defects in iron responsive genes appear to be constitutive (visible at ED and EN) whilst those related to sulphur assimilation are specific to EN. Secondly, from the only four genes that were oppositely affected in *SnRK1α1-OE* and *sesquiα2,* two were related to iron metabolism (*IRP3* and *NEET*).

2.4.4 Tre6P affects SnRK1 activity in mature rosette leaves

SnRK1 is thought to be activated when energy (carbon) is low whilst Tre6P increases when energy in the form of sucrose is high. Accordingly, similar phenotypes could be expected from genetic manipulations that increase SnRK1 activity and those that decrease Tre6P levels whilst similar phenotypes could also be expected from treatments that decrease SnRK1 activity and those that increase Tre6P levels. In agreement with these expectations, *SnRK1α1-OE* plants show metabolic (e.g. high sucrose) and developmental phenotypes such as delayed flowering (Williams et al., 2014; Jeong et al., 2015) that are similar to those reported

for *TPP-OE* (Avonce et al., 2004; Yadav et al., 2014). In turn, SnRK1 loss-of-function mutants show metabolic (low sucrose and higher levels of some organic acids) and developmental phenotypes such as early flowering (Tsai and Gazzarrini, 2012; Filipe et al., 2018), reported for *TPS-OE* and Tre6P accumulation (Avonce et al., 2004; Wahl et al., 2013; Figueroa et al., 2016).

However, these expected responses occur despite the contrasting pattern of Tre6P accumulation in *SnRK1α1-OE* vs *TPP-OE* (higher vs. unchanged compared to wild-type) and in *sesquiα2* vs *TPS-OE* (lower vs. higher compared to wild-type), suggesting that SnRK1 mediates at least some of the effects of Tre6P on these processes. This is further supported by (*i*) the negative correlation between Tre6P accumulation (Figure 2.1B) and the expression of a set of genes that are induced in a SnRK1-dependent manner at EN (Figure 2.5); (*ii*) the fact that more genes were identified as differentially expressed between Col-0 and *SnRK1α1-OE* at ED than at EN, whereas the opposite was true for the *sesquiα2* mutant, for which the number of DEGs at EN far exceeded those at ED; (*iii*) the fact that the expression of these genes during the day is substantially repressed by otsA induction (Figure 2.6). Altogether this suggests that under favourable conditions SnRK1 undergoes repression towards the ED and activation towards the EN and that these changes in SnRK1 activity are at least partly driven by diel changes in Tre6P accumulation. In plants grown under equinoctial conditions, the expression of SnRK1-dependent genes increases during the night (Bläsing et al., 2005; Frank et al., 2018), and increases strongly in an extended night, in the regular night of the starchless *pgm* mutant (Usadel et al., 2008) or in the day and night after transfer to low irradiance (Moraes et al., 2019). This pattern of expression was attributed to progressive depletion of carbon reserves during the night. Moreover, several of these genes, including *PYL5* and *DIN10,* show defective expression at EN in a knockout mutant of bZIP63 (Viana et al., 2021), a transcription factor targeted by SnRK1 (Mair et al., 2015), further supporting the view that the peak in expression of these genes towards the EN requires SnRK1 signaling. Interestingly, expression of a LUCIFERASE (LUC) reporter for the promoter activity of a SnRK1 marker gene (*DIN6::LUC*) declined rapidly during the first half of the night (Frank et al., 2018),

suggesting that maximal accumulation of the endogenous transcript at EN may require mechanisms beyond mere transcriptional induction.

Our conclusion that SnRK1 mediates part of the Tre6P effects on metabolism and gene expression in whole Arabidopsis rosettes, appears to be in conflict with *in vitro* assays in which Tre6P inhibits SnRK1 activity only when extracted from actively growing tissues (Zhang et al., 2009; Nunes et al., 2013). This may be explained by the inability of *in vitro* kinase assays to detect moderate changes in SnRK1 activity (Zhang et al., 2009; Nunes et al., 2013) that can be amplified *in vivo,* leading to clear downstream effects on metabolite and transcript accumulation. Also, as compared to young seedlings, the proportion of SnRK1 that is susceptible to Tre6P inhibition may be much lower in mature leaves and hence appear negligible when both systems are compared. It is also possible that Tre6P affects not only SnRK1 activity but also other aspects of SnRK1 signalling, that are not addressed in *in vitro* activity assays, or that the Tre6P inhibition requires additional factors that are better captured in *in vitro* assays with extracts from sink tissues than from source leaves. Nevertheless, we cannot rule out the possibility that the observed effects are caused by another metabolite in a Tre6P-dependent manner rather than by Tre6P itself.

Although we have thus far mostly considered potentially direct effects of SnRK1 on metabolism and gene expression, it is plausible that these effects could be indirect, caused by perturbations in the circadian clock. An intimate connection between sucrose perception, SnRK1 and clock entrainment and outputs has been demonstrated by several studies (Sanchez-Villarreal et al., 2013; Shin et al., 2017; Frank et al., 2018; Viana et al., 2021). SnRK1 participates in the metabolic entrainment of the clock (Shin et al., 2017; Frank et al., 2018) and this is in part mediated by the bZIP63 transcription factor (Frank et al., 2018; Viana et al., 2021). SnRK1 could alter the clock through the transcription of *RVE2*, the only clock-related component retrieved in our transcriptional analyses [Table 4; (Zhang et al., 2007)] and shown to respond to low carbon conditions (Moraes et al., 2019). Alternatively, SnRK1 could regulate proteins related to the clock, as shown for CRY1 (Yuan et al., 2016). SnRK1 could also act *via* TIME FOR COFFEE (TIC), a circadian clock

regulator downstream of SnRK1 (Sanchez-Villarreal et al., 2013; Shin et al., 2017) which has been implicated in iron homeostasis (Duc et al., 2009).

In conclusion, SnRK1 plays central functions in metabolic and transcriptional regulation under favourable conditions and this is modulated by diel fluctuations in Tre6P levels. SnRK1 is part of the system that translates changes in sucrose levels into changes in Tre6P. SnRK1 also mediates or modulates the effects of Tre6P on the flux of carbon to the TCA cycle. Overall, the effects of SnRK1 depletion on metabolism and transcript abundance were considerably stronger than those of SnRK1 overexpression, suggesting constitutive SnRK1 activation is largely dampened by compensatory negative feedback mechanisms or that additional components (e.g. regulatory subunits) are required for inducing such responses.

2.5 Materials and Methods

2.5.1 Plant material and growth conditions

All *Arabidopsis thaliana* plants used here are in the Columbia (Col-0) background. The *sesquiα2* mutant bears the *snrk1α1-3* mutation (GABI_579E09) in homozygosity and the *snrk1α2-2* mutation (WiscDsLox384F5) in heterozygosity and was previously described (Belda-Palazón et al., 2020). The *SnRK1α1-OE*, AlcR and iOtsA lines were described elsewhere (Jossier et al., 2009; Martins et al., 2013).

Seeds were sown in excess directly on a 1:1 mix of soil (Stender; www.stender.de) and vermiculite [soaked with tap water, supplemented with boron (1.8 mg L^{-1}) and the fungicide Previcur (1.5 ml L^{-1}; Bayer; www.bayer.de)] in round plastic pots (10 cm diameter). Pots were thereafter placed in a cold room (4º C) for 2-3 days before being transferred to growth cabinets (Percival E-36 L, CLF Plant Climatics GmbH, Wertingen, Germany) with the following settings: 12:12 light:dark photoperiod, 22:18º C temperature regime, 60% RH, and 160 µmol m^{-2} s^{-1} irradiance provided by white fluorescent tubes giving a light spectrum as described (Annunziata et al., 2017). The pots were covered with transparent plastic lids during the first 5

days and 2 days later the plants were thinned out to leave 3-5 plants per pot. All pots were well separated to prevent shading and their positions were randomized every 3 days to avoid positional effects. Plants were watered twice a week to ensure soil humidity. To this end, water was added to the trays and excess water (not absorbed by the pots) was removed from the trays after 1h. To avoid pests, plants were treated weekly with *Caenorhabditis elegans* nematodes. Plant harvesting and treatments were started always in the light period of the 20th day of growth. The *sesquiα2* mutant was always pre-selected on 0.5xMS medium supplemented with BASTA (10 µg mL^{-1}) for 6 days and seedlings were thereafter transferred to soil. For ethanol-treated plants (AlcR and iOtsA), a solution of 2% (v/v) ethanol was gently sprayed over the rosettes, 6 h prior to harvest. Whole rosettes were harvested, flash frozen in liquid nitrogen and stored at -80ºC until further analyses.

2.5.2 Metabolite extraction and determination

For metabolite analyses, Col-0, *SnRK1α1-OE* and the *sesquiα2* mutant were harvested at 4-h intervals for a period of 40 h starting at ZT8. Each final sample represents the results obtained from 4-5 biological replicates, each consisting of a pool of 4-5 randomly sampled whole rosettes.

For enzymatic methods, approximately 20 mg of finely ground plant material was extracted twice in boiling 80% (v/v) ethanol buffered with 10 mM HEPES-NaOH (pH 7.0), and once in 50% (v/v) ethanol buffered with 10 mM HEPES-NaOH (pH 7.0). The resulting supernatants were used to measure soluble sugars (glucose, fructose, and sucrose) enzymatically, as described (Stitt *et al.*, 1989). NO_3^- and NO_2^- quantifications were also enzymatically determined from the ethanolic extracts (Cross *et al.*, 2006). Both starch and total protein contents were determined from the insoluble material left after ethanolic extraction, following previously described protocols (Hendriks *et al.*, 2003).

For LC-MS/MS-based quantifications, approximately 20 mg of finely ground plant material was quenched in a 3:7 (v/v) chloroform:methanol mixture at liquid

nitrogen temperature, and allowed to warm up to -20ºC for 2 h. The chloroform phase was then extracted twice with ice-cold ultra-pure water. The two water phases were pooled together and evaporated to dryness in a centrifugal vacuum drier at 20ºC. The resulting pellets were resuspended in 350 µL of ultra-pure water, filtered through a Multiscreen Ultracel-10 (Milipore) membrane to remove high molecular weight components, and diluted 1:10 before assessment by high-performance anion-exchange chromatography coupled to tandem mass spectrometry, as described in (Lunn *et al.*, 2006) with modifications (Figueroa *et al.*, 2016).

2.5.3 Protein extraction, quantification and immunoblotting

For extraction of total protein for the TPS1 immunoblot analyses, whole rosettes (three per replicate) were ground in liquid N_2. Finely ground tissue (approximately 30 mg per sample) was extracted in 1.5 volumes of buffer [50 mM NaCl, 1% Igepal CA-630, 0.5% sodium deoxycholate, 0.1% (w/v) SDS, 50 mM Tris-HCl (pH 8.0), 1 mM EDTA (pH 8.0), supplemented with 50 µM MG132, 50 mM N-ethyl maleimide, 1:20 cOmplete EDTA-free Protease Inhibitor Cocktail (Roche), and 1:500 Phosphatase Inhibitor Cocktails 2 and 3 (Sigma-Aldrich)]. Homogenates were cleared by centrifugation at 21130 x g for 15 minutes at 4°C, and supernatants were used for total protein quantification (Pierce 660 nm protein assay). Single use aliquots of 40 µg total protein were prepared and denatured in Laemmli buffer (Laemmli, 1970) before storage at -20°C. Total protein samples were separated by SDS-PAGE in 7% acrylamide gels, transferred to PVDF membranes (wet transfer at 4°C, 110 V, 60 min) and probed using an 1:3000 dilution of an anti N-terminal TPS1 antibody (Yadav *et al.*, 2014). Chemiluminescent detection was performed using a 1:10000 dilution of Peroxidase AffiniPure goat anti-rabbit IgG (H+L) (Jackson ImmunoResearch), and SuperSignal West Femto Maximum Sensitivity Substrate (Thermo Scientific).

2.5.4 RNA extraction and qRT-PCR

Total RNA was extracted from approximately 50 mg of finely ground tissue, with the Plant Nucleospin RNA extraction kit (Macherey-Nagel), according to the manufacturer's instructions. DNAse-treated RNA (0.5 µg) was used for synthesis of cDNA libraries, using SuperScript III Reverse Transcriptase (Life Technologies), as previously described (Rodrigues *et al.*, 2013). Quantitative real-time RT-PCR (qPCR) was performed in a QuantStudio™ 7 platform (Applied Biosystems®), with the i*Taq*™ Universal SYBR® Green Supermix (Bio-Rad), and the $2^{-\Delta\Delta Ct}$ method for relative quantification (Livak & Schmittgen, 2001). Expression values of SnRK1-induced genes were normalized using the geometric mean of the housekeeping genes *UBQ10*, *UBC21* and *EIF4A* (Vandesompele *et al.*, 2002).

2.5.5 RNA-seq analysis

For RNA-seq analyses, Col-0, *SnRK1α1-OE* and the *sesquiα2* mutant were harvested at the end of the day (ED) and end of the night (EN). Three biological replicates (each composed of a pool of 4-5 randomly sampled whole rosettes) were generated from each genotype and time point. Total RNA was extracted from approximately 50 mg of finely ground tissue, with the Qiagen RNeasy® Plant Mini Kit according to the manufacturer's instructions. RNA integrity was confirmed on an Agilent 2100 Bioanalyzer. Genomic DNA contamination was assessed by qRT-PCR, using primers for an intronic region of the *FCL1* gene. Only RNA samples with A260/A280>2.0, an RNA integrity number (RIN)>7.0, and undetectable gDNA levels, were used for RNA-seq. cDNA libraries were synthesized and sequenced at BGI Genomics (Hong-Kong), using a paired-end strategy and a read length of 150 bp, on their proprietary BGISEQ-500 platform.

Clean reads were mapped to the Arabidopsis reference genome (TAIR10) using HISAT2. All subsequent analyses were done in the R programming environment (v.3.6.3; R Core Team, 2020, https://www.R-project.org/) (see Supporting Information Methods) Common gene names were retrieved with the

biomartr R package (v.0.9.2) (Drost & Paszkowski, 2017) based on gene IDs. Overlaps between different sets of genes were revealed using the Venny online application (http://bioinfogp.cnb.csic.es/tools/venny/index.html). Heat maps for gene expression and metabolite levels were generated using conditional formatting in Excel using maximum and minimum values of Signal log2 ratios for generating the color gradient.

2.5.6 Statistical Analyses

Metabolite measurements were plotted along the experimental time points. Data points represent the average values obtained from the measurement of 4-5 biological replicates, with error bars representing the 95% confidence interval. Each biological replicate is a pool of 4-5 randomly sampled whole rosettes. Statistically significant differences were assessed by one-way ANOVA Sum of Squares Type II, followed by a Tukey's post-hoc test of honestly significant differences.

Tre6P:sucrose regression plots were built using all biological samples harvested at ED (12 h and 36 h after first dawn) and at EN (24 h and 48 h after first dawn), and used for determination of the Pearson's correlation coefficient. Tre6P:sucrose and starch:sucrose ratios were calculated by averaging the ratios obtained for each individual sample at each individual time point. The results of the Tre6P:sucrose and starch:sucrose ratios were then subjected to a *t*-test for identification of statistical significance between genotypes, or to a one-way ANOVA Sum of Squares Type II, followed by a Tukey's post-hoc test of honestly significant differences, respectively.

Rates of starch accumulation and degradation were estimated as described (Moraes *et al.*, 2019), using linear models describing starch levels as a function of time (starch=a.ZT+b).

Statistical analyses were performed using the *R* software (https://www.R-project.org/) and GraphPad Prism version 8.4.0 for Windows (GraphPad Software, La Jolla, California, USA). In all cases a significance level (α) of 0.05 was used.

2.5.7 Accession Numbers

Sequence data from this manuscript is available in the Arabidopsis Genome Initiative database under these accession numbers: *BGAL4*, At5g56870; *DIN10*, At5g20250; *PYL5*, At5g05440; *TPS1*, At1g78580; *FCL1,* At5g65080; *RZPF34,* At5g22920; *TPS8*, At1g70290; *eIF4A*, At3g13920; *UBC21*, At5g25760; *UBQ10*, At4g05320. Sequence data for otsA is available in GenBank, under the accession number X69160.1. RNAseq data have been deposited in the NCBI GEO database under accession number GSE168382.

Acknowledgments

The authors would like to thank the IGC Plant Facility (Vera Nunes) for excellent plant care. This work was supported by Fundação para a Ciência e a Tecnologia through the R&D Unit UIDB/04551/2020 (GREEN-IT - Bioresources for Sustainability), FCT projects LISBOA-01-0145-FEDER-028128 and PTDC/BIA-BID/32347/2017, and FCT fellowships/contracts PD/BD/114361/2016 (BP), SFRH/BPD/116116/2016 (LM), and IF/00804/2013 (EBG), and by the Max Planck Society.

2.6 References

Annunziata MG, Apelt F, Carillo P, Krause U, Feil R, Mengin V, Lauxmann MA, Köhl K, Nikoloski Z, Stitt M, et al (2017) Getting back to nature: A reality check for experiments in controlled environments. J Exp Bot **68**: 4463–4477

Avonce N, Leyman B, Mascorro-Gallardo JO, Van Dijck P, Thevelein JM, Iturriaga G (2004) The arabidopsis trehalose-6-P synthase AtTPS1 gene is a regulator of glucose, abscisic acid, and stress signaling. Plant Physiol **136**: 3649–3659

Baena-González E, Lunn JE (2020) SnRK1 and trehalose 6-phosphate – two ancient pathways converge to regulate plant metabolism and growth. Curr Opin Plant Biol **55**: 52–59

Baena-González E, Rolland F, Thevelein JM, Sheen J (2007) A central integrator of transcription networks in plant stress and energy signalling. Nature **448**: 938–942

Baena-González E, Sheen J (2008) Convergent energy and stress signaling. Trends Plant Sci **13**: 474–482

Belda-Palazón B, Adamo M, Valerio C, Ferreira LJ, Confraria A, Reis-Barata D, Rodrigues A, Meyer C, Rodriguez PL, Baena-González E (2020) A dual function of SnRK2 kinases in the regulation of SnRK1 and plant growth. Nat Plants **6**: 1345–1353

Bläsing OE, Gibon Y, Günther M, Höhne M, Morcuende R, Osuna D, Thimm O, Usadel B, Scheible WR, Stitt M (2005) Sugars and circadian regulation make major contributions to the global regulation of diurnal gene expression in Arabidopsis. Plant Cell **17**: 3257–3281

Broeckx T, Hulsmans S, Rolland F (2016) The plant energy sensor: evolutionary conservation and divergence of SnRK1 structure, regulation, and function. J Exp Bot **67**: 6215–6252

Collakova E, Goyer A, Naponelli V, Krassovskaya I, Gregory JF, Hanson AD, Shachar-Hilla Y (2008) Arabidopsis 10-formyl tetrahydrofolate deformylases are essential for photorespiration. Plant Cell **20**: 1818–1832

Crepin N, Rolland F (2019) SnRK1 activation, signaling, and networking for energy homeostasis. Curr Opin Plant Biol **51**: 29–36

Cross JM, Von Korff M, Altmann T, Bartzetko L, Sulpice R, Gibon Y, Palacios N, Stitt M (2006) Variation of enzyme activities and metabolite levels in 24 arabidopsis accessions growing in carbon-limited conditions. Plant Physiol **142**: 1574–1588

Delorge I, Figueroa CM, Feil R, Lunn JE, Van Dijck P (2015) Trehalose-6-phosphate synthase 1 is not the only active TPS in Arabidopsis thaliana. Biochem J **466**: 283–290

Drost HG, Paszkowski J (2017) Biomartr: Genomic data retrieval with R. Bioinformatics **33**: 1216–1217

Duc C, Cellier F, Lobréaux S, Briat JF, Gaymard F (2009) Regulation of iron homeostasis in Arabidopsis thaliana by the clock regulator time for coffee. J Biol Chem **284**: 36271–36281

Fichtner F, Lunn JE (2021) The Role of Trehalose 6-Phosphate (Tre6P) in Plant Metabolism and Development. Annu Rev Plant Biol **72**: 737–760

Fichtner F, Olas JJ, Feil R, Watanabe M, Krause U, Hoefgen R, Stitt M, Lunn JE (2020) Functional features of TREHALOSE-6-PHOSPHATE SYNTHASE1, an essential enzyme in Arabidopsis. Plant Cell **32**: 1949–1972

Figueroa CM, Feil R, Ishihara H, Watanabe M, Kölling K, Krause U, Höhne M, Encke B, Plaxton WC, Zeeman SC, et al (2016) Trehalose 6-phosphate coordinates organic and amino acid metabolism with carbon availability. Plant J **85**: 410–423

Figueroa CM, Lunn JE (2016) A tale of two sugars: Trehalose 6-phosphate and sucrose. Plant Physiol **172**: 7–27

Filipe O, De Vleesschauwer D, Haeck A, Demeestere K, Höfte M (2018) The energy sensor OsSnRK1a confers broad-spectrum disease resistance in rice. Sci Rep **8**: 3864

Forieri I, Sticht C, Reichelt M, Gretz N, Hawkesford MJ, Malagoli M, Wirtz M, Hell R (2017) System analysis of metabolism and the transcriptome in Arabidopsis thaliana roots reveals differential co-regulation upon iron, sulphur and potassium deficiency. Plant Cell Environ **40**: 95–107

Forieri I, Wirtz M, Hell R (2013) Toward new perspectives on the interaction of iron and sulphur metabolism in plants. Front Plant Sci **4**: 357

Frank A, Matiolli CC, Viana AJC, Hearn TJ, Kusakina J, Belbin FE, Wells Newman D, Yochikawa A, Cano-Ramirez DL, Chembath A, et al (2018) Circadian Entrainment in Arabidopsis by the Sugar-Responsive Transcription Factor bZIP63. Curr Biol **28**: 2597-2606.e6

Graf A, Schlereth A, Stitt M, Smith AM (2010) Circadian control of carbohydrate availability for growth in Arabidopsis plants at night. Proc Natl Acad Sci U S A **107**: 9458–9463

Hendriks JHM, Kolbe A, Gibon Y, Stitt M, Geigenberger P (2003) ADP-Glucose Pyrophosphorylase Is Activated by Posttranslational Redox-Modification in Response to Light and to Sugars in Leaves of Arabidopsis and Other Plant Species. Plant Physiol **133**: 838–849

Hulsmans S, Rodriguez M, De Coninck B, Rolland F (2016) The SnRK1 Energy Sensor in Plant Biotic Interactions. Trends Plant Sci **21**: 648–661

Jeong EY, Seo PJ, Woo JC, Park CM (2015) AKIN10 delays flowering by inactivating IDD8 transcription factor through protein phosphorylation in Arabidopsis. BMC Plant Biol **15**: 110

Jossier M, Bouly JP, Meimoun P, Arjmand A, Lessard P, Hawley S, Grahame Hardie D, Thomas M (2009) SnRK1 (SNF1-related kinase 1) has a central role in sugar and ABA signalling in Arabidopsis thaliana. Plant J **59**: 316–328

Laemmli UK (1970) Cleavage of structural proteins during the assembly of the head of bacteriophage T4. Nature **227**: 680–685

Li C, Qi W, Liang Z, Yang X, Ma Z, Song R (2020) A SnRK1-ZmRFWD3-Opaque2 signaling axis regulates diurnal nitrogen accumulation in maize seeds. Plant Cell **32**: 2823–2841

Li L, Zheng W, Zhu Y, Ye H, Tang B, Arendseea ZW, Jones D, Li R, Ortiz D, Zhao X, et al (2015) QQS orphan gene regulates carbon and nitrogen partitioning across species via NF-YC interactions. Proc Natl Acad Sci U S A **112**: 14734–14739

Li XF, Li YJ, An YH, Xiong LJ, Shao XH, Wang Y, Sun Y (2009) AKINβ1 is involved in the regulation of nitrogen metabolism and sugar signaling in arabidopsis. J Integr Plant Biol **51**: 513–20

Livak KJ, Schmittgen TD (2001) Analysis of relative gene expression data using real-time quantitative PCR and the 2-ΔΔCT method. Methods **25**: 402–408

Lunn JE, Delorge I, Figueroa CM, Van Dijck P, Stitt M (2014) Trehalose metabolism in plants. Plant J **79**: 544–567

Lunn JE, Feil R, Hendriks JHM, Gibon Y, Morcuende R, Osuna D, Scheible WR, Carillo P,

Hajirezaei MR, Stitt M (2006) Sugar-induced increases in trehalose 6-phosphate are correlated with redox activation of ADPglucose pyrophosphorylase and higher rates of starch synthesis in Arabidopsis thaliana. Biochem J **397**: 139–148

Mair A, Pedrotti L, Wurzinger B, Anrather D, Simeunovic A, Weiste C, Valerio C, Dietrich K, Kirchler T, Nägele T, et al (2015) SnRK1-triggered switch of bZIP63 dimerization mediates the low-energy response in plants. Elife. doi: 10.7554/eLife.05828

Margalha L, Confraria A, Baena-González E (2019) SnRK1 and TOR: Modulating growth–defense trade-offs in plant stress responses. J Exp Bot **70**: 2261–2274

Martins MCM, Hejazi M, Fettke J, Steup M, Feil R, Krause U, Arrivault S, Vosloh D, Figueroa CM, Ivakov A, et al (2013) Feedback inhibition of starch degradation in Arabidopsis leaves mediated by trehalose 6-phosphate. Plant Physiol **163**: 1142–1163

Mendoza-Cózatl DG, Gokul A, Carelse MF, Jobe TO, Long TA, Keyster M (2019) Keep talking: Crosstalk between iron and sulphur networks fine-tunes growth and development to promote survival under iron limitation. J Exp Bot **70**: 4197–4210

Moraes TA, Mengin V, Annunziata MG, Encke B, Krohn N, Höhne M, Stitt M (2019) Response of the circadian clock and diel starch turnover to one day of low light or low co2. Plant Physiol **179**: 1457–1478

Nechushtai R, Conlan AR, Harir Y, Song L, Yogev O, Eisenberg-Domovich Y, Livnah O, Michaeli D, Rosen R, Ma V, et al (2012) Characterization of Arabidopsis NEET reveals an ancient role for NEET proteins in iron metabolism. Plant Cell **24**: 2139–54

Nukarinen E, Ngele T, Pedrotti L, Wurzinger B, Mair A, Landgraf R, Börnke F, Hanson J, Teige M, Baena-Gonzalez E, et al (2016) Quantitative phosphoproteomics reveals the role of the AMPK plant ortholog SnRK1 as a metabolic master regulator under energy deprivation. Sci Rep **6**: 31697

Nunes C, Primavesi LF, Patel MK, Martinez-Barajas E, Powers SJ, Sagar R, Fevereiro PS, Davis BG, Paul MJ (2013) Inhibition of SnRK1 by metabolites: Tissue-dependent effects and cooperative inhibition by glucose 1-phosphate in combination with trehalose 6-phosphate. Plant Physiol Biochem **63**: 89–98

Radchuk R, Emery RJN, Weier D, Vigeolas H, Geigenberger P, Lunn JE, Feil R, Weschke W, Weber H (2010) Sucrose non-fermenting kinase 1 (SnRK1) coordinates metabolic and hormonal signals during pea cotyledon growth and differentiation. Plant J **61**: 324–338

Radchuk R, Radchuk V, Weschke W, Borisjuk L, Weber H (2006) Repressing the expression of the SUCROSE NONFERMENTING-1-RELATED PROTEIN KINASE gene in pea embryo causes pleiotropic defects of maturation similar to an abscisic acid-insensitive phenotype. Plant Physiol **140**: 263–278

Ramon M, De Smet I, Vandesteene L, Naudts M, Leyman B, Van Dijck P, Rolland F, Beeckman T, Thevelein JM (2009) Extensive expression regulation and lack of heterologous enzymatic activity of the Class II trehalose metabolism proteins from Arabidopsis thaliana. Plant, Cell Environ **32**: 1015–1032

Rodrigues A, Adamo M, Crozet P, Margalha L, Confraria A, Martinho C, Elias A, Rabissi A, Lumbreras V, González-Guzmán M, et al (2013) ABI1 and PP2CA phosphatases are negative regulators of Snf1-related protein kinase1 signaling in Arabidopsis. Plant Cell **25**: 3871–3884

Rodríguez-Celma J, Chun Pan I, Li W, Lan P, Buckhout TJ, Schmidt W (2013) The transcriptional response of Arabidopsis leaves to Fe deficiency. Front Plant Sci **4**: 276

Ruan YL (2014) Sucrose metabolism: Gateway to diverse carbon use and sugar signaling. Annu Rev Plant Biol **65**: 33–67

Sanchez-Villarreal A, Shin J, Bujdoso N, Obata T, Neumann U, Du SX, Ding Z, Davis AM, Shindo T, Schmelzer E, et al (2013) TIME for COFFEE is an essential component in the maintenance of metabolic homeostasis in Arabidopsis thaliana. Plant J **76**: 188–200

Schwacke R, Ponce-Soto GY, Krause K, Bolger AM, Arsova B, Hallab A, Gruden K, Stitt M, Bolger ME, Usadel B (2019) MapMan4: A Refined Protein Classification and Annotation Framework Applicable to Multi-Omics Data Analysis. Mol Plant **12**: 879–892

Scialdone A, Mugford ST, Feike D, Skeffngton A, Borrill P, Graf A, Smith AM, Howard M (2013) Arabidopsis plants perform arithmetic division to prevent starvation at night. Elife 2:e00669

Shin J, Sánchez-Villarreal A, Davis AM, Du SX, Berendzen KW, Koncz C, Ding Z, Li C, Davis SJ (2017) The metabolic sensor AKIN10 modulates the Arabidopsis circadian clock in a light-dependent manner. Plant Cell Environ **40**: 997–1008

Smith AM, Stitt M (2007) Coordination of carbon supply and plant growth. Plant, Cell Environ **30**: 1126–1149

Stitt M, Lilley RMC, Gerhardt R, Heldt HW (1989) Metabolite levels in specific cells and subcellular compartments of plant leaves. Methods Enzymol **174**: 518–552

Stitt M, Lunn J, Usadel B (2010) Arabidopsis and primary photosynthetic metabolism - More than the icing on the cake. Plant J **61**: 1067–1091

Stitt M, Zeeman SC (2012) Starch turnover: Pathways, regulation and role in growth. Curr Opin Plant Biol **15**: 282–292

Sugden C, Donaghy PG, Halford NG, Hardie DG (1999) Two SNF1-related protein kinases from spinach leaf phosphorylate and inactivate 3-hydroxy-3-methylglutaryl-coenzyme a reductase, nitrate reductase, and sucrose phosphate synthase in vitro. Plant Physiol **120**: 257–74

Sulpice R, Flis A, Ivakov AA, Apelt F, Krohn N, Encke B, Abel C, Feil R, Lunn JE, Stitt M (2014) Arabidopsis coordinates the diurnal regulation of carbon allocation and growth across a wide range of photoperiods. Mol Plant **7**: 137–155

Thimm O, Bläsing O, Gibon Y, Nagel A, Meyer S, Krüger P, Selbig J, Müller LA, Rhee SY, Stitt M (2004) MAPMAN: A user-driven tool to display genomics data sets onto diagrams of metabolic pathways and other biological processes. Plant J **37**: 914–939

Tian T, Liu Y, Yan H, You Q, Yi X, Du Z, Xu W, Su Z (2017) AgriGO v2.0: A GO analysis toolkit for the agricultural community. Nucleic Acids Res **45**: W122–W129

Tsai AYL, Gazzarrini S (2012) AKIN10 and FUSCA3 interact to control lateral organ development and phase transitions in Arabidopsis. Plant J **69**: 809–821

Usadel B, Bläsing OE, Gibon Y, Retzlaff K, Höhne M, Günther M, Stitt M (2008) Global transcript levels respond to small changes of the carbon status during progressive exhaustion of carbohydrates in arabidopsis rosettes. Plant Physiol **146**: 1834–1861

Vandesompele J, De Preter K, Pattyn F, Poppe B, Van Roy N, De Paepe A, Speleman F (2002) Accurate normalization of real-time quantitative RT-PCR data by geometric averaging of multiple internal control genes. Genome Biol **3**: RESEARCH0034

Viana AJC, Matiolli CC, Newman DW, Vieira JGP, Duarte GT, Martins MCM, Gilbault E, Hotta CT, Caldana C, Vincentz M (2021) The sugar-responsive circadian clock regulator bZIP63 modulates plant growth. New Phytol. In Press:

Wahl V, Ponnu J, Schlereth A, Arrivault S, Langenecker T, Franke A, Feil R, Lunn JE, Stitt M,

Schmid M (2013) Regulation of flowering by trehalose-6-phosphate signaling in Arabidopsis thaliana. Science (80-) **339**: 704–707

Wang Y, Wang L, Micallef BJ, Tetlow IJ, Mullen RT, Feil R, Lunn JE, Emes MJ (2020) AKINβ1, a subunit of SnRK1, regulates organic acid metabolism and acts as a global modulator of genes involved in carbon, lipid, and nitrogen metabolism. J Exp Bot **71**: 1010–1028

Williams SP, Rangarajan P, Donahue JL, Hess JE, Gillaspy GE (2014) Regulation of Sucrose non-Fermenting Related Kinase 1 genes in Arabidopsis thaliana. Front Plant Sci **5**: 324

Yadav UP, Ivakov A, Feil R, Duan GY, Walther D, Giavalisco P, Piques M, Carillo P, Hubberten HM, Stitt M, et al (2014) The sucrose-trehalose 6-phosphate (Tre6P) nexus: Specificity and mechanisms of sucrose signalling by Tre6P. J Exp Bot **65**: 1051–1068

Yuan S, Zhang ZW, Zheng C, Zhao ZY, Wang Y, Feng LY, Niu G, Wang CQ, Wang JH, Feng H, et al (2016) Arabidopsis cryptochrome 1 functions in nitrogen regulation of flowering. Proc Natl Acad Sci U S A **113**: 7661–7666

Zhai Z, Keereetaweep J, Liu H, Feil R, Lunn JE, Shanklin J (2018) Trehalose 6-phosphate positively regulates fatty acid synthesis by stabilizing wrinkled1. Plant Cell **30**: 2616–2627

Zhang X, Chen Y, Wang ZY, Chen Z, Gu H, Qu LJ (2007) Constitutive expression of CIR1 (RVE2) affects several circadian-regulated processes and seed germination in Arabidopsis. Plant J **51**: 512–525

Zhang Y, Primavesi LF, Jhurreea D, Andralojc PJ, Mitchell RAC, Powers SJ, Schluepmann H, Delatte T, Wingler A, Paul MJ (2009) Inhibition of SNF1-related protein kinasel activity and regulation of metabolic pathways by trehalose-6-phosphate1. Plant Physiol **149**: 1860–1871

2.7 Supplementary Information

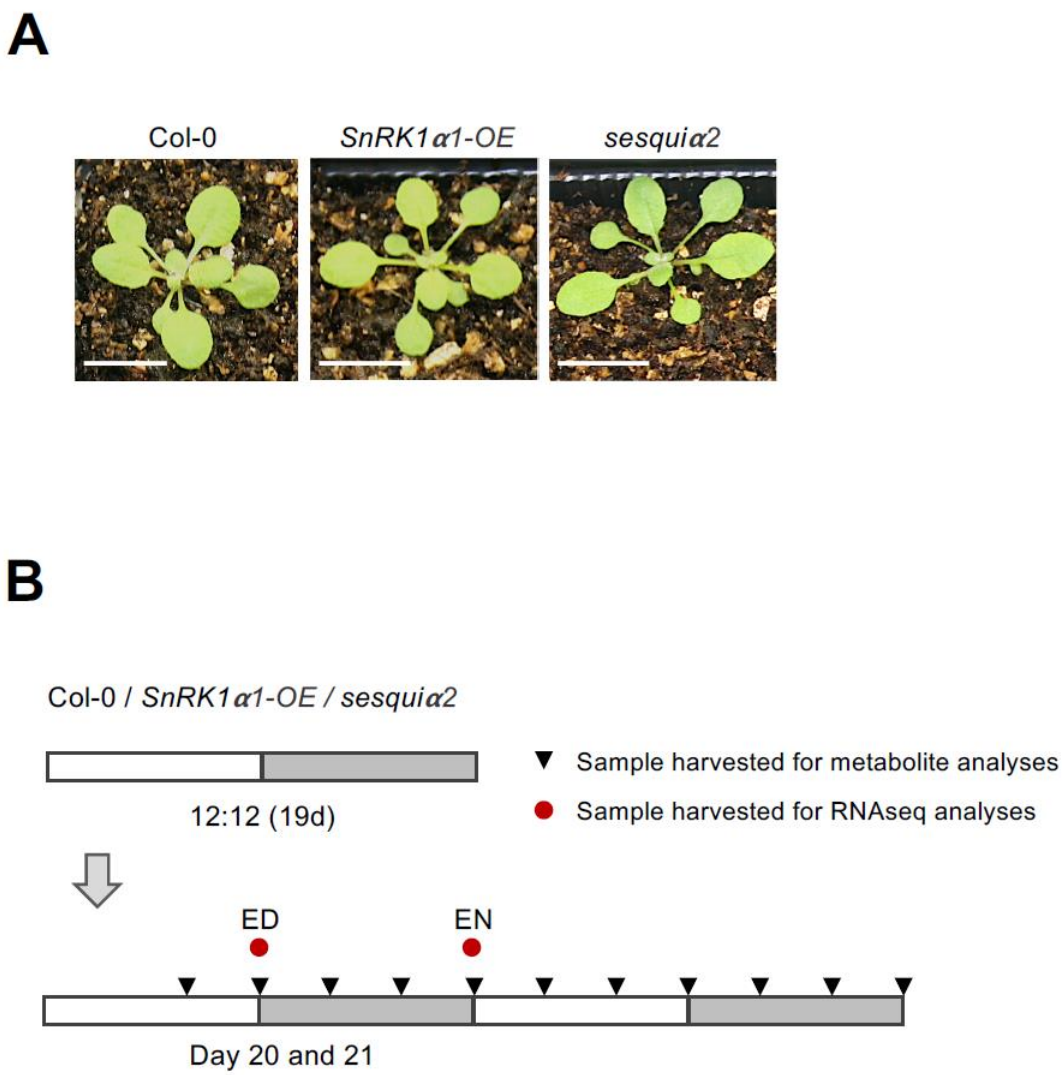

Supplemental Figure 2.1 | Experimental setup for the metabolomic and transcriptomic characterization of SnRK1 mutant lines.
A, Representative pictures of the plants used in these analyses are shown [Col-0, *SnRK1α1-OE*, *sesquiα2*]. Scale bar, 1 cm. **B**, Plants were grown under a 12:12 photoperiod for 19 days. Starting on the 20th day, whole rosettes were harvested every 4 h over a period of 40 h. Black arrows represent the time points used for metabolic measurements, and the red circles represent the end of day (ED) and end of night (EN) time points selected for RNA-seq analyses. The night period is marked in grey.

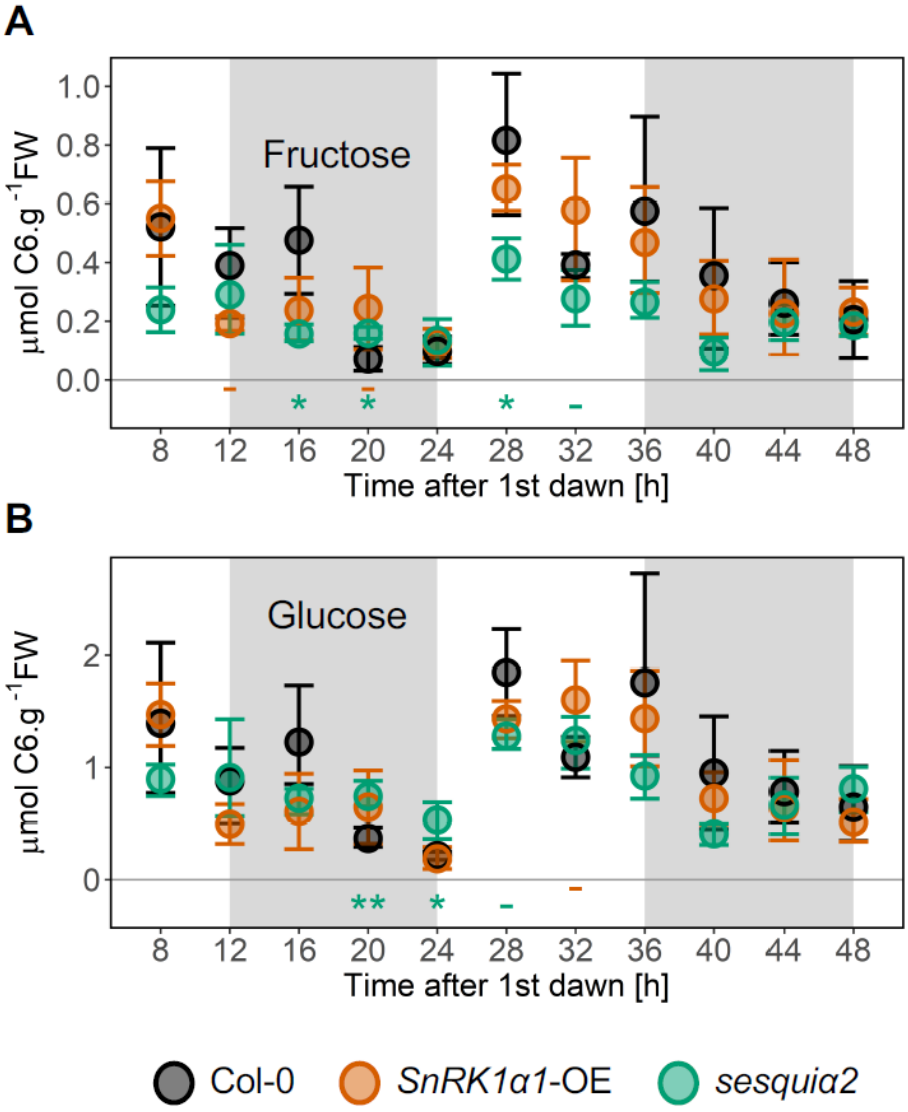

Supplemental Figure 2.2 | Impact of SnRK1 on glucose and fructose accumulation.
Fructose **(A)** and glucose **(B)** levels were quantified from 20-day old Col-0, *SnRK1α1-OE*, and *sesquia2* plants grown under a 12:12 photoperiod and harvested every 4 h. The night period is marked in grey. Graphs show the average of 4-5 biological replicates (each composed of a pool of 4-5 randomly sampled whole rosettes) at each time point, with error bars representing the 95% confidence interval. Asterisks denote statistically significant differences tested at each ZT for both genotypes separately (one-way ANOVA with Tukey's post-hoc test of honestly significant differences, HSD). (-), p<0.1 cases in which the Tukey's HSD resulted non-significant differences; (*), p<0.05; (**), p<0.01.

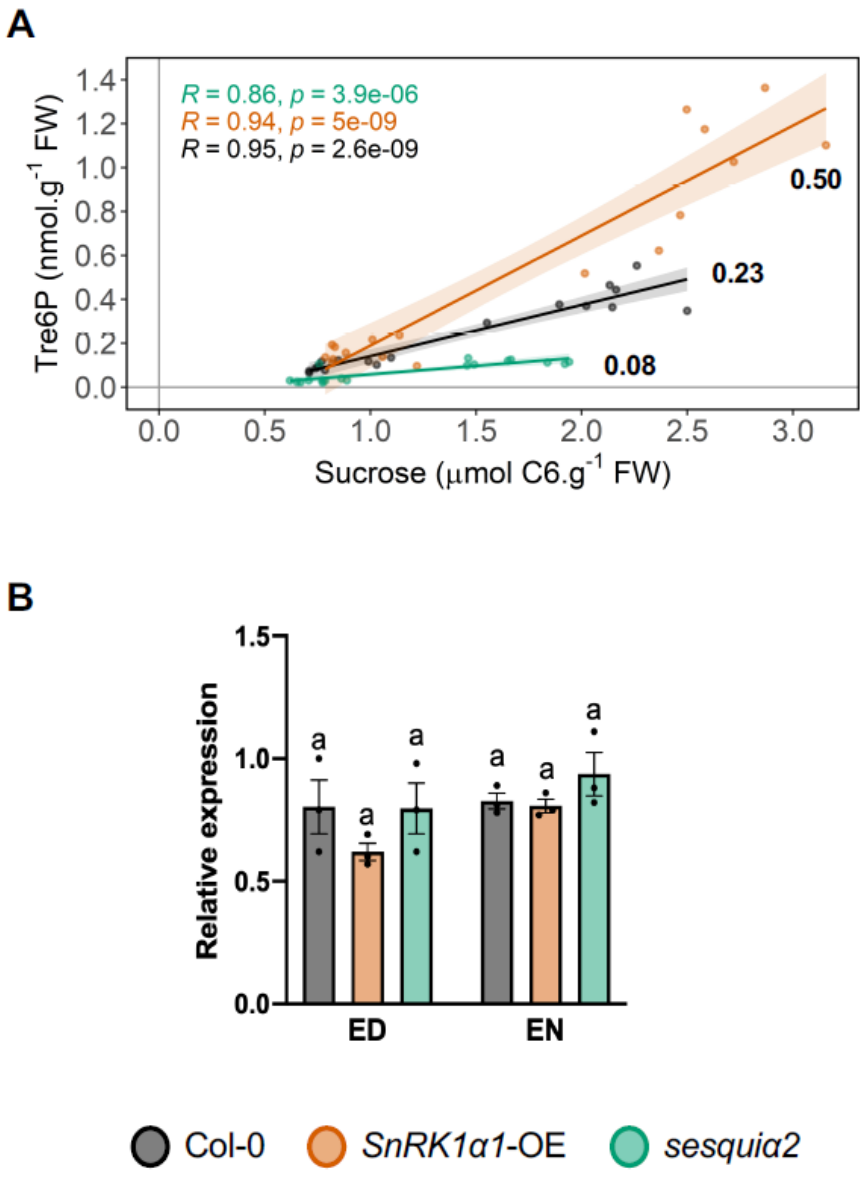

Supplemental Figure 2.3 | Impact of SnRK1 on the sucrose-Tre6P relationship and on *TPS1* transcript accumulation.
A, The sucrose content of samples at the end of the day (ED, 12h and 36h after first dawn) and end of the night (EN, 24h and 48h after first dawn) was plotted against the corresponding values of Tre6P. *R*, Pearson correlation coefficient. Black numbers adjacent to each line indicate the slopes of the corresponding sucrose-Tre6P regression. Sucrose levels correspond to hexose equivalents. **B**, *TPS1* transcript levels quantified by qPCR from 20 d-old Col-0, *SnRK1α1-OE* and *sesquia2* rosettes at ED and EN. Graph corresponds to the average of 3 independent experiments (error bars, SEM). Letters indicate significantly different groups assessed using the ANOVA and Tukey's HSD post-test. Sucrose levels correspond to hexose equivalents

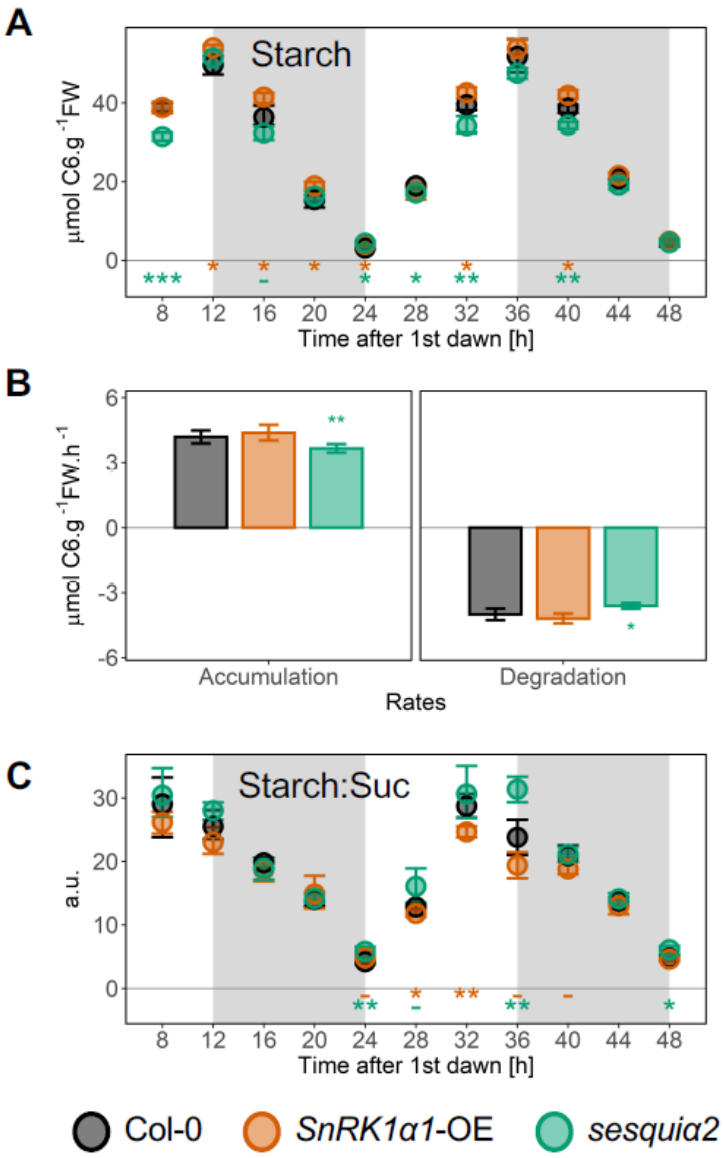

Supplemental Figure 2.4 | Impact of SnRK1 on starch and starch:sucrose ratios.
Twenty-day old Col-0, *SnRK1α1-OE*, and *sesquia2* plants grown under a 12:12 photoperiod were harvested every 4 h for quantifying starch levels **(A),** rates of starch accumulation during the day (left panel) and starch mobilization during the night (right panel) **(B)**, and starch:sucrose ratios **(C)**. The night period is marked in grey. Time series plots show the average of 4-5 biological replicates (each composed of a pool of 4-5 randomly sampled whole rosettes) at each time point, with error bars representing the 95% confidence interval. Asterisks denote statistically significant differences (one-way ANOVA with Tukey HSD post-hoc test). (-), $p<0.1$ cases in which the Tukey's HSD resulted non-significant differences; (*), $p<0.05$; (**), $p<0.01$; (***), $p<0.001$. Starch levels correspond to hexose (C6) equivalents. Rates in panel (B) were calculated as the slope of the linear fit of all biological replicates either in the day or night periods. Statistically significant differences to the control Col-0 was tested for both mutants using ANCOVA; *p*-values reported by asterisks as above.

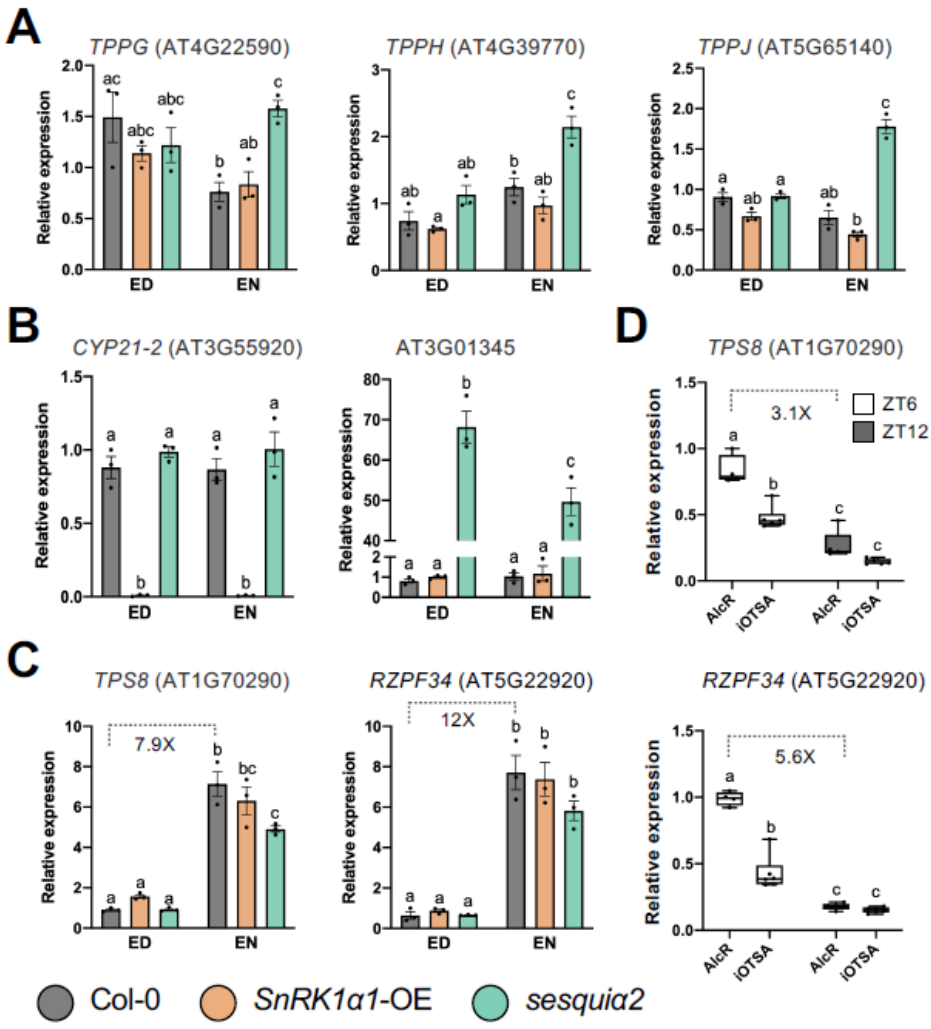

Supplemental Figure 2.5 | Validation of RNA seq and expression of SnRK1 marker genes.
qPCR analyses in the indicated genotypes and time points of selected *TPP* genes retrieved as differentially expressed in *sesquia2* at EN **(A)**, genes affected both at EN and ED in the *SnRK1α1-OE* (left graph) and *sesquia2* (right graph) RNAseq datasets **(B)**, and two SnRK1 marker genes (Baena-Gonzalez et al., 2007) **(C)**. Graphs correspond to the average of three independent experiments (error bars, SEM). Letters indicate significantly different groups assessed using the ANOVA and Tukey's HSD post-test. **D**, Induction of OtsA expression in an ethanol-inducible line (iOtsA) and the corresponding empty vector control (AlcR). Ethanol (2% v/v) was sprayed over the plants at ZT0 or at ZT6 and whole rosettes were harvested after 6 h (ZT6 and ZT12 indicate the time of harvest) for qPCR analyses of two SnRK1 marker genes. Quantification of otsA in these samples is shown in Figure 2.6A. Values denote expression relative to the ZT6 time point of the AlcR line. Boxplots represent 4-5 biological replicates (each consisting of a pool of three randomly harvested rosettes). Lower and upper box boundaries represent the first and third quantiles, respectively, horizontal lines mark the median and whiskers mark the highest and lowest values. Dots represent individual datapoints. Different letters indicate statistically significant differences (p<0.05, one-way ANOVA with Tukey HSD test)

Supplemental Table 2.1 | Metabolite measurements performed in the Col-0, *SnRK1α1-OE,* and *sesquiα2* lines.

Average values and standard deviations are shown for each metabolite at the indicated time points for both the Col-0 control (Table S1a), the *SnRK1α1-OE* line (Table S1b), and the *sesquiα2* mutant (Table S1d). These values were used to calculate the log2 ratios between the two mutants in comparison to the Col-0 control (*SnRK1α1-OE* vs. Col-0, Table S1c; *sesquiα2* vs. Col-0, Table S1e).

TABLE S1A_Col-0 metabolite measurements		Harvest time										
Mean level [nmol/gFW]	Method	Z8	Z12	Z16	Z20	Z24	Z4	Z8	Z12	Z16	Z20	Z24
UDP-glc	LC-MS/MS	64,201	76,359	79,546	59,773	62,392	62,372	64,072	72,125	74,843	85,949	70,265
UDP-Gal	LC-MS/MS	19,077	22,179	24,711	17,990	19,680	18,298	18,460	21,348	21,563	25,435	22,068
Sucrose (as hexose equivalents)	Enzymatic	1386,575	1970,492	1842,906	1099,582	751,458	1480,129	1383,005	2197,037	1861,442	1512,924	935,456
T6P	LC-MS/MS	0,242	0,368	0,214	0,130	0,088	0,226	0,243	0,435	0,219	0,204	0,110
Glucose	Enzymatic	1393,408	880,976	1226,339	367,725	215,410	1845,184	1091,754	1753,328	951,712	784,183	647,770
Fructose	Enzymatic	521,328	389,838	475,896	71,027	96,979	815,992	391,880	574,627	355,162	261,249	205,642
Starch (as hexose equivalents)	Enzymatic	38819,968	49691,737	36352,023	15442,414	3149,454	18953,389	39528,208	51787,631	38674,893	20805,635	4522,036
S6P	LC-MS/MS	0,310	0,378	0,824	0,391	0,334	0,308	0,259	0,347	0,753	0,641	0,432
G6P	LC-MS/MS	147,180	174,483	253,711	165,414	141,693	125,722	155,885	170,254	234,494	174,566	161,987
G1P	LC-MS/MS	14,306	15,994	19,083	13,684	13,698	14,281	13,687	15,022	17,845	19,381	17,464
G1,6BP	LC-MS/MS	3,661	4,016	3,349	2,562	2,653	3,783	3,773	3,803	3,115	3,274	2,728
F6P	LC-MS/MS	41,621	52,097	90,631	42,902	40,141	37,904	41,730	48,943	61,211	53,491	42,508
FBP	LC-MS/MS	1,235	1,377	1,761	1,070	0,639	1,282	1,405	1,361	1,581	1,041	1,097
Gal1P	LC-MS/MS	3,735	3,831	4,836	3,600	3,861	3,370	3,347	3,541	4,318	5,097	4,579
Man6P	LC-MS/MS	27,282	30,132	40,703	29,712	34,264	20,457	26,420	29,374	35,076	37,866	37,581
Unknown Peak Before S6P	LC-MS/MS	0,378	0,335	0,326	0,232	0,265	0,350	0,341	0,356	0,280	0,366	0,342
Glycerate	LC-MS/MS	228,925	240,196	118,207	89,643	157,242	207,925	188,423	236,330	143,103	213,657	142,925
Gly3P	LC-MS/MS	23,363	24,383	19,645	15,267	22,072	20,651	17,485	18,359	19,115	31,628	27,799
3-PGA	LC-MS/MS	103,965	137,560	139,791	107,639	97,147	93,418	120,785	130,237	139,203	94,175	104,228
PEP	LC-MS/MS	12,880	13,608	19,477	15,038	13,232	10,017	12,779	11,950	17,773	7,738	15,552
Pyruvate	LC-MS/MS	174,700	162,381	130,699	104,062	104,462	171,591	165,804	178,776	122,233	129,574	130,154
Unknown Peak After S6P	LC-MS/MS	0,124	0,122	0,119	0,084	0,085	0,133	0,113	0,133	0,103	0,128	0,124
Malate	LC-MS/MS	13083,469	15610,541	9868,444	5933,102	4458,855	12608,587	12233,244	14498,814	8255,421	10704,094	9601,166
Citrate	LC-MS/MS	9588,916	8378,559	10210,036	8983,373	10917,737	10972,849	8828,927	8022,093	8801,390	11522,318	12211,645
Isocitrate	LC-MS/MS	67,207	65,360	64,341	57,801	64,891	72,804	60,457	58,779	58,302	73,119	86,555
2-OG	LC-MS/MS	293,261	306,431	247,400	175,384	160,227	336,213	266,747	296,991	218,683	249,637	245,113
Succinate	LC-MS/MS	299,709	242,610	404,266	333,087	377,159	342,663	235,332	254,842	318,976	395,737	438,426
Fumarate	LC-MS/MS	9128,954	11136,969	6511,546	4595,120	3742,354	9609,903	9552,513	10815,526	5842,064	7739,466	5823,467
Aconitate	LC-MS/MS	93,210	83,927	98,826	86,735	99,352	93,593	83,701	82,674	95,850	104,896	113,109
Unknown Peak 2 After S6P	LC-MS/MS	0,021	0,020	0,024	0,017	0,013	0,021	0,016	0,025	0,022	0,019	0,015
Protein (mg/gFW)	Enzymatic	7,250	7,057	6,797	7,166	8,014	7,632	7,226	7,316	6,795	7,070	7,516
NO2	Enzymatic	458,867	561,850	558,954	544,919	580,662	494,455	560,404	528,397	438,039	484,599	612,949
NO3	Enzymatic	125894,158	138229,740	127686,506	138388,466	130344,865	130618,109	134435,443	135668,293	133073,913	121937,517	125208,341
Shikimate	LC-MS/MS	41,619	49,193	36,684	25,367	26,163	45,740	40,437	44,775	33,692	38,563	27,911
Unknown Peak Before ADP-Glc	LC-MS/MS	0,191	0,258	0,132	0,128	0,166	0,239	0,192	0,246	0,081	0,260	0,150
Unknown Peak Before G1,6BP	LC-MS/MS	1,544	1,479	1,569	1,202	1,289	1,346	1,468	1,599	1,413	1,390	1,329
Unknown Peak After G1,6BP	LC-MS/MS	11,188	12,199	13,452	11,653	13,269	13,673	13,289	12,360	11,904	12,782	14,804
Unknown Peak Before Glycerate	LC-MS/MS	55,428	53,910	47,703	43,006	48,255	63,538	50,143	50,809	46,796	55,555	56,679

TABLE S1A_Col-0 Std Dev		Harvest time										
Mean level [nmol/gFW]	Method	Z8	Z12	Z16	Z20	Z24	Z4	Z8	Z12	Z16	Z20	Z24
UDP-glc	LC-MS/MS	15,534	6,698	11,763	9,644	8,859	13,647	18,790	17,234	10,345	12,863	12,670
UDP-Gal	LC-MS/MS	5,038	2,391	2,950	2,781	3,029	3,474	5,228	5,312	3,286	3,157	3,445
Sucrose (as hexose equivalents)	Enzymatic	302,833	285,949	209,215	114,797	28,384	84,163	116,940	252,649	184,323	123,866	155,432
T6P	LC-MS/MS	0,043	0,061	0,033	0,019	0,019	0,049	0,085	0,093	0,040	0,031	0,023
Glucose	Enzymatic	856,498	419,450	549,296	108,838	45,634	483,721	238,281	926,520	583,744	409,612	412,854
Fructose	Enzymatic	355,713	189,170	232,353	53,725	59,701	269,842	51,835	350,106	272,046	166,508	170,349
Starch (as hexose equivalents)	Enzymatic	1432,086	3006,988	3066,602	2269,069	253,255	532,660	1985,149	4625,848	1192,505	1859,824	1259,832
S6P	LC-MS/MS	0,102	0,084	0,167	0,115	0,064	0,066	0,077	0,058	0,125	0,311	0,158
G6P	LC-MS/MS	14,878	36,650	43,432	29,810	21,502	21,885	49,559	21,213	34,025	21,093	23,243
G1P	LC-MS/MS	4,389	2,439	3,041	1,681	2,298	3,220	4,118	4,607	3,654	4,197	3,218
G1,6BP	LC-MS/MS	0,950	0,342	0,464	0,337	0,548	0,485	1,039	0,689	0,411	0,734	0,391
F6P	LC-MS/MS	6,894	7,946	59,571	6,959	8,491	4,735	11,629	8,590	8,214	9,921	4,714
FBP	LC-MS/MS	0,404	0,312	0,459	0,139	0,137	0,189	0,423	0,425	0,204	0,239	0,510
Gal1P	LC-MS/MS	0,975	0,501	0,642	0,686	0,564	0,758	0,977	0,923	0,771	0,768	0,836
Man6P	LC-MS/MS	4,797	3,687	5,508	7,691	4,887	3,343	7,898	6,600	5,055	4,303	5,792
Unknown Peak Before S6P	LC-MS/MS	0,097	0,108	0,055	0,020	0,039	0,093	0,092	0,094	0,053	0,046	0,063
Glycerate	LC-MS/MS	104,685	91,611	69,912	48,297	53,506	56,552	94,022	63,915	86,397	49,312	88,182
Gly3P	LC-MS/MS	7,399	5,410	4,163	2,289	5,182	7,271	6,721	6,270	3,719	20,422	9,747
3-PGA	LC-MS/MS	10,396	56,185	30,273	21,668	19,627	20,978	40,106	18,563	20,072	16,622	11,214
PEP	LC-MS/MS	5,191	7,862	7,728	5,686	5,618	4,160	3,512	1,983	2,357	2,862	3,693
Pyruvate	LC-MS/MS	65,274	25,577	20,425	39,524	69,012	29,526	46,161	15,531	35,277	32,021	63,393
Unknown Peak After S6P	LC-MS/MS	0,034	0,035	0,024	0,011	0,015	0,028	0,035	0,035	0,018	0,019	0,030
Malate	LC-MS/MS	5321,472	3486,424	3042,617	2333,615	680,926	2447,335	3984,768	3832,353	2154,970	4667,222	3657,266
Citrate	LC-MS/MS	1579,853	1220,653	1566,503	1017,658	979,541	1029,897	2632,522	1642,416	1533,336	1869,566	1839,457
Isocitrate	LC-MS/MS	14,531	10,606	13,066	9,796	11,325	7,109	15,265	13,065	12,132	14,003	13,276
2-OG	LC-MS/MS	123,643	38,017	41,742	35,349	24,078	48,254	83,527	76,501	47,098	98,077	63,316
Succinate	LC-MS/MS	71,447	47,410	65,288	77,244	47,184	78,977	61,595	59,757	81,313	96,013	96,061
Fumarate	LC-MS/MS	3624,058	3156,559	2085,479	2223,623	544,792	2729,464	3803,100	4409,066	1712,220	2787,513	2717,957
Aconitate	LC-MS/MS	16,405	11,580	20,312	9,218	16,662	6,607	24,799	14,024	19,665	18,980	12,302
Unknown Peak 2 After S6P	LC-MS/MS	0,006	0,005	0,002	0,003	0,002	0,003	0,004	0,006	0,005	0,005	0,004
Protein (mg/gFW)	Enzymatic	1,094	0,444	0,528	0,697	1,425	0,314	0,699	0,598	0,456	1,262	1,261
NO2	Enzymatic	55,461	182,501	46,352	197,928	160,099	50,794	117,868	19,186	71,953	91,025	102,420
NO3	Enzymatic	9741,640	5861,069	11426,604	8572,364	7341,427	8997,531	8821,054	7802,169	5248,478	5159,675	2682,221
Shikimate	LC-MS/MS	14,169	11,071	6,160	5,659	5,249	5,883	11,230	9,330	7,195	7,030	6,211
Unknown Peak Before ADP-Glc	LC-MS/MS	0,111	0,088	0,077	0,074	0,072	0,098	0,097	0,161	0,006	0,064	0,073
Unknown Peak Before G1,6BP	LC-MS/MS	0,241	0,080	0,268	0,165	0,277	0,295	0,424	0,326	0,127	0,143	0,276
Unknown Peak After G1,6BP	LC-MS/MS	5,755	1,417	2,757	2,732	3,503	1,596	3,865	2,907	2,031	2,362	4,048
Unknown Peak Before Glycerate	LC-MS/MS	16,948	17,460	13,857	11,472	10,085	13,504	14,935	16,735	15,078	14,505	13,547

TABLE S1B_SnRK1a1- OE metabolite measurements		Harvest time										
Mean level [nmol/gFW]	Method	Z8	Z12	Z16	Z20	Z24	Z4	Z8	Z12	Z16	Z20	Z24
UDP-glc	LC-MS/MS	72,096	61,947	88,112	52,165	53,413	65,371	77,900	60,667	86,451	85,422	52,534
UDP-Gal	LC-MS/MS	21,141	17,583	25,431	15,558	16,775	19,263	22,024	17,637	24,522	24,740	16,819
Sucrose (as hexose equivalents)	Enzymatic	1489,805	2365,200	2239,071	1311,439	827,812	1490,300	1729,348	2802,782	2232,146	1683,341	1049,636
T6P	LC-MS/MS	0,499	0,895	0,470	0,208	0,156	0,414	0,629	1,069	0,540	0,376	0,163
Glucose	Enzymatic	1471,304	496,156	608,638	647,438	186,956	1433,065	1601,065	1435,259	724,325	641,686	513,277
Fructose	Enzymatic	550,390	192,150	237,017	243,449	125,803	650,823	577,642	468,187	275,892	226,259	231,219
Starch (as hexose equivalents)	Enzymatic	38814,276	53961,050	41436,971	18932,652	3994,222	17449,670	42570,114	53812,924	41921,508	21537,132	4844,680
S6P	LC-MS/MS	0,280	0,329	1,096	0,418	0,336	0,336	0,322	0,350	0,972	0,760	0,329
G6P	LC-MS/MS	161,348	180,803	256,575	145,849	119,658	147,820	169,179	179,293	251,639	173,683	116,657
G1P	LC-MS/MS	14,225	13,542	19,134	10,114	11,017	13,077	14,952	12,904	19,383	18,432	11,362
G1,6BP	LC-MS/MS	4,465	3,684	3,533	2,268	2,414	3,002	4,059	3,471	4,181	3,121	2,240
F6P	LC-MS/MS	47,580	54,288	73,868	37,613	33,727	41,895	50,584	54,383	67,571	54,654	32,406
FBP	LC-MS/MS	1,438	1,280	1,509	0,970	0,650	0,907	1,173	1,318	1,877	1,126	0,811
Gal1P	LC-MS/MS	3,644	3,159	5,275	2,773	3,203	3,869	3,746	2,987	5,078	5,015	3,227
Man6P	LC-MS/MS	27,671	29,762	45,693	26,212	27,497	30,187	25,809	26,760	41,251	39,828	27,445
Unknown Peak Before S6P	LC-MS/MS	0,371	0,291	0,357	0,217	0,270	0,322	0,378	0,306	0,390	0,391	0,281
Glycerate	LC-MS/MS	272,090	245,839	165,816	97,959	130,675	166,010	240,645	149,947	145,489	148,576	116,784
Gly3P	LC-MS/MS	24,572	18,757	24,867	14,302	18,577	22,589	21,314	15,316	28,649	23,935	16,984
3-PGA	LC-MS/MS	114,636	115,036	141,050	95,226	85,346	97,773	106,385	100,080	138,076	99,104	77,024
PEP	LC-MS/MS	11,356	11,017	19,074	15,360	12,946	11,952	10,051	9,509	20,007	9,352	10,484
Pyruvate	LC-MS/MS	176,479	140,987	116,048	84,171	97,076	139,202	159,654	128,072	112,908	89,392	86,318
Unknown Peak After S6P	LC-MS/MS	0,140	0,120	0,148	0,080	0,099	0,129	0,139	0,126	0,160	0,158	0,111
Malate	LC-MS/MS	15082,964	12088,964	10824,953	4743,767	5125,726	8813,515	14351,337	11191,024	10854,050	10125,147	6420,074
Citrate	LC-MS/MS	9274,813	7012,701	10968,973	7553,189	9635,868	9531,610	8968,818	6188,595	9944,327	11261,368	9417,438
Isocitrate	LC-MS/MS	69,355	55,207	62,491	47,815	59,359	64,514	65,894	45,833	71,851	71,165	58,662
2-OG	LC-MS/MS	274,228	205,585	188,959	101,580	122,021	206,463	277,428	176,973	222,975	165,727	116,053
Succinate	LC-MS/MS	321,451	180,719	445,509	306,651	363,852	354,726	329,032	212,520	396,695	463,393	378,777
Fumarate	LC-MS/MS	11961,581	9352,294	11519,507	3576,660	4631,840	7281,636	12211,985	9162,011	10253,344	10711,135	5479,711
Aconitate	LC-MS/MS	93,167	70,938	102,611	72,308	89,199	92,373	87,020	61,131	99,689	106,121	81,949
Unknown Peak 2 After S6P	LC-MS/MS	0,019	0,017	0,026	0,012	0,012	0,020	0,017	0,025	0,027	0,023	0,016
Protein (mg/gFW)	Enzymatic	8,353	9,218	8,372	8,051	9,094	8,026	7,963	7,149	8,055	8,366	7,855
NO2	Enzymatic	465,782	468,001	804,001	1047,213	1136,620	613,897	513,810	474,723	472,414	539,003	563,215
NO3	Enzymatic	121372,519	146169,348	140460,242	135519,648	137174,007	134699,119	134177,815	136656,200	129792,892	122095,058	124692,489
Shikimate	LC-MS/MS	47,494	41,778	44,568	22,098	26,048	33,870	46,844	37,547	39,926	37,097	24,043
Unknown Peak Before ADP-Glc	LC-MS/MS	0,221	0,148	0,225	0,063	0,130	0,180	0,252	0,154	0,267	0,279	0,124
Unknown Peak Before G1,6BP	LC-MS/MS	1,593	1,303	1,816	0,968	1,196	1,270	1,241	1,135	1,876	1,480	1,088
Unknown Peak After G1,6BP	LC-MS/MS	12,617	10,555	11,818	9,540	11,338	11,101	10,264	8,896	14,622	11,414	10,669
Unknown Peak Before Glycerate	LC-MS/MS	60,161	51,448	60,260	30,200	46,323	45,620	52,614	41,172	58,527	66,020	43,799

TABLE S1B_SnRK1a1- OE Std Dev		Harvest Time										
Mean level [nmol/gFW]	Method	Z8	Z12	Z16	Z20	Z24	Z4	Z8	Z12	Z16	Z20	Z24
UDP-glc	LC-MS/MS	10,076	20,511	8,380	20,975	9,011	18,872	9,414	16,795	25,318	13,081	16,932
UDP-Gal	LC-MS/MS	2,911	6,133	2,170	6,454	3,130	5,445	2,206	4,989	6,838	3,643	5,150
Sucrose (as hexose equivalents)	Enzymatic	120,101	249,678	301,993	240,835	35,766	278,891	82,865	288,173	86,494	267,339	149,907
T6P	LC-MS/MS	0,049	0,379	0,038	0,087	0,034	0,075	0,083	0,239	0,049	0,060	0,060
Glucose	Enzymatic	359,538	217,706	367,451	451,910	132,217	207,856	476,024	526,194	294,073	478,202	252,069
Fructose	Enzymatic	171,534	29,453	116,769	185,648	64,768	98,953	262,066	225,810	146,490	203,587	106,072
Starch (as hexose equivalents)	Enzymatic	1926,205	939,381	1615,558	1448,437	551,783	2329,032	1658,531	2214,747	1321,704	724,376	827,720
S6P	LC-MS/MS	0,059	0,135	0,187	0,147	0,079	0,125	0,063	0,116	0,502	0,109	0,136
G6P	LC-MS/MS	22,889	41,741	44,241	44,727	15,326	39,893	27,843	43,929	94,986	26,454	29,064
G1P	LC-MS/MS	2,378	5,545	1,738	3,778	2,687	2,999	1,721	4,043	6,457	3,142	4,167
G1,6BP	LC-MS/MS	0,600	0,813	0,282	0,720	0,450	0,219	0,288	0,663	1,071	0,315	0,576
F6P	LC-MS/MS	5,525	17,076	4,971	11,536	5,551	11,827	5,053	14,752	22,729	6,896	9,424
FBP	LC-MS/MS	0,253	0,289	0,417	0,226	0,076	0,258	0,215	0,208	0,556	0,275	0,211
Gal1P	LC-MS/MS	0,588	1,224	0,455	1,012	0,739	1,503	0,583	0,913	1,675	0,839	1,237
Man6P	LC-MS/MS	3,682	8,958	3,327	8,082	4,268	15,479	3,456	7,115	16,143	4,479	8,597
Unknown Peak Before S6P	LC-MS/MS	0,066	0,139	0,045	0,081	0,068	0,062	0,065	0,091	0,047	0,071	0,101
Glycerate	LC-MS/MS	61,873	161,136	92,887	63,239	49,772	76,745	130,469	38,267	9,784	71,444	57,470
Gly3P	LC-MS/MS	7,727	7,160	4,581	6,317	5,774	5,673	4,097	4,224	5,170	5,613	5,815
3-PGA	LC-MS/MS	30,650	15,830	42,118	28,924	13,802	19,659	24,439	8,888	45,132	29,374	18,259
PEP	LC-MS/MS	5,059	2,102	10,236	4,240	4,681	3,661	4,825	3,453	8,306	7,383	2,838
Pyruvate	LC-MS/MS	29,046	51,678	24,834	39,306	15,881	38,309	18,342	58,715	14,612	16,924	14,231
Unknown Peak After S6P	LC-MS/MS	0,027	0,063	0,016	0,038	0,027	0,025	0,027	0,038	0,016	0,027	0,038
Malate	LC-MS/MS	3189,101	5187,394	2116,314	2331,996	1403,686	1653,186	2982,698	3880,929	2827,997	2589,274	2519,199
Citrate	LC-MS/MS	1025,566	1801,216	694,942	2177,714	2360,530	1413,331	1642,688	1163,714	1805,364	1845,958	2858,279
Isocitrate	LC-MS/MS	12,613	21,469	2,791	15,949	16,166	5,653	9,936	12,271	19,559	14,326	19,580
2-OG	LC-MS/MS	29,582	88,106	26,981	39,732	32,098	42,404	37,684	61,397	39,858	34,429	34,904
Succinate	LC-MS/MS	39,085	65,741	37,913	95,356	65,905	83,373	73,020	75,076	113,863	88,309	136,585
Fumarate	LC-MS/MS	3792,087	3811,212	2725,551	1611,280	1472,481	2139,788	4959,974	3152,498	3139,387	3542,209	3222,632
Aconitate	LC-MS/MS	13,889	28,634	3,689	23,847	21,649	14,338	11,815	13,836	29,560	19,994	25,765
Unknown Peak 2 After S6P	LC-MS/MS	0,002	0,006	0,001	0,006	0,003	0,005	0,006	0,007	0,004	0,002	0,006
Protein (mg/gFW)	Enzymatic	0,351	0,483	1,071	0,811	0,421	1,380	0,972	0,405	0,913	0,629	1,041
NO2	Enzymatic	27,243	108,346	289,391	491,120	470,230	117,309	112,071	27,478	36,098	64,841	81,707
NO3	Enzymatic	9092,297	12355,057	6179,142	12998,856	14492,296	6106,217	6430,398	7854,636	6432,696	9687,695	9224,896
Shikimate	LC-MS/MS	8,690	16,513	5,428	6,773	6,295	7,984	9,587	8,471	8,784	7,765	8,591
Unknown Peak Before ADP-Glc	LC-MS/MS	0,138	0,095	0,095	0,061	0,102	0,104	0,093	0,052	0,008	0,120	0,092
Unknown Peak Before G1,6BP	LC-MS/MS	0,209	0,410	0,191	0,347	0,228	0,163	0,138	0,207	0,470	0,252	0,364
Unknown Peak After G1,6BP	LC-MS/MS	2,053	1,488	1,928	1,908	2,045	0,998	1,282	1,118	5,220	1,849	2,606
Unknown Peak Before Glycerate	LC-MS/MS	19,071	26,428	14,097	10,818	15,337	4,267	13,931	11,498	18,170	17,088	21,458

Table S1C_SignalLog2 Ratios_SnRK1a1-OE vs. Col0											
Harvest time	Z8	Z12	Z16	Z20	Z24	Z4	Z8	Z12	Z16	Z20	Z24
UDP-glc	0,167	-0,302	0,148	-0,196	-0,224	0,068	0,282	-0,250	0,208	-0,009	-0,420
UDP-Gal	0,148	-0,335	0,041	-0,210	-0,230	0,074	0,255	-0,276	0,186	-0,040	-0,392
Sucrose	0,104	0,263	0,281	0,254	0,140	0,010	0,322	0,351	0,262	0,154	0,166
T6P	1,044	1,283	1,133	0,679	0,829	0,876	1,372	1,295	1,303	0,878	0,566
Glucose	0,078	-0,828	-1,011	0,816	-0,204	-0,365	0,552	-0,289	-0,394	-0,289	-0,336
Fructose	0,078	-1,021	-1,006	1,777	0,375	-0,326	0,560	-0,296	-0,364	-0,207	0,169
Starch	0,000	0,119	0,189	0,294	0,343	-0,119	0,107	0,055	0,116	0,050	0,099
S6P	-0,146	-0,199	0,411	0,097	0,007	0,124	0,312	0,012	0,370	0,247	-0,393
G6P	0,133	0,051	0,016	-0,182	-0,244	0,234	0,118	0,075	0,102	-0,007	-0,474
G1P	-0,008	-0,240	0,004	-0,436	-0,314	-0,127	0,128	-0,219	0,119	-0,072	-0,620
G1,6BP	0,286	-0,124	0,077	-0,176	-0,136	-0,334	0,105	-0,132	0,425	-0,069	-0,284
F6P	0,193	0,059	-0,295	-0,190	-0,251	0,144	0,278	0,152	0,143	0,031	-0,391
FBP	0,219	-0,105	-0,223	-0,142	0,025	-0,499	-0,260	-0,047	0,247	0,112	-0,435
Gal1P	-0,036	-0,278	0,125	-0,377	-0,270	0,199	0,162	-0,246	0,234	-0,023	-0,505
Man6P	0,020	-0,018	0,167	-0,181	-0,317	0,561	-0,034	-0,134	0,234	0,073	-0,453
Unknown Peak Before S6P	-0,028	-0,204	0,129	-0,099	0,030	-0,120	0,152	-0,217	0,477	0,098	-0,280
Glycerate	0,249	0,034	0,488	0,128	-0,267	-0,325	0,353	-0,656	0,024	-0,524	-0,291
Gly3P	0,073	-0,378	0,340	-0,094	-0,249	0,129	0,286	-0,261	0,584	-0,402	-0,711
3-PGA	0,141	-0,258	0,013	-0,177	-0,187	0,066	-0,183	-0,380	-0,012	0,074	-0,436
PEP	-0,182	-0,305	-0,030	0,031	-0,031	0,255	-0,346	-0,330	0,171	0,273	-0,569
Pyruvate	0,015	-0,204	-0,172	-0,306	-0,106	-0,302	-0,055	-0,481	-0,114	-0,536	-0,592
Unknown Peak After S6P	0,168	-0,019	0,313	-0,060	0,234	-0,050	0,300	-0,085	0,641	0,302	-0,163
Malate	0,205	-0,369	0,133	-0,323	0,201	-0,517	0,230	-0,374	0,395	-0,080	-0,581
Citrate	-0,048	-0,257	0,103	-0,250	-0,180	-0,203	0,023	-0,374	0,176	-0,033	-0,375
Isocitrate	0,045	-0,244	-0,042	-0,274	-0,129	-0,174	0,124	-0,359	0,301	-0,039	-0,561
2-OG	-0,097	-0,576	-0,389	-0,788	-0,393	-0,703	0,057	-0,747	0,028	-0,591	-1,079
Succinate	0,101	-0,425	0,140	-0,119	-0,052	0,050	0,484	-0,262	0,315	0,228	-0,211
Fumarate	0,390	-0,252	0,823	-0,361	0,308	-0,400	0,354	-0,239	0,812	0,469	-0,088
Aconitate	-0,001	-0,243	0,054	-0,262	-0,156	-0,019	0,056	-0,436	0,057	0,017	-0,465
Unknown Peak 2 After S6P	-0,113	-0,200	0,113	-0,471	-0,086	-0,067	0,079	0,051	0,279	0,305	0,105
Protein	0,204	0,385	0,301	0,168	0,182	0,073	0,140	-0,033	0,246	0,243	0,064
NO2	0,022	-0,264	0,524	0,942	0,969	0,312	-0,125	-0,155	0,109	0,154	-0,122
NO3	-0,053	0,081	0,138	-0,030	0,074	0,044	-0,003	0,010	-0,036	0,002	-0,006
Shikimate	0,191	-0,236	0,281	-0,199	-0,006	-0,433	0,212	-0,254	0,245	-0,056	-0,215
Unknown Peak Before ADP-Glc	0,207	-0,801	0,766	-1,023	-0,360	-0,409	0,390	-0,678	1,717	0,103	-0,271
Unknown Peak Before G1,6BP	0,045	-0,183	0,210	-0,313	-0,109	-0,085	-0,242	-0,494	0,409	0,091	-0,289
Unknown Peak After G1,6BP	0,173	-0,209	-0,187	-0,289	-0,227	-0,301	-0,373	-0,474	0,297	-0,163	-0,472
Unknown Peak Before Glycerate	0,118	-0,067	0,337	-0,510	-0,059	-0,478	0,069	-0,303	0,323	0,249	-0,372

TABLE S1D_sesquiα2 metabolite measurements		Harvest time										
Mean level [nmol/gFW]	Method	Z8	Z12	Z16	Z20	Z24	Z4	Z8	Z12	Z16	Z20	Z24
UDP-glc	LC-MS/MS	75,135	77,984	86,428	81,139	56,822	61,690	48,684	72,972	85,936	78,302	50,957
UDP-Gal	LC-MS/MS	20,652	22,335	24,656	24,028	17,633	17,525	14,123	20,560	24,709	22,318	16,855
Sucrose (as hexose equivalents)	Enzymatic	1046,150	1837,680	1713,356	1145,337	751,918	1097,449	1133,967	1519,270	1631,142	1359,504	746,478
T6P	LC-MS/MS	0,055	0,113	0,056	0,049	0,045	0,068	0,060	0,115	0,069	0,055	0,028
Glucose	Enzymatic	896,511	910,342	727,208	743,455	532,651	1280,285	1241,122	924,792	409,375	665,219	810,610
Fructose	Enzymatic	238,958	290,214	156,803	158,744	134,918	411,958	276,364	264,949	95,576	196,721	185,255
Starch (as hexose equivalents)	Enzymatic	31423,904	51344,109	32321,814	16260,185	4399,759	17120,967	34146,547	47510,319	34347,894	19141,845	4533,055
S6P	LC-MS/MS	0,221	0,360	0,616	0,475	0,276	0,257	0,199	0,328	0,713	0,429	0,255
G6P	LC-MS/MS	153,733	166,630	191,494	157,362	128,412	100,613	92,635	134,058	220,083	163,065	107,230
G1P	LC-MS/MS	17,495	16,928	20,922	18,708	14,403	15,056	12,335	16,200	19,532	17,033	12,996
G1,6BP	LC-MS/MS	3,912	4,161	2,821	2,558	2,439	3,385	3,060	3,829	3,052	2,736	2,096
F6P	LC-MS/MS	44,528	49,972	56,422	46,691	34,053	29,523	24,172	34,814	57,171	46,810	29,020
FBP	LC-MS/MS	1,335	1,631	1,019	0,932	0,688	1,185	0,939	1,145	1,397	1,018	0,767
Gal1P	LC-MS/MS	3,488	3,551	4,868	4,290	3,616	3,029	2,628	3,301	4,457	4,068	3,106
Man6P	LC-MS/MS	22,515	27,134	34,999	30,398	28,278	15,482	15,867	23,174	33,374	29,410	22,343
Unknown Peak Before S6P	LC-MS/MS	0,287	0,352	0,274	0,281	0,234	0,339	0,293	0,371	0,278	0,270	0,217
Glycerate	LC-MS/MS	196,385	183,009	106,910	92,209	64,250	106,667	137,809	187,291	83,552	90,103	62,745
Gly3P	LC-MS/MS	19,163	17,422	26,443	20,736	18,534	19,453	15,247	21,468	29,262	16,628	15,393
3-PGA	LC-MS/MS	92,963	95,849	100,469	78,115	86,919	65,315	62,487	75,224	106,853	91,099	65,532
PEP	LC-MS/MS	9,714	11,591	13,727	7,416	15,743	5,620	9,422	8,618	17,191	12,642	9,171
Pyruvate	LC-MS/MS	157,108	149,449	120,383	92,688	80,879	141,689	131,821	160,325	136,025	100,878	70,697
Unknown Peak After S6P	LC-MS/MS	0,111	0,156	0,115	0,111	0,102	0,152	0,113	0,167	0,124	0,103	0,086
Malate	LC-MS/MS	13333,889	15966,109	10312,641	8159,344	5211,233	11990,284	13037,489	18052,377	10543,830	7776,376	5459,036
Citrate	LC-MS/MS	9415,365	10742,224	11005,718	11168,455	11484,588	11575,852	9695,655	11076,955	11500,556	12143,076	11514,954
Isocitrate	LC-MS/MS	98,471	109,144	116,311	107,320	96,405	129,109	94,796	119,011	103,220	100,833	100,687
2-OG	LC-MS/MS	265,115	231,554	210,381	186,008	135,706	311,916	250,544	290,711	217,437	173,170	142,157
Succinate	LC-MS/MS	146,793	148,591	242,572	232,031	220,242	189,413	167,402	171,505	215,113	210,950	195,877
Fumarate	LC-MS/MS	9551,569	13377,063	8814,670	6967,923	4243,141	8877,211	11225,841	14307,513	8619,010	5923,957	4680,154
Aconitate	LC-MS/MS	137,862	156,183	179,914	178,309	155,453	176,854	137,438	165,344	155,016	168,282	160,560
Unknown Peak 2 After S6P	LC-MS/MS	0,012	0,020	0,015	0,016	0,018	0,021	0,015	0,021	0,024	0,016	0,012
Protein (mg/gFW)	Enzymatic	12,172	12,546	13,152	12,223	12,830	11,730	11,964	12,771	12,602	12,957	12,103
NO2	Enzymatic	756,187	1089,456	1154,892	735,500	783,546	671,157	633,087	736,526	732,248	844,161	872,817
NO3	Enzymatic	142010,542	144691,799	138750,397	147085,232	158829,344	148135,167	145832,382	136461,121	133756,439	141140,158	158769,000
Shikimate	LC-MS/MS	37,302	47,104	32,668	30,316	23,401	36,201	34,623	46,800	31,866	27,645	24,015
Unknown Peak Before ADP-Glc	LC-MS/MS	0,052	0,041	0,074	0,073	0,034	0,046	0,038	0,060	0,074	0,090	0,045
Unknown Peak Before G1,6BP	LC-MS/MS	1,064	1,255	1,050	0,993	1,061	1,054	1,132	1,863	1,020	0,992	0,867
Unknown Peak After G1,6BP	LC-MS/MS	12,952	13,371	12,694	11,202	15,246	12,976	14,739	13,755	14,534	13,318	13,058
Unknown Peak Before Glycerate	LC-MS/MS	75,697	85,145	84,988	82,916	61,301	95,850	68,053	89,524	67,289	57,293	55,892

TABLE S1D_sesquiα2 Std Dev		Harvest Time										
Mean level [nmol/gFW]	Method	Z8	Z12	Z16	Z20	Z24	Z4	Z8	Z12	Z16	Z20	Z24
UDP-glc	LC-MS/MS	12,063	3,583	12,074	11,112	5,651	7,065	6,515	10,679	4,795	8,657	9,435
UDP-Gal	LC-MS/MS	2,669	1,818	3,395	2,765	1,247	2,394	1,975	1,522	1,047	1,881	3,171
Sucrose (as hexose equivalents)	Enzymatic	112,997	131,869	66,658	87,034	99,552	231,612	156,170	98,419	108,578	77,678	85,863
T6P	LC-MS/MS	0,006	0,006	0,008	0,007	0,034	0,017	0,014	0,016	0,003	0,007	0,008
Glucose	Enzymatic	175,325	543,425	147,879	147,225	209,100	144,928	282,870	243,244	108,860	317,658	266,375
Fructose	Enzymatic	98,170	187,053	36,126	25,223	104,158	89,408	121,290	69,100	68,396	82,960	48,436
Starch (as hexose equivalents)	Enzymatic	1354,778	2174,463	2219,753	1946,615	942,155	896,027	2797,766	1597,916	1081,224	1726,119	697,518
S6P	LC-MS/MS	0,037	0,038	0,236	0,121	0,064	0,037	0,020	0,060	0,039	0,078	0,092
G6P	LC-MS/MS	22,252	20,926	27,360	15,922	34,690	17,639	17,267	21,613	25,299	11,261	20,594
G1P	LC-MS/MS	2,651	0,664	1,915	2,696	1,206	2,604	1,609	1,359	1,674	2,343	2,467
G1,6BP	LC-MS/MS	0,496	0,305	0,484	0,248	0,254	0,542	0,348	0,679	0,454	0,289	0,358
F6P	LC-MS/MS	7,130	3,522	8,727	4,665	5,424	3,143	3,334	2,580	6,118	6,474	4,767
FBP	LC-MS/MS	0,422	0,468	0,252	0,224	0,182	0,262	0,232	0,244	0,428	0,158	0,091
Gal1P	LC-MS/MS	0,400	0,140	0,162	0,434	0,476	0,420	0,297	0,326	0,333	0,462	0,584
Man6P	LC-MS/MS	1,758	1,126	1,511	2,933	9,785	2,805	1,543	2,915	3,213	2,399	3,609
Unknown Peak Before S6P	LC-MS/MS	0,035	0,019	0,050	0,047	0,030	0,031	0,021	0,045	0,029	0,020	0,041
Glycerate	LC-MS/MS	76,671	18,968	10,684	54,833	15,653	26,412	21,177	22,033	21,267	20,474	12,518
Gly3P	LC-MS/MS	3,444	2,807	5,577	5,442	2,114	1,912	2,085	5,952	4,417	2,170	2,761
3-PGA	LC-MS/MS	23,396	15,801	5,908	3,642	21,062	16,045	9,019	16,925	19,661	14,172	11,886
PEP	LC-MS/MS	4,478	5,501	4,110	1,761	6,092	2,245	2,979	3,703	8,607	4,262	2,198
Pyruvate	LC-MS/MS	16,301	30,048	17,075	6,972	29,629	9,710	24,896	38,876	18,635	22,376	5,940
Unknown Peak After S6P	LC-MS/MS	0,020	0,009	0,016	0,031	0,019	0,011	0,011	0,018	0,013	0,015	0,028
Malate	LC-MS/MS	1508,322	959,400	3453,057	1636,151	2078,215	1211,951	727,172	2503,892	1598,243	1048,880	632,329
Citrate	LC-MS/MS	1327,454	471,417	1320,375	866,369	2358,453	788,524	1276,283	1250,687	1355,009	1241,774	892,386
Isocitrate	LC-MS/MS	18,508	6,025	20,794	12,452	21,602	8,967	11,236	14,307	15,416	8,588	13,862
2-OG	LC-MS/MS	15,151	15,000	43,473	37,526	42,325	35,261	17,050	43,381	25,868	28,609	23,221
Succinate	LC-MS/MS	18,977	7,280	35,590	51,492	61,073	16,503	24,069	25,520	19,700	25,674	30,253
Fumarate	LC-MS/MS	830,475	655,764	3026,943	996,328	1747,772	218,503	1318,253	1455,273	887,217	907,322	737,015
Aconitate	LC-MS/MS	19,519	14,563	22,993	14,613	32,464	8,381	18,849	17,862	12,325	15,920	17,162
Unknown Peak 2 After S6P	LC-MS/MS	0,004	0,003	0,004	0,004	0,010	0,003	0,003	0,004	0,008	0,004	0,004
Protein (mg/gFW)	Enzymatic	1,204	1,746	0,211	0,529	0,525	0,694	0,519	0,235	0,609	1,106	0,610
NO2	Enzymatic	272,114	381,004	588,085	121,751	177,830	26,754	117,329	77,583	164,059	135,320	415,575
NO3	Enzymatic	8459,248	7648,429	13738,816	6995,757	16422,467	12972,217	8056,471	6490,381	5075,890	8643,146	11529,766
Shikimate	LC-MS/MS	4,591	3,808	6,058	5,021	2,920	4,560	4,145	4,812	4,080	2,537	3,394
Unknown Peak Before ADP-Glc	LC-MS/MS	0,044	0,006	0,043	0,024	0,012	0,023	0,017	0,025	0,080	0,036	0,023
Unknown Peak Before G1,6BP	LC-MS/MS	0,137	0,180	0,082	0,114	0,243	0,264	0,141	1,011	0,184	0,089	0,142
Unknown Peak After G1,6BP	LC-MS/MS	2,093	2,109	2,321	1,662	1,814	2,232	2,666	3,449	3,977	1,453	1,321
Unknown Peak Before Glycerate	LC-MS/MS	9,225	4,080	12,789	13,692	10,239	7,040	7,747	19,965	10,438	4,526	3,414

Table S1E_SignalLog2 Ratios_sesquiα2 vs. Col0											
Harvest time	Z8	Z12	Z16	Z20	Z24	Z4	Z8	Z12	Z16	Z20	Z24
UDP-glc	0,227	0,030	0,120	0,441	-0,135	-0,016	-0,396	0,017	0,199	-0,134	-0,464
UDP-Gal	0,114	0,010	-0,003	0,418	-0,158	-0,062	-0,386	-0,054	0,196	-0,189	-0,389
Sucrose	-0,406	-0,101	-0,105	0,059	0,001	-0,432	-0,286	-0,532	-0,191	-0,154	-0,326
T6P	-2,146	-1,697	-1,926	-1,402	-0,950	-1,734	-2,024	-1,922	-1,661	-1,906	-1,991
Glucose	-0,636	0,047	-0,754	1,016	1,306	-0,527	0,185	-0,923	-1,217	-0,237	0,324
Fructose	-1,125	-0,426	-1,602	1,160	0,476	-0,986	-0,504	-1,117	-1,894	-0,409	-0,151
Starch	-0,305	0,047	-0,170	0,074	0,482	-0,147	-0,211	-0,124	-0,171	-0,120	0,004
S6P	-0,486	-0,073	-0,420	0,280	-0,278	-0,261	-0,380	-0,081	-0,077	-0,579	-0,762
G6P	0,063	-0,066	-0,406	-0,072	-0,142	-0,321	-0,751	-0,345	-0,092	-0,098	-0,595
G1P	0,290	0,082	0,133	0,451	0,072	0,076	-0,150	0,109	0,130	-0,186	-0,426
G1,6BP	0,096	0,051	-0,247	-0,003	-0,121	-0,160	-0,302	0,010	-0,029	-0,259	-0,380
F6P	0,097	-0,060	-0,684	0,122	-0,237	-0,360	-0,788	-0,491	-0,099	-0,192	-0,551
FBP	0,112	0,244	-0,789	-0,200	0,107	-0,113	-0,582	-0,250	-0,178	-0,033	-0,515
Gal1P	-0,099	-0,110	0,009	0,253	-0,095	-0,154	-0,349	-0,102	0,046	-0,325	-0,560
Man6P	-0,277	-0,151	-0,218	0,033	-0,277	-0,402	-0,736	-0,342	-0,072	-0,365	-0,750
Unknown Peak Before S6P	-0,395	0,070	-0,251	0,273	-0,179	-0,048	-0,219	0,061	-0,012	-0,439	-0,654
Glycerate	-0,221	-0,392	-0,145	0,041	-1,291	-0,963	-0,451	-0,336	-0,776	-1,246	-1,188
Gly3P	-0,286	-0,485	0,429	0,442	-0,252	-0,086	-0,198	0,226	0,614	-0,928	-0,853
3-PGA	-0,161	-0,521	-0,477	-0,463	-0,161	-0,516	-0,951	-0,792	-0,382	-0,048	-0,669
PEP	-0,407	-0,231	-0,505	-1,020	0,251	-0,834	-0,440	-0,471	-0,048	0,708	-0,762
Pyruvate	-0,153	-0,120	-0,119	-0,167	-0,369	-0,276	-0,331	-0,157	0,154	-0,361	-0,881
Unknown Peak After S6P	-0,168	0,354	-0,051	0,404	0,268	0,186	0,001	0,327	0,268	-0,305	-0,522
Malate	0,027	0,032	0,064	0,460	0,225	-0,073	0,092	0,316	0,353	-0,461	-0,815
Citrate	-0,026	0,359	0,108	0,314	0,073	0,077	0,135	0,466	0,386	0,076	-0,085
Isocitrate	0,551	0,740	0,854	0,893	0,571	0,827	0,649	1,018	0,824	0,464	0,218
2-OG	-0,146	-0,404	-0,234	0,085	-0,240	-0,108	-0,090	-0,031	-0,008	-0,528	-0,786
Succinate	-1,030	-0,707	-0,737	-0,522	-0,776	-0,855	-0,491	-0,571	-0,568	-0,908	-1,162
Fumarate	0,065	0,264	0,437	0,601	0,181	-0,114	0,233	0,404	0,561	-0,386	-0,315
Aconitate	0,565	0,896	0,864	1,040	0,646	0,918	0,715	1,000	0,694	0,682	0,505
Unknown Peak 2 After S6P	-0,748	-0,030	-0,714	-0,152	0,447	-0,006	-0,130	-0,213	0,145	-0,245	-0,291
Protein	0,748	0,830	0,952	0,770	0,679	0,620	0,727	0,804	0,891	0,874	0,687
NO2	0,721	0,955	1,047	0,433	0,432	0,441	0,176	0,479	0,741	0,801	0,510
NO3	0,174	0,066	0,120	0,088	0,285	0,182	0,117	0,008	0,007	0,211	0,343
Shikimate	-0,158	-0,063	-0,167	0,257	-0,161	-0,337	-0,224	0,064	-0,080	-0,480	-0,217
Unknown Peak Before ADP-Glc	-1,884	-2,646	-0,838	-0,811	-2,304	-2,363	-2,331	-2,044	-0,144	-1,525	-1,738
Unknown Peak Before G1,6BP	-0,538	-0,237	-0,580	-0,277	-0,282	-0,354	-0,375	0,220	-0,470	-0,486	-0,617
Unknown Peak After G1,6BP	0,211	0,132	-0,084	-0,057	0,200	-0,076	0,149	0,154	0,288	0,059	-0,181
Unknown Peak Before Glycerate	0,450	0,659	0,833	0,947	0,345	0,593	0,441	0,817	0,524	0,044	-0,020

Other Supplementary Tables (available as electronic files only):

Supplemental Table 2.2 | Differentially expressed genes in the SnRK1α1-OE and sesquiα2 mutants at the end of the day (ED) and end of the night (EN).

Only genes with an FDR< 0.05 and absolute log2FC≥1 were considered as differentially regulated. (a) List of genes upregulated in the SnRK1α1-OE line at ED. (b) List of genes downregulated in the SnRK1α1-OE line at ED. (c) List of genes that are upregulated in the SnRK1α1-OE line at EN. (d) List of genes that are downregulated in the SnRK1α1-OE line at EN. (e) List of genes upregulated in the sesquiα2 mutant at ED. (f) List of genes downregulated in the sesquiα2 mutant at ED. (g) List of genes upregulated in the sesquiα2 mutant at EN. (h) List of genes downregulated in the sesquiα2 mutant at EN.

Supplemental Table 2.3 | Analysis of time point-specific DEGs in SnRK1 mutants.

(a) Genes differentially expressed in the SnRK1α1-OE line both at the end of the day (ED) and end of the night (EN). (b) Genes differentially expressed in the sesquiα2 line both at ED and EN.

Supplemental Table 2.4 | GO enrichment analysis of DEGs in the sesquiα2 mutant.

(a) Enriched GO terms associated with genes differentially expressed in the sesquiα2 mutant both at end of day (ED) and end of night (EN). (b) Enriched GO terms associated with genes differentially expressed in the sesquiα2 mutant only at EN. (c) Enriched GO terms associated with genes differentially expressed in the sesquiα2 mutant only at ED.

Supplemental Table 2.5 | Plant lines, antibodies and primers.
List of all plant lines, antibodies and primers used in this study.

qRT-PCR primers	Name	Sequence
PYL5	PYL5_qPCR_F	GGTCACCGGTGCAACTCC
	PYL5_qPCR_R	CGCGTGGATCATCTGCACC
BGAL4	BGAL4_qPCR_F	CAAGAAGATGCTCCTGGTCC
	BGAL4_qPCR_R	AGCTCCAAGCGATGTAACGG
DIN10	DIN10_qPCR_F	GATTCTTCGTGCTCGACTCC
	DIN10_qPCR_R	TTAGCAAGCTGACACCATCAC
TPS8	TPS8_qPCR_F	CCACAAGGTGTAAGCAAAGG
	TPS8_qPCR_R	CGCGTTCTACCATTTCTCG
RZPF34	RZPF34_qPCR_F	TGCCCTGTATGCTCCAAATC
	RZPF34_qPCR_R	GGGTATGCAGCAACCTCTTC
OTSA (E. coli)	OTSA_qPCR_F	ACTGCGTGACGGGATGAA
	OTSA_qPCR_R	GCAAATTGCGAAAGAACAAGAAC
TPS1	TPS1-qRT-F	TCGTACTCGCACCAATGCTA
	TPS1-qRT-R	TTACATGAACTCACTTGACACT
CYP21	CYP21_qPCR-F	AGTAGTGCGCAAGATCGAAG
	CYP21_qPCR-R	GAAGACGATATTACAAAGAAACTTCTCC
AT3G01345	AT3G01345_qPCR-F	CCTCCTCAACGGAGCACTTC
	AT3G01345_qPCR-R	TTGAGGCCTTGGCAGATTCG
eIF4A	EIF4A_qPCR_F	TCATAGATCTGGTCCTTAAACC
	EIF4B_qPCR_R	GGCAGTCTCTTCGTGCTGAC
UBC21	UBC21_qPCR_F	CTGCGACTCAGGGAATCTTCTAA
	UBC21_qPCR_R	TTGTGCCATTGAATTGAACCC
UBQ10	UBQ10_qPCR_F	GGCCTTGTATAATCCCTGATGAATAAG
	UBQ10_qPCR_R	AAAGAGATAACAGGAACGGAAACATAGT
FCL1	FCL1_qPCR_F	TTTTTTGCCCCCTTCGAATC
	FCL1_qPCR_R	ATCTTCCGCCACCACATTGTAC

Antibody - short name	Antibody - full description	Source	Reference	Dilution	Dilution buffer
Anti-TPS1	Anti-TPS1 (N-terminal)	Custom Made	Yadav et al., 2014 J. Exp. Bot	1:3 000	1% milk in TBS
Anti-Rabbit	Peroxidase Affinipure goat anti-rabbit IgG (H+L)	Jackson Immuno Research	111035144	1:20 000	1% milk in TBS

PLANT LINE	LINE ID	REFERENCE
SnRK1α1-OE		Jossier et al., 2009 Plant J
sesquia2	GABI_579E09 (-/-) x WiscDsLox384F5 (+/-)	Belda-Palazon et al., 2020 Nature Plants
AlcR		Martins et al., 2013 Plant Phys
iOTSA		Martins et al., 2013 Plant Phys

CHAPTER 3

Alternative splicing generates SnRK1β1 protein diversity

Author contributions: Bruno Peixoto, John E. Lunn, Mark Stitt, and Elena Baena-González conceived the research plan and designed the experiments. Bruno Peixoto and Leonor Margalha (RT-PCR) performed the experiments. Melanie Höehne assisted with metabolite profiling. Bruno Peixoto and Elena Baena-González analysed, interpreted data, and wrote the manuscript. John E. Lunn and Mark Stitt interpreted data and edited the manuscript.

3.1 Abstract

SnRK1 is a plant kinase with important energy-conservation functions that acts by modulating metabolic activity and transcriptional programmes. SnRK1 is a heterotrimeric complex, with several of its subunits being encoded by multiple genes. This genetic diversity implies that several SnRK1 complexes are possible, depending on what the subunit composition is. Adding to this already complex picture, alternative splicing of some of the SnRK1 genes is predicted to occur, generating yet more subunit diversity, and potentially increasing the range of molecular functions this kinase can perform. We show in *Arabidopsis thaliana* that one of the regulatory subunits (*SnRK1β1*) can be alternatively spliced into at least three different mRNAs, giving rise to three different proteins. These three β1 subunits accumulate in distinct subcellular compartments where they are capable of interacting with the SnRK1α1 catalytic subunit. Transgenic lines overexpressing the first splice variant (*SnRK1β1.1*) show very mild alterations in primary metabolism, with changes in nitrite levels being compatible with a reduced activation state of nitrate reductase. Altogether, this study reveals a role for alternative splicing in increasing SnRK1 trimer complexity, subcellular localization, and functionality.

3.2 Introduction

Plant SnRK1 is an evolutionarily conserved energy sensing kinase, belonging to the same eukaryotic kinase family as yeast SNF1 and mammalian AMPK (Wurzinger et al., 2018). Like its yeast and mammalian orthologues, SnRK1 functions as a heterotrimeric complex composed by a catalytic α-subunit and two regulatory β- and βγ-subunits (Crozet et al., 2014). Both the catalytic α-subunits and the regulatory β-subunits are encoded by multiple genes in Arabidopsis. The α-subunit comprises an N-terminal kinase catalytic domain and a C-terminal regulatory domain responsible for binding the β-/βγ-subunits and other regulatory factors (Broeckx et al., 2016). The β-subunits traditionally have a variable N-terminal region, a CBM, and a C-terminal domain, that in animals is responsible for mediating

protein-protein interaction with the α- and γ-subunits (Iseli et al., 2005). Amongst the three β-subunits in Arabidopsis (SnRK1β1, SnRK1β2 and SnRK1β3), SnRK1β1 and SnRK1β2 share 49% identity (Bouly et al., 1999) and are the ones most closely related to the yeast and mammalian counterparts. SnRK1β3 is a more divergent subunit that evolved specifically in plants, sharing 50% identity with SnRK1β1, and 41% with SnRK1β2 (Gissot et al., 2004). Nevertheless, and despite lacking the CBM domain, it is capable of complementing a yeast null β-subunit mutant (Gissot et al., 2004; Polge et al., 2008). Besides serving as scaffolds between the α- and γ-subunits, work on yeast and mammals has shown that β-subunits play important roles e.g. in the recruitment of substrates and in the subcellular localization of the kinase (Coccetti et al., 2018; González et al., 2020). In Arabidopsis, transient expression of SnRK1β2 in protoplasts was shown to repress the nuclear translocation of the α-subunit (and thereby its nuclear activities) by virtue of its N-terminal myristoylation (Ramon et al., 2019). Furthermore, artificial enrichment of the α-subunit inside or outside the nucleus had profound consequences on stress responses, growth and development, highlighting the importance of regulating subcellular localization for proper kinase functions (Ramon et al., 2019). The SnRK1β1 subunit has also been shown to be myristoylated, allowing its association to the plasma membrane (Pierre et al., 2007). Intriguingly, *N*-myristoylation mutants show defects in shoot apical meristem differentiation that are at least partially due to their inability to myristoylate the SnRK1β1 subunits (Pierre et al., 2007).

β-subunits contribute also to the regulation of kinase activity e.g. by carbohydrates. The CBM domain of Snf1 and AMPK is known to bind glycogen, localizing the kinase complex to the periphery of the glycogen granules, acting as a regulatory domain that can inhibit kinase activity, and allowing AMPK to act as a glycogen sensor (Polekhina et al., 2003; Wiatrowski et al., 2004; Polekhina et al., 2005; McBride et al., 2009). In plants, evidence for the binding of SnRK1β CBM domains to starch is not yet conclusive, with reports supporting both possibilities (Ávila-Castañeda et al., 2014; Emanuelle et al., 2015; Ruiz-Gayosso et al., 2018). A much less controversial connection to the sugar status exists at the level of transcription, with *SnRK1β1* accumulation being repressed by sugar and light

signals, while induced by darkness and ammonium (Bouly et al., 1999; Polge et al., 2008; Li et al., 2009). Furthermore, *SnRK1β1* expression is negatively correlated with photoperiod length, a feature that contributed to its identification by modelling efforts as a potential "darkness sensor" required for adjusting the rates of starch synthesis and degradation to the duration of the dark period (Pokhilko et al., 2014; Flis et al., 2016). A metanalysis of transcript responses provided by Flis and colleagues also correlated increases in *SnRK1β1* transcript levels with falling sugar levels, responding similarly to genes involved in starch metabolism. On the other hand, *SnRK1β1* transcription was shown to anti-correlate with genes encoding for ribosomal proteins and assembly factors (Flis et al., 2016). At the physiological level, SnRK1β1 has been associated with regulation of nitrogen metabolism, by interacting with, and leading to the phosphorylation-mediated inhibition of NR activity *in planta* (Polge et al., 2008; Li et al., 2009). More recently, a metabolic characterization of a T-DNA insertional mutant for the *SnRK1β1* gene revealed an impact of this subunit on other aspects of primary metabolism, with several sugars accumulating at the expense of organic acids when SnRK1β1 is depleted (Wang et al., 2020). In addition, the predicted alternative splicing of the *SnRK1β1* transcript has been proposed as a potential regulatory mechanism for this subunit (Broeckx et al., 2016). In this study we explore this question and show that alternative splicing generates both protein and functional diversity for this SnRK1 regulatory subunit.

3.3 Results

3.3.1 The three predicted splice variants of *SnRK1β1* are expressed in Arabidopsis

The TAIR database (www.arabidopsis.org) predicts three different mRNA variants for the *AtSnRK1β1* gene (AT5G21170), all of which would result in different protein products (Figure 3.1a-b). To test if these mRNAs are indeed produced, we performed RT-PCR analysis from Columbia-0 (Col-0) seedlings subjected to a 24h night extension, and the corresponding light controls, grown under a long day photoperiod (16h light, 8h darkness). A night extension was used since it is known to

activate SnRK1 signalling and thereby the expression of target genes (Mair et al., 2015). RT-PCR analysis shows amplification of all three splice variants (Figure 3.1c), with a particular enrichment of splice variant 1 in the dark-incubated samples (D), when compared with the light controls (L). This response of the *SnRK1β1.1* splice variant is the same that has been previously described for the *SnRK1β1* gene (Bouly et al., 1999; Baena-González et al., 2007; Polge et al., 2008). Unexpectedly, the primer pair specifically designed for identification of splice form 2 amplified two different fragments in WT. If this is due to the presence of unannotated splice variants, or non-specific amplification is currently unclear. However, the fact that the relative intensity of the two bands differs between light and dark samples, would suggest that these fragments are specific, and that the dark treatment seems to favour the appearance of the smaller *SnRK1β1.2* variant. On the other hand, no unexpected PCR products were observed for *SnRK1β1.3*, which also showed no obvious response to the dark treatment in WT plants.

RT-PCR analysis of three T-DNA insertional mutants of *SnRK1β1* revealed varying degrees of *SnRK1β1.1* depletion in the three lines. The SALK008325 line had a 70% and 60% reduction in this transcript in the L and D treatments, respectively. The reduction was stronger in the SAIL508D10 line, with a 90% reduction in both conditions. Finally, the SAIL40A07 line was the most severely affected, having negligible levels of the *SnRK1β1.1* transcript both in the L and D treatments. Remarkably, the absence of *SnRK1β1.1* expression in the SAIL40A07 line was accompanied by a marked upregulation of the *SnRK1β1.3* transcript, in particular in the L, and by the appearance of an additional amplification product of lower molecular weight (MW) in both L and D samples. Compared to the WT pattern, the relative intensity between the two *SnRK1β1.2* bands also appeared altered in this mutant line, with higher relative abundance of the low MW band in the L than in the D sample. This altered pattern in response to darkness was also visible in the SALK008325 line, although the overall expression level of this splice variant was not altered. The SAIL508D10 line appeared mostly like the WT with regard to the *SnRK1β1.2* and *SnRK1β1.3* transcripts, except for a minor reduction in the levels of the low MW *SnRK1β1.2* band and a very weak amplification of the low MW

SnRK1β1.3 band in the D sample. Taken together, these results support the expression of the predicted *SnRK1β1* splice variants *in planta* and suggest the existence of additional splice forms. Furthermore, from the three T-DNA insertional mutants, SAIL508D10 appears to be the only one where the reduction in *SnRK1β1.1* transcripts is not accompanied by alterations in the levels or splicing pattern of the *SnRK1β1*.2 or *SnRK1β1*.3 transcripts

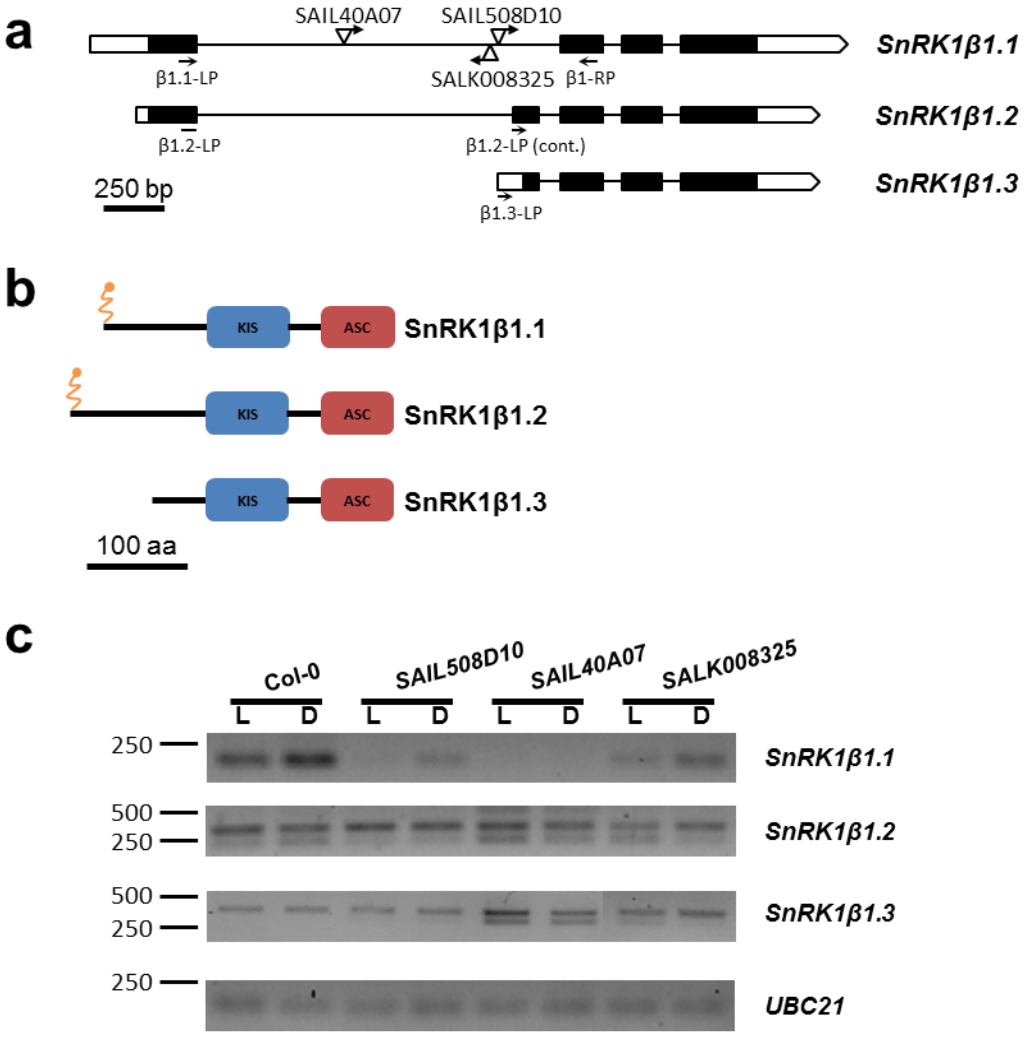

Figure 3.1 | *SnRK1β1* predicted splice variants and expression analysis.
(a) Predicted *SnRK1β1* gene structure, showing the 5´and 3´ UTR (empty boxes), exons (dark boxes), introns (dark thin lines), the site of T-DNA insertion for each mutant line, and the annealing sites of the RT-PCR primers used in **(c)**. **(b)** Predicted SnRK1β1 protein structure, showing the G2 residue bearing N-myristoylation (highlighted in orange), as well as the KIS (Kinase Interacting Sequence) and ASC (Association with SNF1 Kinase) domains (blue and red boxes, respectively). **(c)** RT-PCR analysis of *SnRK1β1* splice variants (*SnRK1β1.1, SnRK1β1.2, SnRK1β1.3)*. cDNA obtained from 8-day old seedlings subjected to a 24h-extended night (D), and the corresponding light controls, maintained under the regular 16:8 photoperiod (L). cDNAs were obtained from Col-0 control plants, and the three insertional mutants described in **(a)**.

3.3.2 The three splice variants of *SnRK1β1* encode proteins with different subcellular localizations

Given our results supporting the expression of the three predicted *SnRK1β1* splice variants *in planta*, and that different protein products are expected to arise from these transcripts, we next investigated potential differences in the subcellular localization of the three *SnRK1β1* gene products. We infiltrated *Nicotiana benthamiana* leaves with *Agrobacterium tumefaciens* harbouring plasmids encoding for C-terminal GFP fusions of all three predicted *SnRK1β1* splice forms and imaged the infected leaf segments 48h after infection.

All three GFP fusions showed different subcellular accumulation patterns (Figure 3.2), with SnRK1β1.1 showing a distinctly punctate expression, while also weakly labelling the inside of the nucleus, but not the nucleolus (Figure 3.2a). SnRK1β1.2-GFP appeared to localize to an endomembrane structure, that could often be seen delineating the nucleus at the cell periphery (Figure 3.2b) whilst SnRK1β1.3 showed a more dispersed localization, labelling the cytosolic, nuclear, and plastidial compartments (Figure 3.2c). To further confirm these observations, the SnRK1β1-GFP fusions were co-expressed in *N. benthamiana* with several subcellular markers. In the case of SnRK1β1.1, the GFP signal in the punctate structures co-localized with the soybean α-1,2-mannosidase I (*Gm*Man1) Golgi marker (Figure 3.3a, Supplemental Figure 3.2a). In the case of SnRK1β1.2 a partial co-localization was observed with the γ-TIP tonoplast marker at 2 days post-infiltration (Figure 3.3b, Supplemental Figure 3.2b). Unfortunately, at this time point, the γ-TIP marker could still be seen largely labelling the peri-nuclear region, indicating that the expression and proper sorting of this subcellular marker was still on-going at 2 days post-inoculation (dpi). Extension of the incubation period to 3 dpi, however, resulted in substantial cell death (data not shown), precluding any imaging analyses and suggesting a role for this subunit in the cell death process. Finally, SnRK1β1.3 largely co-localized with the autofluorescent signal emitted by chlorophyll (Figure 3.3c, Supplemental Figure 3.2c), suggesting a chloroplastidial localization for this isoform. Besides localizing to the interior of the chloroplasts,

SnRK1β1.3-GFP also labelled the cytoplasmic and nuclear compartments (Figure 3.3c). Together, these observations show that alternative splicing of *SnRK1β1* results in β1 subunits with different subcellular localization.

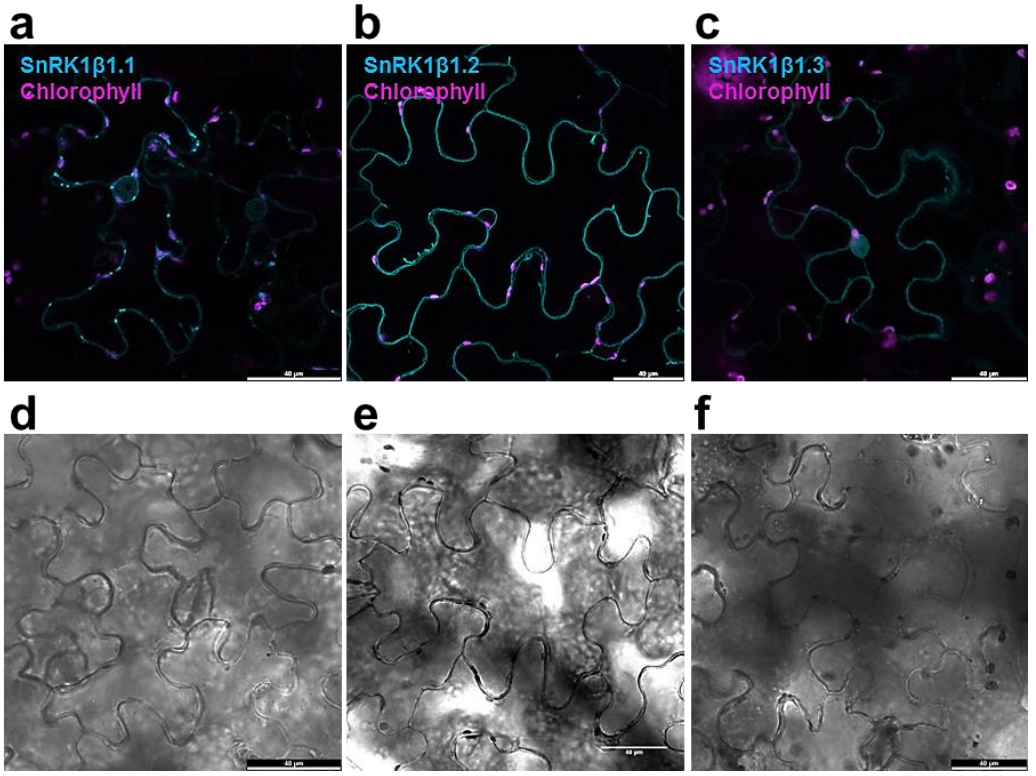

Figure 3.2 | Subcellular localization of SnRK1β1 splice variants.
(a-c) Confocal laser scanning micrographs from *N. benthamiana* epidermis transformed by infiltration of *Agrobacteria* harbouring vectors encoding for C-terminal GFP fusions of the SnRK1β1.1 **(a)**, SnRK1β1.2 **(b)**, and SnRK1β1.3 **(c)** splice variants. GFP fluorescence is shown as cyan, and chlorophyll autofluorescence is shown as magenta. All represented micrographs were taken in a single plane of focus. Brightfield images of the same cells are presented for morphological analysis **(d-f)**. Scale bars: 40 µm.

3.3.3 The SnRK1β1 splice forms interact with the SnRK1α1 catalytic subunit in different subcellular compartments

Given our previous observation that the three SnRK1β1 splice variants yield proteins with different subcellular localizations, we hypothesized that this could result in the recruitment of the SnRK1α1 catalytic subunit to the same subcellular

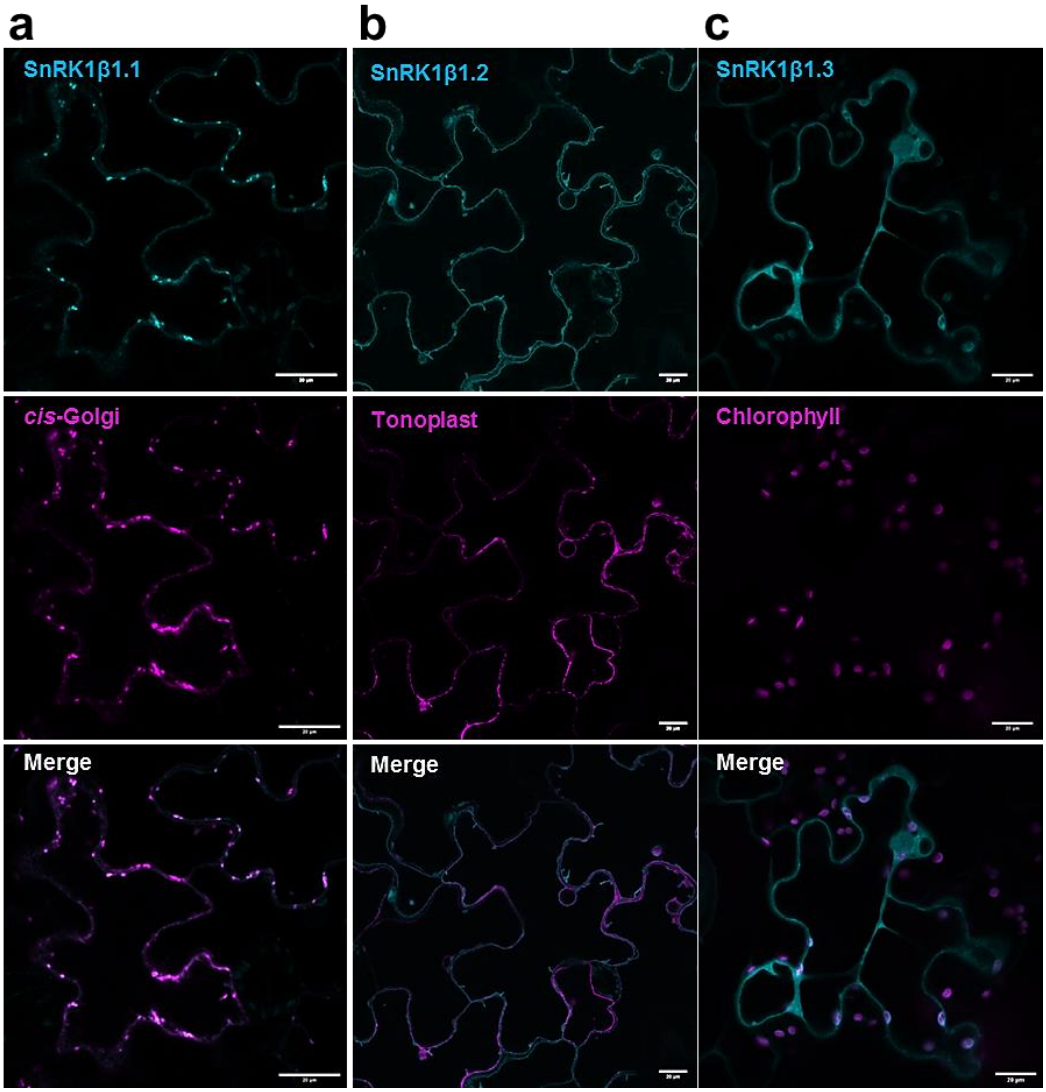

Figure 3.3 | Co-localization analysis of SnRK1β1 splice variants with subcellular markers.
(a,b) Confocal laser scanning micrographs from *N. benthamiana* epidermis co-infiltrated with *Agrobacteria* harbouring vectors encoding for C-terminal GFP fusions of SnRK1β1.1 **(a)** and SnRK1β1.2 **(b)**, with the GmMan1-mCherry *cis*-Golgi marker and the γTIP-mCherry tonoplast marker, respectively. GFP is shown as cyan and mCherry is shown as magenta. **(c)** SnRK1β1.3-GFP was co-localized with chlorophyll autofluorescence (shown as magenta). Fluorescence micrographs were taken at 2 dpi and each channel is shown both isolated and merged. Scale bars: 20 µm.

compartments, potentially exposing the SnRK1 complex to different pools of substrates or other types of interactors. In order to test this hypothesis, we performed bimolecular fluorescent complementation (BiFC) assays in N. benthamiana, using a 2-in-1 system, where the proteins harbouring the YFPN- and

YFPC-fragments are co-expressed from the same vector backbone, together with a cytosolic RFP positive transfection control (Grefen and Blatt, 2012). Confocal laser scanning analysis shows reconstitution of the YFP signal by all three SnRK1β1 splice forms, indicating that all variants are capable of interacting with the SnRK1α1 catalytic subunit in this system (Figure 3.4). Furthermore, the YFP signal localizes to structures morphologically similar to those labelled by the SnRK1β1-GFP variants alone, suggesting that these splice variants might confer different subcellular localizations to the SnRK1 complex.

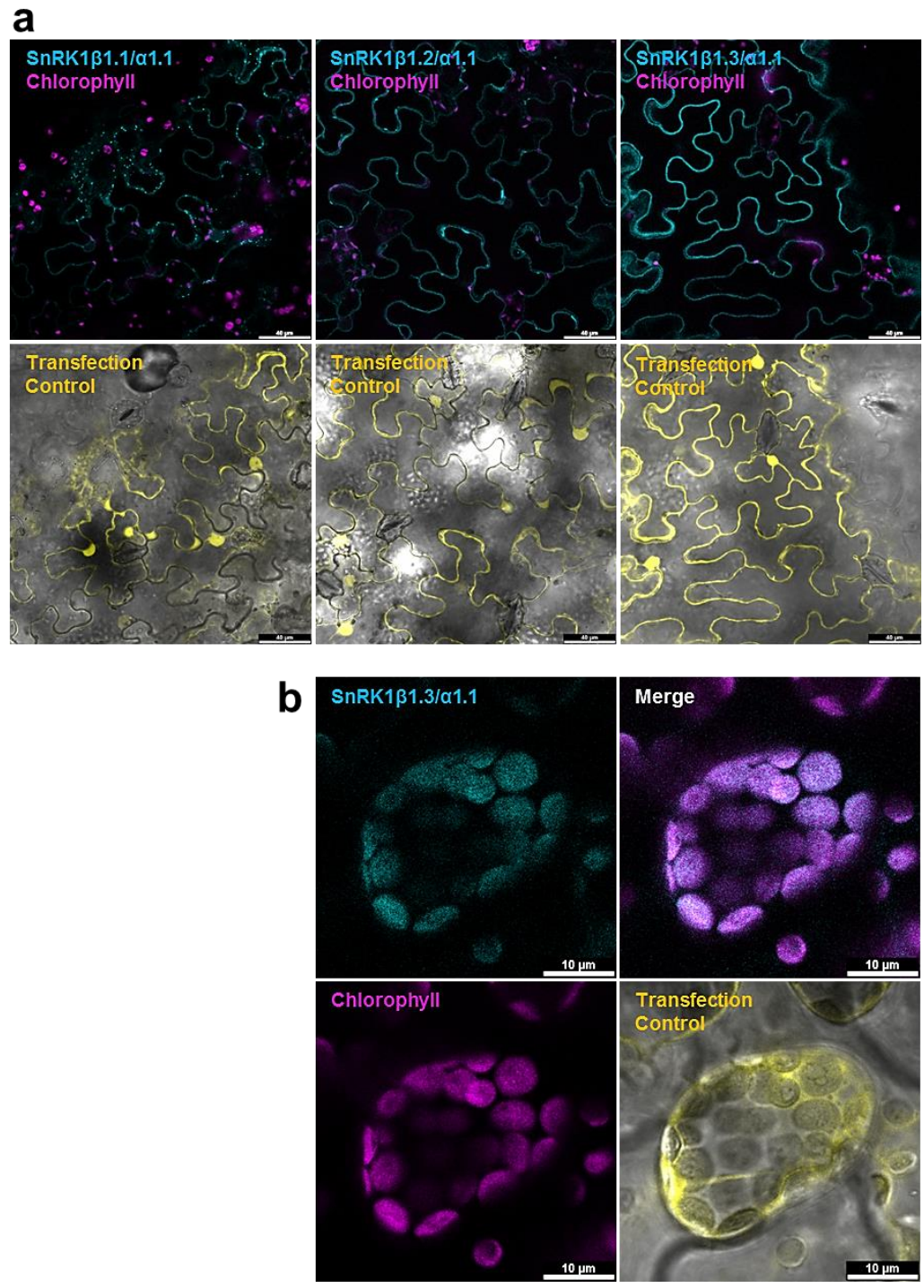

Figure 3.4 | BiFC assays between SnRK1β1 splice variants and the SnRK1α1 catalytic subunit.

(a) The 2-in-1 BiFC system was employed to simultaneously express each corresponding SnRK1β1 splice variant and the catalytic subunit SnRK1α1. Reconstituted YFP fluorescence is shown in cyan. The same vector also encoded for a *35S::RFP* transfection marker, which is

shown in yellow, super-imposed to the brightfield images. There is positive reconstitution of YFP fluorescence between all three SnRK1β1 splice variants and SnRK1α1. **(b)** A detailed view of a mesophyll cell is shown for SnRK1β1.3 and SnRK1α1, where a co-localization with chlorophyll autofluorescence can be observed. Scale bars: 40 µm **(a)**, 10 µm **(b)**.

3.3.4 SnRK1β1 overexpression causes very mild alterations in primary metabolism

Given the known connection between SnRK1 and metabolism and the involvement of the SnRK1β1 subunit in the regulation of NR (Polge et al., 2008; Li et al., 2009), we hypothesized that the β1 subunit is important for the recognition of metabolic enzymes by the SnRK1 kinase and that its genetic manipulation should result in broad changes in metabolism. To test this, we generated constitutive *SnRK1β1.1-HA* overexpression plants (hereafter referred as SnRK1β1.1-OE), selecting two independent lines where overexpression was clearly detected (lines 5.1 and 6.2), and a third, sister line (7.1) where this overexpression was negligible, to be used as a negative control (Supplemental Figure 3.1). Of these SnRK1β1.1-OE lines, line 5.1 was clearly the strongest overexpressor, with line 6.2 showing slightly lower accumulation of the SnRK1β1.1-HA protein. We grew these plants alongside the three T-DNA insertional mutants and their Col-0 controls under short-day (8h light, 16h dark) conditions, with a light intensity of 160 µmol m^{-2} s^{-1}, a growth setup that should generate moderate carbon restriction during vegetative growth (Sulpice et al., 2014). Twenty-day-old whole rosettes were sampled at the ED and EN, and analysed for a total of 13 different metabolites related to carbon and nitrogen metabolism (Supplemental Table 3.1).

We were surprised to find that under our experimental conditions, most of the measured metabolites showed no consistent differences between the SnRK1β1.1-OE lines and WT (Supplemental Figure 3.3). The only exception was nitrite, whose levels at the ED were modestly but significantly reduced in the two overexpressor lines (5.1 and 6.2), but not in their negative control sibling (7.1) (Figure 3.5). This reduction in nitrite levels is compatible with the known repression of NR activity by SnRK1 (McMichael et al., 1995; Moorhead et al., 1996; Li et al., 2009). However, we could not find concomitant changes in the levels of nitrate in

these plants. We also observed no significant differences in other downstream metabolites associated with nitrogen metabolism (e.g total protein content), although there was a subtle, but not statistically significant trend of decreased total amino-acid content in the overexpressor lines (Supplemental Figure 3.3d). In addition, sucrose and malate levels were mildly reduced at the ED in the overexpressor lines, with this effect being more prominent in the 5.1 line that shows the highest degree of SnRK1β1 overexpression. However, in none of these cases the differences reached statistical significance. On the other hand, the T-DNA insertional mutants did not show statistically significant differences for any of the measured metabolites, except the SAIL508D10 line, in which a mild reduction in total protein content at the EN reached statistical significance (Supplemental Figure 3.3d). The other T-DNA lines also showed a similar subtle, yet non-significant, trend of reduced protein accumulation at the EN. With regard to sugar content, no statistically significant changes could be detected for any of the T-DNA lines, although all three mutants showed a very subtle decrease in the levels of fructose at the ED (Supplemental Figure 3.3b). Overall, primary metabolism was only weakly affected by manipulation of the SnRK1β1 subunit and these effects could mostly be detected at the ED.

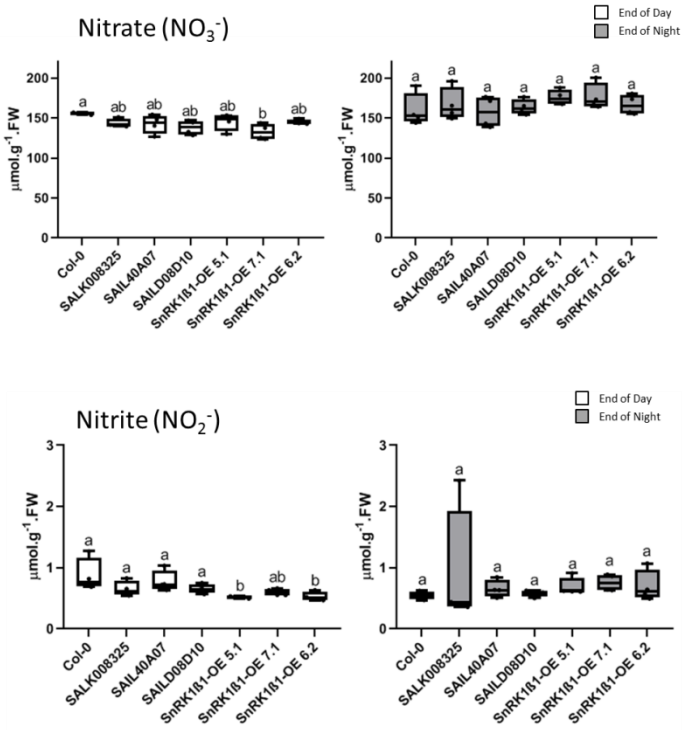

Figure 3.5 | Nitrite, but not nitrate, levels are altered in *SnRK1β1* mutant lines.
Nitrate and nitrite levels were determined for three independent T-DNA insertional mutants and three independent *SnRK1β1.1-OE* lines, and compared against a Col-0 control line at the end of the day (white boxes) and at the end of the night (grey boxes). Nitrate levels show no consistent change between lines at either of the tested time points. Nitrite levels show a subtle decrease for the two *SnRK1β1.1-OE* lines at the end of the day time point, but not for the WT-like sister line (7.1). Boxplots represent 4 biological replicates (each consisting of a pool of 4-5 randomly harvested rosettes). Lower and upper box boundaries represent the first and third quantiles, respectively, horizontal lines mark the median and whiskers mark the highest and lowest values. Dots represent individual datapoints. Different letters indicate statistically significant differences (p<0.05, one-way ANOVA with Tukey HSD test).

3.4 Discussion

SnRK1 plays important roles in plant growth and development as well as in the response to biotic and abiotic stress. However, little is known about how it is regulated. Mechanisms, such as T-loop phosphorylation of SnRK1 are known to be essential for proper functioning of the kinase but, in contrast to AMPK, increases in SnRK1α T-loop phosphorylation do not always correlate with activation of SnRK1 signalling (Baena-González et al., 2007; Fragoso et al., 2009; Coello et al., 2012;

Rodrigues et al., 2013). Most of the other regulatory mechanisms described in plants thus far relate to: (1) the control of its half-life *via* interaction with proteins such as 5PTase13 (Ananieva et al., 2008), PRL1 (Bhalerao et al., 1999) or the SUMO machinery (Crozet et al., 2016); (2) its physical sequestration (Rodrigues et al., 2013; Belda-Palazón et al., 2020); (3) its regulation by sugars (Zhang et al., 2009; Nunes et al., 2013; Zhai et al., 2018). Recent work in Arabidopsis also highlighted the importance of subcellular localization for SnRK1 function (Cho et al., 2012; Ramon et al., 2019). Alternative splicing has been previously proposed as a potential regulatory mechanism, capable of increasing SnRK1 subunit diversity (Broeckx et al., 2016), but such possibility had not been previously investigated.

In this work, we explored the potential biological relevance of alternative splicing for SnRK1 localisation and function, using the SnRK1β1 regulatory subunit as a study case. The TAIR database predicts a minimum of three differentially spliced mRNAs for this gene, all resulting in different protein products. We first confirmed by RT-PCR that these three *SnRK1β1* mRNA variants are indeed expressed *in planta*, opening the possibility that the corresponding proteins play different molecular and/or physiological roles. The amplification of unexpected bands with the primer pairs designed specifically for *SnRK1β1.2* and *SnRK1β1.3* may indicate the existence of additional, non-annotated splice variants, but sequencing data will be required in the future to confirm this. Our RT-PCR data also shows that, despite having no expression of the *SnRK1β1.1* splice variant, one of the T-DNA insertional mutants (SAIL40A07) has elevated levels of the *SnRK1β1.2* and *SnRK1β1.3* variants. This could suggest that reduced *SnRK1β1.1* accumulation is compensated by increased expression of the other splice variants. However, compared to the SAIL40A07 line, the SAILD508D10 line shows an even stronger depletion of the *SnRK1β1.1* transcript in the L and D samples, but little to no change in the levels of *SnRK1β1.2* and *SnRK1β1.3*. It is therefore unclear what may be the cause behind the upregulation of *SnRK1β1.2,* and in particular *SnRK1β1.3,* in the SAIL40A07 line. One obvious difference between this and the other T-DNA lines is the site of the T-DNA insertion, which lies in the first half of the first intron in the case of SAIL40A07 and at the end of the second half of the same intron in the other two

lines. Whether such a compensatory mechanism occurs or not is therefore not clear and more sensitive qRT-PCR analyses should be employed to address this question. The complex splicing patterns of *SnRK1β1* in these three T-DNA insertional mutants makes particularly difficult the interpretation of our results as well as of those reported by Wang and colleagues. A full *snrk1β1* loss-of-function mutant, as well as splice-variant-specific complementation lines would be required in the future to investigate the function of these SnRK1β1 variants.

To start characterizing these novel splice variants, we first overexpressed the corresponding GFP-tagged versions in *N. benthamiana* and imaged their subcellular localization. Using this approach, we were able to show that the three SnRK1β1 splice variants accumulate in distinct subcellular compartments, supporting the hypothesis that they may play different functions at these locations. Our imaging results for SnRK1β1.1 show that this protein accumulates in the Golgi apparatus (GA), in agreement with a previous report (Wang et al., 2020). The function of SnRK1 at this particular sub-cellular compartment is currently unknown. SnRK1 interacts with and phosphorylates 3-hydroxy-3-methylglutaryl coenzyme-A reductase (HMGR), an enzyme of isoprenoid biosynthesis that is localized to the endoplasmic reticulum (ER) (Sugden et al., 1999; Robertlee et al., 2017). It is possible that the interaction between these two proteins occurs at the ER-GA interface, potentially in a SnRK1β1.1-dependent manner. The fact that both splice variants 1 and 2 retain their N-myristoylation sites would imply that these two subunits associate, at least partly, with membranes. The Golgi localization described by Wang and colleagues (Wang et al., 2020) was also shown to depend on myristoylation, but SnRK1β1.1 could also be localized to the inside of the nucleus, both in the Wang study and in our report. It is currently unclear whether this nuclear localization holds true physiological relevance, or if it is a simple artefact due to overexpression of the SnRK1β1.1 protein.

There are currently no reports regarding the exact subcellular localization of SnRK1β1.2. Based on the morphology of the structure labelled by this subunit at 2dpi, we hypothesized that this subunit could be at the tonoplast. However, our co-

localization experiments with γ-TIP were inconclusive and further studies will be needed to establish this. A tonoplast localization would nevertheless be in agreement with the reported localization of AMPK to the lysosome surface in animal cells. Upon activation, AMPK was shown to be recruited to the late endosome/lysosome, leading to the endosomal dissociation and inactivation of mTORC1, in what has been described as a “switch” between anabolic and catabolic metabolism (Zhang et al., 2014).

Finally, SnRK1β1.3 appears to be localized to the cytoplasm/nucleus, consistent with the fact that this alternative splice form is truncated at the N-terminus, losing the G2 residue required for myristoylation. Our observation that this subunit could also accumulate inside the chloroplast was more surprising, but analysis of the peptide sequence of SnRK1β1.3 by TargetP-2.0 (http://www.cbs.dtu.dk/services/TargetP-2.0/) (Armenteros et al., 2019) led to the identification of a putative signal peptide (data not shown), further supporting this result. It will be important to validate this prediction by assessing the effects of truncating the putative signal peptide of SnRK1β1.3 on the subcellular localization of this subunit. The previous observations of SnRK1β1 inside the plastid (Ruiz-Gayosso et al., 2018) did not account for alternative splicing events of the subunit. It will be interesting to further explore phosphate and starch-associated phenotypes in lines with altered levels of *SnRK1β1.3* as a starting point to understanding how functionally relevant these events are *in planta*.

It is commonly accepted that the subcellular localisation of the SnRK1 complex is determined by the regulatory β subunit associated to it, although this is mostly based on observations from yeast and animal systems, and was only recently observed in plants for the SnRK1β2 subunit (reviewed in Polge and Thomas, 2007; Broeckx et al., 2016; Ramon et al., 2019). By using BiFC, we showed that all three SnRK1β1 splice variants are capable of interacting with SnRK1α1, the predominant catalytic subunit (Jossier et al., 2009). Interaction between SnRK1β1 and SnRK1α1 appears to occur at the same subcellular compartment labelled by the corresponding β1 splice variant, suggesting that the interaction with this regulatory subunit confers

the SnRK1 complex a particular subcellular localization. This may indicate a hierarchical control of subcellular localization where the presence of the β-subunits would override the nuclear localization signals found in the α-subunit. Co-expression experiments between the SnRK1α subunits and the three SnRK1β1 splice variants followed by confocal imaging of the α-subunit would allow confirmation of this model.

The potential ability of splice variants 1 and 2 for retaining the α1 subunit in the cytosol prompted the hypothesis that their overexpression could potentiate SnRK1 function towards cytosolic targets, such as metabolic enzymes involved in glycolysis and organic acid synthesis. This, together with the fact the SnRK1β1.1 subunit had been previously implicated in the regulation of NR (Li et al., 2009), led us to focus first on this splice variant. To our surprise, the only metabolite significantly affected in the *SnRK1β1.1-OE* lines was nitrite. The observed reduction in nitrite levels caused by SnRK1β1.1 overexpression is in accordance with the known negative effect of SnRK1 on NR activity, *via* interaction with the β1 subunit (McMichael et al., 1995; Moorhead et al., 1996; Li et al., 2009). In addition, there were subtle, but statistically non-significant reductions in the content of sucrose, malate and total amino-acids in the *SnRK1β1.1-OE* lines at the ED, with this effect being more prominent in the line with the highest level of SnRK1β1.1 overexpression (5.1). This suggests an overall repressive effect of SnRK1β1.1 on carbon and nitrogen metabolism. Under our experimental settings we were unable to reproduce the striking metabolic alterations previously described for one of the T-DNA insertional mutants (SALK008325; Wang et al., 2020). One possible explanation that could account for the substantial differences between the two studies, are the light conditions employed. The Wang study used long-day (16h light, 8h dark) conditions, known to provide enough carbon input for unrestrained growth (Sulpice et al., 2014). Our study focused instead on a short-day (8h light, 16h darkness) photoperiod, which is known to cause carbon limitation (Gibon et al., 2004; Stitt et al., 2010; Sulpice et al., 2014; Mengin et al., 2017; Moraes et al., 2019). It is likely that this difference in photoperiod length and carbon availability plays an important role in the impact of SnRK1β1.1 on metabolism, particularly when considering the model proposed by Pokhilko and colleagues (Pokhilko et al., 2014). This model predicts

that the SnRK1β1 subunit acts as a “dark sensor”, transmitting information about the length of the night. Under this assumption, overexpression of SnRK1β1 should result in the signalling of a longer night, with concomitant changes in the rates of starch synthesis and mobilisation (Pokhilko et al., 2014). However, this effect might be masked if the plants are grown under short-day/long-night conditions, such as ours. The mild metabolic phenotype observed with the SALK008325 line under our experimental settings is more puzzling. Under short-day conditions a *SnRK1β1* knock-out line would be expected to suffer more dramatic metabolic misregulation, due to the mismatch between the abundance of the “dark sensor” and the length of the dark period. Even if we consider the fact that the SALK008325 line is the least affected in terms of *SnRK1β1* expression, or the presence of potential compensatory mechanisms, these would still not satisfactorily explain the differences between our observations and those of the Wang study (Wang et al., 2020). The most likely explanation is that additional variables, such as soil quality and the concentrations of N, P, and other nutrients may have a strong impact that was unaccounted for in both studies.

Overall, our results demonstrate the importance of alternative splicing for generating SnRK1 subunit diversity, allowing for the modulation of subcellular localization, and potentially, the molecular functions associated to this kinase. More experimental data and improved genetic tools will be needed in the future to better understand the relevance of each splice variant in metabolic regulation and other functions of SnRK1 signalling.

3.5 Materials and Methods

3.5.1 Plant Material and Growth Conditions

All *Arabidopsis thaliana* plants used in this study are in the Columbia-0 (Col-0) background. For detecting the presence of *SnRK1β1* transcripts, seedlings were plated on 0.5x MS, 0.2% Glucose, and grown for 8 days under a 16h light, 100 µmol

$m^{-2}s^{-1}$, 22 ºC / 8h dark, 18 ºC regime. For the dark treatment, plates were covered (D) or not (L) with aluminium foil for 24h. Following treatment, the seedlings were rapidly harvested, flash frozen in liquid N_2 and stored at -80 ºC until further processing. For the metabolic characterization, plants were germinated in pots and grown for 19 days under an 8:16 light:dark photoperiod, with a light intensity of 160 µmol m^{-2} s^{-1} and a temperature regime of 22:18 ºC. Each pot contained between 3 and 5 plants well separated from each other to prevent shading, and the pots were randomized in the growth chamber every other day to avoid positional effects. Plants were kept well-watered at all times. Whole rosettes were quickly harvested at the end of the day and end of the night time points, flash frozen with liquid N_2 and stored at -80 ºC until further processing.

3.5.2 RNA extraction, cDNA synthesis and RT-PCR

Total RNA was isolated from seedlings using the TRIzol reagent (Life Technologies), and subsequently treated with RNase-Free DNase (Promega). 1 µg of DNase-treated total RNA was used for synthesising cDNA libraries, using SuperScript III Reverse Transcriptase (Life Technologies), as previously described (Rodrigues et al., 2013). Reverse transcription polymerase chain reaction (RT-PCR) was used to assess the presence and relative abundance of each *SnRK1β1* splice variant, using the *UBC21* housekeeping gene as loading control.

3.5.3 DNA Constructs

The coding sequences of *SnRK1β1* splice variants were amplified from cDNA from plate-grown, 8d-old Arabidopsis seedlings treated under light (control) and darkness, as described in the previous section on *Plant material and growth conditions*. All splice variants were amplified with primers introducing BamHI/StuI sites at their 5' and 3' ends, respectively, and cloned into the pHBT95 vector (Yoo et al., 2007), upstream of a 2xHA tag coding sequence and under the control of a

minimal 35*S* promoter. *SnRK1β1.2* was isolated in a two-step process, by cloning first exons 1-2 as a fragment and exons 2-5 as a second fragment. The resulting products were thereafter combined in a single PCR reaction to reconstitute the entire CDS, using the shared 2nd exon as a bridging sequence. BamHI/StuI enzyme adapters were inserted at the 5' and 3' ends, respectively. For the GFP-tagged versions, the CDS of each SnRK1β1 variant were subcloned from the pHBT95 vector, to the binary vector pCB302, upstream of a GFP coding sequence, and also under control of a *35S* promoter. For the BiFC constructs, the CDS of the catalytic subunit SnRK1α1.1 was cloned into a pDONR containing *attL1* and *attL4* recombination sites, and the CDS of the different SnRK1β1 splice variants were cloned into a pDONR containing *attL3* and *attL2* sites. These entry vectors were thereafter recombined into the pBiFC-2in1-CC vector (Grefen and Blatt, 2012), where both proteins are expressed with C-terminal fusions of the YFP fragments. Subcellular localization markers were acquired as plasmids from ABRC (www.arabidopsis.org) and were previously described (Nelson et al., 2007).

3.5.4 Infiltration of *Nicotiana benthamiana* leaves

Agrobacterium tumefaciens, strain GV3101 (pMP90) was transformed with each GFP-tagged pCB302 construct. Clones were screened by colony PCR and positive clones were selected for infiltration of *Nicotiana benthamiana* leaves. Briefly, 1 mL of fully grown bacterial culture was pelleted by centrifugation at room temperature. The pellet was washed once in infiltration buffer [10 mM $MgCl_2$ and 10 mM MES] and once in infiltration buffer supplemented with 100 µM acetosyringone and was finally resuspended in 1 mL of the same acetosyringone-supplemented buffer. The resulting bacterial suspension was diluted to a final OD_{600} of 0.5, unless otherwise stated. This Agrobacterium solution was used to infiltrate tobacco leaves through the stomata of the lower epidermis, by using a 1 mL syringe without needle. For co-infiltration experiments, bacterial strains containing their respective constructs were mixed prior to leaf infiltration, with subcellular markers being diluted to a final OD_{600} of 0.1. *Agrobacteria* containing

the p19 viral suppressor were employed in all infiltration experiments, at an OD_{600} of 0.5.

3.5.5 Laser Scanning Confocal Imaging

Unless otherwise stated, fluorescence was analysed 48h after tobacco leaf infiltration. Leaf squares were randomly sampled from the infected leaves, infiltrated with sterile deionized water and mounted in water for microscopic observation. Imaging was performed on a Leica SP5 setup, under a 40x water-immersion objective. The laser lines 488 nm, 514 nm, and 561 nm were used and their spectral detection adjusted for the emission of GFP, YFP, and mCherry, respectively, under a sequential scanning regime.

3.5.6 Metabolite extraction and determination

Metabolites were extracted from 20d-old soil-grown rosettes (see *Plant material and growth conditions*) of Col-0, *SnRK1β1.1-OE* lines and the T-DNA insertional *snrk1β1* mutants. Approximately 20 mg of finely ground tissue was extracted twice in boiling 80% (v/v) ethanol buffered with 10 mM HEPES-NaOH (pH 7.0), and once in 50% (v/v) ethanol buffered with 10 mM HEPES-NaOH (pH 7.0). The resulting supernatants were pooled together and used for the enzymatic determination of soluble sugars (glucose, fructose, and sucrose), as previously described (Stitt et al., 1989). NO_3 and NO_2 measurements were determined enzymatically from the ethanolic extracts, as described in (Cross et al., 2006). Starch and total protein were determined from the insoluble material left after ethanolic extraction, as previously described (Hendriks et al., 2003).

3.5.7 Protein extraction and western blot analysis

For extracting total protein for the SnRK1β1.1-HA immunoblot analyses, whole rosettes were ground in liquid nitrogen. Finely ground tissue was extracted in 1,5 volumes of RIPA buffer [25 mM Tris-HCl (pH 8,0), 1 mM EDTA, 0,5 mM EGTA, 1% Triton X-100, 0,1% sodium deoxycholate, 0,1% SDS, 150 mM NaCl, supplemented with 1:50 cOmplete EDTA-free Protease Inhibitor Cocktail (Roche), and 1:500 Phosphatase Inhibitor Cocktails 2 and 3 (Sigma-Aldrich)]. Crude extracts were cleared by centrifugation at 15000 rpm for 15 minutes at 4 ºC, and the supernatants were used for total protein quantification (Pierce 660 nm protein assay). Single use aliquots of 60 µg total protein were prepared and denatured in Laemmli buffer (Laemmli, 1970) before storage at -20 ºC. Protein samples were separated by SDS-PAGE in 10% acrylamide gels, transferred to PVDF membranes (semi-dry transfer, 15 V, 60 minutes) and probed with a 1:1000 dilution of an anti-HA High Affinity antibody (Roche-Portugal). A 1:10000 dilution of Peroxidase AffiniPure goat anti-rat IgG (H+L) (Jackson ImmunoResearch) was used for primary antibody detection. Chemiluminescent detection was performed using Amersham ECL Western Blotting Detection Reagent (GE Healthcare).

3.5.8 Statistical Analyses

Metabolite measurements were separated by time point (ED vs EN) and plotted according to genotype. Box-plots show the complete data range of 4 biological replicates, with each biological replicate representing a pool of 3-5 randomly harvested whole rosettes. Lower and upper box boundaries represent the first and third quantiles, respectively, whereas horizontal lines mark the median and whiskers represent the highest and lowest values; all individual data points are shown. Statistically significant differences were assessed by one-way ANOVA Sum of Squares Type II, followed by a Tukey's post-hoc test of honestly significant differences. In all cases a significance level (α) of 0.05 was used.

3.5.9 Accession Numbers

Sequence data from this manuscript is available in the Arabidopsis Genome Initiative database under these accession numbers: *UBC21*, At5g25760, *SnRK1β1*, At5g21170.

Acknowledgments

We would like to thank Vera Nunes (IGC Plant Facility) and Britta Hausmann (Max Planck Green Team) for invaluable help with plant growth and management and Ana Confraria for comments on the manuscript. This work was supported by the Fundação para a Ciência e Tecnologia through the R&D Unit UIDB/04551/2020 (GREEN-IT - Bioresources for Sustainability), FCT projects LISBOA-01-0145-FEDER-028128 and PTDC/BIA-BID/32347/2017, and by the fellowships/contracts PD/BD/114361/2016 (BP), SFRH/BPD/116116/2016 (LM), and IF/00804/2013 (EBG).

3.6 References

Ananieva, E.A., Gillaspy, G.E., Ely, A., Burnette, R.N., and Erickson, F. Les (2008). Interaction of the WD40 domain of a myoinositol polyphosphate 5-phosphatase with SnRK1 links inositol, sugar, and stress signaling. Plant Physiol. **148**: 1868–1882.

Armenteros, J.J.A., Salvatore, M., Emanuelsson, O., Winther, O., Von Heijne, G., Elofsson, A., and Nielsen, H. (2019). Detecting sequence signals in targeting peptides using deep learning. Life Sci. Alliance **2**: 1–14.

Ávila-Castañeda, A., Gutiérrez-Granados, N., Ruiz-Gayosso, A., Sosa-Peinado, A., Martínez-Barajas, E., and Coello, P. (2014). Structural and functional basis for starch binding in the SnRK1 subunits AKINβ2 and AKINβγ. Front. Plant Sci. **5**: 1–8.

Baena-González, E., Rolland, F., Thevelein, J.M., and Sheen, J. (2007). A central integrator of transcription networks in plant stress and energy signalling. Nature **448**: 938–942.

Belda-Palazón, B., Adamo, M., Valerio, C., Ferreira, L.J., Confraria, A., Reis-Barata, D., Rodrigues, A., Meyer, C., Rodriguez, P.L., and Baena-González, E. (2020). A dual function of SnRK2 kinases in the regulation of SnRK1 and plant growth. Nat. Plants **6**.

Bhalerao, R.P., Salchert, K., Bakó, L., Ökrész, L., Szabados, L., Muranaka, T., Machida, Y., Schell,

J., and Koncz, C. (1999). Regulatory interaction of PRL1 WD protein with Arabidopsis SNF1-like protein kinases. Proc. Natl. Acad. Sci. U. S. A. **96**: 5322–5327.

Bouly, J.P., Gissot, L., Lessard, P., Kreis, M., and Thomas, M. (1999). Arabidopsis thaliana proteins related to the yeast SIP and SNF4 interact with AKINα1, an SNF1-like protein kinase. Plant J. **18**: 541–550.

Broeckx, T., Hulsmans, S., and Rolland, F. (2016). The plant energy sensor: evolutionary conservation and divergence of SnRK1 structure, regulation, and function. J. Exp. Bot. **67**: 6215–6252.

Cho, Y.H., Hong, J.W., Kim, E.C., and Yoo, S.D. (2012). Regulatory functions of SnRK1 in stress-responsive gene expression and in plant growth and development. Plant Physiol. **158**: 1955–1964.

Coccetti, P., Nicastro, R., and Tripodi, F. (2018). Conventional and emerging roles of the energy sensor snf1/AMPK in saccharomyces cerevisiae. Microb. Cell **5**: 482–494.

Coello, P., Hirano, E., Hey, S.J., Muttucumaru, N., Martinez-Barajas, E., Parry, M.A.J., and Halford, N.G. (2012). Evidence that abscisic acid promotes degradation of SNF1-related protein kinase (SnRK) 1 in wheat and activation of a putative calcium-dependent SnRK2. J. Exp. Bot. **63**: 913–924.

Cross, J.M., Von Korff, M., Altmann, T., Bartzetko, L., Sulpice, R., Gibon, Y., Palacios, N., and Stitt, M. (2006). Variation of enzyme activities and metabolite levels in 24 arabidopsis accessions growing in carbon-limited conditions. Plant Physiol. **142**: 1574–1588.

Crozet, P., Margalha, L., Butowt, R., Fernandes, N., Elias, C.A., Orosa, B., Tomanov, K., Teige, M., Bachmair, A., Sadanandom, A., and Baena-González, E. (2016). SUMOylation represses SnRK1 signaling in Arabidopsis. Plant J. **85**: 120–133.

Crozet, P., Margalha, L., Confraria, A., Rodrigues, A., Martinho, C., Adamo, M., Elias, C.A., and Baena-González, E. (2014). Mechanisms of regulation of SNF1/AMPK/SnRK1 protein kinases. Front. Plant Sci. **5**: 1–17.

Emanuelle, S., Hossain, M.I., Moller, I.E., Pedersen, H.L., Van De Meene, A.M.L., Doblin, M.S., Koay, A., Oakhill, J.S., Scott, J.W., Willats, W.G.T., Kemp, B.E., Bacic, A., Gooley, P.R., and Stapleton, D.I. (2015). SnRK1 from Arabidopsis thaliana is an atypical AMPK. Plant J. **82**: 183–192.

Flis, A., Sulpice, R., Seaton, D.D., Ivakov, A.A., Liput, M., Abel, C., Millar, A.J., and Stitt, M. (2016). Photoperiod-dependent changes in the phase of core clock transcripts and global transcriptional outputs at dawn and dusk in Arabidopsis. Plant Cell Environ. **39**: 1955–1981.

Fragoso, S., Espíndola, L., Páez-Valencia, J., Gamboa, A., Camacho, Y., Martínez-Barajas, E., and Coello, P. (2009). SnRK1 isoforms AKIN10 and AKIN11 are differentially regulated in Arabidopsis plants under phosphate starvation. Plant Physiol. **149**: 1906–1916.

Gibon, Y., Blaesing, O.E., Hannemann, J., Carillo, P., Höhne, M., Hendriks, J.H.M., Palacios, N., Cross, J., Selbig, J., and Stitt, M. (2004). A robot-based platform to measure multiple enzyme activities in Arabidopsis using a set of cycling assays: Comparison of changes of enzyme activities and transcript levels during diurnal cycles and in prolonged darkness. Plant Cell **16**: 3304–3325.

Gissot, L., Polge, C., Bouly, J.P., Lemaitre, T., Kreis, M., and Thomas, M. (2004). AKINβ3, a plant specific SnRK1 protein, is lacking domains present in yeast and mammals non-catalytic β-subunits. Plant Mol. Biol. **56**: 747–759.

González, A., Hall, M.N., Lin, S.C., and Hardie, D.G. (2020). AMPK and TOR: The Yin and Yang of Cellular Nutrient Sensing and Growth Control. Cell Metab. **31**: 472–492.

Grefen, C. and Blatt, M.R. (2012). A 2in1 cloning system enables ratiometric bimolecular fluorescence complementation (rBiFC). Biotechniques **53**: 311–314.

Hendriks, J.H.M., Kolbe, A., Gibon, Y., Stitt, M., and Geigenberger, P. (2003). ADP-Glucose Pyrophosphorylase Is Activated by Posttranslational Redox-Modification in Response to Light and to Sugars in Leaves of Arabidopsis and Other Plant Species. Plant Physiol. **133**: 838–849.

Iseli, T.J., Walter, M., Van Denderen, B.J.W., Katsis, F., Witters, L.A., Kemp, B.E., Michell, B.J., and Stapleton, D. (2005). AMP-activated protein kinase β subunit tethers α and γ subunits via its c-terminal sequence (186-270). J. Biol. Chem. **280**: 13395–13400.

Jossier, M., Bouly, J.-P., Meimoun, P., Arjmand, A., Lessard, P., Hawley, S., Grahame Hardie, D., and Thomas, M. (2009). SnRK1 (SNF1-related kinase 1) has a central role in sugar and ABA signalling in Arabidopsis thaliana. Plant J. **59**: 316–328.

Laemmli, U.K. (1970). Cleavage of structural proteins during the assembly of the head of bacteriophage T4. Nature **227**: 680–685.

Li, X.-F., Li, Y.-J., An, Y.-H., Xiong, L.-J., Shao, X.-H., Wang, Y., and Sun, Y. (2009). AKINβ1 is Involved in the Regulation of Nitrogen Metabolism and Sugar Signaling in Arabidopsis. J. Integr. Plant Biol. **51**: 513–520.

Mair, A., Pedrotti, L., Wurzinger, B., Anrather, D., Simeunovic, A., Weiste, C., Valerio, C., Dietrich, K., Kirchler, T., Nägele, T., Carbajosa, J.V., Hanson, J., Baena-González, E., Chaban, C., Weckwerth, W., Dröge-Laser, W., and Teige, M. (2015). SnRK1-triggered switch of bZIP63 dimerization mediates the low-energy response in plants. Elife **4**: 1–33.

McBride, A., Ghilagaber, S., Nikolaev, A., and Hardie, D.G. (2009). The Glycogen-Binding Domain on the AMPK β Subunit Allows the Kinase to Act as a Glycogen Sensor. Cell Metab. **9**: 23–34.

McMichael, R.W., Bachmann, M., and Huber, S.C. (1995). Spinach leaf sucrose-phosphate synthase and nitrate reductase are phosphorylated/inactivated by multiple protein kinases in vitro. Plant Physiol. **108**: 1077–1082.

Mengin, V., Pyl, E.T., Moraes, T.A., Sulpice, R., Krohn, N., Encke, B., and Stitt, M. (2017). Photosynthate partitioning to starch in arabidopsis thaliana is insensitive to light intensity but sensitive to photoperiod due to a restriction on growth in the light in short photoperiods. Plant Cell Environ. **40**: 2608–2627.

Moorhead, G., Douglas, P., Morrice, N., Scarabel, M., Aitken, A., and MacKintosh, C. (1996). Phosphorylated nitrate reductase from spinach leaves is inhibited by 14- 3-3 proteins and activated by fusicoccin. Curr. Biol. **6**: 1104–1113.

Moraes, T.A., Mengin, V., Annunziata, M.G., Encke, B., Krohn, N., Höhne, M., and Stitt, M. (2019). Response of the Circadian Clock and Diel Starch Turnover to One Day of Low Light or Low CO 2. Plant Physiol. **179**: 1457–1478.

Nelson, B.K., Cai, X., and Nebenführ, A. (2007). A multicolored set of in vivo organelle markers for co-localization studies in Arabidopsis and other plants. Plant J. **51**: 1126–1136.

Nunes, C., Primavesi, L.F., Patel, M.K., Martinez-Barajas, E., Powers, S.J., Sagar, R., Fevereiro, P.S., Davis, B.G., and Paul, M.J. (2013). Inhibition of SnRK1 by metabolites: Tissue-dependent effects and cooperative inhibition by glucose 1-phosphate in combination with trehalose 6-phosphate. Plant Physiol. Biochem. **63**: 89–98.

Pierre, M., Traverso, J.A., Boisson, B., Domenichini, S., Bouchez, D., Giglione, C., and Meinnel, T. (2007). N-myristoylation regulates the SnRK1 pathway in arabidopsis. Plant Cell **19**: 2804–2821.

Pokhilko, A., Flis, A., Sulpice, R., Stitt, M., and Ebenhöh, O. (2014). Adjustment of carbon fluxes to light conditions regulates the daily turnover of starch in plants: A computational model. Mol. Biosyst. **10**: 613–627.

Polekhina, G., Gupta, A., Van Denderen, B.J.W., Feil, S.C., Kemp, B.E., Stapleton, D., and Parker, M.W. (2005). Structural basis for glycogen recognition by AMP-activated protein kinase. Structure **13**: 1453–1462.

Polekhina, G., Gupta, A., Michell, B.J., van Denderen, B., Murthy, S., Feil, S.C., Jennings, I.G., Campbell, D.J., Witters, L.A., Parker, M.W., Kemp, B.E., and Stapleton, D. (2003). AMPK β Subunit Targets Metabolic Stress Sensing to Glycogen. Curr. Biol. **13**: 867–871.

Polge, C., Jossier, M., Crozet, P., Gissot, L., and Thomas, M. (2008). β-subunits of the SnRK1 complexes share a common ancestral function together with expression and function specificities; physical interaction with nitrate reductase specifically occurs via AKINβ1-subunit. Plant Physiol. **148**: 1570–1582.

Polge, C. and Thomas, M. (2007). SNF1/AMPK/SnRK1 kinases, global regulators at the heart of energy control? Trends Plant Sci. **12**: 20–28.

Ramon, M., Dang, T.V.T., Broeckx, T., Hulsmans, S., Crepin, N., Sheen, J., and Rolland, F. (2019). Default activation and nuclear translocation of the plant cellular energy sensor SnRK1 regulate metabolic stress responses and development. Plant Cell **31**: 1614–1632.

Robertlee, J., Kobayashi, K., Suzuki, M., and Muranaka, T. (2017). AKIN10, a representative Arabidopsis SNF1-related protein kinase 1 (SnRK1), phosphorylates and downregulates plant HMG-CoA reductase. FEBS Lett. **591**: 1159–1166.

Rodrigues, A., Adamo, M., Crozet, P., Margalha, L., Confraria, A., Martinho, C., Elias, A., Rabissi, A., Lumbreras, V., González-Guzmán, M., Antoni, R., Rodriguez, P.L., and Baena-González, E. (2013). ABI1 and PP2CA phosphatases are negative regulators of Snf1-related protein kinase1 signaling in Arabidopsis. Plant Cell **25**: 3871–3884.

Ruiz-Gayosso, A., Rodríguez-Sotres, R., Martínez-Barajas, E., and Coello, P. (2018). A role for the carbohydrate-binding module (CBM) in regulatory SnRK1 subunits: the effect of maltose on SnRK1 activity. Plant J. **96**: 163–175.

Stitt, M., Lilley, R.M.C., Gerhardt, R., and Heldt, H.W. (1989). Metabolite levels in specific cells and subcellular compartments of plant leaves. Methods Enzymol. **174**: 518–552.

Stitt, M., Lunn, J., and Usadel, B. (2010). Arabidopsis and primary photosynthetic metabolism - More than the icing on the cake. Plant J. **61**: 1067–1091.

Sugden, C., Crawford, R.M., Halford, N.G., and Hardie, D.G. (1999). Regulation of spinach SNF1-related (SnRK1) kinases by protein kinases and phosphatases is associated with phosphorylation of the T loop and is regulated by 5'-AMP. Plant J. **19**: 433–439.

Sulpice, R., Flis, A., Ivakov, A.A., Apelt, F., Krohn, N., Encke, B., Abel, C., Feil, R., Lunn, J.E., and Stitt, M. (2014). Arabidopsis coordinates the diurnal regulation of carbon allocation and growth across a wide range of Photoperiods. Mol. Plant **7**: 137–155.

Wang, Y., Wang, L., Micallef, B.J., Tetlow, I.J., Mullen, R.T., Feil, R., Lunn, J.E., and Emes, M.J. (2020). AKINβ1, a subunit of SnRK1, regulates organic acid metabolism and acts as a global modulator of genes involved in carbon, lipid, and nitrogen metabolism. J. Exp. Bot. **71**: 1010–1028.

Wiatrowski, H.A., van Denderen, B.J.W., Berkey, C.D., Kemp, B.E., Stapleton, D., and Carlson, M. (2004). Mutations in the Gal83 Glycogen-Binding Domain Activate the Snf1/Gal83 Kinase Pathway by a Glycogen-Independent Mechanism. Mol. Cell. Biol. **24**: 352–361.

Wurzinger, B., Nukarinen, E., Nägele, T., Weckwerth, W., and Teige, M. (2018). The snrk1 kinase as central mediator of energy signaling between different organelles. Plant Physiol. **176**: 1085–1094.

Yoo, S.D., Cho, Y.H., and Sheen, J. (2007). Arabidopsis mesophyll protoplasts: A versatile cell system for transient gene expression analysis. Nat. Protoc. **2**: 1565–1572.

Zhai, Z., Keereetaweep, J., Liu, H., Feil, R., Lunn, J.E., and Shanklin, J. (2018). Trehalose 6-phosphate positively regulates fatty acid synthesis by stabilizing wrinkled1[open]. Plant Cell **30**: 2616–2627.

Zhang, C.S., Jiang, B., Li, M., Zhu, M., Peng, Y., Zhang, Y.L., Wu, Y.Q., Li, T.Y., Liang, Y., Lu, Z., Lian, G., Liu, Q., Guo, H., Yin, Z., Ye, Z., Han, J., Wu, J.W., Yin, H., Lin, S.Y., and Lin, S.C. (2014). The lysosomal v-ATPase-ragulator complex is a common activator for AMPK and mTORC1, acting as a switch between catabolism and anabolism. Cell Metab. **20**: 526–540.

Zhang, Y., Primavesi, L.F., Jhurreea, D., Andralojc, P.J., Mitchell, R.A.C., Powers, S.J., Schluepmann, H., Delatte, T., Wingler, A., and Paul, M.J. (2009). Inhibition of SNF1-related protein kinasel activity and regulation of metabolic pathways by trehalose-6-phosphate1[w][OA]. Plant Physiol. **149**: 1860–1871.

3.7 Supplementary Data

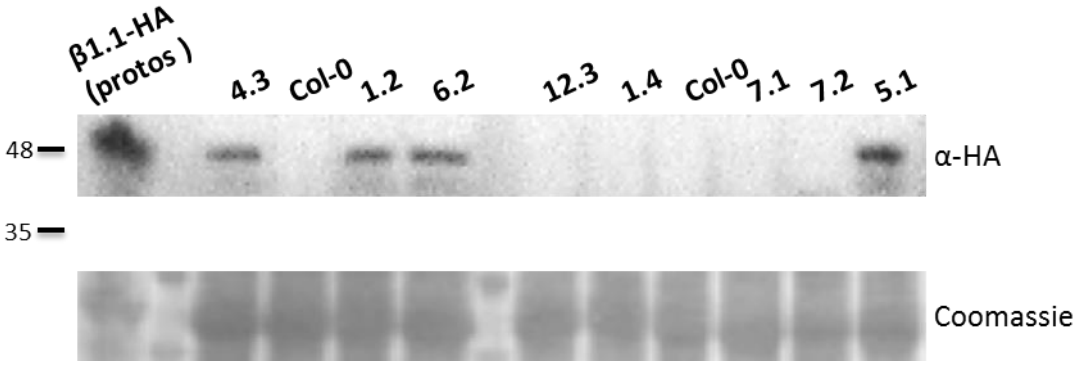

Supplemental Figure 3.1 | Western blot analysis of several *SnRK1β1.1-OE* lines.
Western blot analysis of several independent *SnRK1β1.1-OE* lines, using an antibody against the HA tag. Line 5.1 shows the strongest degree of protein accumulation. Lines 6.2, 5.1 were chosen as representatives for overexpression of SnRK1β1.1, whereas line 7.1 was used as a WT-like control. Coomassie blue staining of total protein is shown as loading control.

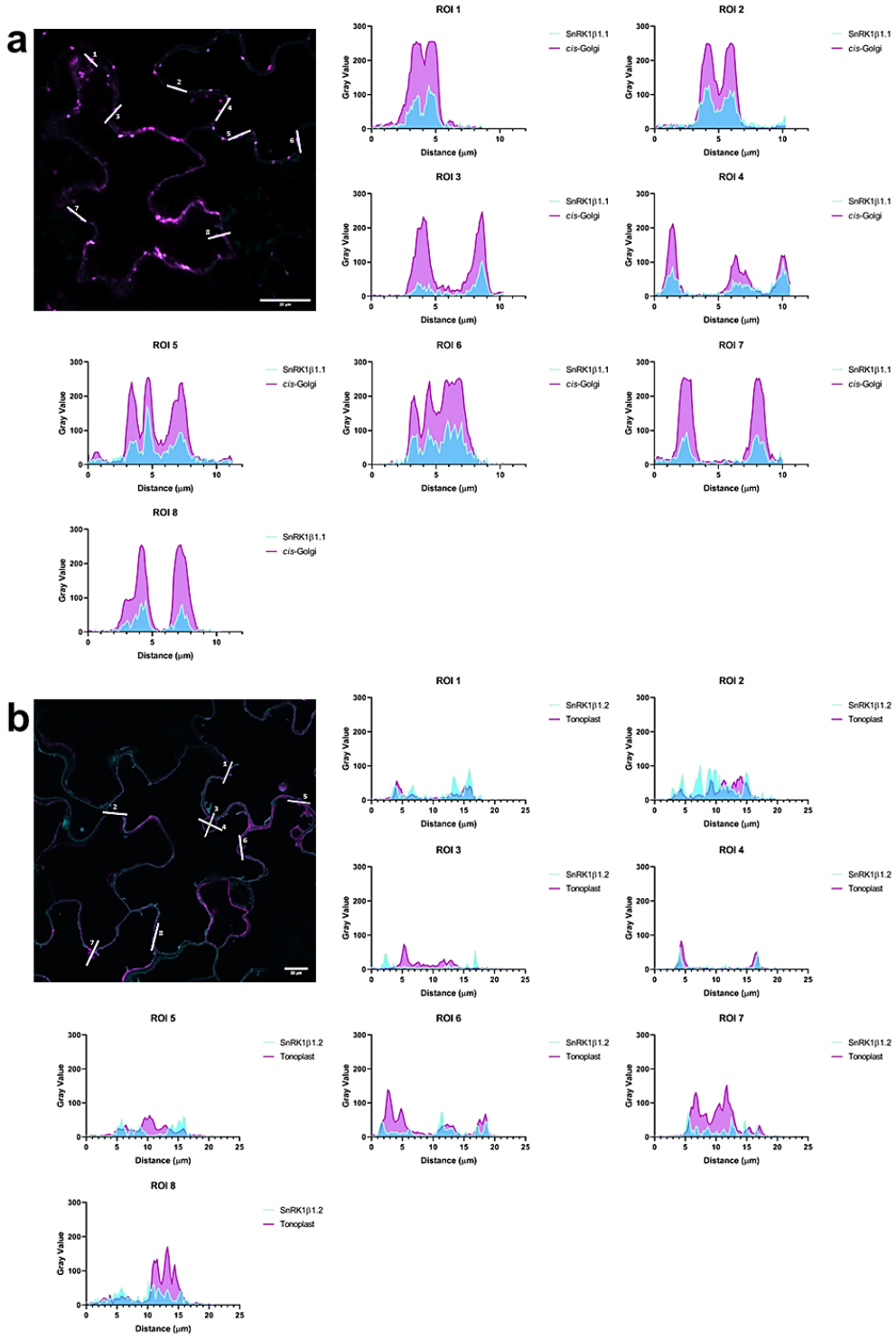
a
ROI 1
ROI 2
ROI 3
ROI 4
ROI 5
ROI 6
ROI 7
ROI 8
Gray Value
Distance (μm)
SnRK1β1.1
cis-Golgi
b
ROI 1
ROI 2
ROI 3
ROI 4
ROI 5
ROI 6
ROI 7
ROI 8
Gray Value
Distance (μm)
SnRK1β1.2
Tonoplast

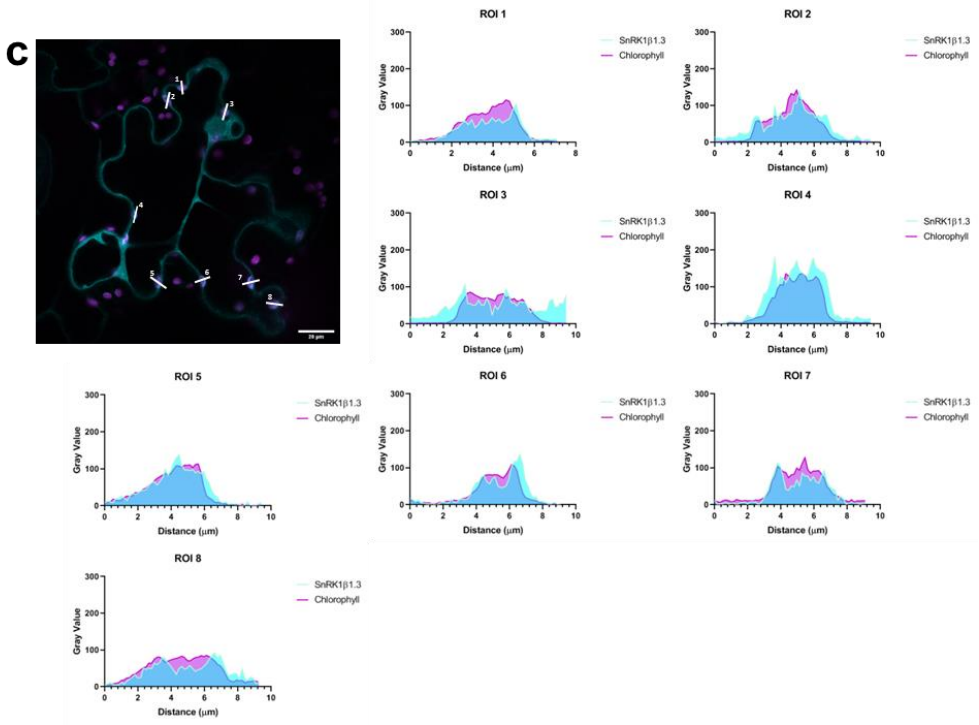

Supplemental Figure 3.2 | Quantification of co-localization between SnRK1β1 splice variants and several subcellular markers.
(a-c) For quantification of co-localization, eight independent zones from the micrographs presented in Fig. 3 were selected. A horizontal line was drawn along the micrograph, and the grey intensity values of both fluorescent channels was measured and plotted as a histogram. Overlap of the histogram peaks illustrates a positive co-localization between SnRK1β1.1-GFP and the *cis*-Golgi marker (*Gm*Man1-mCherry) **(a).** The overall signal intensity of both SnRK1β1.2-GFP and γ-TIP-mCherry was very low, but a partial co-localization could be observed in some, but not all, of the regions analysed **(b)**. SnRK1β1.3-GFP consistently co-localized with chlorophyll autofluorescence, indicating a putative chloroplastidial localization for this splice variant **(c)**. Scale bars: 20 µm.

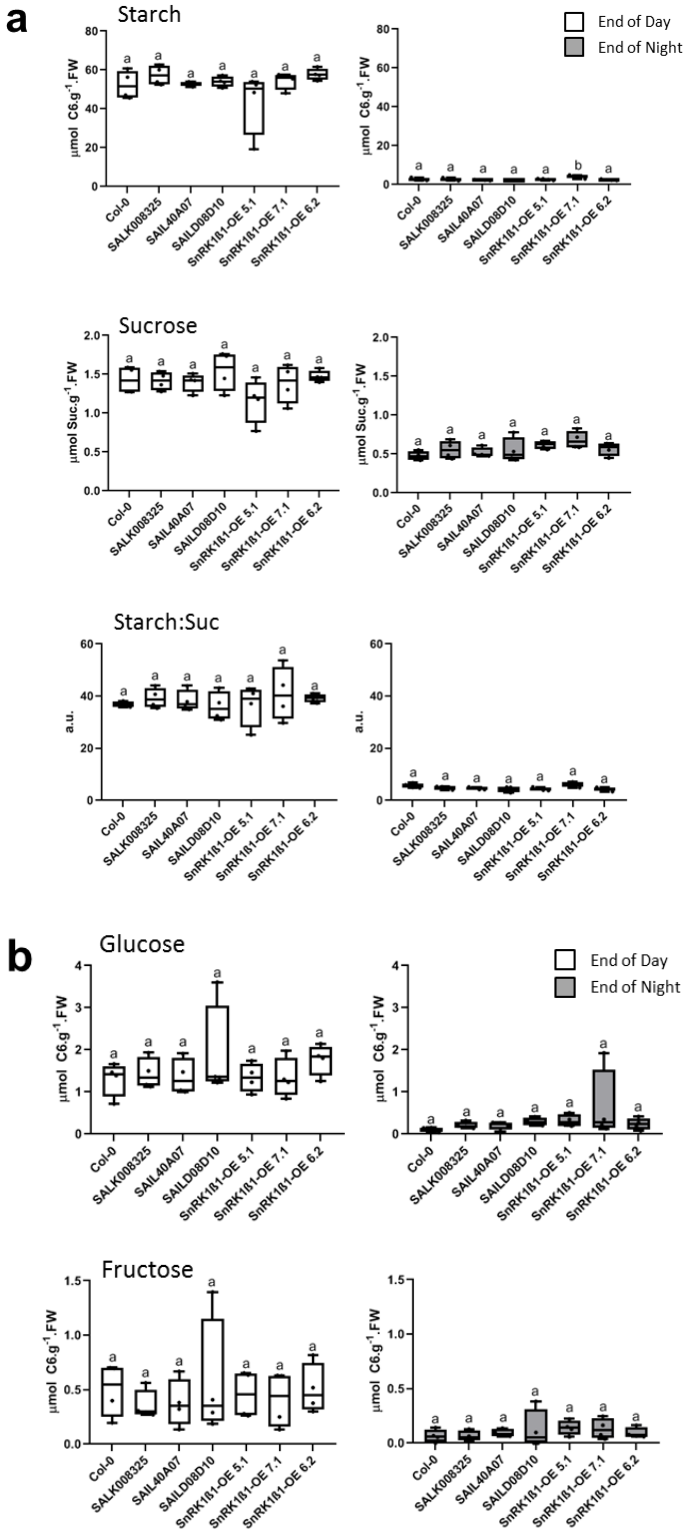
a
Starch
End of Day
End of Night
µmol C6.g-1.FW
Sucrose
µmol Suc.g-1.FW
Starch:Suc
a.u.
b
Glucose
Fructose
Col-0
SALK008325
SAIL40A07
SAILD08D10
SnRK1ß1-OE 5.1
SnRK1ß1-OE 7.1
SnRK1ß1-OE 6.2

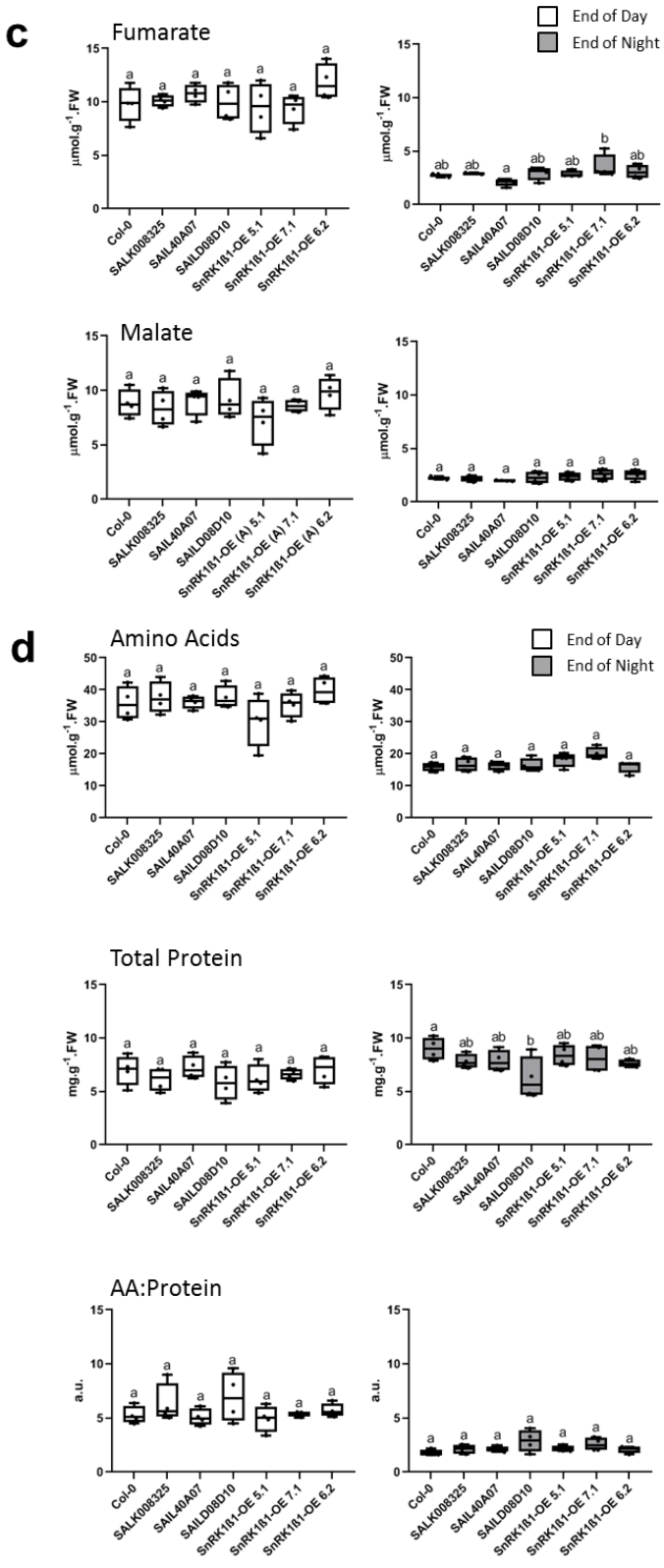
c
Fumarate
End of Day
End of Night
µmol.g-1.FW
Malate
d
Amino Acids
Total Protein
mg.g-1.FW
AA:Protein
a.u.
Col-0
SALK008325
SAIL40A07
SAILD08D10
SnRK1ß1-OE 5.1
SnRK1ß1-OE 7.1
SnRK1ß1-OE 6.2
SnRK1ß1-OE (A) 5.1
SnRK1ß1-OE (A) 7.1
SnRK1ß1-OE (A) 6.2

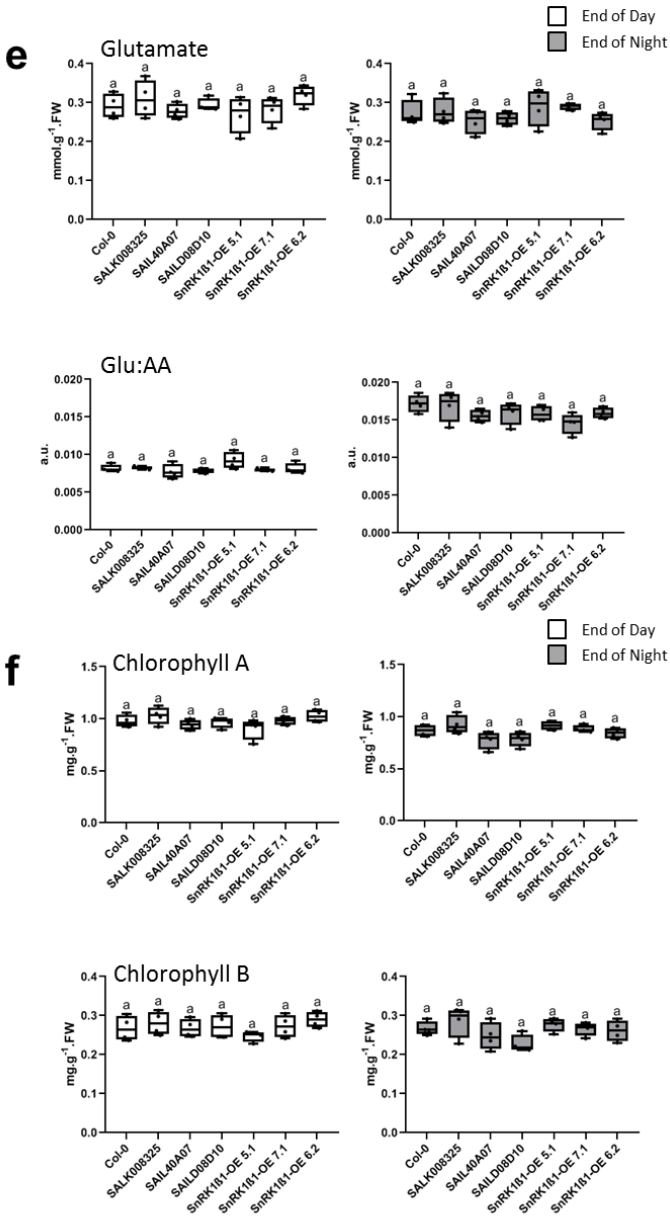

Supplemental Figure 3.3 | Metabolite profiling of *SnRK1β1* mutant lines.
Metabolites related to carbon and nitrogen metabolism were determined for three independent T-DNA insertional mutants and three independent *SnRK1β1.1-OE* lines, and compared against a Col-0 control line at the end of the day (white boxes) and at the end of the night (grey boxes). **(a)** Starch and sucrose levels show no statistically significant differences between the *SnRK1β1* mutant lines and the wildtype, although mildly decreased sucrose accumulation was observed in the *SnRK1β1.1-OE* lines at the end of the day. Similarly to starch, the starch:sucrose ratios remained unaltered in all of the lines, at either time point. Boxplots represent 4 biological replicates (each consisting of a pool of 4-5 randomly harvested rosettes). **(b-c)** Glucose, fructose, fumarate and malate levels show no statistically significant differences between the *SnRK1β1* mutant lines and the wildtype, although mildly reduced malate accumulation was observed in the *SnRK1β1.1-OE* lines at the end of the day **(c)**. **(d)** The total

amino-acid pool and total protein levels show no statistically significant differences between lines, although the *SnRK1β1.1-OE* lines show a tendency of lower amino-acid accumulation at the end of the day. **(e)** Glutamate levels show no statistically significant change between lines. The abundance of glutamate in relation to the entire amino-acid pool (Glu:AA) also remains unchanged **(e)**. Chlorophyll content shows no statistically significant differences between lines, although a subtle decrease in chlorophyll B content was observed in the strongest overexpressor line (5.1) at the ED **(f)**. Lower and upper box boundaries represent the first and third quantiles, respectively, horizontal lines mark the median and whiskers mark the highest and lowest values. Dots represent individual datapoints. Different letters indicate statistically significant differences (p<0.05, one-way ANOVA with Tukey HSD test).

Supplemental Table 3.1 | Metabolite measurements performed in the Col-0, *SnRK1β1.1-OE*, and *snrk1β1* lines.

Average values and standard deviations are shown for each metabolite at both time points (ED and EN) for the Col-0 control (Table S1a), the three *SnRK1β1.1-OE* lines (Table S1b), and the three *snrk1β1* T-DNA insertional mutant lines (Table S1d). These values were used to calculate the log2 ratios between the OE and T-DNA mutants in comparison to the WT (*SnRK1β1-OE* vs Col-0, Table S1c; *snrk1β1* vs Col-0, Table S1e).

TABLE S1A_Col-0 metabolite measurements				Std Dev	
Mean level [µmol/gFW]	Method	End of Day	End of Night	End of Day	End of Night
Sucrose	Enzymatic	1,424	0,481	0,149	0,049
Glucose	Enzymatic	1,310	0,109	0,356	0,046
Fructose	Enzymatic	0,499	0,067	0,213	0,051
Starch	Enzymatic	52,430	2,734	6,284	0,641
Malate	Enzymatic	8,830	2,235	1,101	0,134
Fumarate	Enzymatic	9,786	2,767	1,447	0,139
Protein (mg/gFW)	Enzymatic	6,963	9,011	1,228	0,916
NO2	Enzymatic	0,875	0,548	0,233	0,058
NO3	Enzymatic	155,300	159,800	1,193	17,816
Total Amino-acids	Enzymatic	35,900	15,900	4,546	1,155
Glutamate (mmol/gFW)	Enzymatic	0,292	0,273	0,027	0,028
Chlorophyll A (mg/gFW)	-	0,976	0,869	0,052	0,049
Chlorophyll B (mg/gFW)	-	0,267	0,267	0,027	0,015

TABLE S1B_SnRK1b1-OE metabolite measurements							
		SnRK1b1-OE 5.1		SnRK1b1-OE 6.2		SnRK1b1-OE 7.1	
Mean level [µmol/gFW]	Method	End of Day	End of Night	End of Day	End of Night	End of Day	End of Night
Sucrose	Enzymatic	1,158	0,618	1,475	0,566	1,380	0,681
Glucose	Enzymatic	1,344	0,316	1,765	0,239	1,335	0,654
Fructose	Enzymatic	0,458	0,139	0,504	0,091	0,411	0,131
Starch	Enzymatic	43,550	2,705	57,790	2,431	54,520	4,138
Malate	Enzymatic	7,175	2,396	9,733	2,539	8,566	2,576
Fumarate	Enzymatic	9,447	2,848	11,870	3,067	9,358	3,562
Protein (mg/gFW)	Enzymatic	6,173	8,406	7,055	7,629	6,599	8,086
NO2	Enzymatic	0,515	0,689	0,528	0,697	0,602	0,756
NO3	Enzymatic	145,200	175,500	145,200	166,600	132,600	176,200
Total Amino-acids	Enzymatic	30,050	18,160	39,610	16,000	35,430	20,110
Glutamate (mmol/gFW)	Enzymatic	0,271	0,288	0,320	0,253	0,283	0,291
Chlorophyll A (mg/gFW)	-	0,903	0,916	1,025	0,844	0,980	0,884
Chlorophyll B (mg/gFW)	-	0,248	0,277	0,290	0,261	0,273	0,266

Std Dev						
	SnRK1b1-OE 5.1		SnRK1b1-OE 6.2		SnRK1b1-OE 7.1	
	End of Day	End of Night	End of Day	End of Night	End of Day	End of Night
Sucrose	0,286	0,053	0,075	0,087	0,250	0,114
Glucose	0,340	0,143	0,374	0,142	0,469	0,854
Fructose	0,216	0,068	0,228	0,049	0,257	0,094
Starch	16,310	0,467	2,960	0,330	4,398	0,895
Malate	2,194	0,402	1,519	0,467	0,583	0,490
Fumarate	2,375	0,297	1,690	0,631	1,408	1,122
Protein (mg/gFW)	1,319	0,983	1,382	0,332	0,526	1,275
NO2	0,016	0,149	0,074	0,257	0,055	0,137
NO3	10,820	9,653	2,958	12,330	9,723	16,610
Total Amino-acids	7,919	2,187	4,350	1,905	3,995	1,904
Glutamate (mmol/gFW)	0,047	0,048	0,026	0,023	0,034	0,008
Chlorophyll A (mg/gFW)	0,101	0,046	0,058	0,050	0,038	0,034
Chlorophyll B (mg/gFW)	0,014	0,017	0,020	0,027	0,028	0,018

Table S1C_SignalLog2 Ratios_SnRK1b1-OE vs. Col0

	SnRK1b1-OE 5.1		SnRK1b1-OE 6.2		SnRK1b1-OE 7.1	
Harvest time	End of Day	End of Night	End of Day	End of Night	End of Day	End of Night
Sucrose	-0,298	0,363	0,051	0,235	-0,045	0,502
Glucose	0,037	1,536	0,430	1,132	0,027	2,583
Fructose	-0,123	1,063	0,015	0,456	-0,279	0,976
Starch	-0,268	-0,015	0,140	-0,169	0,056	0,598
Malate	-0,299	0,100	0,140	0,184	-0,044	0,205
Fumarate	-0,051	0,042	0,279	0,149	-0,065	0,364
Protein (mg/gFW)	-0,174	-0,100	0,019	-0,240	-0,077	-0,156
NO2	-0,765	0,330	-0,728	0,347	-0,540	0,464
NO3	-0,097	0,135	-0,097	0,060	-0,228	0,141
Total Amino-acids	-0,257	0,192	0,142	0,009	-0,019	0,339
Glutamate	-0,108	0,078	0,132	-0,110	-0,046	0,090
Chlorophyll A	-0,112	0,075	0,071	-0,043	0,006	0,023
Chlorophyll B	-0,106	0,052	0,118	-0,033	0,033	-0,005

TABLE S1D_snrk1b1 metabolite measurements							
		SALK008325		SAIL40A07		SAILD08510	
Mean level [µmol/gFW]	Method	End of Day	End of Night	End of Day	End of Night	End of Day	End of Night
Sucrose	Enzymatic	1,415	0,555	1,396	0,519	1,543	0,546
Glucose	Enzymatic	1,435	0,207	1,358	0,203	1,885	0,293
Fructose	Enzymatic	0,359	0,064	0,377	0,092	0,570	0,120
Starch	Enzymatic	57,270	2,685	52,900	2,360	54,000	2,200
Malate	Enzymatic	8,336	2,183	8,959	1,994	9,176	2,286
Fumarate	Enzymatic	10,090	2,914	10,790	2,070	9,951	2,932
Protein (mg/gFW)	Enzymatic	6,131	7,807	7,223	7,842	5,818	6,198
NO2	Enzymatic	0,655	0,910	0,781	0,657	0,655	0,583
NO3	Enzymatic	143,300	166,900	142,300	157,400	138,100	163,500
Total Amino-acids	Enzymatic	37,570	16,550	36,090	16,260	37,570	16,430
Glutamate (mmol/gFW)	Enzymatic	0,310	0,277	0,278	0,253	0,294	0,260
Chlorophyll A (mg/gFW)	-	1,028	0,921	0,945	0,775	0,966	0,785
Chlorophyll B (mg/gFW)	-	0,281	0,286	0,268	0,248	0,272	0,228

Std Dev						
	SALK008325		SAIL40A07		SAILD08510	
	End of Day	End of Night	End of Day	End of Night	End of Day	End of Night
Sucrose	0,117	0,114	0,119	0,063	0,254	0,162
Glucose	0,370	0,080	0,427	0,095	1,150	0,088
Fructose	0,137	0,047	0,221	0,034	0,559	0,181
Starch	4,890	0,726	1,243	0,246	2,652	0,108
Malate	1,625	0,278	1,260	0,053	1,843	0,532
Fumarate	0,535	0,073	0,840	0,332	1,686	0,631
Protein (mg/gFW)	1,127	0,673	1,087	1,017	1,609	1,983
NO2	0,124	1,010	0,175	0,141	0,075	0,054
NO3	5,315	20,670	11,790	19,270	8,877	9,697
Total Amino-acids	4,923	2,209	1,955	1,354	3,708	2,069
Glutamate (mmol/gFW)	0,047	0,033	0,019	0,032	0,017	0,016
Chlorophyll A (mg/gFW)	0,084	0,088	0,047	0,083	0,052	0,070
Chlorophyll B (mg/gFW)	0,030	0,040	0,023	0,035	0,031	0,023

Table S1E_SignalLog2 Ratios_snrk1b1 vs. Col0

	SALK008325		SAIL40A07		SAILD08510	
Harvest time	**End of Day**	**End of Night**	**End of Day**	**End of Night**	**End of Day**	**End of Night**
Sucrose	-0,009	0,207	-0,029	0,111	0,116	0,185
Glucose	0,131	0,923	0,052	0,893	0,525	1,426
Fructose	-0,475	-0,055	-0,403	0,470	0,194	0,852
Starch	0,127	-0,026	0,013	-0,212	0,043	-0,314
Malate	-0,083	-0,034	0,021	-0,165	0,055	0,033
Fumarate	0,044	0,075	0,141	-0,419	0,024	0,084
Protein (mg/gFW)	-0,184	-0,207	0,053	-0,200	-0,259	-0,540
NO2	-0,417	0,731	-0,164	0,262	-0,417	0,088
NO3	-0,116	0,063	-0,126	-0,022	-0,169	0,033
Total Amino-acids	0,066	0,058	0,008	0,032	0,066	0,047
Glutamate	0,090	0,022	-0,069	-0,109	0,013	-0,074
Chlorophyll A	0,075	0,083	-0,047	-0,166	-0,015	-0,147
Chlorophyll B	0,072	0,099	0,006	-0,110	0,028	-0,232

Supplemental Table 3.2 | Plant lines, antibodies and primers.
List of all plant lines, antibodies and primers used in this study.

Cloning Primers	Name	Sequence
SnRK1β1.1	Beta1 TAIR Fw_BamHI	CGGGATCCATGGGAAATGCGAACGGCAAAG
	Beta1 TAIR Rev_StuI	AAGGCCTCCGTGTGAGCGGTTTGTAGAGGAC
SnRK1β1.2	AKINB1.2_Exon2_CloningF	GCCCACATTGTTATTCCACG
	AKINB1.2_Exon2_CloningR	ATCCGACACGAAATGCAGCCATTAGG
SnRK1β1.3	AKINB1.3_BamHI_F	CGGGATCCATGCGTCACCTCTTCCATTGTTTA

RT-PCR Primers	Name	Sequence
SnRK1β1.1	β1.1-LP	TTATTCGCTCCTCAGGTTCC
	β1-RP	GGTAGGGATTCCTTGCTCTG
SnRK1β1.2	β1.2-LP	TTATTCGCTCCTCAGCCCACATTG
SnRK1β1.3	β1.3-LP	GTTGCTATATTCATTTTCGACTCC

Antibody - short name	Antibody - full description	Source	Reference	Dilution	Dilution buffer
Anti-HA	Anti-HA High Affinity	Roche-Portugal	11867423001	1:1 000	1% milk in TBS
Anti-Rat	Peroxidase Affinipure goat anti-rat IgG	Jackson Immuno Research	112035167	1:10 000	1% milk in TBS

PLANT LINE	LINE ID	REFERENCE
SnRK1β1.1-OE	*SnRK1β1.1-OE (5.1)*	This work
	SnRK1β1.1-OE (6.2)	This work
	SnRK1β1.1-OE (7.1)	This work
SALK008325	SALK008325	Li et al., 2009 JIPB
SAIL40A07	SAIL40A07	This work
SAIL508D10	SAIL508D10	This work

Construct	Reference	Description
G-rk *CD3-967*	Nelson et al., 2007 TPJ	Cytoplasmic and transmembrane domain (first 49 aminoacids) of *Gm*Man1, soybean α-1,2-mannosidase I with a C-terminal fusion to an mCherry fluorescent protein
vac-rk *CD3-975*	Nelson et al., 2007 TPJ	γ-TIP with a C-terminal fusion to an mCherry fluorescent protein
35S::SnRK1β1.1-GFP	This work	Coding sequence (CDS) of the *SnRK1β1.1* transcript, with a C-terminal fusion to a GFP
35S::SnRK1β1.2-GFP	This work	CDS of the *SnRK1β1.2* transcript, with a C-terminal fusion to a GFP
35S::SnRK1β1.3-GFP	This work	CDs of the *SnRK1β1.3* transcript, with a C-terminal fusion to a GFP
35S::SnRK1β1.1-nYFP, 35S::SnRK1α1-cYFP, 35S::RFP	This work	CDS of the *SnRK1β1.1* transcript, with a C-terminal fusion to the nYFP fragment, CDS of the *SnRK1α1* transcript, with a C-terminal fusion to the cYFP fragment, and a cytosolic RFP transfection marker
35S::SnRK1β1.2-nYFP, 35S::SnRK1α1-cYFP, 35S::RFP	This work	CDS of the *SnRK1β1.2* transcript, with a C-terminal fusion to the nYFP fragment, CDS of the *SnRK1α1* transcript, with a C-terminal fusion to the cYFP fragment, and a cytosolic RFP transfection marker
35S::SnRK1β1.3-nYFP, 35S::SnRK1α1-cYFP, 35S::RFP	This work	CDS of the *SnRK1β1.3* transcript, with a C-terminal fusion to the nYFP fragment, CDS of the *SnRK1α1* transcript, with a C-terminal fusion to the cYFP fragment, and a cytosolic RFP transfection marker

CHAPTER 4

General Discussion and Future Perspectives

4.1 SnRK1 is necessary also under favourable growth conditions

SnRK1/Snf1/AMPK kinases are universally known as master regulators of metabolism and cellular energy homeostasis, functioning as “fuel-gauges” in eukaryotic organisms (Ghillebert et al., 2011). The plant SnRK1 plays diverse and important functions in energy management in response to both biotic and abiotic stress, and, consequently, it is viewed mostly as a regulator of stress responses (Baena-González et al., 2007; Baena-González and Sheen, 2008; Crepin and Rolland, 2019). However, manipulation of SnRK1 impacts also multiple aspects of growth and development and full *SnRK1α1* knockouts appear not to be viable, further highlighting the centrality of this kinase (Margalha et al., 2019; Baena-González and Lunn, 2020). It is currently unclear if the impossibility of obtaining a double *snrk1α1 snrk1α2* mutant is due to SnRK1 being required at a specific developmental stage, or if normal SnRK1 function is necessary at all times for normal plant growth and development (Baena-González et al., 2007; Ramon et al., 2013; Gao et al., 2016; Ramon et al., 2019).

In this thesis, I identified important functions for the SnRK1 kinase at the metabolic and gene expression levels, under favourable growth conditions. My work uncovered a multilevel involvement of SnRK1 in sucrose homeostasis, both through the regulation of photoassimilate partitioning between sucrose and the TCA cycle, and through the modulation of Tre6P accumulation in response to sucrose. I also describe novel regulatory aspects of SnRK1 that link its activity to the regular daily cycles of sugar accumulation and to different subcellular localizations that potentially provide access to different protein substrates.

.

4.2 SnRK1 links the sucrose status to Tre6P

Even though the sucrose-Tre6P nexus model is widely accepted to explain sucrose homeostasis, the mechanism by which increases in sucrose result in

concomitant increases in Tre6P is not understood. It is only known that this response is independent of transcription, but not of protein synthesis, but the actual protein that must be synthetized in order for an increase in sucrose to result in increased levels of Tre6P accumulation remains unknown (Yadav et al., 2014).

In chapter 2, we identified Tre6P itself as one of the metabolites most sensitive to the genetic manipulation of SnRK1. According to the sucrose-Tre6P nexus model, an increase in the endogenous sucrose levels leads to an increase in Tre6P (Yadav et al., 2014). Indeed, we observed that the *SnRK1α1-OE* line had increased sucrose and Tre6P levels, whereas the opposite was true for the *sesquiα2* line. Given that SnRK1 activity is often associated with growth-repression and decreased carbon consumption, it is not surprising that *SnRK1α1* overexpression results in a sucrose accumulation phenotype. If sucrose consumption was the only altered process in the SnRK1 mutants one would expect that the change in Tre6P levels would be proportional to that of sucrose, just enough to signal the extra available sucrose. However, Tre6P is disproportionally affected compared to sucrose, leading to a shift in the Tre6P:Suc ratio, that is up to 92% higher in the overexpressor line and 64% lower in the *sesquiα2* background, when compared to WT values. This observation suggests that SnRK1 is part of the mechanism that links sucrose to Tre6P. This mechanism becomes overly responsive in the *SnRK1α1-OE* line, providing a molecular basis for the previously described phenotypes of sugar hypersensitivity of these plants (Jossier et al., 2009). The relationship between sucrose and Tre6P has been explored in great detail over a wide range of growth conditions, tissues and plant species (see Chapter 1 for details). Increased Tre6P:Suc ratios are typically associated with metabolically active tissues, so it was unexpected that overexpression of *SnRK1α1* also led to a higher Tre6P:Suc ratio. This supports the view that SnRK1 is required under favourable growth conditions to drive growth, potentially explaining the inability to obtain a full *SnRK1α* knock-out mutant (see section 4.4 for a more detailed discussion).

The marked impact of SnRK1 on Tre6P levels suggested that SnRK1 modulates Tre6P synthesis from Glc6P and UDPGlc (*via* TPS enzymes), and/or Tre6P

dephosphorylation into trehalose (*via* TPP enzymes), with those two hypotheses being non-mutually exclusive. In Arabidopsis TPS1 plays an important regulatory role in Tre6P synthesis (Eastmond et al., 2002; Gómez et al., 2010; Delorge et al., 2015), as was recently demonstrated by the detailed characterization of *tps1* complementation lines expressing various mutated TPS1 variants (Fichtner, Olas, et al., 2020). We therefore examined the patterns of accumulation of TPS1, but could find no differences at either the transcript or protein levels, except for a decrease in total TPS1 abundance at the end of the day (ED) in the *SnRK1α1-OE* line. This decrease in TPS1 abundance is anti-correlated with the pattern of Tre6P accumulation, raising the possibility that, *in planta,* TPS1 is repressed by the accumulation of its product. However, despite the fact that changes in TPS1 protein abundance cannot explain the observed patterns of Tre6P accumulation, it is plausible that TPS1 activity is regulated by mechanisms that do not impact its protein levels. In this context, one intriguing possibility is that TPS1 is itself a target of SnRK1-mediated phosphorylation, and indeed, using a recently published *in silico* analysis tool [PhosMoS, (Carianopol et al., 2020)], we could predict a single full SnRK1 phosphorylation site at residue S252, and several other partial SnRK1 phosphorylation sites (data not shown). This specific S252 residue has recently been investigated by Fichtner and colleagues, who generated both phosphomutant (S252A) and phosphomimetic (S252D) variants. Under their experimental settings (16h long-day photoperiods), only a very subtle increase in Tre6P levels could be detected at ZT10 in the phosphomutant line and no changes in the phosphomimetic mutant (Fichtner, Olas, et al., 2020). Although not supporting a functional role for the phosphorylation of this residue, these results are insufficient to discard the hypothesis that TPS1, or some other intermediary factor, is regulated by the SnRK1 kinase.

On the other hand, the strongly reduced levels of Tre6P in the *sesquiα2* line also cannot be explained by differences in TPS1 accumulation, but we detected increased transcript abundance for four different *TPP* genes (*TPPD*, *TPPG*, *TPPJ*, and *TPPH*), at the end of the night (EN), when Tre6P levels are lowest. This raises the possibility that SnRK1 is involved in Tre6P dephosphorylation. TPP enzymes have been the target of substantially less characterization and study, but all eleven

proteins appear to have some degree of tissue-specificity and catalytic activity (Vandesteene et al., 2012) and could undoubtedly contribute to Tre6P signalling in different plant tissues. It is puzzling that we can only detect enhanced accumulation of *TPP* transcripts in the *sesquiα2* line at EN, when Tre6P levels show the least difference between this mutant and the WT. We currently do not have information regarding the abundance of the corresponding TPP proteins during the day-night cycle, and it is possible that this upregulation at the end of the night is in preparation for the following light period, preventing Tre6P from rising to WT levels in the *sesquiα2* background. It will be important to analyse how much these transcriptional differences reflect protein abundance, in order to determine if TPPs play a role in the altered Tre6P accumulation of the *SnRK1α* mutants. Nevertheless, the fact that, despite its high Tre6P content, the *SnRK1α1-OE* mutant had WT levels of *TPPs* suggests that transcriptional regulation of TPPs may not be the main mechanism by which SnRK1 affects Tre6P levels.

4.3 SnRK1 links Tre6P to carbon and nitrogen metabolism

Besides the altered response of Tre6P to sucrose levels, the *sesquiα2* line showed a metabolic profile of decreased glycolytic intermediate accumulation, compared to the WT. In addition, it showed higher contents of several organic acids, namely citrate, aconitate, and isocitrate, with a concomitant decrease in the levels of succinate. Increased diversion of carbon away from glycolysis, towards the synthesis of organic acids would be typically associated with elevated Tre6P levels (Figueroa et al., 2016). The fact that this “high Tre6P” profile is present in a line with remarkably low Tre6P levels suggests that the previously described effects of Tre6P in controlling the flux of carbon occur *via* inhibition of the SnRK1 kinase.

Interestingly, the accumulation of organic acids was not equally affected in the *sesquiα2* and iOtsA lines: succinate, and to a lower extent 2-OG, accumulated to lower levels in the *sesquiα2* compared to WT, whilst their accumulation was higher in the iOtsA background compared to the AlcR control. The reason behind these

differences is currently unclear. One may be differing responses to an induced increase in Tre6P and constitutive changes in SnRK1 expression. Alternatively, the work of Ruiz-Gayosso and colleagues (Ruiz-Gayosso et al., 2018) shows that during the day-night cycle, the subunits conforming the SnRK1 heterotrimer suffer a shift, with the SnRK1β3 subunit preferentially binding to the complex at the ED. This shift in SnRK1 trimer composition has a measurable impact on the dynamics of the kinase, making it susceptible to maltose, which acts by enhancing SnRK1 kinase activity *in vitro*. It is thus possible that such diurnal shifts in SnRK1 subunit composition lead to differential sensitivities to Tre6P-mediated inhibition, as opposed to a loss-of-function approach that, by targeting both catalytic subunits, should equally impair any SnRK1 trimer that is formed. In order to further disentangle this question, a deeper characterization would be needed of SnRK1 trimer composition during the day-night cycle, and under specific stress conditions and developmental stages. This issue gains even more relevance, when considering the results of chapter 3, with alternative splicing potentially contributing to a higher diversity of SnRK1 trimers.

There are several possible explanations why only a part of the TCA cycle is affected upon SnRK1 depletion, with the non-cyclical operation of the TCA cycle in illuminated leaves being the simplest one (Sweetlove et al., 2010). Under this assumption, an increased investment of 2-OG towards nitrogen assimilation and/or photorespiration could help explain the observed differences and, indeed, an enhanced flux of carbon towards nitrogen assimilation would be compatible with the known inhibitory function of SnRK1 over NR activity (McMichael et al., 1995; Moorhead et al., 1996). On the other hand, our transcriptomic analyses identified the photorespiration gene *PURU2* (encoding a 10-formyl tetrahydrofolate deformylase) as being downregulated in the *SnRK1α1-OE*, opening up the possibility that SnRK1 is involved in the inhibition of photorespiration. Photorespiration is the process by which 2-phosphoglycolate, a toxic by-product from the oxygenase reaction mediated by RubisCO, can be detoxified back into 3-PGA, *via* a series of reactions that span over three different subcellular compartments (the plastid, peroxisome and mitochondria) (Eisenhut et al., 2019). An over activated photorespiratory pathway in

the *sesquia2* line would be compatible with the observed decreased levels of the intermediates glycerate, Gly3P and 2-OG, but not of 3-PGA, the final metabolite in the pathway (see Chapter 2, Sup Table 1). Regardless, photorespiration remains an attractive pathway, since it provides a point of interaction between carbon, nitrogen, organic acid and sulphur metabolism (Eisenhut et al., 2019), all processes apparently affected by SnRK1.

Alternatively, the recent description of a TCA cycle metabolon (Sweetlove and Fernie, 2018) could also provide an exciting new hypothesis to explain these results. In mitochondria isolated from potato tubers, all eight TCA cycle enzymes engage in binary protein-protein interactions, giving rise to a full TCA cycle metabolon linking the catalytic subunits of sequential enzymes (Zhang et al., 2017). Using the protein-protein interaction data generated by Zhang and colleagues, we can effectively look at succinate dehydrogenase (and by extension, to succinate) as the starting point of the metabolon, which is capable of at least partial channelling of metabolites all the way to isocitrate. Since these two organic acids are the most affected ones in the *sesquia2* line, with a very substantial decrease in the levels of succinate and a very substantial increase in the levels of isocitrate, one could hypothesize that SnRK1 acts to destabilize the TCA cycle metabolon. Although exciting, this explanation is highly speculative, given our current lack of knowledge regarding (1) interactions between SnRK1 and the enzymes involved in the TCA cycle, (2) the lack of reports of SnRK1 inside the mitochondria (where the metabolon is presumably localized), and (3) the currently unclear physiological effects of the formation of such metabolons. Nevertheless, this hypothesis could provide the backbone for advancing our understanding on how SnRK1 impacts central metabolism. Regardless of the purpose behind the uneven effects of SnRK1 on the TCA cycle, it remains relevant to explore potential alterations of TCA cycle enzymes in the SnRK1 mutants. To gain mechanistic understanding of how SnRK1 influences organic acid metabolism, it will be important to identify which of the enzymes, if any, are targeted by SnRK1, and in which way these putative phosphorylation events may affect their enzymatic properties.

Previous work by Figueroa and colleagues showed that a transient increase in Tre6P results in post-translational activation of PEPC and NR (Figueroa et al., 2016). In the case of NR, the potentially increased diversion of organic acids towards nitrogen assimilation of the *sesquiα2* mutant is consistent with the established connection between SnRK1 and NR. Phosphorylation of NR by SnRK1 leads to its recognition by 14-3-3 proteins and its subsequent inactivation (McMichael et al., 1995; Moorhead et al., 1996). Although such connection to SnRK1 has not been made in the case of PEPC, it is plausible that it exists, and that either PEPC directly, or its upstream kinase (PEPCK) are targeted by SnRK1 for phosphorylation, resulting in the downstream reduction of the flux of carbon between glycolysis, the TCA cycle, and organic acid synthesis. To test such hypothesis, the *SnRK1α1-OE* and *sesquiα2* lines could be used to measure total PEPC activity to investigate potential differences in the mutants. The expectation is that carbon would flow more readily *via* PEPC in the *sesquiα2* background, similar to what was observed for the iOtsA lines (Figueroa et al., 2016), providing further confirmation that the effects of Tre6P on metabolism are mediated by SnRK1. Preliminary *in silico* analyses of the PEPC1 protein sequence using the PhosMos tool (Carianopol et al., 2020) identified S440 as a full SnRK1 phosphorylation site (data not shown). This residue is conserved across all four PEPC genes from Arabidopsis, therefore providing a good starting point for investigating a functional link between SnRK1 and PEPC. The fact that this residue is in close proximity to the Glc6P-binding allosteric site of the enzyme, also provides a possible mechanism by which SnRK1 might impact on PEPC activity. PEPC has been considered of large interest for the development of strategies to increase plant biomass production (Ku et al., 2001). However, the only known protein with regulatory functions over this enzyme is PEPCK, modulating PEPC sensitivity to malate-mediated inhibition (Jiao and Chollet, 1989). Determining if SnRK1 can also regulate PEPC activity might open new directions for PEPC manipulation and thereby have significant impact in the development of novel, more productive plant varieties.

Preliminary analysis of T-DNA insertional and overexpression mutants for *SnRK1β1.1* show a surprisingly stable metabolic landscape under our experimental

settings (Chapter 3). These results contrast with those obtained by Wang and colleagues, who reported severe alterations at the level of sugars and organic acids in a *snrk1β1* T-DNA insertion mutant (SALK008325) (Wang et al., 2020). Under 16h long-day photoperiods, this line had a metabolic profile opposite of what we observed in the *sesquiα2* mutant, with higher levels of soluble sugar and starch, but reduced accumulation of organic acids (Wang et al., 2020). It is currently unclear why we were unable to reproduce the results of the Wang report, but an obvious difference between both studies is the photoperiod employed. In our study we employed a short-day (8h light; 16h dark) photoperiod that should cause carbon restriction during growth, whereas in the Wang study, mutants were grown under a 16h light, 8h dark long-day photoperiod. The difference in carbon availability between both experimental setups could lead to different SnRK1 activation states, potentially masking phenotypes under certain growth conditions. Another potential difference, yet more difficult to control for, is the type of soil employed in the two studies, which could differ in nutrient content and thereby influence in different ways SnRK1 activity. To test these hypotheses, it will be interesting to further characterize the impact of SnRK1 mutations in primary metabolism, both under different photoperiods and carbon availability regimes (high vs low sugar availability) and under different supply of nutrients, such as nitrogen, phosphate, iron and sulphur. Finally, our RT-PCR analysis of the SALK008325 and other T-DNA insertional mutants paints a complex picture, where *SnRK1β1.1* does appear to be knocked-down, but *SnRK1β1.3* might be overexpressed, raising questions about the adequacy of these mutants for functional studies of the SnRK1β1.1 subunit.

A previous study analysed the impact of *SnRK1β1* overexpression by generating overexpressor lines of the *SnRK1β1.1* variant, similar to the ones used in this work. The authors showed that by overexpressing *SnRK1β1.1*, NR activity was reduced to less than 10% of WT levels, with little to no impact on SPS activity (Li et al., 2009). This suggests that our observation of reduced NO_2^- levels in the *SnRK1β1.1-OE* is likely due to the reduced activation state of NR in this background. To further explore this hypothesis, the levels of glutamine and glutamate in both the *SnRK1α* and *SnRK1β1* backgrounds should be determined. This would also expand

our understanding on how SnRK1 coordinates carbon and nitrogen metabolism. Complementing the analysis of the *sesquiα2* mutant with the measurement of NR and SPS activities could further help us understand a potential coordination between the α and β1 subunits in the regulation of C-N balance.

We were surprised by the very subtle differences in the patterns of starch accumulation of the two SnRK1 mutants. Considering the previously described connection between Tre6P and starch dynamics (Kolbe et al., 2005; Martins et al., 2013; Figueroa et al., 2016; Dos Anjos et al., 2018), and the substantial impact of SnRK1 manipulation on Tre6P accumulation, we expected starch levels to be more strongly affected.

Starch content was significantly different only in the *sesquiα2* line, where a decreased rate of both synthesis and mobilisation could be estimated. High Tre6P plants accumulate excess starch but the precise molecular mechanisms behind this remain unclear. Early work suggested redox-mediated activation of AGPase as the underlying mechanism (Kolbe et al., 2005), but this could not be reproduced in a later study (Martins et al., 2013). Additionally, if the effects of high Tre6P on starch were mediated *via* inhibition of SnRK1, the *sesquiα2* line should present a starch excess phenotype (Kolbe et al., 2005; Martins et al., 2013), which was not observed. Indeed, later studies showed that starch is not necessarily increased following an induced increase in Tre6P (Figueroa et al., 2016), calling into question if Tre6P directly regulates starch accumulation. This is an important question, as starch accumulation is tightly regulated, with an increased allocation of photosynthate to starch in carbon-restricted conditions, for example in low light compared to high light, or in short days compared to long days (Smith and Stitt, 2007; Mengin et al., 2017; Moraes et al., 2019). However, this may be more related to a restriction of growth that leads to higher leaf sugars and a resulting increase in starch accumulation than to direct regulation of the starch synthesis pathway (Mengin et al., 2017; Moraes et al., 2019). Whether SnRK1 and, possibly changes in expression of *SnRK1β1* (as suggested by Pokhilko et al., 2014) are involved in this restriction of growth and resulting stimulation of starch accumulation remains an open question that could be

investigated by growing lines with modified expression of *SnRK1α* and *SnRK1β* in different light intensities or photoperiod durations.

The reduction in starch mobilization in the *sesquiα2* line is, in principle, compatible with the hypothesis that the effects of Tre6P on starch are mediated by SnRK1. However, the reduced starch mobilisation could be more easily explained by the fact that the *sesquiα2* mutant reaches the end of the day with less starch than the WT. Arabidopsis adjusts starch mobilization so that approximately 95% of all carbon reserves are consumed by dawn (Gibon et al., 2004; Graf et al., 2010). This system is very robust and can compensate for changes in starch levels that are far more dramatic than the ones we observed in the *sesquiα2* line (Graf et al., 2010; Scialdone et al., 2013).

On the other hand, Tre6P is thought to affect starch mobilisation at the early steps of cyclical phosphorylation and dephosphorylation of the starch granule. However, Tre6P did not have a direct impact on the catalytic activity of enzymes involved in starch degradation nor on their protein abundance, suggesting this effect is indirect (Martins et al., 2013). Alternately, Tre6P might act on previously undiscovered components of the starch degradation pathway and the network that regulates it. If SnRK1 was to mediate the effects of Tre6P on starch, it should localize inside chloroplasts where these enzymes reside, and indeed a few studies report the presence of SnRK1 subunits in this organelle (Fragoso et al., 2009; Ruiz-Gayosso et al., 2018). Physical interaction between SnRK1α2 and SEX4, involved in starch granule dephosphorylation, has also been previously reported (Fordham-Skelton et al., 2002), and laforin, the functional equivalent of SEX4 in humans, is phosphorylated by AMPK in a process that is essential for proper glycogen metabolism (Gentry et al., 2007; Solaz-Fuster et al., 2008; Raththagala et al., 2015).

The work presented in Chapter 3 also shows a putative chloroplastidial localization for the novel SnRK1β1.3 splice variant. This strengthens the hypothesis that this heterotrimeric kinase plays a role in plastidial metabolism, and provides a possible mechanism for the previously reported plastidial localization of the SnRK1 catalytic subunits (Fragoso et al., 2009). The SnRK1α1/β3/βγ complex that forms at

the ED, and its connections with maltose, one of the main products of starch degradation (Ruiz-Gayosso et al., 2018), is yet another indirect link between SnRK1 and the plastid. Despite all of the circumstantial evidence linking SnRK1 to the chloroplast in general, and starch metabolism in particular, genetic manipulation of either the catalytic α or regulatory β1 subunits in my work did not lead to any substantial changes in starch content, or the pattern of accumulation and mobilisation during the light-dark cycle.

More work is necessary to conclusively link SnRK1 with starch metabolism. It is possible that SnRK1 modulates starch metabolism in response to unexpected environmental challenges, which we did not test in our experimental settings. We focused instead on characterizing SnRK1α/β1 mutant lines under favourable growth conditions. However, given the tight connection between SnRK1 signalling and the response to stress, the obvious next step would be to submit these plants to environmental challenges known to alter energy availability, and characterize their responses. Nukarinen and colleagues previously subjected a *snrk1* loss-of-function mutant to a 6h night extension, performing metabolite profiling over that time period (Nukarinen et al., 2016). Interestingly, the results of this study matched our own, with the *snrk1* mutant presenting reduced levels of sucrose and several glycolytic intermediates and an increased level of organic acids, particularly during the night extension (Nukarinen et al., 2016). However, such an experimental setting, where most carbon resources will have already been depleted at the onset of the night extension, might not be the most informative, particularly when aiming at understanding the impact of SnRK1 on starch metabolism. Instead, I propose that a sudden early dusk, and the monitoring of metabolism over the following night and day periods might provide better clues as to how manipulation of SnRK1 impacts on the ability of the plant to cope with environmental challenges at the metabolic and transcriptional levels. Alternatively, plants might be subjected to a single day of low light and then returned to growth irradiance, as in Moraes *et al.* (2019). This might have the advantage that there would be less perturbation of photoperiod and circadian signalling.

4.4 SnRK1 is potentially linked to Fe and S metabolism

At the gene expression level, the RNA-seq analysis of Chapter 2 identified genes related to iron (Fe) and sulphur (S) metabolism as being strongly dependent on the SnRK1 kinase. In the *sesquiα2* mutant, Fe metabolism genes were markedly downregulated at EN and ED, whereas genes associated with S metabolism were upregulated at the EN only. Fe^{2+} and S^{2-} are highly reactive nutrients that must be kept under tight metabolic control to minimize cellular damage [reviewed in Mendoza-Cózatl et al., 2019]. Iron and sulphur metabolism is tightly coordinated, with Fe excess leading to a S deficiency response, and *vice-versa* (Forieri et al., 2013, 2017; Mendoza-Cózatl et al., 2019). With the currently available gene expression data, it is not possible to determine which of these two nutrients is primarily affected by SnRK1α manipulation, and which one responds as a compensatory mechanism. However, the fact that the Fe-responsive genes appear constitutively altered, and the fact that of the four genes that show opposite responses between the *SnRK1α* gain- and loss-of-function mutants, two are Fe-responsive genes (*IRP3* and *NEET*), strongly suggests that SnRK1 plays a direct effect on the regulation of Fe-responsive genes. It is also difficult to assess at what level mineral nutrition is actually affected in these mutants. The transcriptional response would suggest an excess of Fe in the *sesquiα2* line, implying that SnRK1 plays a role in maintaining Fe homeostasis, but ionomic measurements must be performed to confirm this hypothesis.

Aconitase cannot operate in the absence of either Fe or S, since it requires Fe-S clusters as co-factors, leading to the accumulation of citrate (Mendoza-Cózatl et al., 2019). The *SnRK1α1-OE* line shows slightly reduced levels of isocitrate, which could be an indication of Fe deficiency, but these are not accompanied by an accumulation of citrate, so it is unclear if the reduction in isocitrate levels is due to deficient Fe levels, or some other more general effect on the TCA cycle. It is also currently unknown how genetic manipulation of SnRK1 might affect Fe and S metabolism at other levels, besides gene expression. One of the most important Fe storage compartments is the vacuole, where we observed accumulation of the

SnRK1β1.2 subunit at the tonoplast. To determine if such localization is functionally connected to Fe-metabolism, lines overexpressing SnRK1β1.2 could be grown under different Fe supplementation regimes and their response could be assessed by qPCR analysis of Fe-responsive genes. Such overexpressor lines would also be a good tool for identifying protein interactors and thereby providing leads about the processes affected by SnRK1.

4.5 Tre6P impacts SnRK1 in mature leaves

Looking at the genes identified as downregulated in the *sesquia2* mutant in the RNA-seq analysis of chapter 2, we found a significant overlap with the genes previously reported to be induced by transient *SnRK1α1* overexpression in Arabidopsis protoplasts (Baena-González et al., 2007). These observations were further confirmed by qPCR, and suggest that SnRK1 signalling is progressively activated during the dark period, peaking at the EN, and then progressively repressed during the light period, reaching a minimum at the ED. This daily pattern of gene expression was anti-correlated with the levels of Tre6P accumulation, during the day-night cycle, and aligns highest SnRK1 activity to the time when the carbon status is at its lowest. These results and interpretation are in line with the work of Ruiz-Gayosso and colleagues, who measured higher *in vitro* kinase activities from SnRK1βγ immunoprecipitates (IPs) when leaves were harvested at dawn than when they were harvested at dusk (Ruiz-Gayosso et al., 2018).

Employing an ethanol-inducible iOtsA overexpressor line we could not only confirm the observation that SnRK1 marker genes are progressively repressed along the day, but we could also show that this behaviour is indeed influenced by the endogenous Tre6P levels. Furthermore, these results were obtained from 20d-old rosettes, indicating that Tre6P is able to inhibit SnRK1 in mature leaves. This challenges the view that Tre6P inhibits SnRK1 only on extracts obtained from very young, actively growing tissues (Zhang et al., 2009; Nunes et al., 2013). Whether this repression involves the same factor of actively growing tissues, the SnRK1

upstream kinases (SnAKs) (Zhang et al., 2009; Zhai et al., 2018), or other factor(s) remains to be addressed. A possible reason for detecting SnRK1 repression by Tre6P in our study with mature rosettes but not in the Zhang and Nunes studies (Zhang et al., 2009; Nunes et al., 2013) could be the sensitivity of the employed readouts. Gene expression, as used in our study, is likely to be a more sensitive readout of SnRK1 activity due to signal amplification cascades that typically occur *in vivo*, as compared to the more linear responses commonly observed in *in vitro* studies.

Despite our current lack of knowledge regarding the impact of the SnRK1 kinase in plant metabolism, it is becoming increasingly apparent that more precise tools are required to fully understand and dissect the physiological relevance of this kinase. Recent analyses of Tre6P metabolism have disclosed highly localized effects that cannot be easily studied in constitutive transgenic lines (Fichtner, Barbier, et al., 2020). This is likely the same for SnRK1 signalling. In this study we looked specifically at whole rosettes in constitutive gain- and loss-of-function mutants. These lines will still be useful for furthering our understanding of how other tissues adjust their metabolic landscapes in response to SnRK1 manipulation, as well as for investigating the role of SnRK1 on carbon partitioning and homeostasis at the whole plant level. However, it would be important to increase our level of precision by generating tissue- or cell-specific overexpression or knock-out lines of specific SnRK1 subunits as well as inducible mutants, similar to those already in use to study Tre6P signalling (Martins et al., 2013; Figueroa et al., 2016; Fichtner, Barbier, et al., 2020). This would minimize pleiotropic effects and facilitate the interpretation of the resulting phenotypes. One possibility would be to apply a strategy similar to the one used for *tps1* complementation lines, rescuing SnRK1 expression only during embryo and early seedling development, to determine if SnRK1 is required also at later stages of vegetative and reproductive growth. The fact that SnRK1 depletion *via* virus-induced gene silencing (VIGS) results in growth arrest (Baena-González et al., 2007), already argues in favour of the hypothesis. Furthermore, the very low Tre6P levels observed in the *sesquia2* line suggest that a full *snrk1* knock-out in Arabidopsis would result in unsustainably low Tre6P levels, followed by an inability to

regulate sucrose homeostasis. Such a plant line would likely phenocopy the *tps1* mutant, providing an explanation as to why this knock-out has never been successfully obtained in Arabidopsis.

The development of inducible systems (both for overexpression and loss-of-function), lines with altered SnRK1 levels in a tissue-specific manner, or the complementation of the *sesquiα2* background with hypomorphic SnRK1α variants, should all be useful in further elucidating the relevance of this kinase during favourable growth conditions. It would also be important to analyse if and how the photosynthetic capacity of these SnRK1 mutants is affected, as this could provide further insight into the observed effects on carbon accumulation in the glycolytic and starch biosynthetic pathways. A link between SnRK1 and photosynthesis has been observed at the gene expression level, with transient *SnRK1α1* overexpression leading to upregulation of several photosynthetic genes (Baena-González et al., 2007). Furthermore, SnRK1 was recently shown to promote stomata development, presumably as a way to enhance photosynthetic capacity when carbon levels are low (Han et al., 2020). Curiously, mammalian AMPK plays an important role in the hypothalamus, stimulating appetite when blood glucose levels decline [reviewed in López, 2018]. It is therefore tempting to propose that the potentially stimulatory effect of SnRK1 on carbon assimilation could be the functional equivalent of AMPK function in the regulation of appetite and that both would ultimately promote carbon intake by the organism.

Attacking the catalytic subunits, although effective, invariably results in the complete removal of all SnRK1 functions simultaneously, and is more likely to result in deleterious and pleiotropic effects. Obtaining a full knock-out line for *SnRK1β1* will be important for investigating further the impact of this subunit on metabolism. This would also allow the generation of complementation lines with the specific *SnRK1β1* splice variants identified in chapter 3, which, together with *SnRK1β1.2* and *SnRK1β1.3* overexpressor lines, would provide a full set of tools to dissect their functions. Knock-out mutants of regulatory β and βγ SnRK1 subunits might also be a more precise way of characterizing the roles of the SnRK1 kinase, as this will allow

targeting only specific subsets of its cellular functions. Such a knock-out line would also open the possibility of complementing it with *SnRK1β1* under the control of an inducible promoter, which might be a quite direct way to learn how this regulatory subunit modifies SnRK1 function. Indeed, deeper genetic analysis of the roles of the regulatory subunits may be a useful strategy for future research.

It is widely accepted that the β regulatory subunits are involved in the subcellular localization of the SnRK1 trimer, and in that way help in regulating its function, by defining which SnRK1 targets are accessible to the kinase at a given time (Coccetti et al., 2018; Ramon et al., 2019; González et al., 2020). Our results in chapter 3 show that alternative splicing events targeting the *SnRK1β1* transcript generate both new RNA and protein diversity. We confirmed the existence of all three predicted mRNA forms of *SnRK1β1 in planta* and showed how their protein products accumulate at different subcellular localizations when overexpressed in tobacco leaf epidermis. We also provide preliminary data supporting the ability of SnRK1α1 to interact with all three β1 splice variants, although these results should be further confirmed by other methodologies, such as co-IP experiments. Questions such as which interacting partners are specific to each β1 subunit, or how these subunits impact SnRK1 function, such as gene expression or metabolism, must be addressed in future experiments. Our initial characterization of the SnRK1β1.1 subunit is also an important first step in broadening our understanding of how SnRK1 influences primary metabolism. Our results obtained with the SnRK1α mutant lines are relevant, but do not provide information regarding which SnRK1αβγ complexes are involved in the regulation of primary metabolism, or if the catalytic subunits are sufficient for the regulation of these processes as independent entities (see Ramon et al. 2019).

Finally, it is important to note that the work presented in this thesis was performed from a SnRK1-perspective, providing an overview of the relevance of SnRK1 for metabolism. However, to effectively regulate metabolism, feedback mechanisms must be in place that link metabolic information to SnRK1 activity. In this context, inducible knockdowns or overexpressors of enzymes involved in

glycolysis, the TCA cycle and starch metabolism could be valuable tools to investigate possible impacts of metabolism on SnRK1 signalling, allowing us to have a more complete picture of the interplay between these different pathways, and how metabolism feeds back into SnRK1 signalling.

In conclusion, this work advances the field of SnRK1 signalling and plant central metabolism in several ways (refer to Figure 4.1 for a graphical representation):

- **Alternative splicing of *SnRK1β1* can act as a source of SnRK1 subunit diversity.** This finding will contribute to our understanding of the composition of SnRK1αβγ heterotrimers *in vivo*, as well as of their specialised functions at the molecular and physiological levels.
- **SnRK1 is part of the system that links sucrose to Tre6P accumulation.** Genetic manipulation of SnRK1 results in altered levels of Tre6P. The fact that Tre6P still responds to sucrose and that the two sugars are highly correlated in the SnRK1 mutants along the day-night cycle is evidence that neither synthesis nor degradation of Tre6P is lost. Instead, the altered relationship between these two sugars in the SnRK1 mutants is more likely to be explained by a role of SnRK1 in linking sucrose to Tre6P. Much has been published about the effects of Tre6P on SnRK1 function, but this work is the first to describe a reciprocal effect of SnRK1 on Tre6P. These results redefine our understanding of the relationship between these two molecular players and might change the way previous work related to the physiological effects of SnRK1 might be interpreted.
- **SnRK1 mediates at least partly the effects of Tre6P on metabolism.** SnRK1 depletion causes low Tre6P accumulation but leads to metabolic phenotypes associated to high Tre6P. Conversely, SnRK1 overexpression causes high Tre6P accumulation but does not lead to metabolic phenotypes associated to high Tre6P. These observations suggest that SnRK1 acts as an effector of Tre6P, at least with regard to metabolic adjustments.
- **Tre6P inhibits SnRK1 in mature rosettes**. Inducible overexpression of otsA (as a means to increase Tre6P levels) represses expression of SnRK1-

induced genes, supporting a repressive action of Tre6P on SnRK1 signalling in autotrophic adult tissues. This is further supported by the metabolic signatures of the SnRK1 mutants described in the previous paragraph. This idea challenges the currently accepted view that such repression occurs only in very young and actively proliferating tissues.

- **The daily fluctuations of Tre6P lead to daily fluctuations in SnRK1 activity.** This allows a fine-tuning of SnRK1 activation during the day-night cycle, maximizing its effects on gene expression at the EN, when carbon resources are at their lowest, and minimizing its effects at the ED, when carbon resources are highest. It also challenges the established view that SnRK1 is activate (and plays an important role) only during stress conditions.

Overall, this thesis brings novel insight into how SnRK1 modulates metabolism and gene expression, particularly in the absence of stress in the context of regular day-night cycles. The SnRK1-Tre6P relationship must also be redefined, and the sucrose-Tre6P nexus adjusted to account for the relevance of SnRK1 activity in linking sucrose to Tre6P and *vice-versa*. It now becomes relevant to revisit the previously published studies on SnRK1 and reassess if impaired Tre6P accumulation and/or signalling could explain the occasionally contradictory results of SnRK1 manipulation in different tissues and plant species. This thesis will also serve as a basis for designing future experiments that can further expand our mechanistic understanding behind the impact of SnRK1 and Tre6P on plant metabolism, physiology and development.

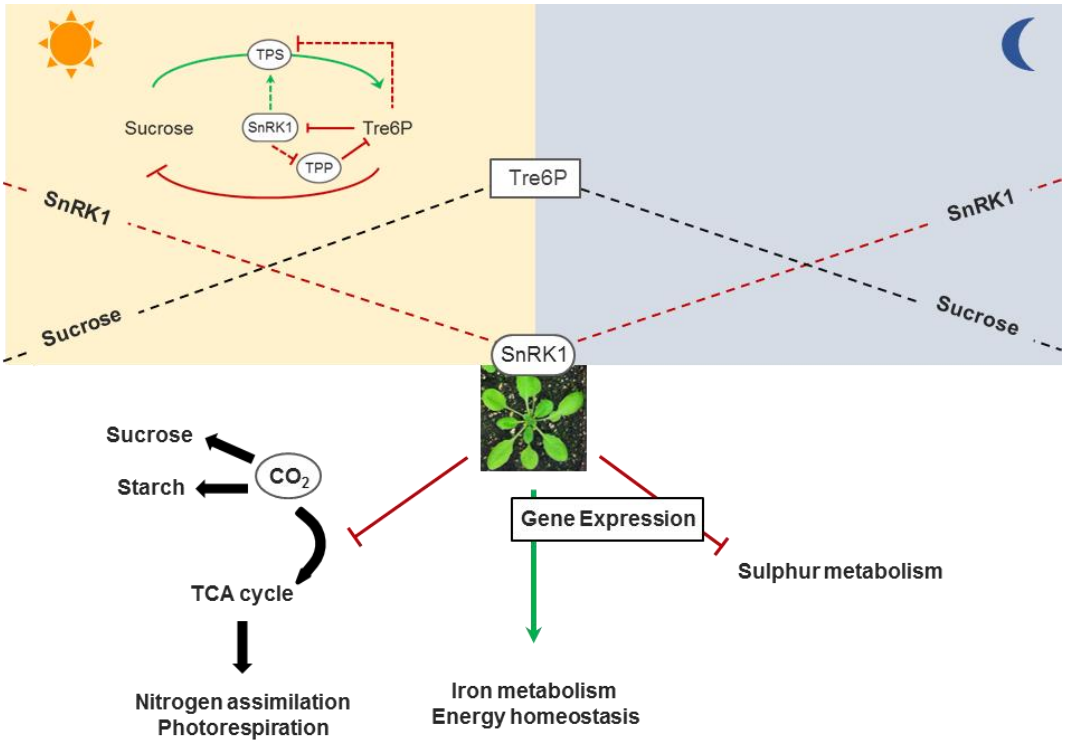

Figure 4.1 | Model for the sucrose-Tre6P-SnRK1 interplay and its relevance for the control of carbon metabolism and gene expression in source leaves.
Sucrose accumulation during the day leads to a parallel increase in Tre6P levels, inducing mechanisms that maintain sucrose homeostasis. SnRK1 appears to be required for translating sucrose information into adequate Tre6P levels, but this does not involve changes in TPS1 protein accumulation. However, excessive Tre6P accumulation may trigger negative feedback mechanisms that repress TPS1 accumulation in the *SnRK1α1-OE* at ED. The build-up of Tre6P during the day results in a progressive repression of SnRK1 activity. This enables an enhanced flux of carbon into the TCA cycle, contributing to a decrease in sucrose levels. This observation implies that SnRK1 is involved in the translation of the Tre6P signal to the downstream metabolic adjustments that have been attributed to increased Tre6P levels. Declining sucrose and Tre6P levels during the night lead to the gradual activation of SnRK1, which reaches maximal activity at dawn. Lack of SnRK1 activity in the *sesquiα2* mutant alters the expression of 275 genes (235 at EN and 40 at ED) related to iron and sulphur metabolism, and energy homeostasis.

4.6 References

Dos Anjos, L., Pandey, P.K., Moraes, T.A., Feil, R., Lunn, J.E., and Stitt, M. (2018). Feedback regulation by trehalose 6-phosphate slows down starch mobilization below the rate that would exhaust starch reserves at dawn in Arabidopsis leaves. Plant Direct **2**: e00078.

Baena-González, E. and Lunn, J.E. (2020). SnRK1 and trehalose 6-phosphate – two ancient pathways converge to regulate plant metabolism and growth. Curr. Opin. Plant Biol. **55**: 52–59.

Baena-González, E., Rolland, F., Thevelein, J.M., and Sheen, J. (2007). A central integrator of transcription networks in plant stress and energy signalling. Nature **448**: 938–942.

Baena-González, E. and Sheen, J. (2008). Convergent energy and stress signaling. Trends Plant Sci. **13**: 474–482.

Carianopol, C.S., Chan, A.L., Dong, S., Provart, N.J., Lumba, S., and Gazzarrini, S. (2020). An abscisic acid-responsive protein interaction network for sucrose non-fermenting related kinase1 in abiotic stress response. Commun. Biol. **3**: 1–15.

Coccetti, P., Nicastro, R., and Tripodi, F. (2018). Conventional and emerging roles of the energy sensor snf1/AMPK in saccharomyces cerevisiae. Microb. Cell **5**: 482–494.

Crepin, N. and Rolland, F. (2019). SnRK1 activation, signaling, and networking for energy homeostasis. Curr. Opin. Plant Biol. **51**: 29–36.

Delorge, I., Figueroa, C.M., Feil, R., Lunn, J.E., and Van Dijck, P. (2015). Trehalose-6-phosphate synthase 1 is not the only active TPS in Arabidopsis thaliana. Biochem. J. **466**: 283–290.

Eastmond, P.J., Van Dijken, A.J.H., Spielman, M., Kerr, A., Tissier, A.F., Dickinson, H.G., Jones, J.D.G., Smeekens, S.C., and Graham, I.A. (2002). Trehalose-6-phosphate synthase 1, which catalyses the first step in trehalose synthesis, is essential for Arabidopsis embryo maturation. Plant J. **29**: 225–235.

Eisenhut, M., Roell, M.S., and Weber, A.P.M. (2019). Mechanistic understanding of photorespiration paves the way to a new green revolution. New Phytol. **223**: 1762–1769.

Fichtner, F., Barbier, F.F., Annunziata, M.G., Feil, R., Olas, J.J., Mueller-Roeber, B., Stitt, M., Beveridge, C.A., and Lunn, J.E. (2020). Regulation of shoot branching in Arabidopsis by trehalose 6-phosphate. New Phytol. **13**: nph.17006.

Fichtner, F., Olas, J.J., Feil, R., Watanabe, M., Krause, U., Hoefgen, R., Stitt, M., and Lunn, J.E. (2020). Functional features of TREHALOSE-6-PHOSPHATE SYNTHASE1, an essential enzyme in Arabidopsis. Plant Cell **32**: 1949–1972.

Figueroa, C.M., Feil, R., Ishihara, H., Watanabe, M., Kölling, K., Krause, U., Höhne, M., Encke, B., Plaxton, W.C., Zeeman, S.C., Li, Z., Schulze, W.X., Hoefgen, R., Stitt, M., and Lunn, J.E. (2016). Trehalose 6-phosphate coordinates organic and amino acid metabolism with carbon availability. Plant J. **85**: 410–423.

Fordham-Skelton, A.P., Chilley, P., Lumbreras, V., Reignoux, S., Fenton, T.R., Dahm, C.C., Pages, M., and Gatehouse, J.A. (2002). A novel higher plant protein tyrosine phosphatase interacts with SNF1-related protein kinases via a KIS (kinase interaction sequence) domain. Plant J. **29**: 705–715.

Forieri, I., Sticht, C., Reichelt, M., Gretz, N., Hawkesford, M.J., Malagoli, M., Wirtz, M., and Hell, R. (2017). System analysis of metabolism and the transcriptome in Arabidopsis thaliana roots reveals differential co-regulation upon iron, sulphur and potassium deficiency. Plant Cell Environ.

Forieri, I., Wirtz, M., and Hell, R. (2013). Toward new perspectives on the interaction of iron and sulphur metabolism in plants. Front. Plant Sci.

Fragoso, S., Espíndola, L., Páez-Valencia, J., Gamboa, A., Camacho, Y., Martínez-Barajas, E., and Coello, P. (2009). SnRK1 isoforms AKIN10 and AKIN11 are differentially regulated in Arabidopsis plants under phosphate starvation. Plant Physiol. **149**: 1906–1916.

Gao, X.Q., Liu, C.Z., Li, D.D., Zhao, T.T., Li, F., Jia, X.N., Zhao, X.Y., and Zhang, X.S. (2016). The Arabidopsis KINβγ Subunit of the SnRK1 Complex Regulates Pollen Hydration on the Stigma by Mediating the Level of Reactive Oxygen Species in Pollen. PLoS Genet. **12**: 1–25.

Gentry, M.S., Dowen, R.H., Worby, C.A., Mattoo, S., Ecker, J.R., and Dixon, J.E. (2007). The phosphatase laforin crosses evolutionary boundaries and links carbohydrate metabolism to neuronal disease. J. Cell Biol. **178**: 477–488.

Ghillebert, R., Swinnen, E., Wen, J., Vandesteene, L., Ramon, M., Norga, K., Rolland, F., and Winderickx, J. (2011). The AMPK/SNF1/SnRK1 fuel gauge and energy regulator: Structure, function and regulation. FEBS J. **278**: 3978–3990.

Gibon, Y., Blaesing, O.E., Hannemann, J., Carillo, P., Höhne, M., Hendriks, J.H.M., Palacios, N., Cross, J., Selbig, J., and Stitt, M. (2004). A robot-based platform to measure multiple enzyme activities in Arabidopsis using a set of cycling assays: Comparison of changes of enzyme activities and transcript levels during diurnal cycles and in prolonged darkness. Plant Cell **16**: 3304–3325.

Gómez, L.D., Gilday, A., Feil, R., Lunn, J.E., and Graham, I.A. (2010). AtTPS1-mediated trehalose 6-phosphate synthesis is essential for embryogenic and vegetative growth and responsiveness to ABA in germinating seeds and stomatal guard cells. Plant J. **64**: 1–13.

González, A., Hall, M.N., Lin, S.C., and Hardie, D.G. (2020). AMPK and TOR: The Yin and Yang of Cellular Nutrient Sensing and Growth Control. Cell Metab. **31**: 472–492.

Graf, A., Schlereth, A., Stitt, M., and Smith, A.M. (2010). Circadian control of carbohydrate availability for growth in Arabidopsis plants at night. Proc. Natl. Acad. Sci. U. S. A. **107**: 9458–9463.

Han, C., Liu, Y., Shi, W., Qiao, Y., Wang, L., Tian, Y., Fan, M., Deng, Z., Lau, O.S., De Jaeger, G., and Bai, M.Y. (2020). KIN10 promotes stomatal development through stabilization of the SPEECHLESS transcription factor. Nat. Commun. **11**.

Jiao, J.A. and Chollet, R. (1989). Regulatory seryl-phosphorylation of C4 phosphoenolpyruvate carboxylase by a soluble protein kinase from maize leaves. Arch. Biochem. Biophys. **269**: 526–535.

Jossier, M., Bouly, J.-P., Meimoun, P., Arjmand, A., Lessard, P., Hawley, S., Grahame Hardie, D., and Thomas, M. (2009). SnRK1 (SNF1-related kinase 1) has a central role in sugar and ABA signalling in Arabidopsis thaliana. Plant J. **59**: 316–328.

Kolbe, A., Tiessen, A., Schluepmann, H., Paul, M., Ulrich, S., and Geigenberger, P. (2005). Trehalose 6-phosphate regulates starch synthesis via posttranslational redox activation of ADP-glucose pyrophosphorylase. **102**: 2–7.

Ku, M.S.B., Cho, D., Li, X., Jiao, D.M., Pinto, M., Miyao, M., and Matsuoka, M. (2001). Introduction of genes encoding C4 photosynthesis enzymes into rice plants: Physiological consequences. Novartis Found. Symp. **236**: 100–116.

Li, X.-F., Li, Y.-J., An, Y.-H., Xiong, L.-J., Shao, X.-H., Wang, Y., and Sun, Y. (2009). AKINβ1 is Involved in the Regulation of Nitrogen Metabolism and Sugar Signaling in Arabidopsis. J. Integr. Plant Biol. **51**: 513–520.

López, M. (2018). Hypothalamic AMPK and energy balance. Eur. J. Clin. Invest. **48**: 1–10.

Margalha, L., Confraria, A., and Baena-González, E. (2019). SnRK1 and TOR: Modulating growth–defense trade-offs in plant stress responses. J. Exp. Bot. **70**: 2261–2274.

Martins, M.C.M., Hejazi, M., Fettke, J., Steup, M., Feil, R., Krause, U., Arrivault, S., Vosloh, D., Figueroa, C.M., Ivakov, A., Yadav, U.P., Piques, M., Metzner, D., Stitt, M., and Lunn, J.E. (2013). Feedback inhibition of starch degradation in Arabidopsis leaves mediated by trehalose 6-phosphate. Plant Physiol. **163**: 1142–1163.

McMichael, R.W., Bachmann, M., and Huber, S.C. (1995). Spinach leaf sucrose-phosphate synthase and nitrate reductase are phosphorylated/inactivated by multiple protein kinases in vitro. Plant Physiol. **108**: 1077–1082.

Mendoza-Cózatl, D.G., Gokul, A., Carelse, M.F., Jobe, T.O., Long, T.A., and Keyster, M. (2019). Keep talking: crosstalk between iron and sulphur networks fine-tunes growth and development to promote survival under iron limitation. J. Exp. Bot. **70**: 4197–4210.

Mengin, V., Pyl, E.T., Moraes, T.A., Sulpice, R., Krohn, N., Encke, B., and Stitt, M. (2017). Photosynthate partitioning to starch in arabidopsis thaliana is insensitive to light intensity but sensitive to photoperiod due to a restriction on growth in the light in short photoperiods. Plant Cell Environ. **40**: 2608–2627.

Moorhead, G., Douglas, P., Morrice, N., Scarabel, M., Aitken, A., and MacKintosh, C. (1996). Phosphorylated nitrate reductase from spinach leaves is inhibited by 14- 3-3 proteins and activated by fusicoccin. Curr. Biol. **6**: 1104–1113.

Moraes, T.A., Mengin, V., Annunziata, M.G., Encke, B., Krohn, N., Höhne, M., and Stitt, M. (2019). Response of the Circadian Clock and Diel Starch Turnover to One Day of Low Light or Low CO 2. Plant Physiol. **179**: 1457–1478.

Nukarinen, E., Ngele, T., Pedrotti, L., Wurzinger, B., Mair, A., Landgraf, R., Börnke, F., Hanson, J., Teige, M., Baena-Gonzalez, E., Dröge-Laser, W., and Weckwerth, W. (2016). Quantitative phosphoproteomics reveals the role of the AMPK plant ortholog SnRK1 as a metabolic master regulator under energy deprivation. Sci. Rep. **6**: 31697.

Nunes, C., Primavesi, L.F., Patel, M.K., Martinez-Barajas, E., Powers, S.J., Sagar, R., Fevereiro, P.S., Davis, B.G., and Paul, M.J. (2013). Inhibition of SnRK1 by metabolites: Tissue-dependent effects and cooperative inhibition by glucose 1-phosphate in combination with trehalose 6-phosphate. Plant Physiol. Biochem. **63**: 89–98.

Pokhilko, A., Flis, A., Sulpice, R., Stitt, M., and Ebenhöh, O. (2014). Adjustment of carbon fluxes to light conditions regulates the daily turnover of starch in plants: A computational model. Mol. Biosyst. **10**: 613–627.

Ramon, M., Dang, T.V.T., Broeckx, T., Hulsmans, S., Crepin, N., Sheen, J., and Rolland, F. (2019). Default activation and nuclear translocation of the plant cellular energy sensor SnRK1 regulate metabolic stress responses and development. Plant Cell **31**: 1614–1632.

Ramon, M., Ruelens, P., Li, Y., Sheen, J., Geuten, K., and Rolland, F. (2013). The hybrid Four-CBS-Domain KINβγ subunit functions as the canonical γ subunit of the plant energy sensor SnRK1. Plant J. **75**: 11–25.

Raththagala, M., Brewer, M.K., Parker, M.W., Sherwood, A.R., Wong, B.K., Hsu, S., Bridges, T.M., Paasch, B.C., Hellman, L.M., Husodo, S., Meekins, D.A., Taylor, A.O., Turner, B.D., Auger, K.D., Dukhande, V. V., Chakravarthy, S., Sanz, P., Woods, V.L., Li, S., Vander Kooi, C.W., et al. (2015). Structural mechanism of laforin function in glycogen dephosphorylation and lafora disease. Mol. Cell **57**: 261–272.

Ruiz-Gayosso, A., Rodríguez-Sotres, R., Martínez-Barajas, E., and Coello, P. (2018). A role for the carbohydrate-binding module (CBM) in regulatory SnRK1 subunits: the effect of maltose on SnRK1 activity. Plant J. **96**: 163–175.

Scialdone, A., Mugford, S.T., Feike, D., Skeffngton, A., Borrill, P., Graf, A., Smith, A.M., and Howard, M. (2013). Arabidopsis plants perform arithmetic division to prevent starvation at night. Elife: 2:e00669.

Smith, A.M. and Stitt, M. (2007). Coordination of carbon supply and plant growth. Plant, Cell Environ. **30**: 1126–1149.

Solaz-Fuster, M.C., Gimeno-Alcañiz, J.V., Ros, S., Fernandez-Sanchez, M.E., Garcia-Fojeda, B., Garcia, O.C., Vilchez, D., Dominguez, J., Garcia-Rocha, M., Sanchez-Piris, M., Aguado, C., Knecht, E., Serratosa, J., Guinovart, J.J., Sanz, P., and De Córdoba, S.R. (2008). Regulation of glycogen synthesis by the laforin - Malin complex is modulated by the AMP-activated protein kinase pathway. Hum. Mol. Genet. **17**: 667–678.

Sweetlove, L.J., Beard, K.F.M., Nunes-Nesi, A., Fernie, A.R., and Ratcliffe, R.G. (2010). Not just a circle: flux modes in the plant TCA cycle. Trends Plant Sci. **15**: 462–470.

Sweetlove, L.J. and Fernie, A.R. (2018). The role of dynamic enzyme assemblies and substrate channelling in metabolic regulation. Nat. Commun. **9**.

Vandesteene, L., López-Galvis, L., Vanneste, K., Feil, R., Maere, S., Lammens, W., Rolland, F., Lunn, J.E., Avonce, N., Beeckman, T., and van Dijck, P. (2012). Expansive evolution of the TREHALOSE-6-PHOSPHATE PHOSPHATASE gene family in Arabidopsis. Plant Physiol. **160**: 884–896.

Wang, Y., Wang, L., Micallef, B.J., Tetlow, I.J., Mullen, R.T., Feil, R., Lunn, J.E., and Emes, M.J. (2020). AKINβ1, a subunit of SnRK1, regulates organic acid metabolism and acts as a global modulator of genes involved in carbon, lipid, and nitrogen metabolism. J. Exp. Bot. **71**: 1010–1028.

Yadav, U.P., Ivakov, A., Feil, R., Duan, G.Y., Walther, D., Giavalisco, P., Piques, M., Carillo, P., Hubberten, H.M., Stitt, M., and Lunn, J.E. (2014). The sucrose-trehalose 6-phosphate (Tre6P) nexus: Specificity and mechanisms of sucrose signalling by. J. Exp. Bot. **65**: 1051–1068.

Zhai, Z., Keereetaweep, J., Liu, H., Feil, R., Lunn, J.E., and Shanklin, J. (2018). Trehalose 6-phosphate positively regulates fatty acid synthesis by stabilizing wrinkled1[open]. Plant Cell **30**: 2616–2627.

Zhang, Y., Beard, K.F.M., Swart, C., Bergmann, S., Krahnert, I., Nikoloski, Z., Graf, A., George Ratcliffe, R., Sweetlove, L.J., Fernie, A.R., and Obata, T. (2017). Protein-protein interactions and metabolite channelling in the plant tricarboxylic acid cycle. Nat. Commun. **8**.

Zhang, Y., Primavesi, L.F., Jhurreea, D., Andralojc, P.J., Mitchell, R.A.C., Powers, S.J., Schluepmann, H., Delatte, T., Wingler, A., and Paul, M.J. (2009). Inhibition of SNF1-related protein kinasel activity and regulation of metabolic pathways by trehalose-6-phosphate1[w][OA]. Plant Physiol. **149**: 1860–1871.